



National Library
of Canada

Bibliothèque nationale
du Canada

Canadian Theses Service

Service des thèses canadiennes

Ottawa, Canada
K1A 0N4

NOTICE

The quality of this microform is heavily dependent upon the quality of the original thesis submitted for microfilming. Every effort has been made to ensure the highest quality of reproduction possible.

If pages are missing, contact the university which granted the degree.

Some pages may have indistinct print especially if the original pages were typed with a poor typewriter ribbon or if the university sent us an inferior photocopy.

Reproduction in full or in part of this microform is governed by the Canadian Copyright Act, R.S.C. 1970, c. C-30, and subsequent amendments.

AVIS

La qualité de cette microforme dépend grandement de la qualité de la thèse soumise au microfilmage. Nous avons tout fait pour assurer une qualité supérieure de reproduction.

S'il manque des pages, veuillez communiquer avec l'université qui a conféré le grade.

La qualité d'impression de certaines pages peut laisser à désirer, surtout si les pages originales ont été dactylographiées à l'aide d'un ruban usé ou si l'université nous a fait parvenir une photocopie de qualité inférieure.

La reproduction, même partielle, de cette microforme est soumise à la Loi canadienne sur le droit d'auteur, SRC 1970, c. C-30, et ses amendements subséquents.

THE ISOTOPIC DEPENDENCE OF BORN-OPPENHEIMER BREAKDOWN
EFFECTS: APPLICATION OF A HAMILTONIAN CORRECTION
APPROACH TO THE REPRESENTATION OF SPECTROSCOPIC LINE
POSITIONS OF HF/DF AND HCl/DCI

by

PHOTOS GEORGE HAJIGEORGIOU
B.Sc.(Hon.), Dalhousie University, 1984.

Submitted in partial fulfillment of
the requirements for the degree of
DOCTOR OF PHILOSOPHY

at

Dalhousie University
Halifax, Nova Scotia, Canada

August 1990

© Copyright by Photos George Hajigeorgiou, 1990



National Library
of Canada

Bibliothèque nationale
du Canada

Canadian Theses Service Service des thèses canadiennes

Ottawa, Canada
K1A 0N4

The author has granted an irrevocable non-exclusive licence allowing the National Library of Canada to reproduce, loan, distribute or sell copies of his/her thesis by any means and in any form or format, making this thesis available to interested persons.

The author retains ownership of the copyright in his/her thesis. Neither the thesis nor substantial extracts from it may be printed or otherwise reproduced without his/her permission.

L'auteur a accordé une licence irrévocable et non exclusive permettant à la Bibliothèque nationale du Canada de reproduire, prêter, distribuer ou vendre des copies de sa thèse de quelque manière et sous quelque forme que ce soit pour mettre des exemplaires de cette thèse à la disposition des personnes intéressées.

L'auteur conserve la propriété du droit d'auteur qui protège sa thèse. Ni la thèse ni des extraits substantiels de celle-ci ne doivent être imprimés ou autrement reproduits sans son autorisation.

ISBN 0-315-64580-6

Canada

To my family

TABLE OF CONTENTS

	PAGE
LIST OF TABLES	xii
LIST OF FIGURES	xviii
ABSTRACT	xxi
LIST OF ABBREVIATIONS AND SYMBOLS	xxii
ACKNOWLEDGEMENTS	xxvi
CHAPTER 1 GENERAL INTRODUCTION	1
CHAPTER 2 THEORETICAL BACKGROUND AND NUMERICAL TECHNIQUES	5
2.1 <i>The JWKB Approach</i>	5
2.2 <i>The Dunham and Dunham-type Solutions</i>	7
2.3 <i>Rydberg-Klein-Rees-Vanderslice Potentials</i>	9
2.4 <i>The Concept of Molecular Structure: The Born-Oppenheimer Approximation</i>	14
2.5 <i>The Adiabatic Separation of Electronic States</i>	18
2.6 <i>Nonadiabatic Theory</i>	22
2.7 <i>Effective Hamiltonians for Radial Motion</i>	24
2.8 <i>The Isotopic Dependence of Molecular Constants</i>	29
2.9 <i>Centrifugal Distortion Constants for Diatomic Molecules</i>	31
2.10 <i>The Method of Least-Squares</i>	36

	PAGE
2.10.1 <i>Introduction</i>	36
2.10.2 <i>Weighted Linear Least-Squares</i>	38
2.10.3 <i>Correlated Least-Squares (Merging)</i>	40
2.10.4 <i>Weighted Nonlinear Least-Squares</i>	43
2.11 <i>Numerical Solution of the Radial Wave Equation</i>	45
2.11.1 <i>Truly Bound States</i>	45
2.11.2 <i>Quasibound States (Orbiting Resonances)</i>	53
 CHAPTER 3 IMPROVED HAMILTONIAN OPERATORS FOR RADIAL MOTION	 59
PART A: SEMICLASSICAL METHODS	59
3.1 <i>Direct Inclusion of 3rd-Order JWKB Phase Integral</i>	61
3.2 <i>Indirect Inclusion of Higher-Order JWKB Terms</i>	62
3.3 <i>Extended Dunham and Dunham-type Methods</i>	66
 PART B: QUANTUM MECHANICAL METHODS	 68
3.4 <i>Direct Perturbation Methods</i>	68
3.5 <i>Inverse Methods</i>	69
3.5.1 <i>Semiempirical Correction Methods</i>	69

	PAGE
3.5.2 <i>Inverse Perturbation Analysis (IPA)</i>	70
3.5.3 <i>A Hamiltonian Correction Approach</i>	76
3.5.3 (a) <i>Introduction</i>	76
3.5.3 (b) <i>Numerical Procedure</i>	78
3.5.3 (c) <i>Mathematical Model</i>	79
3.5.3 (d) <i>Model Testing</i>	82
3.5.3 (d.1) <i>General Description of the Problem</i>	82
3.5.3 (d.2) <i>Model Hamiltonians and Synthetic Spectra</i>	87
3.5.3 (d.3) <i>Trial Operators and Least-Squares Fit</i>	90
3.5.3 (d.4) <i>Radial Functions and Discussion</i>	97
 CHAPTER 4 ROTATIONAL ANALYSIS OF THE $B^1\Sigma^+ - X^1\Sigma^+$	
EMISSION BANDS OF $D^{35}\text{Cl}$	111
4.1 <i>Introduction</i>	111
4.2 <i>Experimental Details</i>	115
4.3 <i>Wavelength Calibration</i>	120
4.4 <i>Analysis of Molecular Spectrum</i>	121
4.5 <i>RKR/V Potentials and Electronic Isotope Shift</i>	128
4.6 <i>Rydberg \approx non-Rydberg Interactions</i>	133

	PAGE
CHAPTER 5 SPECTROSCOPIC INVESTIGATIONS OF DEUTERIUM FLUORIDE	143
PART A: FOURIER TRANSFORM SPECTROSCOPY OF DF	143
5.1 <i>Basic Principles of Fourier Transform Spectroscopy</i>	143
5.2 <i>Experimental</i>	147
5.3 <i>Analysis</i>	148
PART B: SPECTROGRAPHIC STUDY OF THE $B^1\Sigma^+ - X^1\Sigma^+$ EMISSION BAND SYSTEM IN THE ULTRAVIOLET	154
5.4 <i>Introduction</i>	154
5.5 <i>Experimental Details</i>	158
5.6 <i>Rotational Assignments</i>	163
5.7 <i>Molecular Parameters</i>	164
5.8 <i>RKR Potential Curves for DF</i>	166
5.9 <i>Dissociation Energy of $DF(X^1\Sigma^+)$</i>	170
5.10 <i>Electronic Isotope Shift</i>	181

	PAGE
CHAPTER 6 ISOTOPIC BEHAVIOUR OF BORN-OPPENHEIMER BREAKDOWN: THE $B^1\Sigma^+$ AND $X^1\Sigma^+$ STATES OF HCl AND DCI	183
6.1 <i>Introduction</i>	183
6.2 <i>The Multi-Isotopomer Problem</i>	186
6.3 <i>Determination of Effective Hamiltonian Operators</i>	188
6.3.1 <i>Selection of Data</i>	188
6.3.2 <i>Assignment of $D^{37}\text{Cl } B^1\Sigma^+ - X^1\Sigma^+$ Bands</i>	193
6.3.3 <i>Initial Operators and Hamiltonian Correction Model</i>	193
6.3.4 <i>Least-Squares Fit and Radial Operators</i>	198
6.4 <i>Isotopic Variation of Equilibrium Bond Lengths</i>	220
6.5 <i>Perturbation Calculation of Centrifugal Distortion</i>	229
6.6 <i>Tritium Chloride</i>	242
6.7 <i>Higher-Order JWKB Effects in the RKR Procedure</i>	245
6.8 <i>Nonuniqueness in the Hamiltonian Operators: Further Comments</i>	246
6.9 <i>The Adiabatic Correction at the Potential Minimum</i>	252

	PAGE
CHAPTER 7 ISOTOPIC BEHAVIOUR OF BORN-OPPENHEIMER BREAKDOWN: THE $B^1\Sigma^+$ AND $X^1\Sigma^+$ STATES OF HF AND DF	255
7.1 <i>Introduction</i>	255
7.2 <i>Analysis</i>	261
7.2.1 <i>Selection of Data</i>	261
7.2.2 <i>Trial Operators</i>	262
7.2.3 <i>Least-Squares Fitting</i>	269
7.3 <i>Results and Discussion</i>	273
7.3.1 <i>Radial Functions and Eigenvalues for HF and DF</i>	273
7.3.2 <i>Predissociation in $X^1\Sigma^+$</i>	282
7.3.3 <i>The Dissociation Energy of $X^1\Sigma^+$</i>	287
7.3.4 <i>The Electronic Isotope Shift</i>	298
7.3.5 <i>Perturbation Calculation of Centrifugal Distortion</i>	298
7.3.6 <i>Vibrational Index at Dissociation</i>	305
7.3.7 <i>Tritium Fluoride</i>	312
7.3.8 <i>Equilibrium Bond Lengths</i>	316
7.3.9 <i>Radiative Transition Probabilities</i>	319

CHAPTER 8 REVIEW OF HAMILTONIAN CORRECTION

APPROACH	337
8.1 <i>Comparison with a Conventional Analysis</i>	337
8.1.1 <i>Physical Significance</i>	337
8.1.2 <i>General Fitting, Extrapolation and Interpolation Ability</i>	339
8.1.3 <i>Stability</i>	341
8.1.4 <i>Compactness</i>	341
8.2 <i>Suggestions for Improved Procedures</i>	343
8.2.1 <i>Improved Compactness</i>	343
8.2.2 <i>Extension to Higher-Order Perturbation Theory</i>	345
8.2.3 <i>Direct Nonlinear Least-Squares Fits to Analytical Operators</i>	347
8.3 <i>Concluding Remarks</i>	349
APPENDICES	350
BIBLIOGRAPHY	351

LIST OF TABLES

TABLE NUMBER	TITLE	PAGE
2.1	Test of Algorithm for Solution of Radial Wave Equation: Parameters of Analytical Potential Functions	50
2.2	Test of Algorithm for Solution of Radial Wave Equation: A Comparison of Calculated with Exact Energies	51
3.1	Fundamental Band of $\text{HF}(X^1\Sigma^+)$: Demonstration of Inadequacy of RKR Potential in Predicting Observables	60
3.2	Synthetic Spectroscopic Data Base for the Model Calculations	88
3.3	Parameters of Hamiltonian Operators for the Model Calculations	89
3.4	Basis Functions for Model Calculations	94
3.5	Results of the Model Calculations: Radial Functions	96
3.6	Results of Least-Squares Fit for the Model DF 4-14 ($B \rightarrow X$) Band	98
3.7	Results of the Model Calculations: Energies and Widths of Selected Quasibound Levels	99
4.1	Franck-Condon Factors for the $B^1\Sigma^+ - X^1\Sigma^+$ Band System of D^{35}Cl for Selected Values of J .	126

TABLE NUMBER	TITLE	PAGE
4.2	Least-Squares Fits for Individuals Bands of the $B^1\Sigma^+ - X^1\Sigma^+$ Band System of $D^{35}\text{Cl}$	129
4.3	Merged Parameters (cm^{-1}) for the $X^1\Sigma^+$ and $B^1\Sigma^+$ States of $D^{35}\text{Cl}$	131
4.4	Merged Vibronic Energies (cm^{-1}) for the $B^1\Sigma^+$ and $X^1\Sigma^+$ States of $D^{35}\text{Cl}$	132
4.5	RKRV Turning Points for the $X^1\Sigma^+$ and $B^1\Sigma^+$ States of $D^{35}\text{Cl}$	134
5.1	Fourier Transform Line Positions of $\text{DF}(X^1\Sigma^+)$	153
5.2	Dunham Coefficients (cm^{-1}) for $\text{DF}(X^1\Sigma^+)$	153
5.3	Least-Squares Fits for Individual Bands of the $B \rightarrow X$ Band System of DF	165
5.4	Merged Parameters (cm^{-1}) for the $X^1\Sigma^+$ and $B^1\Sigma^+$ States of DF	167
5.5	Merged Vibronic Terms (cm^{-1}) for the $B^1\Sigma^+$ and $X^1\Sigma^+$ States of DF	168
5.6	Equilibrium Vibrational-Rotational Parameters for the $B^1\Sigma^+$ State of DF	169
5.7	RKRV Turning Points for the $X^1\Sigma^+$ and $B^1\Sigma^+$ States of DF	171
5.8	A Test of the LCD Method: Energies and Widths of Model Potential Quasibound Levels	174

TABLE NUMBER	TITLE	PAGE
5.9	Rotational Predissociation in the $X^1\Sigma^+$ State of DF: Determination of the Dissociation Energy	178
6.1	Summary of Vibrational-Rotational Data for HCl/DCI	189
6.2	Trial Potential Functions for the $X^1\Sigma^+$ and $B^1\Sigma^+$ States of HCl	196
6.3	Final Assignments for HCl($B - X$)	199
6.4	Final Assignments for DCI($B - X$)	201
6.5	Fitted Coefficients (p_k) for Correction Functions	204
6.6	Internuclear Potentials for the $X^1\Sigma^+$ States of $H^{35}Cl$ and $H^{37}Cl$	207
6.7	Internuclear Potentials for the $X^1\Sigma^+$ States of $D^{35}Cl$ and $D^{37}Cl$	208
6.8	Internuclear Potentials for the $B^1\Sigma^+$ States of $H^{35}Cl$ and $H^{37}Cl$	209
6.9	Internuclear Potentials for the $B^1\Sigma^+$ States of $D^{35}Cl$ and $D^{37}Cl$	210
6.10	Radial Variation of Matrix Element $\langle A^1\Pi L_x X^1\Sigma^+ \rangle$ for HCl	221
6.11	Isotopic Dependence of Equilibrium Internuclear Separations for HCl	224
6.12	Atomic and Reduced Molecular Masses	226
6.13	Quantum Mechanical Molecular Constants for $HCl(X^1\Sigma^+)$	231

TABLE NUMBER	TITLE	PAGE
6.14	Quantum Mechanical Molecular Constants for $\text{HCl}(B^1\Sigma^+)$	234
6.15	Quantum Mechanical Molecular Constants for $\text{DCI}(X^1\Sigma^+)$	235
6.16	Quantum Mechanical Molecular Constants for $\text{DCI}(B^1\Sigma^+)$	239
6.17	Rotational and Centrifugal Distortion Constants for HCl : Calculation of Far-Infrared Transitions for H^{35}Cl and H^{37}Cl	240
6.18	Calculated Eigenvalues and Rotational Constants for TCI : Comparison of Observed and Calculated Microwave Transitions	244
7.1	Summary of Experimental Data Base for HF/DF	263
7.2	Internuclear Potentials for the $X^1\Sigma^+$ States of HF and DF	280
7.3	Internuclear Potentials for the $B^1\Sigma^+$ States of HF and DF	281
7.4	Coefficients d_{Xi} for Nuclear-Mass-Independent Part of $g(R)$	283
7.5	Rotational Predissociation in $X^1\Sigma^+$: Calculated Energies and Widths of Selected Quasibound Levels for HF and DF	288

TABLE NUMBER	TITLE	PAGE
7.6	The Dissociation Energies (cm^{-1}) of Ground State HF and DF: A Comparison of Several Methods of Determination	297
7.7	Quantum Mechanical Molecular Constants for HF/DF($X^1\Sigma^+$)	300
7.8	Quantum Mechanical Molecular Constants for HF/DF($B^1\Sigma^+$)	304
7.9	Calculation of HF($X^1\Sigma^+$) Pure Rotational Transitions from Quantum Mechanical Rotational and Centrifugal Distortion Constants	306
7.10	Tentative Rotational Assignments (cm^{-1}) for the 6-27 Band of the $B - X$ System of Deuterium Fluoride	313
7.11	Merged Molecular Constants (cm^{-1}) for TF($X^1\Sigma^+$)	315
7.12	Quantum Mechanical Molecular Constants (cm^{-1}) for TF($X^1\Sigma^+$)	317
7.13	Isotopic Dependence of Equilibrium Internuclear Separations	318
7.14	Dipole Moment Coefficients for the $X^1\Sigma^+$ States of HF and DF	322
7.15	Rotationless Matrix Elements and Einstein Coefficients for HF($X^1\Sigma^+$)	323
7.16	Rotationless Matrix Elements and Einstein Coefficients for DF($X^1\Sigma^+$)	326

TABLE NUMBER	TITLE	PAGE
7.17	Electric Dipole Moment (D) for the Ground States of HF and DF	332
7.18	A Calculation of the Rotational Dependence of Franck-Condon Factors for the $B^1\Sigma^+ - X^1\Sigma^+$ Band System of DF	333
8.1	Test of First-Order Perturbation Theory	346

LIST OF FIGURES

FIGURE NUMBER	TITLE	PAGE
2.1	Illustration of the RKR _V potential inversion procedure	10
2.2	Graphical representation of a quasibound level	54
3.1	Arrangement of electronic states for the model calculations	84
3.2	The correction function $\Delta U_X(R)$ for the model calculations	101
3.3	The isotopically invariant component of the ground state $g(R)$ function for the model calculations	104
3.4	The function $\Delta U_B(R)$ for the model calculations	106
3.5	The function $\Delta U_X^H(R)$ for the model calculations	108
4.1	Arrangement of low-lying electronic states of HCl(DCl)	113
4.2	Schematic of the 10.7-m concave grating vacuum spectrograph	116
4.3	A small portion of the $B^1\Sigma^+ \rightarrow X^1\Sigma^+$ emission band system of DCl	122
4.4	Determination of the absolute vibrational numbering for the $B^1\Sigma^+$ state of DCl	136
4.5	Perturbations in the $B^1\Sigma^+$ state of HCl	138
4.6	Perturbations in the $B^1\Sigma^+$ state of DCl	140

FIGURE NUMBER	TITLE	PAGE
5.1	Interferometer unit of a Fourier transform spectrometer	145
5.2	A small portion of the far-infrared spectrum of DF	149
5.3	A plot of calibrant error versus frequency	151
5.4	Low-lying electronic states of hydrogen fluoride	156
5.5	A small portion of the $\text{DF}(B^1\Sigma^+ \rightarrow X^1\Sigma^+)$ emission spectrum	160
5.6	Limiting curve of dissociation (LCD) plots of model data	175
5.7	Limiting curve of dissociation (LCD) plot for $\text{DF}(X^1\Sigma^+)$	179
6.1	The estimated function $U_X^{\text{H}}(R)$ for $\text{HCl/DCI}(X^1\Sigma^+)$	212
6.2	The estimated function $U_X^{\text{Cl}}(R)$ for $\text{HCl/DCI}(X^1\Sigma^+)$	214
6.3	The estimated function $U_B^{\text{H}}(R)$ for $\text{HCl/DCI}(B^1\Sigma^+)$	216
6.4	The estimated function $\tilde{R}_X^{\text{H}}(R)$ for $\text{HCl/DCI}(X^1\Sigma^+)$	218
6.5	Mass-scaled higher-order JWKB corrections for the $X^1\Sigma^+$ state of HCl/DCI	247
7.1	Quantum mechanical inconsistency of an RKR potential for the $X^1\Sigma^+$ state of HF	257
7.2	The experimentally determined function $U_X^{\text{H}}(R)$ for $\text{HF/DF}(X^1\Sigma^+)$	273

FIGURE NUMBER	TITLE	PAGE
7.3	The experimentally determined function $U_B^H(R)$ for HF/DF($B^1\Sigma^+$)	276
7.4	The function $\tilde{R}_X^H(R)$ for the $X^1\Sigma^+$ state of HF/DF	279
7.5	Interaction between the $A^1\Pi$ and $X^1\Sigma^+$ states of HF(DF)	285
7.6	Locus of barrier maximum (LBM) plots for HF/DF($X^1\Sigma^+$)	293
7.7	Estimation of v_D for HF($X^1\Sigma^+$)	308
7.8	Estimation of v_D for DF($X^1\Sigma^+$)	310

ABSTRACT

Pure rotational transitions of $\text{DF}(X^1\Sigma^+)$ with $1 \leq J'' \leq 8$ in $v'' = 0$ were obtained precisely with a state-of-the-art Fourier transform spectrometer. These data were combined with selected spectroscopic data for $\text{DF}(v'' = 0-4)$ in a least-squares determination of Dunham coefficients.

The $B^1\Sigma^+ - X^1\Sigma^+$ ultraviolet emission band system of DF was recorded spectrographically in the region 205-275 nm. Computer assisted rotational analyses of 41 bands with $0 \leq v' \leq 5$ and $16 \leq v'' \leq 26$ resulted in band origins and rotational parameters for both electronic states.

The $B^1\Sigma^+ - X^1\Sigma^+$ emission bands of DCl in the region 166-240 nm were photographed in higher orders of a 10.7-m concave grating vacuum spectrograph. Rotational analyses of 56 bands of D^{35}Cl with $v' = 0-7$ and $v'' = 11-23$ furnished molecular parameters for both states.

All reliable literature data for the $X^1\Sigma^+(v'' = 0-19)$ and $B^1\Sigma^+(v' = 0-10)$ states of HF and the $X^1\Sigma^+(v'' = 0-26)$ and $B^1\Sigma^+(v' = 0-7)$ states of DF were employed to determine isotopically self-consistent radial operators which take full account of Born-Oppenheimer breakdown. The dissociation energy of $\text{DF}(X^1\Sigma^+)$ was estimated as $\mathcal{D}_e = 49338(45) \text{ cm}^{-1}$ and the vibrational index at dissociation as $v_D = 29.2(5)$. The electronic isotope shift of $B^1\Sigma^+$ was estimated as $\Delta T_e = -2.48(7) \text{ cm}^{-1}$. Rotationally dependent Franck-Condon factors for the $B \rightarrow X$ transition and Einstein coefficients for spontaneous emission in $X^1\Sigma^+$ were calculated. Rotational assignments for the $B^1\Sigma^+ - X^1\Sigma^+$ emission band system of DF were extended significantly.

A similar analysis of data for H^{35}Cl , H^{37}Cl , D^{35}Cl , and D^{37}Cl was performed. A simultaneous four-isotopomer least-squares fit of 8497 line positions resulted in Born-Oppenheimer potentials for the $B^1\Sigma^+$ and $X^1\Sigma^+$ states and radial functions which describe adiabatic and nonadiabatic effects. The electronic isotope shift of $B^1\Sigma^+$ was obtained as $\Delta T_e = -11.11(3) \text{ cm}^{-1}$. Rotational assignments for the $B^1\Sigma^+ - X^1\Sigma^+$ emission band system of D^{35}Cl were extended and the first set of assignments for the $B \rightarrow X$ system of D^{37}Cl was obtained. Quantum mechanical rotational and centrifugal distortion constants were calculated for TCl. As was the case for HF/DF, the repulsive $A^1\Pi$ state of HCl/DCl was found to perturb significantly the energy level manifold of $X^1\Sigma^+$ in a heterogeneous fashion.

LIST OF ABBREVIATIONS AND SYMBOLS

α	Morse potential anharmonicity parameter
α_e	Vibration-rotation coupling constant
\AA	Ångstrom unit (1×10^{-10} m)
$A_{v'J'}^{v''J''}$	Einstein coefficient for spontaneous emission
$B(R)$	$B(R) = \hbar^2/2\mu R^2$. Instantaneous rotational constant
B_v	Rotational constant for vibrational level v
B_e	Equilibrium rotational constant
β	$\beta = (\hbar^2/2\mu)^{1/2} = (16.857\,631\,4/\mu)^{1/2}$, in spectroscopic units
$\hat{\beta}$	Least-squares parameter estimate
c	Speed of light ($2.997\,924\,58 \times 10^8$ m s ⁻¹)
c_i	Partial charge of atom i
C_6	Van der Waals dispersion coefficient
CI	Configuration Interaction
C_{ij}	Least-squares correlation coefficient
$C_{nn}(R)$	Adiabatic correction
$C_{nm}(R)$	Nonadiabatic mixing matrix element
CPU	Central Processing Unit
D	Equilibrium electric dipole moment
\mathcal{D}_e	Diatomic internuclear dissociation energy with reference to the potential minimum
D_v	Centrifugal distortion constant; coefficient of $[J(J + 1)]^2$
Δ_{kl}	Mass-scaling parameter

Δ_R	Nuclear Laplacian operator
e	Elementary electronic charge ($1.602\,177\,33(49) \times 10^{-19}$ C)
E	Energy
EGS	Extended Geometric Series
E_{vJ}	Rovibrational energy
ϵ	Spectral measurement precision
ϵ_0	Permittivity of vacuum ($8.854\,187\,816 \times 10^{-12}$ F m ⁻¹)
f	Degrees of freedom
f_v	RKRV improper integral
F_{vJ}	Rovibrational energy
$F(v, J)$	Rovibrational energy
g_J	Gyromagnetic ratio
g_v	RKRV improper integral
G_v	Vibrational energy
\mathcal{H}	Quantum mechanical Hamiltonian operator
\hbar	$\hbar = h/2\pi$, h is Planck's constant ($6.626\,075\,5(40) \times 10^{-34}$ J s)
H_v	Centrifugal distortion constant; coefficient of $[J(J + 1)]^3$
J	Rotational quantum number
JWKB	Jeffreys-Wentzel-Kramers-Brillouin
\mathcal{K}	$\mathcal{K} = J(J + 1)$
Λ	Electronic orbital angular momentum
L_v	Centrifugal distortion constant; coefficient of $[J(J + 1)]^4$

LBM	Locus of barrier maximum
LCD	Limiting curve of dissociation
M	Nuclear mass
m_e	Electron rest mass ($9.109\,389\,7(54) \times 10^{-31}$ kg)
M_p	Proton rest mass ($1.672\,623\,1(10) \times 10^{-27}$ kg)
μ	Diatomic reduced mass
$\mu(R)$	Electric dipole moment function
M_v	Centrifugal distortion constant; coefficient of $[J(J + 1)]^5$
MVLU	Minimum-variance linear unbiased
n	Principal quantum number
N_A	Avogadro constant ($6.022\,136\,7(36) \times 10^{23}$ mol ⁻¹)
ν_i	Spectral transition frequency
ν_0	Vibronic band origin
ω_e	Vibrational constant; coefficient of $(v + \frac{1}{2})$
$\omega_e x_e$	Vibrational constant; coefficient of $(v + \frac{1}{2})^2$
P	Momentum operator
PMO	Perturbed Morse Oscillator
$\Psi(q, Q)$	Schrödinger total wavefunction
$\psi(R)$	Schrödinger radial wavefunction
$\psi(r, R)$	Schrödinger total wavefunction
$\Psi^{\text{JWKB}}(R)$	JWKB radial wavefunction
$\psi_w(R)$	Schrödinger rovibrational (radial) wavefunction

r	Instantaneous electronic coordinate
R	Instantaneous internuclear coordinate
R_e	Equilibrium internuclear separation
RKRV	Rydberg-Klein-Rees-Vanderslice
$\hat{\sigma}$	Least-squares standard deviation
T_e	Electronic term value
T_v	Vibronic energy
U_{kl}	Extended-Dunham energy expansion isotopically invariant coefficient
$U(R)$	Potential energy function
v	Vibrational quantum number
v_D	Vibrational index at dissociation
VUV	Vacuum ultraviolet
W	Energy
$\langle X \rangle$	Quantum mechanical expectation value
ξ	Reduced internuclear coordinate
Y_{kl}	Dunham energy expansion coefficient
Z	Nuclear charge

ACKNOWLEDGEMENTS

I would like to thank Prof. John Coxon for his competent and enthusiastic supervision of this research. I thank him for his support, understanding, for his encouragement and provision of opportunity in becoming acquainted with various aspects of experimental molecular spectroscopy, as well as for his ample availability despite unusual family commitments. I also thank him for his efforts and interest in enhancing the appearance of this thesis. The friendship I received from the Coxon household is deeply appreciated.

I should like to thank Dr. K. P. Huber for his interest in and expert direction of the spectrographic experiments as well as for his gracious hospitality during my stay at the Herzberg Institute of Astrophysics, National Research Council of Canada, Ottawa. Mr. F. Alberti is thanked especially for his advice, technical assistance and persistence in obtaining the photographic plates. Mr. M. Barnett is thanked for his assistance in transferring data to magnetic tape.

Dr. J. W. C. Johns of the Herzberg Institute of Astrophysics is thanked for his direction of the interferometric experiments, for providing measurements of the fundamental band of DF, and for several discussions. He is also thanked for his hospitality during my stay in Ottawa. Mr. W. Neil is thanked for his assistance with the Fourier transform experiments.

Dr. R. J. Le Roy is thanked for several discussions during the course of this work.

I thank my family for their love, support and encouragement during my entire university career. Dr. William Hare, his wife Niki and their children are thanked for their valued friendship, advice and encouragement during my years in Halifax.

I thank my friends and all the members of the Chemistry Department. I would like to thank especially the gang of the "Hellenic Sound" for making the past few months such a pleasure. Past and present members of this research group are thanked for their friendship and comraderie.

Dalhousie University and the W. C. Sumner Foundation are thanked for financial support in the form of graduate fellowships.

Finally, I thank the Lord for giving me the strength and patience to complete this work.

CHAPTER 1

GENERAL INTRODUCTION

In the earlier part of this century, Erwin Schrödinger published a series of articles (1) on the wave mechanical description of matter at the atomic level. Schrödinger's theory had far-reaching implications and influenced the development of most areas of physical science. In the field of molecular spectroscopy, the new wave mechanics was swiftly adopted as it provided much improved interpretations of simple spectra over the old quantum theory results.

All the stationary state energies, E , and wavefunctions, Ψ , of a quantum mechanical system are obtained as solutions of the time-independent Schrödinger equation,

$$\mathcal{H}(q, Q) \Psi(q, Q) = E \Psi(q, Q). \quad (1.1)$$

Despite the deceptively simple appearance of this eigenvalue equation, an exact solution is usually far from straightforward. The main problem is that the eigenfunctions correlate the electronic coordinates, q , with those of the nuclei, Q .

In 1927 Born and Oppenheimer (2) achieved a significant simplification of the diatomic wave equation. In the absence of external magnetic and electric fields, the total wavefunction was factored into electronic and nuclear parts and any interaction between the two motions thus neglected. An important result emerging from the Born-Oppenheimer treatment was the concept of a potential energy function, describing the behaviour of a chemical bond as

a function of internuclear separation.

Much effort has been directed towards the development of procedures for the determination of potential functions from basic principles and from the results of spectroscopic experiments. *Ab initio* methods varying in degree of sophistication are applied routinely to the problem. It is found, however, that such methodology provides results which approach spectroscopic accuracy only for relatively simple one- or two-electron diatomics. For many-electron systems, the average-field approximations of quantum methods give results which are significantly inconsistent with experimental observation. Fortunately, more accurate methods are available whereby spectroscopically derived "molecular constants" can be inverted to the internuclear potential.

A direct inversion method which is widely employed to generate diatomic potentials is the semiclassical RKR procedure. This, however, is an approximate method only; in recent years, improvement in the precision of spectral measurements has necessitated a review of this inversion scheme. This has stimulated the development of improved numerical procedures whose end products are internuclear potential functions that are consistent with experimental results, within the precision of the measurements.

One such method is employed in the present work to bring about a better understanding of the electronic structures and spectra of the diatomic hydrogen halides HF and HCl. In order to achieve this, it has been necessary to go beyond the Born-Oppenheimer approximation. Spectroscopic information has been employed to determine effective radial (nuclear) Hamiltonian operators which consider adequately the coupling of electronic and nuclear motions. Despite the widely held belief that these simple diatomic systems have long been well understood, interesting results presented in this thesis

demonstrate clearly that previous characterizations in terms of molecular constants precluded a comprehensive understanding of the molecular states and their interactions.

In order to investigate the isotopic dependence of Born-Oppenheimer breakdown in HF and HCl it has been necessary to incorporate spectral data of several isotopomers. Due to the inferior quality or complete absence of some data, comprehensive spectrographic investigations of the ultraviolet $B^1\Sigma^+ \rightarrow X^1\Sigma^+$ emission band systems of DF and DCl have been undertaken. Also, a few very precise far-infrared transitions in $v'' = 0$, and the fundamental band of DF in the infrared, have been studied by interferometric techniques.

A review of some relevant theory is presented in the second chapter. The semiclassical RKR equations are developed and their theoretical basis, the JWKB quantization condition, is outlined. The Born-Oppenheimer principle is explained and its shortcomings are clearly indicated. It is shown how electronic-nuclear coupling can be described by employing effective Hamiltonian operators that include implicitly the effects of excited electronic states on nuclear motion. Chapter 2 also deals with computational procedures important to this work. The statistical fitting method of least-squares, which has been of crucial importance to the completion of the present work, is described. Of equal importance was the numerical solution of the radial wave equation for a general potential function, and this is therefore also described.

The third chapter reviews previous attempts to improve semiclassical RKR potentials. The numerical correction method applied here to HF and HCl is considered in particular detail; model calculations are carried out and the effectiveness and limitations of the procedure are assessed.

The fourth and fifth chapters describe the acquisition of new experimental information on DF and DCl. Chapter 4 reports a conventional rotational analysis for the $B^1\Sigma^+ \rightarrow X^1\Sigma^+$ electronic band system of DCl in the ultraviolet and vacuum ultraviolet. Chapter 5 is divided into two parts; the first describes a Fourier transform study of DF($v'' = 0, 1$), and in the second part a rotational analysis of the ultraviolet $B^1\Sigma^+ \rightarrow X^1\Sigma^+$ emission band system is reported.

In the sixth and seventh chapters a numerical method is employed to determine radial Hamiltonian operators from spectroscopic data. Chapter 6 describes the application of the procedure to a spectroscopic data base of the isotopomers H^{35}Cl , H^{37}Cl , D^{35}Cl , and D^{37}Cl . In Chapter 7 a similar analysis is made of the spectroscopic information available for the isotopomers HF and DF. An important result of both analyses concerns the detection of rotationally dependent energy shifts in the rovibrational levels of the ground $X^1\Sigma^+$ states arising from a strong second-order perturbation by the low-lying repulsive $A^1\Pi$ state.

In the concluding chapter, the numerical method employed to derive radial operators for HF and HCl is discussed briefly. The procedure is reviewed objectively and suggestions for improved methods are provided.

CHAPTER 2

THEORETICAL BACKGROUND AND NUMERICAL TECHNIQUES

2.1 *The JWKB Approach*

Within the Schrödinger equation framework, it is possible to obtain exact analytic solutions for a relatively few, often physically uninteresting quantum mechanical systems. In practice, it is necessary to apply approximate methods, as in the case for the solutions of the one-dimensional radial wave equation. Aside from the usual tools of quantum mechanics, which include perturbational and variational approaches, methods which investigate the asymptotic behaviour of the wave equation can be employed.

One such procedure, for which an enormous literature exists, was developed by Jeffreys (3), Wentzel (4), Kramers (5), and Brillouin (6). Although this is abbreviated as JWKB in the present work, it is not uncommon to find the alternatives WKB and WKBJ in the literature. The method is based on a transformation of the one dimensional Schrödinger equation,

$$\frac{d^2\psi(R)}{dR^2} + \frac{2\mu}{\hbar^2} [E - U(R)] \psi(R) = 0. \quad (2.1)$$

The total energy of the system is denoted by E , and its potential energy by $U(R)$; $\psi(R)$ is the associated wavefunction and μ the reduced molecular mass. Insertion of the JWKB wavefunction (7),

$$\Psi^{\text{JWKB}}(R) = e^{(i/\hbar)\Theta}, \quad (2.2)$$

where,

$$\Theta = \Theta_0 + \hbar \Theta_1 + \hbar^2 \Theta_2 + \dots, \quad (2.3)$$

can be followed by solution of the wave equation to any desired order. Substitution of the classical component Θ_0 into Eq. (2.2) yields the modified differential equation,

$$(i\hbar/2\mu)d^2\Theta_0/dR^2 - (2\mu)^{-1}(d\Theta_0/dR)^2 + [E - U(R)] = 0. \quad (2.4)$$

If quantal effects are considered small in comparison to the classical, the leftmost term can be omitted, whereupon Eq. (2.4) suffers a reduction in order. Straightforward integration yields the classical action integral,

$$\Theta_0 = \pm \int \sqrt{2\mu[E - U(R)]} dR. \quad (2.5)$$

Dunham (8) has shown that if the classical component of the JWKB wavefunction is employed only, and appropriate boundary conditions are imposed, the Bohr quantization condition,

$$\int_{R_1}^{R_2} \sqrt{2\mu[E - U(R)]} dR = 2\pi\hbar v, \quad (2.6)$$

emerges. This old quantum theory result can be improved further by including quantum effects partially through Θ_1 , leading to the Bohr-Sommerfeld half-integer quantization condition,

$$\int_{R_1}^{R_2} \sqrt{2\mu[E - U(R)]} dR = 2\pi\hbar (v + 1/2), \quad (2.7)$$

where R_1 and R_2 are the classical turning points of motion and the quantum number for the oscillation can assume the values $v = 0, 1, 2 \dots$, etc. This is also known as the semiclassical JWKB quantization condition.

If the first three terms of the expansion Eq. (2.3) are retained, a two-term JWKB quantization condition arises and can be written as,

$$\frac{1}{\pi\beta} \int_{R_1}^{R_2} [E - U(R)]^{1/2} dR - \frac{\beta}{96\pi} \oint_{\Gamma} U''(R) [E - U(R)]^{-3/2} dR = v + \frac{1}{2}, \quad (2.8)$$

where $\beta = (\hbar^2/2\mu)^{1/2}$ and the contour of integration Γ encloses the portion of the real line for which $U(R) < E$. Initial applications of this and higher order conditions were concerned with the calculation of the eigenvalues of empirical analytical potential functions (9, 10).

The JWKB method has been criticized by Killingbeck (11) for its inherent restriction to the classical region of motion; he pointed out that tunnelling corrections beyond the classical turning points should be considered. As an alternative to JWKB methodology, Killingbeck proposed a formulation based on Young's local momentum concept (12) and obtained preliminary numerical results for symmetric oscillators that surpassed the two-term JWKB quantization condition in accuracy. An alternate method stemming from work in the early 1930's, was proposed following the rediscovery of the Milne differential equation (13) by Korsch and Laurent (14). The new procedure was developed both for truly bound (14), as well as quasibound (15) energy levels.

2.2 The Dunham and Dunham-type Solutions

Dunham (16) was the first to recognize an important application of the JWKB method to the diatomic problem. Starting with the two-term quantization condition, Eq. (2.8), Dunham assumed a potential energy function of the form,

$$U(R) = a_0 \xi^2 (1 + a_1 \xi + a_2 \xi^2 + \dots) +$$

$$B_e J(J + 1)(1 - 2\xi + 3\xi^2 - \dots), \quad (2.9)$$

where $\xi = (R - R_e)/R_e$. R_e and B_e are the equilibrium internuclear separation and rotational constant, respectively, and the rotational quantum number is denoted by J . Dunham arrived at the energy level expression,

$$E_{vJ} = \sum_{kl} Y_{kl}(v + \frac{1}{2})^k [J(J + 1)]^l, \quad (2.10)$$

where the coefficients of the double summation, Y_{kl} , were defined in terms of the potential expansion coefficients, a_n . The usual application of Dunham's result involves fitting spectral line positions to a model constructed on the basis of Eq. (2.10). The determination of the Y_{kl} is followed by an estimation of the potential equilibrium derivative terms, a_n . By this simple inversion procedure, experimentally derived positions of stationary energy states are employed to deduce the molecular structure.

The main weakness of Dunham's approach rests with the choice of the reduced internuclear coordinate, ξ . The radius of convergence of this expansion is $2R_e$, making the model unreliable for extrapolation to larger R . Also, the potential function adopted by Dunham fails to describe properly the long-range diatomic interaction, the theoretical formulation of which is well understood (17). Following Dunham's pioneering effort, other authors (18-20) adopted different choices for ξ in an attempt to improve the convergence of the series. Despite some improvement, these models also remain deficient in their description of the long-range forces.

2.3 Rydberg-Klein-Rees-Vanderslice Potentials

If the rovibrational energy levels are known from experiment, it is possible to use another semiclassical method to determine the potential energy function. The procedure developed by Rydberg (21), and soon thereafter also discussed by Klein (22), exploited the half-integer quantization condition in generating the classical turning points of motion from experimental information, without assuming any particular analytic form for the potential. Rees (23) later provided a graphical working formulation of Klein's equations, but the large number of tedious manual calculations required made the method cumbersome; as a result it did not enjoy wide use before the advent of digital computers. Another factor contributing to the slow initial progress of this method is the fact that the precision of experimental data often did not warrant a more extensive description than was provided by closed term value expressions of empirical potential-like functions. The subsequent treatment of Vanderslice *et al.* (24) was successful at painting a clear picture of the physical significance of the procedure and demonstrated the efficacy of performing such calculations with digital computers.

The following derivation of the Rydberg-Klein-Rees-Vanderslice (RKR) expressions follows mainly that given in Ref. (24). As shown in Fig. 2.1, the area enclosed by the potential function $U(R)$ and energy level E is given by,

$$A(E, J) = \int_{R_1}^{R_2} [E - U_J(R)] dR, \quad (2.11)$$

where $U_J(R) = U_0(R) + \beta^2 J(J+1)/R^2$, the effective potential including the kinetic energy of rotation. The partial derivatives

Figure 2.1

Illustration of the RKR V potential inversion procedure. R_1 and R_2 are the inner and outer classical turning points, respectively. The shaded area bound by energy E and the potential well is denoted by A .

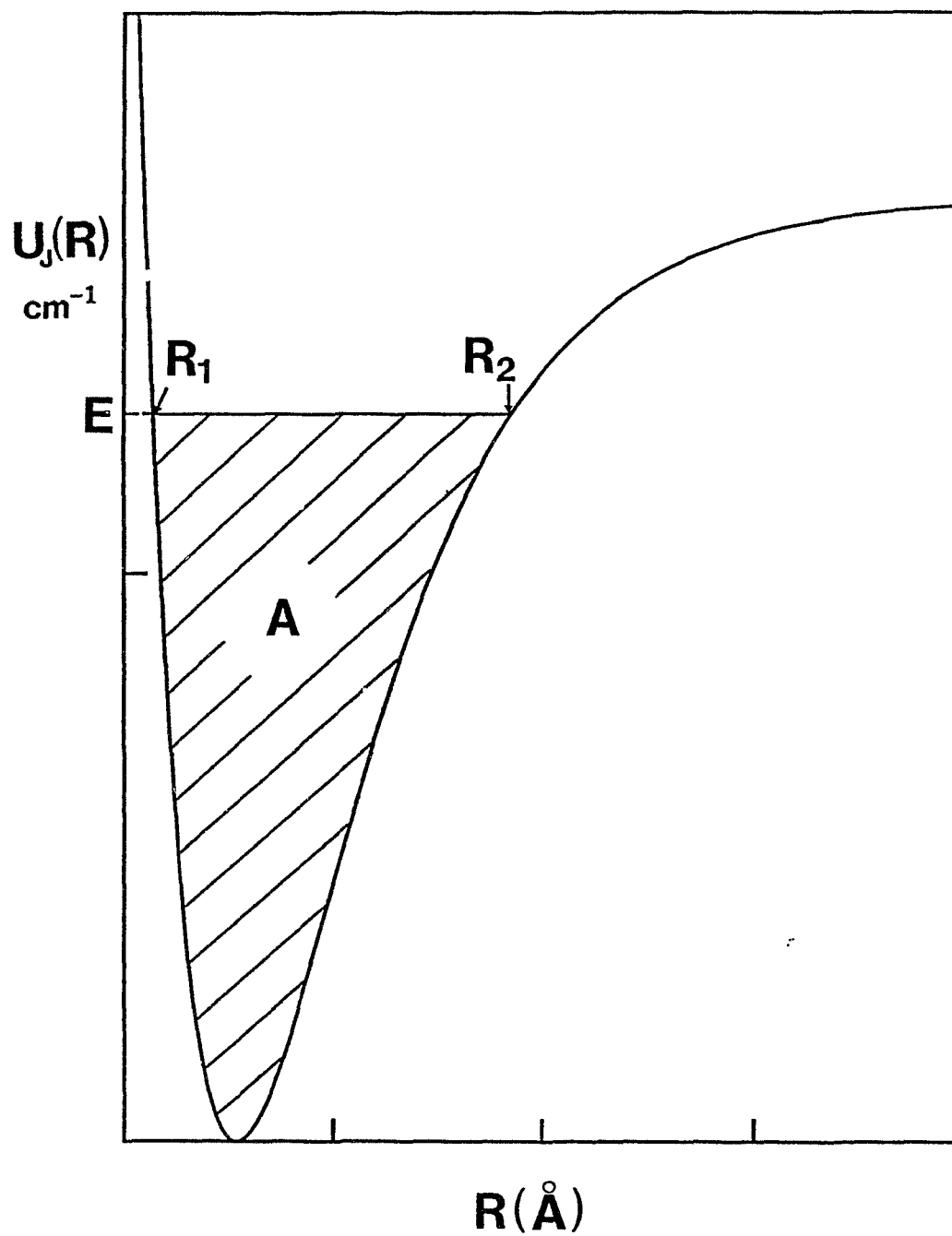


Figure 2.1

$$[\partial A(E, J)/\partial E]_J = \int_{R_1}^{R_2} dR = R_2 - R_1, \quad (2.12)$$

$$[\partial A(E, J)/\partial J(J + 1)]_E = -\beta^2 \int_{R_1}^{R_2} R^{-2} dR = -\beta^2 (R_2^{-1} - R_1^{-1}), \quad (2.13)$$

allow for a unique determination of the two classical turning points. It is now necessary to relate the experimentally derived energy terms to the area integral. This is accomplished through the Eulerian integral of the type,

$$E - U_J(R) = \frac{2}{\pi} \int_{U_0}^E \left(\frac{E - E'}{E' - U_J(R)} \right)^{1/2} dE', \quad (2.14)$$

where E' are the (quantum number) parametrized energy terms and U_0 is the minimum of energy. It is then possible to express the area integral as,

$$A(E, J) = \frac{2}{\pi} \int_U^E \sqrt{E - E'} dE' \int_{R_1}^{R_2} \frac{dR}{\sqrt{E' - U_J(R)}}. \quad (2.15)$$

The next step in the derivation involves the manipulation of the first-order JWKB quantization condition to bring it in a form compatible with the rightmost integral above. The semiclassical eigenvalue condition,

$$v' + \frac{1}{2} = (\pi\beta)^{-1} \int_{R_1}^{R_2} \sqrt{E' - U_J(R)} dR, \quad (2.16)$$

can be differentiated once to give,

$$d(v' + \frac{1}{2})/dE' = (2\pi\beta)^{-1} \int_{R_1}^{R_2} \frac{dR}{\sqrt{E' - U_J(R)}}, \quad (2.17)$$

allowing the area integral to be cast as,

$$A(E, J) = 4\beta \int_U^E \sqrt{E - E'} dE' d(v' + 1/2)/dE' =$$

$$4\beta \int_{v_e + 1/2}^{v + 1/2} \sqrt{E - E'} d(v' + 1/2). \quad (2.18)$$

Since $d(v' + 1/2) = dv'$, we can write,

$$A(E, J) = 4\beta \int_{v_e}^v \sqrt{E - E'} dv', \quad (2.19)$$

which is essentially the usual $S(E, J)$ "auxiliary" function from which most derivations of the RKR equations begin. Differentiating partially with respect to E and $J(J + 1)$, and setting the appropriate terms to Eqs. (2.12), and (2.13) respectively, one obtains the relevant expressions,

$$2f = R_2 - R_1 = 2\beta \int_{v_e}^v \frac{dv'}{\sqrt{E - E'}}, \quad (2.20)$$

and

$$2g = R_1^{-1} - R_2^{-1} = 2\beta^{-1} \int_{v_e}^v \frac{\partial E' / \partial J(J+1)}{\sqrt{E - E'}} dv' = 2\beta^{-1} \int_{v_e}^v \frac{B_{v'}}{\sqrt{E - E'}} dv', \quad (2.21)$$

where $B_{v'}$ is a rotational constant. The two functions f and g make it possible to extract the classical turning points from,

$$R_{1,2}(v) = [f_v/g_v + f_v^2]^{1/2} \pm f_v, \quad (2.22)$$

where the $+$ and $-$ signs refer to the inner (R_1) and outer (R_2) turning points, respectively, for vibrational level v .

2.4 The Concept of Molecular Structure: The Born-Oppenheimer Approximation

The Born-Oppenheimer approximation (2) is the cornerstone of modern molecular physics. Proposed in 1927, it facilitated an exact solution of the wave equation for one-electron diatomic systems such as the H_2^+ molecule. Although the general three-body problem is theoretically impossible to solve exactly, both for classical and quantum mechanical systems, casting the particles into a confocal elliptical coordinate system allows for a separation of variables and hence facilitates a restricted type of solution.

In their original treatment, Born and Oppenheimer (2) applied perturbation theory to achieve a separation between the motions of the electrons and those of the nuclear vibrations. A working formalism for the separate quantization of the two motions was thus set up. Their argument was based on the relatively large differential between values for the mass of the electron and of typical nuclei. Since the nucleus-electron mass ratio is large, it is expected that electrons will average their motion adequately during the course of a single nuclear vibration, so that, to a good approximation, the nuclei can be regarded as stationary. This allows for the computation of electronic eigenvalues with a parametric dependence on the internuclear coordinate.

The precise nature of the ansatz can be best elucidated by the conventional mathematical formulation (25). In solving the total Schrödinger eigenvalue equation,

$$\mathcal{H}_{\text{total}}(r, R) \Psi_{\text{total}}(r, R) = E \Psi_{\text{total}}(r, R), \quad (2.23)$$

the total molecular Hamiltonian operator for a diatomic system AB can be expressed as,

$$\mathcal{H}_{\text{total}}(r, R) = \left[\frac{P_A^2}{2M_A} + \frac{P_B^2}{2M_B} \right] + \left[\sum_i \frac{P_i^2}{2m_e} + \frac{e^2}{4\pi\epsilon_0} \left\{ \frac{Z_A Z_B}{R} - \sum_i \frac{Z_A}{r_{A_i}} - \sum_i \frac{Z_B}{r_{B_i}} + \frac{1}{2} \sum_i \sum_{i \neq j} \frac{1}{r_{ij}} \right\} \right], \quad (2.24)$$

where r and R refer to electronic and nuclear coordinates, respectively. Specifically, r_{A_i} and r_{B_i} are the instantaneous distances of electron i and nuclei A and B, and the r_{ij} are instantaneous interelectronic separations. The internuclear separation is given by R . The nuclear charges are $Z_A e$ and $Z_B e$, where e is the elementary electronic charge and the Z_k give the number of protons. The nuclear and electronic masses are given by M_k and m_e , respectively, and the symbol P represents a momentum operator; ϵ_0 is the permittivity of free space. The total energy operator can be written as,

$$\mathcal{H}_{\text{total}}(R) = \mathcal{H}_{\text{nuc}}(R) + \mathcal{H}_{\text{elec}}(r, R), \quad (2.25)$$

where $\mathcal{H}_{\text{nuc}}(R)$ and $\mathcal{H}_{\text{elec}}(r, R)$ correspond to the terms in square brackets in Eq. (2.24).

The first part of the approximation involves the separation of the total eigenfunction into electronic and nuclear components,

$$\Psi_{\text{total}}(r, R) = \psi_{\text{elec}}(r, R) \psi_{\text{nuc}}(R), \quad (2.26)$$

where $\psi_{\text{elec}}(r, R)$ satisfies the eigenvalue equation,

$$\mathcal{H}_{\text{elec}}(r, R) \psi_{\text{elec}}(r, R) = E_{\text{elec}}(R) \psi_{\text{elec}}(r, R). \quad (2.27)$$

Since the nuclei are considered as fixed, the $Z_A Z_B / R$ term contributes to $E_{\text{elec}}(R)$ parametrically and need not be considered explicitly in the solution

of Eq. (2.27). This results in an effective potential energy, $U(R)$, for nuclear motion. Direct substitution of Eqs. (2.25, 2.26) in the total Schrödinger equation, Eq. (2.23), then yields,

$$[\mathcal{H}_{\text{nuc}}(R) + \mathcal{H}_{\text{elec}}(r, R)]\psi_{\text{nuc}}(R)\psi_{\text{elec}}(r, R) = E_{\text{total}}\psi_{\text{nuc}}(R)\psi_{\text{elec}}(r, R). \quad (2.28)$$

Multiplying through and discarding terms containing $\mathcal{H}_{\text{elec}}(r, R)\psi_{\text{nuc}}(r, R)$, one obtains,

$$\begin{aligned} \psi_{\text{elec}}(r, R)\mathcal{H}_{\text{nuc}}(R)\psi_{\text{nuc}}(R) + \psi_{\text{nuc}}(R)\mathcal{H}_{\text{nuc}}(R)\psi_{\text{elec}}(r, R) + \\ \psi_{\text{nuc}}(R)\mathcal{H}_{\text{elec}}(r, R)\psi_{\text{elec}}(r, R) = E_{\text{total}}\psi_{\text{nuc}}(R)\psi_{\text{elec}}(r, R). \end{aligned} \quad (2.29)$$

Substituting the right-hand side of Eq. (2.27) in Eq. (2.29) and rearranging yields,

$$\begin{aligned} \psi_{\text{elec}}(r, R)\mathcal{H}_{\text{nuc}}(R)\psi_{\text{nuc}}(R) + \psi_{\text{nuc}}(R)\mathcal{H}_{\text{nuc}}(R)\psi_{\text{elec}}(r, R) = \\ \psi_{\text{elec}}(r, R)[E_{\text{total}} - U(R)]\psi_{\text{nuc}}(R). \end{aligned} \quad (2.30)$$

The omission of the underlined term constitutes the second part of the approximation; in this fashion all interaction between nuclear and electronic motions is eliminated. A subsequent division of Eq. (2.30) by $\psi_{\text{elec}}(r, R)$ followed by rearrangement gives the quantization expression,

$$\mathcal{H}_{\text{nuc}}(R)\psi_{\text{nuc}}(R) = [E_{\text{total}} - U(R)]\psi_{\text{nuc}}(R), \quad (2.31)$$

for nuclear motion. The entire procedure can be regarded as a simple separation of variables rationalized by the observation that the electronic Laplacian is orders of magnitude greater than its nuclear counterpart.

While the treatment given above, obviously inspired by the typical smallness of the m_e/M_k ratio, seemingly achieves the desired separation, it is

thought by some that the argument was too hastily accepted. Woolley and Sutcliffe (26) contend that the Born-Oppenheimer treatment was devised in an attempt to rationalize an already existing school of thought consisting of a preconceived (classical) notion of molecular structure in terms of a well-defined potential energy surface, distinct bonds and angles. Although these authors fail to suggest practical alternatives, they bring to light some of the dangers associated with the blind use of the Born-Oppenheimer approximation. At a deeper level of the solution of the wave equation, it can be shown that the concept of a potential energy function is not preserved.

In an independent examination into the causes leading to the apparent separation between nuclear and electronic motions, Essén (27) also expresses dissatisfaction with the original treatment of Born and Oppenheimer (2). Essén's view of a molecule, which is also shared by Bader (28), is supported by application of the quantum mechanical virial theorem to the description of Coulombic interactions. According to this view, it is not the smallness of the m_e/M_k ratio that leads to the observed separation, but rather the derived form for the Coulombic interaction between collective (vibrational) and individual (electronic) internal molecular motions. Bader (28) views a molecule as a network of essentially neutral subsystems, which can be likened to atoms, that interact weakly, in analogy with the conventional notion of bonds, arranged spatially in some orientation, forming the concept of a molecular structure. Bader then distinguishes molecular structure from molecular *geometry*, stating that his definition of molecular structure survives beyond the clamped-nuclei approximation, whereas the concept of molecular geometry does not. In accord with this theoretical setup, the solution for the total system then simply requires that a separate virial

theorem be solved for each subsystem.

Essén (27) did not provide a working formalism in his analysis. This was achieved, to a limited degree, in recent work by Monkhorst (29). Employing the coupled-cluster approach to treat the electrons and nuclei on the same quantum mechanical footing, Monkhorst gave a lucid description of how the computational effort should proceed in obtaining positions for both stationary and time-dependent states. The coupled-cluster approach has since been implemented computationally and is in routine use for *ab initio* calculations.

Despite the philosophical objections of some, a potential energy function for vibrational motion remains as indispensable a tool to the molecular spectroscopist as the electronic wavefunction is to the quantum chemist. The whole of infrared spectroscopy, with particular emphasis on radiative transition probabilities, appears to be impossible without it. It should be realized at the outset however, that a potential function far outside the Born-Oppenheimer approximation should be regarded as a useful mathematical tool only. Often, at higher energy, a network of crossings of zeroth-order curves occurs; in this case a potential energy function is devoid of any physical meaning.

2.5 *The Adiabatic Separation of Electronic States*

The Born-Oppenheimer approximation neglects all avenues by which nuclear vibrations can affect the electronic motions. A preliminary intuitive examination of this limitation suggests two situations which can disturb the efficient averaging of the electronic mass/charge distribution about a dinuclear framework. The most obvious arises in the case of increasingly energetic vibrations. Here, the separation begins to break down as the

electrons cannot average their motions as efficiently in the course of the now significantly more rapid nuclear oscillations. This renders the electronic potential $E_{\text{elec}}(R)$ inappropriate for governing the nuclear vibrations.

The Born-Oppenheimer description of an electronic state is short-sighted in one more respect. It assumes that no interactions between electronic states occur. This can be shown to be false, most effectively by a mathematical treatment. In a comprehensive review article, Kołos (25) develops rigorously the different levels of approximation at which the radial wave equation can be solved. The exact radial Schrödinger equation, which considers the coupling of nuclear and electronic motions within a single electronic state, as well as the coupling between rovibronic levels of different electronic states, can be written as,

$$\begin{aligned} \left[-(2\mu)^{-1}\Delta_R + U_n^{\text{BO}}(R) + C_{nn}(R) - E \right] \psi_n^{\text{nuc}}(R) = \\ - \sum_{m \neq n} C_{nm}(R) \psi_m^{\text{nuc}}(R), \end{aligned} \quad (2.32)$$

where Δ_R is the nuclear Laplacian operator and $U_n^{\text{BO}}(R)$ the Born-Oppenheimer potential for electronic state n . The term $C_{nn}(R)$ is known as the adiabatic correction and is given by,

$$C_{nn}(R) = \int \psi_n^{\text{elec}}(r, R) \mathcal{H}'(R) \psi_n^{\text{elec}}(r, R) dr, \quad (2.33)$$

where the perturbing Hamiltonian is given by,

$$\mathcal{H}'(R) = (8\mu)^{-1} \left\{ \sum_{i=1}^n \nabla_{r_i} \right\}^2 - (2\mu_a)^{-1} \nabla_R \sum_{i=1}^n \nabla_{r_i}, \quad (2.34)$$

where $\nabla_q = \partial^2/\partial q^2$ and the reduced masses are defined as,

$$\mu^{-1} = M_A^{-1} + M_B^{-1}, \quad (2.35)$$

$$\mu_a^{-1} = -M_A^{-1} + M_B^{-1}. \quad (2.36)$$

The cross-terms $\nabla_R \nabla_r$ in Eq. (2.34) represent the mass-polarization effect, which induces the electrons to follow the motion of the nuclei. This effect is, for example, responsible for the finite dipole moment in the homonuclear diatomic HD (25). The terms $C_{nm}(R)$ in Eq. (2.32) are off-diagonal matrix elements coupling electronic state n to excited states m . Their explicit form is at this point unimportant. Within the realms of the *adiabatic approximation* considered here, these terms are neglected. In addition, the effective potential for nuclear motion now contains the radial term $C_{nn}(R)$ and is collectively referred to as the adiabatic potential. Within this formulation, the radial wave equation is still of a second-order *homogeneous* type and the concept of a unique potential energy function survives.

The adiabatic approximation can be expected to provide a good description for a well-isolated ground electronic state. Since the matrix elements $C_{nm}(R)$, which describe the effects of excited rovibronic states on the electronic motions of electronic state n , are inversely proportional to the nuclear masses, the adiabatic approximation should be less accurate for light molecules. The adiabatic solutions of the simple molecular systems H_2 and H_2^+ are in fact shown (25, 30) to be unsuccessful at predicting the positions of the vibrational levels of the rotationless ground states which are known quite accurately from spectroscopic observation.

When interactions between electronic states are of significant magnitude, the concept of a potential function is not preserved. Neglecting electronic state coupling for the moment, it is possible to improve further on the

adiabatic potential. There are two more effects which have not yet been considered. First, due to a relativistic Lorentzian transformation of the electronic masses, the simplistic “rest-mass” wave description of Schrödinger fails to describe the effects arising from special relativity. These are larger for the faster moving inner core electrons of heavy atoms and can be shown to follow a Z/n dependence, where n is the principle quantum number and Z is the nuclear charge number. For the relatively light systems for which traditional *ab initio* methods are most successful, the relativistic effects are small. In general, to ensure a theoretically proper inclusion of these in the electronic and nuclear energies, one must solve the relativistic wave equation of Dirac (31). Alternatively, if the terms omitted in Schrödinger’s treatment are small, they can be estimated by conventional perturbation theory.

Additional corrections are predicted from the branch of quantum electrodynamics that deals with self-interactions (32). Since the bound electrons in a molecular system cannot be separated from their charge radiation fields, they will undergo continuous absorption and re-emission of virtual photons, the pairs existing for times dictated by the energy-time uncertainty principle. The photons are not detectable experimentally (hence the label ‘virtual’). The electron can be viewed as being continuously “bathed” in these virtual particles leading to a self-energy associated with each electron, whether bound or free. The classical electrodynamical treatment of this phenomenon predicts unphysical infinite energy shifts. The infinities are removed by performing a mass-renormalization, whereby a mass contribution δm , due to quantum fluctuations of the electromagnetic field, is added to the mass m_0 of a hypothetical chargeless electron. m_0 is not an

observable, but the effective observed mass, $m_0 + \delta m$, or m_e , is now associated with finite shifts in the positions of the system's energy levels. At yet a deeper level, *relativistic* quantum electrodynamics describes an analogous renormalization of the electronic *charge*, introducing a further shift in energy, evidently much less important. These quantum-field effects are often referred to as radiative corrections. The experimental detection of these Lamb (32) shifts in atoms cannot be rationalized by either Schrödinger's or Dirac's wave mechanics.

The adiabatic function corrected for relativistic and radiative effects can then be regarded as the best possible function which preserves the concept of a potential energy curve.

2.6 Nonadiabatic Theory

The explicit consideration of terms connecting rovibronic levels of different electronic states leads to an exact solution of the radial wave equation, Eq. (2.32). These off-diagonal *nonadiabatic* terms give a full account of the electron-nuclear motion interactions. In this case, the problem involves the solution of an inhomogeneous differential equation, but in practice it is not approached in this fashion; an exception is found in the article by Hutson and Howard (33).

A nonadiabatic calculation begins with the best possible potential function, as defined above. The rovibrational energy eigenvalues of the electronic state in question are calculated by solving the homogeneous problem and second-order nonadiabatic corrections are applied to the *eigenvalues*. These contributions are normally small enough to warrant a nondegenerate perturbation treatment. A radial nonadiabatic correction function cannot be

added to the best possible potential, as can be seen from Eq. (2.32), if the problem is to be approached in a *truly* direct fashion; there is no simple way in which Eq. (2.32) can be manipulated to transform the terms on the right-hand side to the form of a unique effective radial correction to the adiabatic function. In fact, Bishop and Shih (30) have shown that a plausible solution would involve a separate potential for each vibrational level. In an *ab initio* sense, there cannot exist a unique potential function which describes nonadiabatic corrections simultaneously in all the bound levels.

Although the task of calculating nonadiabatic corrections reliably is enormous, requiring an accurate description of excited state electronic wavefunctions and potentials, these computations are usually not attempted for a more important reason. The bottleneck in an electronic calculation of this sort is the solution to the fixed-nuclei problem. At the Hartree-Fock level, variational methods suffer from the need to account for electron correlation. Although this effect can be included by employing configuration interaction (CI) wavefunctions, such calculations demand considerable CPU time and mass storage (34). In the zeroth-order solution of Eq. (2.27), the instantaneous repulsions between pairs of electrons are not accounted for properly, and an iteratively improved average-field approximation is applied. For "heavy" diatomic systems, the relativistic corrections are considerable; the magnitude of these effects is often large enough that convergence in a perturbational calculation cannot be ensured. The inapplicability of conventional quantum tools to this problem has prompted the development of a field of research that is still in its infancy.

For these reasons, exhaustive nonadiabatic calculations have only been carried out for one- and two-electron diatomic systems. It should be noted

that the agreement between experimental measurements and *ab initio* calculations for the ground state of HD^+ has reached the 0.001 cm^{-1} level (30). The agreement between *ab initio* estimates of the bond dissociation energies for the isotopomers of molecular hydrogen with the experimentally derived values is most remarkable (35, 36). This problem has been the subject of an interesting long-term interplay between theory and experiment, where improvements to the methodology of both fields were in the end needed to achieve the present day agreement.

2.7 Effective Hamiltonians for Radial Motion

In the adiabatic approximation, electronic state interactions are not accounted for so that energy levels of one state are completely oblivious to those of distant or nearby states. An exact nonadiabatic solution constitutes an enormous computational task. Nonetheless, spectroscopic observables reflect all internal and external perturbations to which the eigenstates are subjected.

Improvement in the resolving power of spectroscopic instruments over the years has led to more precise determinations of the energy level positions and revealed inconsistencies in the predicted interrelationships between the molecular constants for different isotopic forms of a diatomic molecule. The illuminating review article of Van Vleck (37) considered the various causes resulting in such inconsistencies. The experimentally derived constants ω_e^{exp} and B_e^{exp} were shown to differ from their zero-order values, ω_e and B_e , by small isotopically variant corrections, so that the simple isotopic relations,

$$\omega_e/\omega_e' = (\mu'/\mu)^{1/2}, \quad (2.37)$$

and

$$B_e/B'_e = \mu'/\mu, \quad (2.38)$$

where the primes refer to isotopic substitution, could not be satisfied. Briefly, four causes were implicated: the incompleteness of the JWKB expansion in Dunham's treatment, adiabatic corrections, and nonadiabatic perturbations of two types. Those arising from coupling of electronic states with the same orbital angular momentum, Λ , were termed *homogeneous*, and those mixing states differing by a unit in Λ were named *heterogeneous* interactions. Theoretical expressions were provided through which the estimation of such deviations could, in principle, be carried out, and their limiting behaviour for certain cases was discussed.

Owing to the aforementioned difficulties associated with a reliable *ab initio* estimation of these terms, the work of Van Vleck served chiefly as a qualitative guide to the understanding of the causes, offering little in terms of a quantitative analysis, except for the simplest cases, and then only with approximate analytical electronic wavefunctions. Since these effects follow well understood isotopic behaviour, and since the experimental observables inherently hold all information relating to these, it should be possible to contrive an inversion procedure by which reliable quantitative descriptions become available.

Fortunately, the nonadiabatic problem can be cast in a form that proves to be more useful. A perturbation treatment of Eq. (2.32) can decouple distant excited states from a ground state, projecting the (small) nonadiabatic interactions onto the adiabatic Hamiltonian of the lower state. These, then, appear as additional radial functions modifying the adiabatic

Hamiltonian operator without altering the homogeneous nature of the eigenvalue equation. This effective Hamiltonian operator is characterized by eigenvalues which are essentially identical to those of the exact Hamiltonian. The procedure for accomplishing this, is known as the Van Vleck, or electronic contact transformation (38). It appears, upon reflection, that the key to preserving the concept of a potential energy function is the requirement that a *homogeneous* differential equation describe the system. The inhomogeneous wave equation is thus essentially equivalent with an infinite nondegenerate perturbation expansion resulting in an homogeneous problem. It would seem, then, that within the validity of the Van Vleck transformation, a potential energy function is preserved. This concept is sustained as long as the nondegeneracy of the perturbation can be ensured.

Since the pioneering treatment of Van Vleck, three independent works have appeared in the literature that present effective vibration-rotation Hamiltonians for a diatomic molecule. In the consideration of energy shifts associated with non-Born-Oppenheimer behaviour in $^1\Sigma$ states, Herman and Asgharian (39) derived the effective radial Hamiltonian operator,

$$\begin{aligned} \mathcal{H}_n^{\text{eff}}(R) = & (2\mu_{\text{at}})^{-1}[1 + (m_e/m_p)g_2(R)]P_R^2 + \\ & (2\mu_{\text{at}})^{-1}[1 + (m_e/m_p)g_1(R)]J(J+1) + U_n^{\text{ad}}(R), \end{aligned} \quad (2.39)$$

where $U_n^{\text{ad}}(R)$ is the adiabatic potential, and μ_{at} is defined with atomic rather than nuclear masses. m_p is the mass of a proton and the radial functions $g_1(R)$ and $g_2(R)$ represent heterogeneous and homogeneous perturbations, respectively. These two Born-Oppenheimer breakdown contributions are of the order of m_e/m_p , in line with the errors expected in making the

Born-Oppenheimer approximation.

A discussion of the physical significance of these functions with regard to the electronic structure of a $^1\Sigma$ state is appropriate. In a Born-Oppenheimer rotating oscillator there is complete separation of the electronic and the nuclear motions, and $g_1(R)$ and $g_2(R)$ are both uniformly zero. The effective radial Hamiltonian thus collapses to the adiabatic operator. However, as the energy of vibration increases, some of the nuclear excitation is transferred to the electronic cloud, coupling electronic and vibrational motions and consequently also the ground $^1\Sigma$ state to excited $^1\Sigma$ states. In an analogous fashion, as the frequency of rotation increases, some of the nuclear angular momentum is transferred to the valence electrons, distorting the otherwise cylindrical symmetry of the electronic distribution along the internuclear axis. This results in a net nonzero electronic angular momentum along the internuclear axis which imparts a partial Π character onto the Σ state, along with a net magnetic moment. Accordingly, matrix elements coupling $^1\Sigma$ states to $^1\Pi$ states assume finite values. Since the valence electrons acquire a finite moment, they can interact with an applied magnetic field and the molecule is now characterized by a Zeeman spectrum.

The results of Bunker and Moss (40) bear general similarity to those of Herman and Asgharian (39). However, the effective Hamiltonian,

$$\mathcal{H}_n^{\text{eff}}(R) = (2\mu)^{-1}g_{\text{vib}}(R)P_R^2 + B(R)[1 + g_{\text{rot}}(R)]J(J+1) + U_n^{\text{na}}(R), \quad (2.40)$$

where $B(R) = \hbar^2/2\mu R^2$, is now defined with $U_n^{\text{na}}(R)$. This potential is no longer the adiabatic potential, but in addition contains nonadiabatic contributions. These arise naturally by subjecting the isomorphic $^1\Sigma$ Hamiltonian to a contact transformation and extending the resultant effective operator to the

perturbation order required to give rise to such effects. The analogy of $g_{\text{rot}}(R)$ and $g_{\text{vib}}(R)$ to $g_1(R)$ and $g_2(R)$ in Eq. (2.39) should be obvious. In an ensuing application of this operator to the H_2 and D_2 isotopomers, Bunker *et al.* (41) chose to model these nonadiabatic functions with effective constant values, and achieved moderate success in describing the rovibrational energy levels, with residuals displaying systematic trends.

The formulations of Herman and Asgharian (39) and Bunker and Moss (40) were aimed primarily towards an *ab initio* type of analysis. The more recent work of Watson (42) presents the Born-Oppenheimer breakdown problem in a manner amenable to a JWKB treatment, and thus is more tractable for the incorporation of experimental data in the estimation of relevant effects. Watson begins with the Born-Oppenheimer operator and treats the correction terms separately. The expression for the deviations of rovibrational level positions from their Born-Oppenheimer values in electronic state n is given by,

$$\Delta E_n(v, J) = \sum_i (m_e/M_i) \langle \psi_{vJ} | (\beta_{\text{at}}^2/R^2) J(J+1) \tilde{R}_i^{(n)}(R) + \tilde{S}_i^{(n)}(R) | \psi_{vJ} \rangle, \quad (2.41)$$

where the index i refers to each atom and the $\langle \psi_{vJ} |$ are rovibronic state vectors; β_{at}^2 contains the reduced molecular mass constructed with atomic masses. The functions $\tilde{R}_i^{(n)}(R)$ and $\tilde{S}_i^{(n)}(R)$ are defined as,

$$\tilde{R}_i^{(n)}(R) = R_i^{(n)}(R) - R^{-1} \int_{R_0}^R Q_i^{(n)}(R) dR, \quad (2.42)$$

$$\tilde{S}_i^{(n)}(R) = S_i^{(n)}(R) + \frac{1}{2} [\partial U^{\text{BO}}(R)/\partial R] \int_{R_0}^R Q_i^{(n)}(R) dR, \quad (2.43)$$

in terms of the isotopically invariant functions, $Q_i^{(n)}(R)$, $R_i^{(n)}(R)$, and $S_i^{(n)}(R)$. To the accuracy envisaged by Watson, $S_i^{(n)}(R)$ represents the pure

adiabatic correction. The purely nonadiabatic functions $Q_i^{(n)}(R)$ and $R_i^{(n)}(R)$ represent homogeneous and heterogeneous perturbations, respectively, for atomic subsystems i . The expression for the energy corrections, Eq. (2.41), is conveniently in the form of the first-order Rayleigh-Schrödinger perturbation theory result. Regarding the kernel as a perturbing Hamiltonian, an effective (first-order) operator for radial motion can be written as,

$$\mathcal{H}_n^{\text{eff}} = (2\mu_{\text{at}})^{-1}P_R^2 + (\beta_{\text{at}}^2/R^2)J(J+1)[1 + \sum_i (m_e/M_i)\tilde{R}_i^{(n)}(R)] + U_n^{\text{eff}}(R), \quad (2.44)$$

where,

$$U_n^{\text{eff}}(R) = U_n^{\text{BO}}(R) + \sum_i (m_e/M_i)\tilde{S}_i^{(n)}(R). \quad (2.45)$$

Examination of Eqs. (2.42, 2.43) reveals at once the uncertainty associated with unique determinations of $\tilde{S}_i^{(n)}(R)$ and $\tilde{R}_i^{(n)}(R)$, on account of the unspecified value of R_0 . Although different functions would result for different values of R_0 , Watson (42) states that this does not affect the value of the energy correction $\Delta E_n(v, J)$; addition of $-\lambda/R$ to $\tilde{R}_i^{(n)}(R)$ with a corresponding addition of $(\lambda/2)[\partial U^{\text{BO}}(R)/\partial R]$ to $\tilde{S}_i^{(n)}(R)$, would result in identical energy corrections. From the experimentalist's point of view, this uncertainty results because there is no simple experimental method for extracting any information relating to the vibrationally induced perturbation of electronic cloud averaging, *i.e.* the pure homogeneous effects. Thus, as the effective Hamiltonian, Eq. (2.44), suggests, the effects of $R_i^{(n)}(R)$, $Q_i^{(n)}(R)$ and $S_i^{(n)}(R)$ are experimentally inseparable.

2.8 The Isotopic Dependence of Molecular Constants

As indicated in the previous section, improvements in the resolution of

spectroscopic instruments helped reveal significant inconsistencies in the simple isotopic relations describing diatomic molecular constants. Although in the early days these defects were discovered from the spectra of hydrides and deuterides, nowadays it has been possible to detect significant Born-Oppenheimer breakdown effects in the high resolution spectra of such relatively heavy diatomics as InCl (43) and MgCl (44). A rather interesting case of what appears to be a relativistic breakdown of the Born-Oppenheimer approximation has been reported recently for thallium chloride (45).

Within the framework of Dunham's semiclassical treatment, the Y_{kl} parameters in Eq. (2.10) can be related to a set of isotopically invariant constants U_{kl} according to,

$$Y_{kl} = U_{kl} \mu^{-(k+2l)/2}, \quad (2.46)$$

providing for a unified description of data for different isotopomers. A rigorous account of Born-Oppenheimer breakdown effects, as well as consideration of the two-term JWKB quantization condition, leads to the modified relationship (42),

$$Y_{kl} = U_{kl} \mu^{-(k+2l)/2} \{1 + m_e \Delta_{kl}^a / M_a + m_e \Delta_{kl}^b / M_b + \mathcal{O}(m_e^2 / M_i^2)\}, \quad (2.47)$$

which gives better descriptions of experimental line positions for isotopically related molecules. The isotopically invariant U_{kl} can be regarded as the molecular constants of the Born-Oppenheimer potential. The mass-scaling parameters Δ_{kl}^i are composed of contributions from adiabatic and nonadiabatic coupling, as well as from higher-order JWKB phase integrals, and are normally of the order of unity. The term $\mathcal{O}(m_e^2 / M_i^2)$ emphasizes that the exact expression should include contributions from additional mass-scaling

parameters with mass weights beginning with m_e^2/M_i^2 . These are normally neglected as they are too small to characterize experimentally. Eq. (2.47) was employed by Coxon and Ogilvie (46) in a simultaneous least-squares reduction of spectroscopic lines for isotopomers of HCl.

In recent years, it has become preferable to approach the problem from a different perspective. Instead of concentrating on the determination of the coefficients of power series in $(v + \frac{1}{2})$ and $J(J + 1)$, efforts have been directed towards the estimation of the radial variation of elements of effective radial Hamiltonian operators which include non-Born-Oppenheimer effects. It is from these radial functions, after all, that the concept of molecular constants is born. It is possible, then, with a proper understanding of the mass dependence of such effects, to formulate the reduction procedure in a manner which allows the simultaneous incorporation of data for various isotopomers. If desired, it is possible to calculate the molecular parameters, using fully quantum mechanical methods, following a determination of the Hamiltonian operators. These would arise naturally by subjecting the radial operator to a vibrational contact transformation yielding an expression that operates within a single vibrational state. This is entirely analogous to subjecting the exact multi-electronic state operator to a Van Vleck, or electronic contact transformation, to yield a function that operates within a single electronic state.

2.9 Centrifugal Distortion Constants for Diatomic Molecules

An appreciation for the need and general usefulness of rotational and centrifugal distortion constants can be gained by reviewing the results of Dunham's theory (16). The most practical result of Dunham can be regarded as

the compact representation of rovibronic energies in terms of a double power series in $(v + \frac{1}{2})$ and $J(J + 1)$. Although Dunham provided explicit expressions for the (interrelated) Y_{kl} coefficients in terms of the potential parameters, these are ordinarily treated as free parameters in least-squares fits of spectral data. The molecular constant model also provides a theoretical basis for performing interpolation and (cautious) extrapolation to new members of a set of spectroscopic line positions. An additional advantage of this methodology is that the coefficients of such expansions can be employed in any of several inversion schemes to yield the internuclear potential, allowing for the estimation of molecular intensity factors by considering the associated wavefunctions.

There exist many methods for the estimation of centrifugal distortion constants. A straightforward procedure involves the representation of spectral line frequencies as,

$$\nu_i(v', v'', J', J'') = \nu_0(v', v'') + F(v', J') - F(v'', J''), \quad (2.48)$$

where

$$F(v, J) = B_v \mathcal{K} - D_v \mathcal{K}^2 + H_v \mathcal{K}^3 + L_v \mathcal{K}^4 + M_v \mathcal{K}^5 + \dots, \quad (2.49)$$

and $\mathcal{K} = J(J + 1)$ for a diatomic molecule in a $^1\Sigma$ state. Subsequent fitting of line positions to this model furnishes estimates of rotational and centrifugal constants for the two states involved. The vibrational term energies can then be extracted from the fitted band origins, $\nu_0(v', v'')$, and can be used along with the rotational constants, B_v , to yield first-order RKR turning-points.

There are two problems with this procedure. The first deals with the possibility of estimated constants absorbing some contribution from missing constants due to the required truncation of the power series in \mathcal{K} . The

additional effect of interparameter correlation in the least-squares procedure renders the rotational constants as effective least-squares parameters which serve only to represent the data from which they were derived, lack a strict physical meaning, and have little extrapolation ability. Also, for sufficiently large powers of \mathcal{K} and values of J , the procedure can encounter computational round-off error problems, which may necessitate the use of quadruple precision arithmetic.

The second problem is theoretical in origin. As a result of electronic state interactions, the rotational and centrifugal distortion constants lose their usual mechanical meaning. Use of contaminated rotational constants in the ensuing generation of RKR potential curves is inconsistent with the derivation of the semiclassical inversion procedure, and the resulting functions will not be fully decoupled from neighbouring electronic states.

Centrifugal distortion constants can also be calculated if a potential energy curve is available. Two basic approaches involve semiclassical and quantum mechanical methods. Within the JWKB picture, Kirschner and Watson (47) developed and employed a semiclassical perturbation theory to estimate the centrifugal distortion constants of $\text{CO}(X^1\Sigma^+)$. The method was found to be increasingly unstable towards the dissociation limit and its accompanying complexity made it unattractive for routine use. Barwell (48) devised a procedure which removed the near-dissociation problems, so that semiclassical quadratures could be evaluated to obtain the constants over the entire range of potential energy. This was made possible by considering the theoretically predicted (49) form of the long-range potential in the first-order JWKB quantization condition.

There are three quantum mechanical methods for calculating centrifugal

distortion constants for a diatomic molecule. The first, introduced by Moody and Beckel (50), was termed the eigenvalue-fitting method. Here, the vibrational-rotational eigenvalues of a potential energy function were found and subsequently fitted to a power series in \mathcal{K} , giving at once B_v , D_v , H_v , etc. The second method, discussed by Tellinghuisen (51), exploited the relationship,

$$B_v(J) = \frac{\partial G(v, J)}{\partial \mathcal{K}} = \beta^2 \langle \psi_{vJ} | R^{-2} | \psi_{vJ} \rangle = B_v - 2D_v \mathcal{K} + 3H_v \mathcal{K}^2 + \dots, (2.50)$$

where calculation of the expectation values for different values of J of given v followed by a least-squares fit to a power series in \mathcal{K} led to estimates of the constants. This is known as the energy-derivative method. These two fitting methods suffer from similar problems as the experimental method above. Moreover, the energy-derivative method makes the explicit assumption that rotational constants are given as expectation values of R^{-2} . A neglect of heterogeneous contributions to $B_v(J)$ is made. The eigenvalue-fitting method also assumes this, albeit implicitly, by constructing rotational potentials on the basis of a centrifugal term $\beta^2 \mathcal{K}/R^2$.

The third, and most fundamental quantum mechanical method is based on the application of Rayleigh-Schrödinger perturbation theory. Developed by Albritton and co-workers (52), this procedure defines the rotational and centrifugal distortion constants as perturbation energies of the rotational Hamiltonian operator β^2/R^2 . Expressing first and higher order wavefunction corrections in terms of summations over zero-order terms, these authors obtained,

$$B_v = \beta^2 \langle \psi_v | R^{-2} | \psi_v \rangle, \quad (2.51)$$

$$D_v = \beta^4 \sum_{v'} \frac{\langle \psi_{v'} | R^{-2} | \psi_v \rangle^2}{E_v^{(1)} - E_{v'}^{(0)}}, \quad (2.52)$$

etc., where for D_v the special symbol emphasizes that a summation should be considered over the bound vibrational levels and an integration carried out over the continuum. Since the computational algorithm neglects altogether the continuum contributions, second and higher order constants become increasingly unreliable as the dissociation limit is approached. This traditional perturbation procedure is also inefficient computationally owing to the great number of summation operations, particularly for higher-order perturbation energies.

In recent work, Hutson (53) was able to circumvent the sum-over-states expressions by considering a *direct* perturbation calculation. This was made possible by employing Hutson and Howard's novel numerical procedure (34) for solving reliably an inhomogeneous differential equation. For first- and second-order wavefunction corrections made orthogonal to the zero-order eigenfunctions, expressions for the rotational and centrifugal distortion constants are (53, 54),

$$B_v = \langle \psi_v^{(0)} | \mathcal{H}' | \psi_v^{(0)} \rangle, \quad (2.53)$$

$$D_v = - \langle \psi_v^{(0)} | \mathcal{H}' | \psi_v^{(1)} \rangle, \quad (2.54)$$

$$H_v = \langle \psi_v^{(1)} | \mathcal{H}' - B_v | \psi_v^{(1)} \rangle, \quad (2.55)$$

$$L_v = \langle \psi_v^{(1)} | \mathcal{H}' - B_v | \psi_v^{(2)} \rangle + D_v \langle \psi_v^{(1)} | \psi_v^{(1)} \rangle, \quad (2.56)$$

$$M_v = \langle \psi_v^{(2)} | \mathcal{H}' - B_v | \psi_v^{(2)} \rangle + 2D_v \langle \psi_v^{(1)} | \psi_v^{(2)} \rangle - H_v \langle \psi_v^{(1)} | \psi_v^{(1)} \rangle, \quad (2.57)$$

where the perturbing Hamiltonian is $\mathcal{H}' = \beta^2/R^2$. This method gives constants

which are, in principle, reliable up to the dissociation limit. Of course, for very high vibrational levels, an extended integration range is required to ensure that all significant portions of the wavefunction are sampled, rendering the procedure somewhat inefficient for such levels. This latter problem was overcome recently by Pajunen (55) through the reformulation of the perturbation problem in terms of the Prüfer phase function. The method does not involve wavefunctions explicitly, but the natural oscillatory behaviour of the Prüfer function makes the procedure more reliable for high vibrational levels, where the highly oscillatory structure of the wavefunction could make previous methods less reliable due to insufficient sampling.

2.10 The Method of Least-Squares

2.10.1 Introduction

The fruitful interplay between the experimentalist and the theoretician during the first half of this century led to the development of theoretical models which could be applied to the representation of spectroscopic data. However, without the modern electronic computer, the spectroscopist was required to draw upon tedious and often unreliable methods for relating spectral features to physical models. Although approximate graphical procedures (56) allowed the experimentalist to become more directly involved with the analysis by exploiting an intimate familiarity with the experimental information, they failed to provide reliable estimates for the molecular parameters and their uncertainties, and were inherently limited in power and scope.

Nowadays, fast digital computers are readily available; this has contributed tremendously to the growth and maturity of the field of molecular

spectroscopy. With a variety of options available for fitting equations to data, it is necessary to justify a preference for any one in particular. Some of the better known fit criteria are, least absolute deviation, least-squared deviation, maximum likelihood, minimum chi-squared, the simplex method, and others. However, the method of minimum-variance, or least-squares (57), has gained an almost universal acceptance as a standard fitting technique. In molecular spectroscopy, whether it is used for the purpose of calibrating the wavelengths of a spectrum on a photographic plate, or for extracting meaningful estimates of molecular constants from spectral line positions, the method of least-squares enjoys wide popularity, primarily because of the advantageous properties associated with the estimates it provides.

The estimates furnished by least-squares are the most precise unbiased estimates that are linear functions of the measurements (57). These are usually termed minimum-variance linear unbiased (MVLU) estimates. The 'unbiased' attribute is the most important because it indicates that the procedure *itself* will not introduce any systematic error into the estimates, whereas this is often not the case for other fit criteria.

It is important to examine briefly the assumptions of the least-squares method. First, a perfect model is presumed. This is rarely the case, as it appears that time and again nature evades being modelled perfectly by mathematics; hence it is important to establish the adequacy of a chosen model through critical tests where possible or practical, before applying it to experimental data. The linear regression method assumes a model which depends linearly on the parameters, although it is possible to obtain MVLU estimates for a nonlinear model. Another important assumption is that the measurements must be described by some distribution function (not necessarily Gaussian)

with zero-mean and a finite error variance. Accordingly, the systematic component in the measurement error should be zero; that is, if an estimate is determined from the same data set measured many times, with measurements subject only to *random* error, the deviation from the “true” value would average to zero. When this is not the case, as is found occasionally for spectroscopic data, it should be realized that the ‘unbiased’ property is rendered useless and the estimates should be viewed with suspicion. Finally, the independent variable is assumed to be without error. While this is normally not a problem for many spectroscopic applications, as the independent variables are often quantum numbers, the general problem in which both variables are subject to finite errors has been solved (58).

2.10.2 Weighted Linear Least-Squares

The general linear least-squares problem can be expressed most concisely in matrix notation as,

$$\mathbf{y} = \mathbf{X}\boldsymbol{\beta} + \boldsymbol{\epsilon}, \quad (2.58)$$

where

$$\mathbf{y} = \begin{bmatrix} y_1 \\ y_2 \\ \vdots \\ y_n \end{bmatrix}, \quad \boldsymbol{\beta} = \begin{bmatrix} \beta_1 \\ \beta_2 \\ \vdots \\ \beta_n \end{bmatrix}, \quad \boldsymbol{\epsilon} = \begin{bmatrix} \epsilon_1 \\ \epsilon_2 \\ \vdots \\ \epsilon_n \end{bmatrix}. \quad (2.59)$$

\mathbf{y} contains the experimental data, $\boldsymbol{\beta}$ is the column vector containing the parameters to be estimated, $\boldsymbol{\epsilon}$ contains the (unknown) measurement errors, and \mathbf{X} is the coefficient matrix. Application of the least-squares criterion to this linear system yields the MVLU values $\hat{\boldsymbol{\beta}}$ that minimize the sum of the squares

between the measurements \mathbf{y} and the calculated values $\hat{\mathbf{y}}$, as

$$\hat{\beta} = (\mathbf{X}^T \mathbf{W} \mathbf{X})^{-1} \mathbf{X}^T \mathbf{W} \mathbf{y}. \quad (2.60)$$

Alternatively,

$$\hat{\beta} = (\mathbf{X}^T \Phi^{-1} \mathbf{X})^{-1} \mathbf{X}^T \Phi^{-1} \mathbf{y}, \quad (2.61)$$

where the weight matrix (\mathbf{W}) is the reciprocal of the measurement error dispersion matrix \mathbf{M} , which is in turn given in terms of the diagonal matrix Φ of the measurement errors. More specifically, in matrix form,

$$\Phi = \begin{bmatrix} \sigma_1^2 & & 0 \\ & \sigma_2^2 & \\ 0 & & \ddots \\ & & & \sigma_n^2 \end{bmatrix}, \quad \mathbf{M} = \begin{bmatrix} \sigma_1^2/\sigma_n^2 & & 0 \\ & \sigma_2^2/\sigma_n^2 & \\ 0 & & \ddots \\ & & & 1 \end{bmatrix}, \quad (2.62)$$

so that $\Phi = \sigma_n^2 \mathbf{M}$. The σ_i^2 are unknown variances, but the ratios σ_i^2/σ_j^2 , for $i \neq j$ are assumed to be known. σ_n^2 is an unknown common factor and the weight matrix is simply $\mathbf{W} = \mathbf{M}^{-1}$. The common unknown factor σ_n^2 is calculated from

$$\hat{\sigma}_n^2 = f^{-1} (\mathbf{y} - \mathbf{X} \hat{\beta})^T \mathbf{W} (\mathbf{y} - \mathbf{X} \hat{\beta}), \quad (2.63)$$

where f are the degrees of freedom. The variance-covariance matrix, Θ , of the molecular parameters is calculated from

$$\Theta = \hat{\sigma}_n^2 (\mathbf{X}^T \mathbf{W} \mathbf{X})^{-1} = \hat{\sigma}_n^2 \mathbf{V}, \quad (2.64)$$

where \mathbf{V} is the dispersion matrix with the obvious value $(\mathbf{X}^T \mathbf{W} \mathbf{X})^{-1}$. This matrix is important as it gives an indication of the degree of interdependence of the least-squares estimates. An often more immediately helpful indicator of parameter interdependence is the correlation coefficient matrix element, C_{ij} , given by

$$C_{ij} = \hat{\Theta}_{ij} / (\hat{\Theta}_{ii} \hat{\Theta}_{jj})^{1/2}, \quad (2.65)$$

the diagonal elements of which have values of unity and the off-diagonal elements take values which range from -1 to $+1$. Absolute off-diagonal values near unity indicate strong correlation between the pair of estimates involved; this means that there is a mutual influence in the determination of the two estimates. In applications to real data this usually serves to reduce the physical significance of both estimates.

Finally, it should be obvious that if the weight matrix equals the unity matrix \mathbf{I} , that is, if all the data are weighted equally, the results given above collapse precisely to those of the unweighted formulation.

2.10.3 Correlated Least-Squares (Merging)

The problem of combining multiple estimates of least-squares parameters for the purpose of obtaining an optimum set of single MVLU values cannot be resolved satisfactorily by a simple weighted averaging scheme. Although this takes account of the potentially different precisions of such estimates, it overlooks correlations that link a set of estimates together.

A procedure which facilitates a statistically sound solution to this problem has been described by Albritton *et al.* (57). Here, a single-step merge formulation was proposed whereby results from separate *unweighted* single band fits were merged together to yield an optimum set of constants. The unattractive alternative of a simultaneous *weighted* multi-band fit makes the single-step approach advantageous in terms of the significantly reduced computational demands on storage and execution time that can be achieved. An additional benefit of this approach is the improved manner in which relative

systematic error in a subset can be unmasked. Furthermore, the results of the single-step approach are completely equivalent to those of the weighted multi-band fit.

The merge approach considers the output of k individual band fits as the input to another least-squares fit which reduces a set of m redundant input parameters to a final set of p unique estimates. The solution of m equations of the type

$$y = \tilde{X}\tilde{\beta} + \delta, \quad (2.66)$$

is considered where

y is the vector containing m input parameters,

\tilde{X} maps the input and output parameters,

$\tilde{\beta}$ contains the p output parameters,

δ are unknown (*interrelated*) errors.

Albritton *et al.* (57) stressed that the δ are interrelated through the variance-covariance matrices associated with the redundant input constants, and that it is precisely these (known) interrelations which form the basis of the merge approach. A minimization of $\delta^T \delta$ yields p nonredundant parameters

$$\hat{\beta}_M = (\tilde{X}^T \hat{\Phi}^{-1} \tilde{X})^{-1} \tilde{X}^T \hat{\Phi}^{-1} y, \quad (2.67)$$

where $\hat{\Phi}$ is a matrix containing the individual variance-covariance matrices associated with each separate single band fit, so that

$$\hat{\Phi} = \begin{bmatrix} \hat{\Theta}_1 & & 0 \\ & \hat{\Theta}_2 & \\ 0 & & \hat{\Theta}_k \end{bmatrix}. \quad (2.68)$$

The estimated variance of the merge fit is given by

$$\hat{\sigma}_M^2 = f_M^{-1}(\mathbf{y} - \tilde{\mathbf{X}}\hat{\beta}_M)^T \hat{\Phi}^{-1}(\mathbf{y} - \tilde{\mathbf{X}}\hat{\beta}_M), \quad (2.69)$$

where $f_M = m - p$ are the degrees of freedom of the merge fit. The variance-covariance matrix associated with the merged constants is

$$\hat{\Theta}_M = \hat{\sigma}_M^2 \mathbf{V}_M, \quad (2.70)$$

defined with the $p \times p$ dispersion matrix

$$\mathbf{V}_M = (\tilde{\mathbf{X}}^T \hat{\Phi}^{-1} \tilde{\mathbf{X}})^{-1}. \quad (2.71)$$

Despite the advantages gained by adopting the single-step merge approach, in large applications it quickly becomes apparent that detection of systematic error in individual subsets can be a time consuming matter. It must be accomplished through the systematic exclusion of suspect subsets in repeated single-step merges. For this reason, Coxon (59) investigated the possibility of carrying out merge fits in a stepwise fashion. The stepwise approach considers the output of several single-step merges as input into a grand merge, shown to give results that are identical to that of a single-step procedure. In direct analogy to the single-step result, the stepwise approach gives the expression

$$\hat{\beta}_{SM} = (\tilde{\mathbf{X}}^T \hat{\Phi}_M^{-1} \tilde{\mathbf{X}})^{-1} \tilde{\mathbf{X}}^T \hat{\Phi}_M^{-1} \hat{\beta}_M, \quad (2.72)$$

for the stepwise merge MVLU parameter estimates $\hat{\beta}_{SM}$. The estimated stepwise merge variance is given by

$$\hat{\sigma}_{SM}^2 = f_{SM}^{-1}(\hat{\beta}_M - \tilde{\mathbf{X}}\hat{\beta}_{SM})^T \hat{\Phi}_M^{-1}(\hat{\beta}_M - \tilde{\mathbf{X}}\hat{\beta}_{SM}). \quad (2.73)$$

The weight matrix $\hat{\Phi}_M$ is not composed by the variance-covariance matrices associated with the single-step merged constants, as might first be expected. Coxon (59) found that in order to obtain results identical to those of the

single-step approach, the weight matrix had to be defined as

$$\hat{\Phi}_M = \begin{bmatrix} (\hat{V}_M)_1 & & 0 \\ & (\hat{V}_M)_2 & \\ 0 & & \ddots & \\ & & & (\hat{V}_M)_q \end{bmatrix}, \quad (2.74)$$

where the $(\hat{V}_M)_i$ are the dispersion matrices from the q single-step merge fits. This difference is at the heart of the stepwise approach. The variance of an equivalent single-step grand merge of several stepwise merges is calculated by

$$\hat{\sigma}_{GM}^2 f_{GM} = \hat{\sigma}_{SM1}^2 f_{SM1} + \hat{\sigma}_{SM2}^2 f_{SM2} + \dots, \quad (2.75)$$

where $f_{GM} = f_{SM1} + f_{SM2} + \dots$, f_{SMi} being the degrees of freedom for stepwise merge i .

2.10.4 Weighted Nonlinear Least-Squares

There are many interesting intrinsically nonlinear problems in chemical physics and molecular spectroscopy. The direct reduction of line positions to molecular constants for $^2\Pi$ states, the fitting of spectral line profiles to Gaussian, Lorentzian, or Voigt models, and the representation of RKR turning points by flexible analytical potential functions, are just a few.

For a set of k observations Y , the nonlinear problem can be written as,

$$Y = f(\xi_1, \xi_2, \dots, \xi_k; \theta_1, \theta_2, \dots, \theta_p) + \epsilon, \quad (2.76)$$

or simply, $Y = f(\Xi, \Theta) + \epsilon$. The object here is to obtain least-squares estimates $\hat{\theta}$ in an iterative fashion from a *linearized* problem. The linearization is achieved by expanding $f(\Xi, \Theta)$ in a Taylor series,

$$f(\Xi, \Theta) = f(\Xi, \Theta_0) + \sum_{i=1}^p \left[\frac{\partial f(\Xi, \Theta)}{\partial \theta_i} \right]_{\Theta=\Theta_0} (\theta_i - \theta_{i0}) +$$

$$\frac{1}{2} \sum_{i=1}^p \left[\frac{\partial^2 f(\Xi, \Theta)}{\partial \theta_i^2} \right]_{\Theta=\Theta_0} (\theta_i - \theta_{i0})^2 + \dots, \quad (2.77)$$

where the Θ_0 are initial trial values of the parameters. Birss (60) has proposed using the Hellmann-Feynman theorem (61, 62) in evaluating the second derivatives to achieve improved convergence. These terms are neglected here. The resultant pseudolinear system of equations can be written succinctly in matrix form as

$$\Delta Y = Z \Delta \theta, \quad (2.78)$$

where, for the j th iteration,

$$\Delta Y = \begin{bmatrix} \Delta y_{1j} \\ \Delta y_{2j} \\ \vdots \\ \Delta y_{kj} \end{bmatrix}, \quad \Delta \theta = \begin{bmatrix} \Delta \theta_{1j} \\ \Delta \theta_{2j} \\ \vdots \\ \Delta \theta_{kj} \end{bmatrix}, \quad (2.79)$$

and

$$Z = \begin{bmatrix} \left[\frac{\partial f}{\partial \theta_1} \right]_{1j} & \left[\frac{\partial f}{\partial \theta_2} \right]_{1j} & \dots & \left[\frac{\partial f}{\partial \theta_p} \right]_{1j} \\ \left[\frac{\partial f}{\partial \theta_1} \right]_{2j} & \left[\frac{\partial f}{\partial \theta_2} \right]_{2j} & \dots & \left[\frac{\partial f}{\partial \theta_p} \right]_{2j} \\ \cdot & \cdot & \dots & \cdot \\ \cdot & \cdot & \dots & \cdot \\ \cdot & \cdot & \dots & \cdot \\ \left[\frac{\partial f}{\partial \theta_1} \right]_{kj} & \left[\frac{\partial f}{\partial \theta_2} \right]_{kj} & \dots & \left[\frac{\partial f}{\partial \theta_p} \right]_{kj} \end{bmatrix}, \quad (2.80)$$

where $\Delta Y = f(\Xi, \Theta) - f(\Xi, \Theta_0)$, from Eq. (2.77) above, and $\Delta \theta = \theta_i - \theta_{i0}$. The key to rapid convergence is the method of estimation of the first derivatives.

Although methods can vary in degree of sophistication, a simple finite-difference approach was found adequate in applications found in this work.

A minimization must be applied to the error sum of squares,

$$S = (\Delta Y)^T(\Delta Y), \quad (2.81)$$

to obtain the parameter correction estimates

$$\Delta\theta = (Z^T W Z)^{-1} Z^T \Delta Y, \quad (2.82)$$

such that the θ of the current (j th) iteration are

$$\theta_{i,j} = \theta_{i,j-1} + \Delta\theta_{i,j}. \quad (2.83)$$

The procedure is iterated until a specified convergence criterion in the sum of the squares is met. After convergence, an indication of the goodness of the fit can be obtained from

$$\hat{\sigma} = f^{-1} \left[\sum_{i=1}^n \Delta Y_i^2 \right]^{1/2}. \quad (2.84)$$

The variance-covariance matrix is

$$\hat{\Theta} = \hat{\sigma}^2 \mathbf{V}, \quad (2.85)$$

defined with the dispersion matrix

$$\mathbf{V} = (Z^T W Z)^{-1}. \quad (2.86)$$

The square roots of the diagonal variance-covariance elements give estimated standard errors for the parameters.

2.11 Numerical Solution of the Radial Wave Equation

2.11.1 Truly Bound States

One the most useful applications of numerical methods to the field of

molecular spectroscopy is undoubtedly in obtaining solutions of the central-field eigenvalue problem. The present work rests on the availability of a trustworthy solution of the radial wave equation.

The location of truly bound levels, that is, those which lie below the dissociation limit, is accomplished through the procedure usually ascribed to Cooley (63). The computer program used in this work includes the subsequent modifications of Zare and Cashion (64). For a diatomic molecule regarded as a symmetric top, solution of the Schrödinger equation expressed in polar spherical coordinates is preceded by a separation of the problem into angular and radial parts so that

$$\Psi = \rho(R) Y_{J\Lambda M}(\Theta, \Phi, \phi), \quad (2.87)$$

is an acceptable solution. The $Y_{J\Lambda M}$ are hypergeometric functions and should not be confused with Dunham's Y_{kl} (16). $\rho(R)$ are the solutions of the radial wave equation expressed in dimensionless form as,

$$d^2\rho(R)/dR^2 = [U(R) - E] \rho(R), \quad (2.88)$$

where $U(R)$ is the effective rotational potential,

$$U(R) = E_{el}(R) + Z_a Z_b / R + [\mathcal{K} - \Lambda^2] / R^2, \quad (2.89)$$

and E is the vibrational eigenvalue. $E_{el}(R)$ is the electronic energy having a parametric dependence on internuclear distance, and $Z_a Z_b / R$ is the nuclear Coulombic repulsion term. The last term in Eq. (2.89) is the kinetic energy of nuclear rotation.

The program of Zare and Cashion (64) considers the modified second-order differential equation,

$$d^2S(R)/dR = [U(R) - E] S(R), \quad (2.90)$$

where $S(R) = R \rho(R)$, automatically ensuring the inclusion of volume element $R^2 dR$ in subsequent expectation value calculations.

Application of Numerov's (65) sixth-order difference equation,

$$-T_{i-1} + 2T_i - T_{i+1} + h^2(U_i - E) P_i = 0, \quad (2.91)$$

where $P_i = P(R_i)$ is an initial non-normalized solution and,

$$T_i = [1 - (h^2/12)(U_i - E)] P_i, \quad (2.92)$$

$$U_i = U(R_i),$$

$$h = R_{i+1} - R_i,$$

yields a solution associated with an error of $(h^6/240) d^6 P_i / dR^6$. The integration is performed in a bidirectional mode with inward and outward integrations starting at the last and first mesh points, respectively. The inward integration is initialized by applying the boundary conditions,

$$P_n = 10^{-30}, \quad (2.93)$$

and

$$P_{n-1} = P_n e^{[R_n \sqrt{U_n - E} - R_{n-1} \sqrt{U_{n-1} - E}]}, \quad (2.94)$$

with a trial value E . Eq. (2.94) is derived from the JWKB wavefunction and its use at the beginning of the inward solution is justified so long as the potential is slowly approaching an asymptote near R_n . The inward (decreasing- R) integration continues until the first extremum of the wavefunction is detected, at R_m .

The outward (increasing- R) integration begins with the boundary conditions,

$$P_0 = 0, P_1 = 10^{-20}. \quad (2.95)$$

The solution proceeds in accord with Eq. (2.91) until the radial distance R_m is reached, that is, at the place where the inward integration was terminated. At this point, the inward and outward solutions are made mutually consistent through division by their respective non-normalized values at R_m ; hence at the joint between the inward and outward integrations the solution has the same value ($P_m = 1$), but likely suffers from a discontinuity in slope.

The potentially different slopes between the two curves at the crossing-point R_m are used to correct the trial energy value, E . A simple expression for such a correction is given by,

$$\Delta E = (P'_{out} - P'_{in}) / \int_0^\infty [P(R)]^2 dR, \quad (2.96)$$

where P'_{out} and P'_{in} give the first derivatives at R_m from the outward and inward integration, respectively. Improved convergence can be achieved through the use of the Newton-Raphson result,

$$\Delta E = -F(E)/F'(E), \quad (2.97)$$

where the correction function is

$$F(E) = h^{-2}(-T_{m-1} + 2T_m - T_{m+1}) + (U_m - E) P_m, \quad (2.98)$$

and its derivative is given by

$$F'(E) = - \sum_{j=1}^n P_j^2. \quad (2.99)$$

The procedure is iterated until $|\Delta E| \leq \epsilon$, where ϵ is a preset convergence criterion. Following convergence, the normalized solution is obtained as,

$$S_i = P_i / \left[h \sum_{j=1}^n P_j^2 \right]^{1/2}, \quad i = 1, 2, \dots, n. \quad (2.100)$$

It was decided to test the accuracy of the procedure using model potential functions for which the wave equation is solvable exactly. For the case of no nuclear rotation ($J = 0$), the radial wave equation can be solved essentially exactly with the Morse potential function,

$$U(R) = \mathcal{D}_e \left[1 - e^{-\alpha(R - R_e)} \right]^2. \quad (2.101)$$

An analytical expression for the vibrational eigenvalue emerges,

$$G_v = \omega_e(v + 1/2) - \omega_e x_e(v + 1/2)^2, \quad (2.102)$$

with

$$\omega_e = 2\alpha\beta(\mathcal{D}_e)^{1/2}, \quad (2.103)$$

$$\omega_e x_e = (\alpha\beta)^2. \quad (2.104)$$

Choosing appropriate values for α and \mathcal{D}_e allows for the procedure to be tested very near dissociation. Table 2.1 gives the parameters α , \mathcal{D}_e , ω_e , and $\omega_e x_e$ for the Morse potential employed here. Cashion (64) also tested the procedure using a Morse potential; variables such as integration interval size and number of points were thus not investigated here. It should be noted, however, that in specific applications, these factors were thoroughly explored. The main objective of the present test is to ensure and demonstrate the proper operation of the computer program, which is of critical importance to this research. The eigenvalue convergence criterion employed was 10^{-6} cm^{-1} . Results from the program are compared to the true (exact) energies in Table 2.2.

TABLE 2.1

Test of Algorithm for Solution of Radial Wave Equation:
Parameters of Analytical Potential Functions

Morse Potential	Fues-Kratzer Potential
$R_e = 1.000 \text{ \AA}$	$R_e = 0.916 \ 835 \ 9 \text{ \AA}$
$\mathcal{D}_e = 31 \ 250 \text{ cm}^{-1}$	$\mathcal{D}_e = 49 \ 375 \text{ cm}^{-1}$
$\mu = 1.685 \ 763 \ 14 \text{ amu}$	$\mu = 0.957 \ 055 \ 282 \text{ amu}$
$R_{\min} = 0.40 \text{ \AA}$	$R_{\min} = 0.40 \text{ \AA}$
$R_{\max} = 6.40 \text{ \AA}$	$R_{\max} = 8.40 \text{ \AA}$
$h = 0.002 \text{ \AA}$	$h = 0.0025 \text{ \AA}$
$\epsilon = 10^{-6} \text{ cm}^{-1}$	$\epsilon = 10^{-4} \text{ cm}^{-1}$
$\omega_e = 2500 \text{ cm}^{-1}$	
$\omega_e x_e = 50 \text{ cm}^{-1}$	

Morse potential can be constructed from Eq. (2.101). Fues-Kratzer potential is defined by Eq. (2.105). R_e is the equilibrium internuclear separation, \mathcal{D}_e is the dissociation limit and μ is the reduced molecular mass. The functions were constructed in the range R_{\min} to R_{\max} with a mesh size of h . The radial wave equation was solved with a convergence criterion of ϵ . The energy parameters ω_e and $\omega_e x_e$ are defined by Eqs. (2.103) and (2.104), respectively.

TABLE 2.2

Test of Algorithm for Solution of Radial Wave Equation:
A Comparison of Calculated with Exact Energies (cm^{-1})

Morse Potential					
v	E^{exact}	$10^6 \times \Delta E$	v	E^{exact}	$10^6 \times \Delta E$
0	1237.5	2	12	23437.5	1530
1	3637.5	15	13	24637.5	1646
2	5937.5	49	14	25737.5	1725
3	8137.5	111	15	26737.5	1762
4	10237.5	205	16	27637.5	1752
5	12237.5	330	17	28437.5	1695
6	14137.5	482	18	29137.5	1589
7	15937.5	654	19	29737.5	1436
8	17637.5	839	20	30237.5	1241
9	19237.5	1028	21	30637.5	1008
10	20737.5	1212	22	30937.5	743
11	22137.5	1382	23	31137.5	456
			24	31237.5	-753
Fues-Kratzer Potential ^a					
v	$J = 0$	$J = 5$	$J = 10$	$J = 15$	$J = 20$
0	0.0000	0.0000	-0.0001	-0.0001	-0.0001
4	-0.0001	-0.0001	-0.0001	-0.0001	-0.0002
8	-0.0002	-0.0002	-0.0001	-0.0001	-0.0001
12	-0.0013	-0.0006	-0.0002	-0.0002	-0.0002
16	-0.0044	-0.0022	-0.0003	-0.0001	-0.0002
20	-0.0109	-0.0055	-0.0009	-0.0001	-0.0003

^aEntries for Fues-Kratzer potential are the discrepancies between the exact (Eq. 2.106) and calculated (numerical solution of the radial wave equation) energies, in cm^{-1} .

In order to ensure the proper operation of the program for the rotational case, the Fues-Kratzer potential,

$$U(R) = \mathcal{D}_e[1 + \chi^2 - 2\chi], \quad (2.105)$$

with $\chi = R_e/R$, was used. The Fues-Kratzer Schrödinger equation is solvable exactly for all values of v and J . The terms are given by (66),

$$E_{vJ} = \mathcal{D}_e - \frac{k \mathcal{D}_e}{\left[(v + \frac{1}{2}) + [J(J + 1) + \frac{1}{4} + k]^{1/2} \right]^2}, \quad (2.106)$$

where

$$k = R_e^2 \mathcal{D}_e / \beta^2. \quad (2.107)$$

The parameters of the potential and the rotational eigenvalue test results are given in Tables 2.1 and 2.2, respectively.

It is noteworthy that the Cooley predictor-corrector procedure is not the only method available for solving the one-dimensional Schrödinger equation. A series of papers (67-69) dealing with an application of the quantum mechanical variational method appeared in the late 1960's and early 1970's. Basis sets were constructed as linear combinations of the well-known wavefunctions of the harmonic oscillator, and later the eigenfunctions of a Morse potential. All these attempts met with moderate success. In view of an already existing successful method (64), application of the variational method to the problem appears to be of academic value only. More reliable alternatives include the "Log-Derivative Method" (70), the Prüfer phase function method (55), and the "Canonical Functions Method" (CFM) proposed by Kobeissi *et al.* (71). Recently, Tellinghuisen (72) showed that the CFM method is formally and numerically equivalent to the procedure of Cooley (63), provided that both

algorithms are implemented with the Numerov integration formula. The Cooley-Numerov method was, however, shown to be computationally more efficient.

2.11.2 *Quasibound States (Orbiting Resonances)*

Adjustment of the rotationless potential by the centrifugal term $\beta^2 J(J + 1)/R^2$ yields effective rotational functions, characterized by a barrier. As shown in Figure 2.2, energy states which exist above the asymptote are associated with three turning points. These quasibound states are not *truly* bound but possess a finite probability of penetrating the barrier in a nonradiative fashion. Associated with these metastable levels are finite lifetimes and widths related by the uncertainty principle of energy and time. The spectroscopic detection, in emission, of a gradual broadening of rotational lines with increasing J , followed by an abrupt disappearance of the structure, provides convincing proof that a predissociation is occurring. A quantitative analysis of this information yields an estimate for the dissociation energy.

The theoretical description of quasibound states can be accomplished by a variety of methods. Since the "exact" methods of quantum mechanics are often tedious to use, approximate boundary condition schemes have proven to be of great value in locating orbiting resonances. These were reviewed and tested by Le Roy and Liu (73). Their results suggested that the Airy function boundary condition is reliable for the type of resonances encountered in this work.

The Airy function boundary condition derivation assumes that the rotational potential near the third turning point can be approximated by a

Figure 2.2

Graphical representation of a quasibound level. E_{v0} and E_{vJ} are vibrational energies corresponding to rotationless and rotational potential curves, respectively. (R_1^0, R_2^0) , and (R_1^J, R_2^J) are the inner and outer classical turning points for the case of rotationless and rotational potentials, respectively. The third turning point for the rotational potential curve is given by R_3^J .

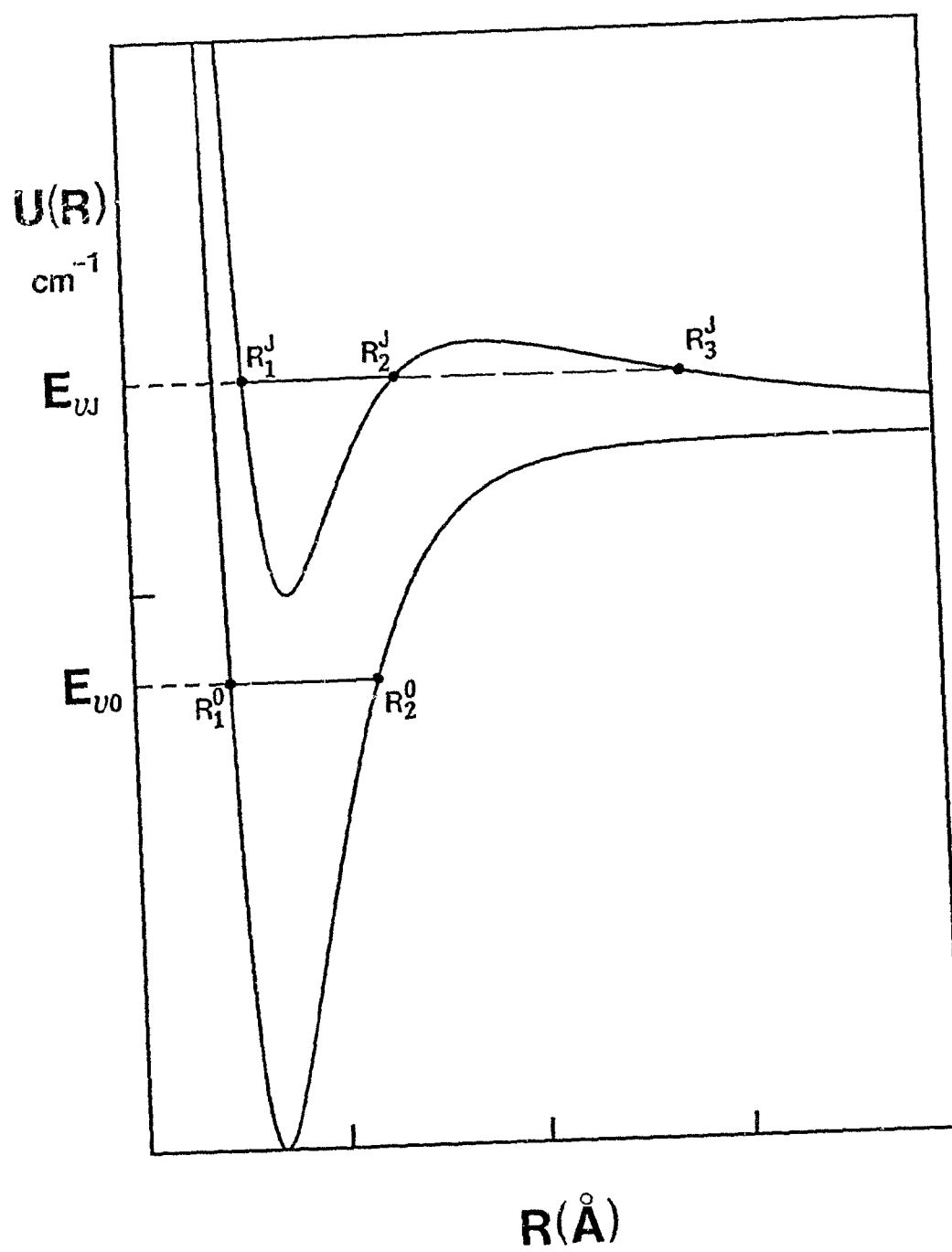


Figure 2.2

straight line. Application of the uniform approximation (73) to the problem casts the wavefunction at the outermost turning point as an Airy function of the second kind, $Bi(-z)$ (74). Along with a boundary condition at $R = 0$, the problem is transformed into the one-dimensional eigenvalue type, which allows the procedure to be incorporated directly in Cooley's algorithm. Since the approximation requires the three turning points to be spaced well apart, the increasing proximity of the second and third turning points with increasing energy makes the method more reliable for resonances well below the barrier maximum and totally inapplicable above it. It was shown (73) that the error in the prediction of quasibound energies with the Airy BC is approximately 5% of Γ , where Γ is the full width at half-height of the energy state. Tiemann (75), however, has shown recently that these estimates could deviate by as much as 20% and in an unpredictable direction. For the types of resonances that can be detected spectrographically ($\Gamma \leq 1 \text{ cm}^{-1}$), the error in the calculated position is almost indistinguishable from the experimental uncertainty.

The treatment of the resonance *widths* follows a different path. Conceptually, the simplest approach views the width as the ratio of the probability of barrier penetration to the period of oscillation in the potential well (76, 77), so that by the uncertainty principle,

$$\Gamma = \hbar\omega/t_{vib}, \quad (2.108)$$

where

$$\omega = \exp\left\{-\frac{(8\mu)^{1/2}}{\hbar} \int_{R_2(E)}^{R_3(E)} [U(R) - E]^{1/2} dR\right\}, \quad (2.109)$$

and

$$t_{vib} = (2\mu)^{1/2} \int_{R_1(E)}^{R_2(E)} [E - U(R)]^{-1/2} dR. \quad (2.110)$$

This semiclassical recipe was found (77) to yield widths that were within $\sim 12\%$ of more accurate estimates, for $H_2(X^1\Sigma^+)$. The widths reported in the present work were calculated by a more complicated prescription. Le Roy's QBOUND subroutine (78) originally provided the simple width given above; however, following the recent article of Connor and Smith (79), the code appears to have been modified to calculate the width in the semiclassical uniform approximation as,

$$\Gamma = 2\hbar t_{vib} w(\epsilon)/\pi, \quad (2.111)$$

where

$$w(\epsilon) = \frac{[1 + e^{2\pi\epsilon}]^{1/2} - 1}{[1 + e^{2\pi\epsilon}]^{1/2} + 1}, \quad (2.112)$$

and ϵ is the quadrature through the barrier.

Unfortunately, it is not as easy to verify the accuracy of level positions for quasibound states as it was for truly bound states. The rotational solution for the Morse oscillator is, as stated above, not truly exact. The Fues-Kratzer eigenvalue formula is of little use here since this potential cannot form a potential barrier. There simply does not appear to be any absolute standard for direct comparison. This has forced previous investigators to rely on *ab initio* results for positions, and well-studied experimental systems for widths. Some promise was offered by a relatively obscure article by Tietz (80) where an analytical potential was developed, having an exact solution in closed form for the eigenvalues. It was found

that adjustment of one of the potential parameters led to the formation and controlled the magnitude of an inherent potential maximum. With the exact eigenvalue expression at hand it appeared at first that this might offer a sound way of evaluating the accuracy of approximate methods. However, there appears to be an error associated with the energy expression; in any case, a solution was only considered for a *real* wavefunction; the case $E \geq \mathcal{Q}_e$, where the wavefunction enters the complex plane, was not considered by Tietz (80).

CHAPTER 3
IMPROVED HAMILTONIAN OPERATORS FOR RADIAL MOTION
PART A: SEMICLASSICAL METHODS

The first-order RKR_V potential inversion procedure is popular because of the relatively easy calculations involved and the usually excellent potentials it provides. Additionally, it is an almost unique procedure, failing to define the behaviour of the curve only below the ground vibrational level. Reliable evaluation of the improper integrals f and g has been the subject of numerous articles in the literature (81-85), and the first-order problem can be considered adequately resolved.

However, the advent of laser and interferometric methods brought an accompanying improvement in the precision of spectroscopic data; this has served to demonstrate convincingly the limitations of the first-order RKR_V approximation. It is often found that the quantum mechanical expectation values of first-order RKR_V functions fail to describe observables within the measurement uncertainties. A case in point is the fundamental band of HF, obtained experimentally by Fourier transform techniques (86). Table 3.1 shows a comparison of observed frequencies and those calculated on the basis of quantum mechanical eigenvalues of the RKR_V curve of Di Lonardo and Douglas (87).

The inadequacy of the semiclassically approximate RKR_V potential inversion procedure derives primarily from the neglect of higher-order JWKB phase integrals in its derivation. On account of the correspondence principle (88), a semiclassical JWKB formulation is expected to be less

TABLE 3.1

Fundamental Band of HF($X^1\Sigma^+$): Demonstration of Inadequacy of RKR
Potential in Predicting Observables

J	$P(J)$	$\Delta P(J)$	$ \Delta P(J)/\epsilon $	$R(J)$	$\Delta R(J)$	$ \Delta R(J)/\epsilon $
0				4001.0127	-0.0235	47.0
1	3920.3328	-0.0210	42.0	4038.9882	-0.0259	51.8
2	3877.7289	-0.0214	42.8	4075.3231	-0.0295	59.0
3	3833.6846	-0.0320	46.0	4109.9709	-0.0343	68.6
4	3788.2533	-0.0255	51.0	4142.8863	-0.0401	80.2
5	3741.4890	-0.0291	58.2	4174.0267	-0.0469	93.8
6	3693.4467	-0.0336	67.2	4203.3509	-0.0548	109.8
7	3644.1822	-0.0395	79.0	4230.8197	-0.0638	127.6
8	3593.7520	-0.0465	93.0	4256.3958	-0.0736	147.2
9	3542.2127	-0.0537	107.4	4280.0442	-0.0838	167.6
10	3489.6214	-0.0620	124.0	4301.7319	-0.0953	190.6
11	3436.0358	-0.0698	139.6	4321.4284	-0.1080	216.0

The quantities $\Delta P(J)$ and $\Delta R(J)$ refer to observed-calculated line positions (cm^{-1}) for the P - and R -branches, respectively. ϵ is the experimental error estimate; $\epsilon = 0.0005 \text{ cm}^{-1}$ for this band.

reliable where quantal effects are significant. Better results can therefore be obtained for heavy molecules and high values of the quantum numbers. In this section, methods for improving first-order RKR Hamiltonians are reviewed.

3.1 *Direct Inclusion of 3rd-Order JWKB Phase Integral*

The first documented method for incorporating exactly the second finite JWKB integral in the RKR procedure is due to Vanderslice and co-workers (89). This derivation was followed by an application to the ground state of molecular hydrogen (90). A solution was obtained in an iterative fashion, whereby a repetitively improved first-order curve was used to estimate the second-order RKR (third-order JWKB) corrections to the turning points. Some difficulty was encountered in fitting the potential derivative required for the second-order corrections to a power series in $U^{1/2}$. This was due to the large values of dU/dR at small internuclear separations and led to problems with the uniqueness and stability of the procedure. Furthermore, the corrections obtained were of the order of the uncertainties in the first-order turning points indicating that highly precise data are required for a proper evaluation of such effects.

A mathematically equivalent procedure for second-order RKR calculations was presented by Kirschner and Watson (47). This was applied to the ground $X^1\Sigma^+$ state of CO, and despite the need for intermediate least-squares fits, the calculations provided a potential which could recover satisfactorily the input G_v and B_v values. The Rydberg-Klein-Dunham second-order calculations of McKeever (91) for the ground state of H_2 appear to be equally successful. Here, it was shown that the previous results of Davies and Vanderslice (90)

were overestimates of the second-order corrections to the turning points.

A rigorous derivation of a two-term RKR procedure was undertaken by Le Roy (92). The resulting expressions for the f and g integrals included explicitly the effects of the third-order JWKB integral. The solution proceeds in an iterative fashion but so far there do not appear to be any published applications of this procedure.

3.2 Indirect Inclusion of Higher-Order JWKB Terms

It is possible to include the effects of higher-order phase integrals while avoiding the mathematical and numerical complexities associated with their explicit evaluation.

By far the simplest procedure of this type was proposed by Kaiser (93). The contributions from the second JWKB term were considered in the modified quantization condition,

$$\oint \sqrt{E_{vJ} - U(R)} dR = 2\pi\beta(v + \frac{1}{2} + \Delta), \quad (3.1)$$

where Δ was treated most concisely by Kirschner and Watson (47), obtaining

$$\Delta = \frac{\beta}{64\pi} \lim_{E \rightarrow 0} \oint (dU/dR)^2 [E - U(R)]^{-5/2} dR. \quad (3.2)$$

Kaiser (93) gave the simple result,

$$\Delta = Y_{00}/Y_{10}, \quad (3.3)$$

where the Dunham coefficient Y_{00} was approximated by

$$Y_{00} = \frac{(B_e - \omega_e x_e)}{4} + \frac{\alpha_e \omega_e}{12B_e} + \frac{(\alpha_e \omega_e)^2}{144B_e^3}, \quad (3.4)$$

defined with the usual vibrational-rotational parameters. This adjusts the positions of all vibrational levels by a constant amount and simply requires that first-order RKR integrals be evaluated from the modified lower limit,

$$v_0^{\text{eff}} = -\frac{1}{2} - \Delta, \quad (3.5)$$

reducing sharply the work required to obtain what is presumably in effect a second-order RKR potential. Recent work (94), however, has shown that the Kaiser modification may lead to results for the g integral that are often inferior to those of an unmodified first-order calculation. This is because, even though the Kaiser correction considers the second JWKB term, it fixes its value to that at the potential minimum (94), *i.e.* the condition that $E \rightarrow 0$ in Eq. (3.2) above.

The approach of Huffaker (95) considered the evaluation of turning points in terms of two power series given as analytic functions of the spectroscopic constants. Second-order JWKB terms were introduced effectively by making corrections to spectroscopic constants based on Huffaker's Perturbed Morse Oscillator (PMO) model (96),

$$U^{\text{PMO}}(R) = \tau \left[y^2 + \sum_n b_n y^n \right], \quad (3.6)$$

where

$$y = 1 - \exp[-a(R - R_e)]. \quad (3.7)$$

This method was applied to the ground electronic states of CO and HF (95) with moderate success, encountering particularly significant problems near the dissociation limit. A breakdown of JWKB theory might be expected immediately near dissociation (97), but it is unlikely that the levels considered by Huffaker (95) enter into this region.

By a similar approach, Coxon and Ogilvie (46) followed Watson's (42) suggestion of correcting experimental values of the U_{kl} for higher-order effects, and used these in a Kaiser unmodified first-order RKR calculation. The resulting potential should then have been equivalent to one obtained by considering higher-order JWKB phase integrals explicitly. Along the same lines, expressions for higher-order contributions to some Dunham coefficients were obtained by Bouanich (98) through perturbation theory.

In more recent work, Schwartz and Le Roy (94) proposed to eliminate the third-order JWKB integral by considering information on two isotopomers simultaneously. The resulting simple expressions were thus exact within the third-order JWKB approximation. Model calculations showed that results were superior to those of both an unmodified first-order calculation and the Kaiser corrected first-order results. At the same time, the model testing suggested that care should be exercised in applying the method. In particular, the procedure was found to be highly sensitive to the precision of the input data, and should be used for very precise measurements only. Also, since the two isotopomers were assumed to have the same potential, the method should not be applied to systems for which the Born-Oppenheimer approximation is significantly deficient. This limitation is unfortunate as it makes the procedure less reliable for light diatomics, the very systems for which higher-order JWKB effects are most significant. These warnings were apparently not heeded in a recent application of the procedure to the isotopic LiH molecules (99). Not surprisingly, improvement over the first-order results was not realized.

A most interesting application of Watson's (100) semiclassical inversion procedure was proposed by Gouedard and Vigue (101). In an attempt to improve

a first-order RKR potential iteratively, these authors identified a function $X(R)$ with a small potential correction, $\Delta U(R)$, and inverted ΔG_v and ΔB_v values to this function. ΔG_v and ΔB_v , the differences between the experimental and quantum mechanical values, became gradually smaller, but it was found that after convergence, the final differences displayed oscillatory behaviour for $\text{CC}(X^1\Sigma^+)$, with better results realized for heavier diatomics. The authors speculated that for a light molecule like CO, quantum effects may be significant, and pointed to their inability in separating calculational from quantum limitations on the method.

A chief criticism of methods that rely on a partial intermediate set of molecular constants is that these constants are not true observables of a system, but have significance only as parameters that define an infinite perturbation expansion. Putting aside, for the moment, any inconsistencies and loss of mechanical significance that may result owing to the method of their estimation, the quantum mechanical identities of these constants, and their effect on the physical significance of RKR potentials must be considered.

Since the molecular constants employed in the estimation of RKR turning points are derived by considering experimental line positions, they must reflect the nonadiabatic interactions experienced by the electronic state in question. This contamination will, to some extent, enter into the classical turning points of motion. In order to gain more insight into this, it is helpful to examine qualitatively the influence of neighbouring electronic states on the values taken by the derived G_v and B_v constants that serve as input for such a calculation. The vibrational terms will deviate from their (generally unknown) adiabatic values through homogeneous mixing of the

unperturbed eigenfunctions. This type of perturbation is fully compatible with a JWKB transformation of the eigenvalue problem, Eq. (2.1), since it will contribute to the adiabatic potential and to the adiabatic rotational constants in a J -independent fashion. Thus the RKR procedure *can* recover homogeneously perturbed potential curves. However, even though a heterogeneous interaction will have no additional effect on the rotationless term values, it can significantly alter the adiabatic (or even homogeneously nonadiabatic) identity of rotational constants. No provisions were made for this type of interaction in the derivation of the RKR equations; the formulation of Klein's g integral assumes that rotational constants are expectation values of R^{-2} . More significantly, a fundamental neglect of heterogeneous coupling is made in the JWKB transformation of the radial wave equation, Eq. (2.1). It is Eq. (2.32) that should be subjected to this transformation. Therefore, although the rotational constants contain all the information on the heterogeneous couplings, the RKR equations have not been set up to extract such information in a theoretically proper fashion. It appears, then, in the matter of electronic state interactions, that semiclassical methods face similar limitations as *ab initio* descriptions; in order to describe the couplings properly, knowledge of excited state potential functions is required. In spite of this, a truly inverse JWKB procedure taking this *implicitly* into account appears to be possible; the recent work of Watson (42) offered an as yet unexplored semiclassical scheme for achieving such a task.

3.3 *Extended Dunham and Dunham-type Methods*

Recently Bessis *et al.* (102) proposed a method for the direct reduction

of vibrational-rotational data to analytical functions describing the radial dependences of various interesting effects. The coefficients of such functions were expressed in terms of familiar spectroscopic parameters. The starting point in a computer-aided perturbation calculation was the Dunham potential. Additional functions were employed to describe the effects of interest, and the coefficients of these were given by unwieldy expressions in terms of the potential parameters and known spectroscopic constants. One application of the method was to the description of the radial variations of the spin-rotation and spin-orbit couplings in the ground state of OH, with encouraging results.

More recently, Ogilvie (103) developed an analogous inversion procedure modelled with the Ogilvie-Tipping reduced potential coordinate (104). In addition to providing less complicated expressions for the coefficients of the radial functions, the work of Ogilvie was superior in another aspect; the Dunham reduced coordinate $x^D = (R - R_e)/R_e$ employed by Bessis *et al.* (102), suffers from a limited radius of convergence ($0 \leq R_c \leq 2R_e$), whereas use of $x^{OT} = 2(R - R_e)/(R + R_e)$, with $0 \leq R_c \leq \infty$, is preferable.

The main criticism of these approaches concerns their ability to describe properly the potential function all the way up to dissociation. It is doubtful whether any single analytic function can achieve this. In addition, the power series functions employed above fail to describe the long-range behaviour of an internuclear potential function. Finally, neither of the analytic formulations has been adapted to include heterogeneous interactions in a theoretically proper fashion. The coefficients would then partially absorb such effects, losing their originally intended identity.

PART B: QUANTUM MECHANICAL METHODS

3.4 Direct Perturbation Methods

Initial efforts involving the application of quantum mechanical perturbation theory to the improvement of potential functions were concerned with systematic corrections to a variety of analytical model functions. Galin *et al.* (105) considered the calculation of Dunham parameters in high orders of perturbation theory, obtained through computer algebraic methods. Subsequently, Burenin (106) formally perturbed a Fues-Kratzer oscillator, using the exact solution for this system as a zeroth-order starting basis. The perturbation expansion was carried out in terms of inverse powers of the internuclear distance, but use of the conventional Rayleigh-Schrödinger approach was avoided. Instead, a different perturbation theory (106) was used, involving a finite number of terms for the energy corrections, in contrast to the conventional infinite expansion method. Only the theoretical layout was presented, and application of the resulting (complicated) procedure does not appear to have been undertaken.

The first "perturbative" expansion on the basis of a Morse oscillator can be attributed to Dunham (16). In more recent work, expressions similar in structure to those of Dunham emerged from the formal perturbative treatment of Huffaker (96). The model was coined the Perturbed Morse Oscillator (PMO) and in later work (107) it was applied to a variety of diatomic states. In its purely theoretical form, the PMO expansion was only moderately successful, encountering particular problems for the ground states of HF and HCl. Thus, despite jargon suggesting otherwise, its current applications find it as a flexible analytic fitting model for the representation of RKR turning

points (95, 108), or *ab initio* results (109).

3.5 Inverse Methods

The label for methods to follow herein as “inverse” is only loosely applied. A *true* inverse method determines the internuclear potential directly from experimental data rather than assume some parametrized functional form and adjust it in a fit to the data (110). In this section, methods which systematically impose corrections to radial Hamiltonian operators to attain agreement with the experimental data are considered. On the other hand, Dunham’s procedure can be regarded as a true inversion of the experimental data to the internuclear potential. This also applies to the procedures considered in sections 3.2.1 and 3.2.2 above.

3.5.1 Semiempirical Correction Methods

The possibility of removing the disagreement between experimental results and those of approximate theoretical methods by using the correction function approach, was first explored by Le Roy and Bernstein (111). The method was applied to $H_2(X^1\Sigma_g^+)$ where the *ab initio* potential of Kołos and Wolniewicz (112) was adjusted by an empirical correction function in an effort to resolve a serious discrepancy in the calculated vibrational intervals from those known precisely from experiment. An interesting result of this work was that either of a pair of empirical correction functions could remove the discrepancy, indicating a displeasing lack of uniqueness.

Kuriyan and Pritchard (113, 114) constructed effective nonadiabatic potential functions for diatomic hydrogen and deuterium, and their molecular

ions using a correction function approach. The method of estimation of such functions involved the interactive piecemeal determination of linear correction patches (113), applied only to the outer limbs of the trial potentials. The work of Ref. (111) showed that the nonuniqueness of the correction procedure would be greatest for the low vibrational levels considered here, so that adjustment of either limb near the minimum would result in similar changes to the eigenvalues. A small criticism of this work (113) concerns the failure to consider any possible alteration of the centrifugal term by heterogeneous nonadiabatic coupling. The importance of these two articles (113, 114) is that they offered an interesting, albeit somewhat unrefined alternative to expensive high-level *ab initio* nonadiabatic calculations.

Some consideration to heterogeneous effects in hydrogen was given in an article by Bunker *et al.* (41), where a centrifugal term of the type,

$$\mathcal{H}_{\text{rot}}(R) = \beta^2 J(J + 1)[1 + \alpha(R)]/R^2, \quad (3.8)$$

was included in fits to low vibrational-rotational energy levels of H_2 and D_2 . However, only partial success was demonstrated, most likely due to the modelling of $\alpha(R)$ by a simple constant.

3.5.2 Inverse Perturbation Analysis (IPA)

A more methodical approach for obtaining potential correction functions from experimental data was proposed by Kosman and Hinze (115). This method begins with a zeroth-order radial Schrödinger equation for a $^1\Sigma$ state,

$$(\mathcal{H}_{\text{vib}}^0 + \mathcal{H}_{\text{rot}}^0)\psi_{vJ}^0 = E_{vJ}^0 \psi_{vJ}^0, \quad (3.9)$$

where

$$\mathcal{H}_{\text{vib}}^0 = -\beta^2 d^2/dR^2 + U_0^0(R), \quad (3.10)$$

and

$$\mathcal{H}_{\text{rot}} = \beta^2 J(J + 1)/R^2. \quad (3.11)$$

It is then assumed that the "true" (effective) rotationless potential differs from the approximate function $U_0^0(R)$ in Eq. (3.10), by a radial correction function $\Delta U(R)$, so that

$$U_0^{\text{eff}}(R) = U_0^0(R) + \Delta U(R), \quad (3.12)$$

where the as yet unknown- correction function can be regarded as a perturbing operator. Rayleigh-Schrödinger perturbation theory provides the *first-order* energy corrections,

$$\Delta E_{vJ} = \langle \psi_{vJ}^0 | \Delta U(R) | \psi_{vJ}^0 \rangle, \quad (3.13)$$

in terms of the zeroth-order radial eigenvectors. Eq. (3.13) is normally encountered in direct applications, whereby an assumed $\Delta U(R)$ function is employed to calculate the first-order energy corrections. Alternatively, a known $\Delta U(R)$ function can be used in conjunction with parametrized eigenvectors $|\psi_{vJ}^0(\alpha_1, \alpha_2, \dots, \alpha_n; R)\rangle$ in a variational calculation.

The inverted perturbation approach seeks to determine $\Delta U(R)$ by assuming that the differences ΔE_{vJ} between the approximate eigenvalues, E_{vJ}^0 , and the experimental terms, E_{vJ}^{exp} , can be described entirely by a first-order model. These differences should actually be expressed as,

$$\Delta E_{vJ} = \langle vJ | \Delta U | vJ \rangle + \sum_{vJ \neq wK} \frac{|\langle vJ | \Delta U | wK \rangle|^2}{E_{vJ}^0 - E_{wK}^0} + \text{higher order terms.} \quad (3.14)$$

The IPA assumes that second- and higher-order terms are small in relation to the first term in Eq. (3.14), and unimportant with regard to the experimental errors.

If the perturbing Hamiltonian $\Delta U(R)$ is expanded in terms of a flexible mathematical basis set,

$$\Delta U(R) = c_i f_i(R), \quad (3.15)$$

and substituted back into Eq. (3.13), a set of linear equations,

$$\Delta E_{vJ} = \sum_i c_i \langle \psi_{vJ}^0 | f_i(R) | \psi_{vJ}^0 \rangle, \quad (3.16)$$

is obtained. In typical applications, this set of linear equations is overdetermined and can be treated effectively by a least-squares minimization procedure to provide estimates of the c_i .

The key approximation of IPA is that the $E_{vJ}^{\text{exp}} - E_{vJ}^0$ differences can be equated to the ΔE_{vJ} first-order corrections of Eq. (3.14). This can be ensured by choosing a trial potential, $U_0^0(R)$, which forms a close approximation for the final effective potential, $U_0^{\text{eff}}(R)$. Since this might not always be possible, and since a *finite* basis set is used to approximate $\Delta U(R)$, it is not expected that the perturbation calculation will converge in one cycle. Therefore, in the IPA formulation of Kosman and Hinze (115), an iterative approach was adopted. This might equally be thought of as an application of the variational theorem since the stepwise improvement of the potential causes a concomitant optimization of the radial eigenfunctions.

Vidal and Scheingraber (116) formulated the IPA in much the same fashion as the previous investigators (115). The key difference was their choice of a basis set; improved convergence was claimed with the nonlinear interpolation,

$$x = \frac{(R - R_e)(R_{\max} - R_{\min})}{(R_{\max} + R_{\min})(R_e + R) - 2(R_{\max}R_{\min} + R_eR)}, \quad (3.17)$$

with R_{\max} and R_{\min} chosen as the outermost and innermost classical turning points, respectively. Their representation for $\Delta U(R)$ was,

$$\Delta U(R) = \sum_i c_i P_i(x) e^{-x^{2n}} \quad (1 \leq n \leq 5) \quad (3.18)$$

where $P_i(x)$ are Legendre polynomials. These authors employed Eq. (3.18) in a fit using a *partial* set of term value differences.

The inverted perturbation procedure can also be discussed in terms of the Hellmann-Feynman (61, 62, 117) theorem (HFT). The HFT equates the rate of change of an eigenvalue with respect to a real parameter, with the expectation value of the rate of change of the potential function with respect to the same parameter, that is,

$$\frac{\partial E}{\partial \lambda} = \langle \Psi | \frac{\partial U(R)}{\partial \lambda} | \Psi \rangle. \quad (3.19)$$

It is easy to show that the first-order perturbation result is actually a limiting case of the HFT. In fact, Epstein (118) went on to derive the conventional second-order result from the HFT, and intimated that the entire Rayleigh-Schrödinger perturbation theory follows from the HFT. However, the relationship between the IPA and the HFT is not as simple as this and derives from the use of a least-squares minimization procedure in the optimization of $U_0^{\text{eff}}(R)$. Consider the simple case of a single electronic state n , characterized by a potential,

$$U_n^{\text{eff}}(R) = [U_n^0(R) + \beta^2 J(J+1)/R^2] + \Delta U_n(R), \quad (3.20)$$

with associated eigenvalues

$$E_{nvJ} = E_{nvJ}^0 + \Delta E_{nvJ}. \quad (3.21)$$

The IPA procedure considers the minimization of eigenvalue residuals, ΔE_{nvJ} , to obtain $\Delta U(R)$. It is possible to write a Hellmann-Feynman theorem for Eq. (3.21) with respect to a set of parameters c_i that define the potential correction $\Delta U(R)$, as

$$\partial E_{nvJ} / \partial c_i = \partial E_{nvJ}^0 / \partial c_i + \partial \Delta E_{nvJ} / \partial c_i \quad (3.22)$$

which is also equal to

$$\partial E_{nvJ} / \partial c_i = \langle nvJ | \partial U_n^{\text{eff}}(R) / \partial c_i | nvJ \rangle, \quad (3.23)$$

leading to the relationship,

$$\partial \Delta E_{nvJ} / \partial c_i = \langle nvJ | \partial \Delta U_n(R) / \partial c_i | nvJ \rangle. \quad (3.24)$$

If $\Delta U_n(R)$ is given by Eq. (3.15) above, the partial derivatives given here assume the explicit form,

$$\partial \Delta E_{nvJ} / \partial c_i = \langle nvJ | f_i(R) | nvJ \rangle. \quad (3.25)$$

These are identically the expectation values (cf. Eq. (3.16)) which form the coefficient matrix for the least-squares fit of the IPA.

The need for an initial potential which forms a close approximation to the final potential has been discussed previously in terms of the reliability of a first-order perturbation model; a good initial potential can reduce the number of iterations required to achieve convergence. However, a slightly different interpretation here finds the use of first-order perturbation theory as the means of linearizing an inherently *nonlinear* problem, that is, the exact relationship between a Hamiltonian operator and its point spectrum. It appears that perturbation theory acts as the agent of a pseudolinearization of

the exact nonlinear problem; partial derivatives required for the least-squares analysis are obtained most accurately as Hellmann-Feynman integrals. The quality of partial derivatives in nonlinear least-squares analysis is a crucial factor in determining the rate of convergence of the problem.

The expressions Eqs. (3.23-3.25) given above were written in terms of the wavefunctions of the final effective potential; in fact, in equating the Hellmann-Feynman treatment with the first-order perturbation setup, the subtle assumption,

$$\partial E_{nvJ} / \partial c_i = \langle \psi_{nvJ}^{\text{eff}} | f_i(R) | \psi_{nvJ}^{\text{eff}} \rangle \approx \langle \psi_{nvJ}^0 | f_i(R) | \psi_{nvJ}^0 \rangle, \quad (3.26)$$

was made. In the usual perturbative treatment, the true wavefunction is expanded,

$$|\psi_{nvJ}^{\text{eff}}\rangle = |\psi_{nvJ}^{(0)}\rangle + \lambda |\psi_{nvJ}^{(1)}\rangle + \lambda^2 |\psi_{nvJ}^{(2)}\rangle + \dots, \quad (3.27)$$

in terms of the zeroth-order eigenfunctions and perturbation corrections. This shows clearly the nature of the first-order perturbation assumption; the first- and higher-order wavefunction corrections are neglected in the first cycle and as the potential function is improved iteratively,

$$|\psi_{nvJ}^{\text{IPA}}\rangle \rightarrow |\psi_{nvJ}^{\text{eff}}\rangle, \quad (3.28)$$

that is, the IPA wavefunctions approach the exact wavefunctions. This is the inverse perturbation formulation of the problem of correcting wavefunctions which is, of course, implicit in the procedure. The IPA wavefunctions are implicitly, and nonlinearly, dependent on the c_i coefficients of the potential correction. This demonstrates the importance of a good initial potential. The expectation values employed in the correction procedure depend critically

on the quality of the trial wavefunctions and will affect the convergence properties of the solution.

Despite the demonstrated success of IPA in describing systems to which it had been applied, it remains theoretically deficient in its ability to describe rotational shifts that arise from a global heterogeneous perturbation. The validity of Eq. (3.11) was not in any way questioned despite the existing article of Herman and Asgharian (39). It would have taken little additional labour to implement a Bunker *et al.* (41) $\alpha(R)J(J + 1)$ contribution to the eigenvalues in the IPA algorithm. The importance of such a term in relation to the experimental errors must be established *statistically* and not *a priori* ignored. Finally, although Korman and Hinze (115) claim the method to be within the adiabatic approximation, it is easy to see that the scheme can absorb homogeneous nonadiabatic perturbations as additional corrections to the rotationless potential curve. Thus, the claim of adiabaticity in the functions derived by the IPA is *not* proven simply by obtaining a satisfactory representation of the spectral data. Adiabatic and homogeneously nonadiabatic corrections are experimentally inseparable and potential functions derived in this fashion must reflect both effects.

3.5.3 A Hamiltonian Correction Approach

3.5.3 (a) Introduction

The procedure described in this section has been developed by Coxon (119, 120) and applied to the description of the quantum energy levels and electronic structure of hydrogen chloride isotopomers. The method is employed in the present work to improve the understanding of the spectra, molecular structures, and electronic state interactions in the hydrides HF,

DF, HCl and DCl. The formulation rests soundly on the theoretical results of Watson (42), allowing Coxon to write an effective radial Hamiltonian for a $^1\Sigma$ electronic state n as,

$$\mathcal{H}_n^{\text{eff}}(R) = P_R^2/(2\mu_{\text{at}}) + \beta_{\text{at}}^2 J(J+1)[1 + q_n(R)]/R^2 + U_n^{\text{eff}}(R), \quad (3.29)$$

defined with atomic masses to take into account the general tendency of the inner electrons to follow closely the motion of the nuclei. The inclination of the valence electrons to “slip” from rapid nuclear vibrations is described by applying a correction to the Born-Oppenheimer potential, as given previously by Eq. (2.45), with radial functions $\tilde{S}_i^n(R)$ for each atomic centre i . The $\tilde{S}_i^n(R)$ can be expressed in terms of two other functions, $S_i^n(R)$ and $Q_i^n(R)$, as in Eq. (2.43). In the formulation of Watson, the $S_i^n(R)$ are pure adiabatic corrections, whereas the work of Bunker and Moss (40) shows that they contain some (small) nonadiabatic component. The functions $Q_i^n(R)$ describe homogeneous nonadiabatic interactions and allow for the vibrationally induced slippage effect.

The slippage of valence electrons during particularly energetic nuclear rotations is characterized by the purely nonadiabatic function $q_n(R)$ given in terms of isotopically invariant functions $\tilde{R}_i^n(R)$,

$$q_n(R) = \sum_i (m_e/M_i) \tilde{R}_i^n(R), \quad (3.30)$$

where, as indicated by Eq. (2.42), $\tilde{R}_i^n(R)$ is expressed in terms of two functions $R_i^n(R)$ and $Q_i^n(R)$. The functions $R_i^n(R)$ are responsible for heterogeneous electronic state mixing. Due to the contributions from $Q_i^n(R)$, the total function $q_n(R)$ is purely nonadiabatic but *not* purely heterogeneous.

3.5.3 (b) Numerical Procedure

Unlike the IPA, the Hamiltonian Correction Approach (HCA) considers the adjustment of *line position residuals* by optimizing term value residuals for two states simultaneously. This is statistically more correct than the separate adjustment of term values, as the process of measuring a spectral line position correlates the two levels. It is also more pleasing conceptually to operate on true observables, the spectral line positions, rather than on derived quantities. The residuals $\Delta\nu$, between the measured line positions, ν_{obs} , and those constructed from the eigenvalues of the trial Hamiltonians, ν_0 , are given by,

$$\Delta\nu_{n'v'J'n''v''J''} = (E_{n'v'J'} - E_{n'v'J'}^0) - (E_{n''v''J''} - E_{n''v''J''}^0). \quad (3.31)$$

The simultaneous adjustment of two ΔE_{nvJ} is accomplished by applying the principles of IPA. Starting with the approximate radial operator

$$\mathcal{H}^0(R) = P_R^2/2\mu_{\text{at}} + U_n^0(R) + \beta_{\text{at}}^2 J(J+1)/R^2, \quad (3.32)$$

the terms

$$\Delta U_n(R) + \beta_{\text{at}}^2 J(J+1)q_n(R)/R^2, \quad (3.33)$$

associated with the difference between the trial and final effective operators, Eqs. (3.32) and (3.29), yield the corrections to the eigenvalues,

$$\Delta E_{nvJ} = \langle \psi_{nvJ}^{\text{eff}} | \Delta U_n(R) | \psi_{nvJ}^{\text{eff}} \rangle + \langle \psi_{nvJ}^{\text{eff}} | g_n(R) | \psi_{nvJ}^{\text{eff}} \rangle J(J+1), \quad (3.34)$$

where $g_n(R) = \beta_{\text{at}}^2 q_n(R)/R^2$. Note that the exact corrections are given as expectation values of the final effective wavefunctions. Now, a first-order approximation for Eq. (3.34) is obtained,

$$\Delta E_{nvJ} \approx \langle \psi_{nvJ}^0 | \Delta U_n(R) | \psi_{nvJ}^0 \rangle + \langle \psi_{nvJ}^0 | g_n(R) | \psi_{nvJ}^0 \rangle J(J+1), \quad (3.35)$$

and the individual kernels are expanded as

$$\Delta U_n(R) = \sum_i c_i \phi_i(R), \quad (3.36)$$

and

$$g_n(R) = \sum_i d_i \vartheta_i(R), \quad (3.37)$$

casting the Δv problem into,

$$\begin{aligned} \Delta v_{n'v'J'n''v''J''} = & \sum_i c'_i \langle \phi'_i \rangle + \sum_i d'_i \langle \vartheta'_i \rangle J'(J'+1) - \\ & \sum_i c''_i \langle \phi''_i \rangle - \sum_i d''_i \langle \vartheta''_i \rangle J''(J''+1), \end{aligned} \quad (3.38)$$

where

$$\langle \phi_i \rangle = \langle \psi_{nvJ}^0 | \phi_i(R) | \psi_{nvJ}^0 \rangle, \quad \langle \vartheta_i \rangle = \langle \psi_{nvJ}^0 | \vartheta_i(R) | \psi_{nvJ}^0 \rangle. \quad (3.39)$$

Weighted linear least-squares optimization is applied to determine estimates of the coefficients. The weighting is achieved as σ_i^{-2} , where σ_i is the estimated measurement uncertainty of the i^{th} line position.

3.5.3 (c) Mathematical Model

In retrospect, the most important consideration in the success of any inverted perturbation approach, is the choice of a mathematical basis for representing the unknown functions. It is also the main weakness of any such procedure; one attempts to determine functions with no prior knowledge of their radial variations. This requires thoughtful selection of a basis set. Also, at the fitting stage, much time consuming trial and error optimization

is not unusual. More will be said on this later, when the HCA is scrutinized through model calculations.

Coxon (120) realized that the use of global functions, which exert an influence over the entire domain of molecular existence, can lead to difficulties. In particular, the determination of such functions is weighted strongly towards the lower vibrational levels, for which highly precise data are often available, paying little regard for spectrographically obtained electronic data. Thus, it was found (119) that highly precise low- ν data could be fitted quite satisfactorily, whereas electronic data fits were characterized by systematic residuals that increased with ν and J . In later work (120), use of functions that imposed corrections in localized regions of coordinate space, removed the systematic trend in the fitted residuals and allowed the inclusion of highly excited rotational levels in the fits.

The mathematical model employed for $\Delta U_n(R)$ in this work is,

$$\Delta U_n(R) = \Delta T_{ne} + a_n S_n(R) + \sum_i b_{ni} G_{ni}(R) + \sum_{ij} c_{nij} F_{nij}(R). \quad (3.40)$$

ΔT_{ne} is an adjustment to a trial electronic term value. The second function, $S_n(R)$, is the first derivative of the trial rotationless potential,

$$S_n(R) = dU_n^0(R)/dR, \quad (3.41)$$

which is approximated by the central-difference formula (121),

$$S_n^k(R) = \frac{-U_{k+2} + 8U_{k+1} - 8U_{k-1} + U_{k-2}}{12h}, \quad (3.42)$$

h being the radial distance between adjacent points in the numerical potential. The derivative term is aimed at translating the potential function along the internuclear coordinate axis without changing the positions of the

energy levels. Use of the first derivative term alone is not correct mathematically. The increment form of the Taylor series (122) defines,

$$U(R + h) = U(R) + h \frac{dU(R)}{dR} + \frac{h^2}{2!} \frac{d^2U(R)}{dR^2} + \frac{h^3}{3!} \frac{d^3U(R)}{dR^3} + \dots, \quad (3.43)$$

as the mathematical transformation required to achieve a translation of the rotationless potential by h units along the radial axis. Clearly, then, use of the $S_n(R)$ function alone ignores second and higher derivative terms. However, the approximation is good for small translations and use of the first derivative alone in this work is justified *a posteriori*. The explicit use of higher than first derivatives in the fitting procedure is possible but would necessitate the use of nonlinear least-squares since the coefficients of derivative terms in the Taylor series expansion, Eq. (3.43), are interrelated.

The $G_{ni}(R)$ are modified Gaussian functions,

$$G_{ni}(R) = (R - R_e) \exp[-\alpha_{nik}(R - R_{ni})^2], \quad (3.44)$$

constructed about a central radial distance R_{ni} . The damping parameters α_{nik} are in general different on either side of R_{ni} ($k = 1$ and 2 refer to $R < R_{ni}$ and $R > R_{ni}$, respectively). For two adjacent Gaussians, G_{ni} and $G_{n,i+1}$, α_{ni2} and $\alpha_{n,i+1,1}$ are chosen such that the damping components of both functions have a value of 0.75 midway between R_{ni} and $R_{n,i+1}$ (120). The 0.75 factor is somewhat arbitrary but Coxon has shown (120) that a fitted function is relatively insensitive to this, provided sufficient overlap between adjacent functions is ensured. Similar conclusions were reached by Hamilton *et al.* (123) in a recent application of a correction procedure employing local Gaussian functions as a basis.

Finally, the $F_{nij}(R)$ functions are defined by

$$F_{ni1}(R) = (R - R_{ne})^i \quad \text{for } R < R_{ne} \text{ and } F_{ni1}(R) = 0 \text{ for } R > R_{ne} \quad (3.45)$$

and

$$F_{ni2}(R) = (R - R_{ne})^i \quad \text{for } R > R_{ne} \text{ and } F_{ni2}(R) = 0 \text{ for } R < R_{ne}, \quad (3.46)$$

allowing for separate radial correction functions for the inner ($j = 1$) and outer ($j = 2$) limbs. R_{ne} is the R_e value for electronic state n .

The representation chosen for the nonadiabatic function $g_n(R)$ is

$$g_n(R) = \sum_i d_{ni} H_{ni}(R), \quad (3.47)$$

where

$$H_{ni}(R) = (R - \mathcal{R}_n)^i - (R_{ne} - \mathcal{R}_n)^i, \quad (3.48)$$

with \mathcal{R}_n chosen to be the smallest internuclear separation to which the data are sensitive.

3.5.3 (d) Model Testing

3.5.3 (d.1) General Description of the Problem

A major assumption of the least-squares method is that the selected model describes the physical problem perfectly. In practice this condition is almost never fulfilled. Here, the *a priori* assumption is made that the effective radial operator given by Eq. (3.29), portrays an adequate theoretical description of the physical problem. The reliability of this assumption can be established absolutely only by extensive *ab initio* calculations that consider explicitly the electronic structures and interactions of all possible states of a quantum mechanical system. This is clearly not practical here. In general, Eq. (3.29) can be trusted insofar as

a contact transformation of the exact Hamiltonian is valid. This requires that electronic states remain fairly well-separated so that any nonadiabatic interactions can be managed by a second-order nondegenerate perturbation scheme.

The primary objective of the model calculations is to test the general reliability of the mathematical basis in reproducing known Hamiltonian operators from synthetic spectra. This will be of help in assessing the strengths and weaknesses of the HCA and will give an indication of the ranges of reliability of derived functions.

The model problem is designed to approximate closely the situations encountered later in this work, where the procedure is applied to real data. Figure 3.1 portrays a hypothetical layout of three electronic states, labelled X , A , and B . The ground singlet X state possesses no axial electronic angular momentum in its unperturbed configuration. It does, however, gain a net magnetic moment through an interaction with its repulsive $A^1\Pi$ neighbour state. The nonadiabatic mixing is small for the low vibrational levels of the ground state, but becomes quite significant as $X^1\Sigma^+$ vibrational levels approach the dissociation limit, where neutral atomic products are shared by the two electronic states. Also, a unique perturber approximation is made, whereby other $^1\Pi$ states are too far away from $X^1\Sigma^+$ to influence its energy level manifold to the precision of the measurements. The (second-order) energy of interaction from the L -uncoupling can then be given approximately by (124),

$$W'_2 = -J(J + 1)\{B(R)\}^2 \frac{L(L + 1)h^2}{E(\Pi) - E(\Sigma)}, \quad (3.49)$$

where only valence electron excitation contributes to the kinetic energy of the nuclei. This expression bears a striking resemblance to the term

Figure 3.1

Arrangement of electronic states for the model calculations. The system is composed of a valence ground state $X^1\Sigma^+$, a repulsive electronic state $A^1\Pi$ which correlates with the X state dissociation products, and an ionic $B^1\Sigma^+$ state at higher energy.

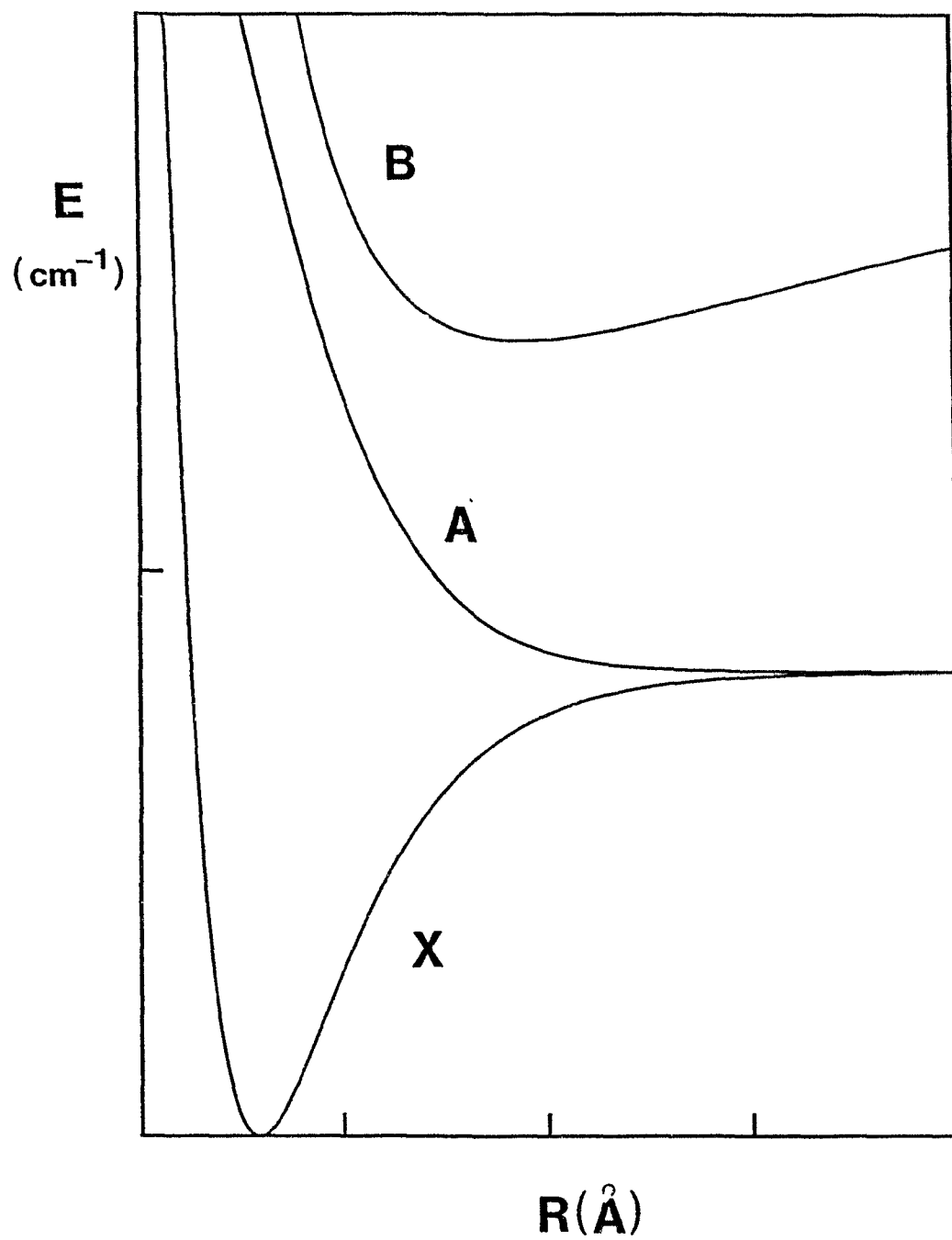


Figure 3.1

$q(R)J(J + 1)$ in the effective operator, Eq. (3.29). In fact, by analogy with a more rigorous treatment (124), $q(R)$ would be given by,

$$q(R) = -4\{B(R)\}^2 \left[2\pi^2 \sum_s N_s m_e \tau_s^2 + \frac{|\langle A^1\Pi | L_x | X^1\Sigma \rangle|^2}{U(A^1\Pi) - U(X^1\Sigma)} \right], \quad (3.50)$$

where the summation is over closed-shell electrons around nuclei of distance τ_s away from the centre of mass. The approximation of pure-precession is not used as it is clearly not realistic for the particular problem at hand

It is evident that the perturbation to bound rotational energy levels will always be negative. This is fully consistent with the second-order Rayleigh-Schrödinger perturbation theory result which dictates that the unperturbed levels of the lower state adjust away (*i.e.* in a negative direction) from the higher-lying perturber. With respect to the electronic state mixing, it is also assumed that the matrix element $\langle A^1\Pi | L_x | X^1\Sigma \rangle$ from which the $L(L + 1)$ term in Eq. (3.49) is derived, is slowly-varying and tends to zero at very small separations and in the limit of dissociation. These arguments are not only helpful in obtaining a reasonable radial variation for the model $q(R)$ function, but also in providing a description that may later be of value in understanding the physics of real molecules.

On the "experimental" front, the emission from the lower vibrational levels of the ionic $B^1\Sigma^+$ state to the upper vibrational levels of the $X^1\Sigma^+$ state has been "studied" photographically in the ultraviolet. The coupling of $B^1\Sigma^+$ to $A^1\Pi$ is assumed to be too small to characterize spectrographically, and mixing of $B^1\Sigma^+$ with high-lying Rydberg states is not of measurable magnitude for the low vibrational levels considered here. The ground state lower vibrational levels are known precisely from Fourier transform spectroscopy,

and an ensuing flame emission "study", examining intermediate vibrational levels, has closed-up the gap between the infrared and ultraviolet data. Spectral data are available both for a hydride HX and its deuteride DX, covering similar energy ranges. The hypothetical halogen atom X has only one stable nuclide. Synthetic spectroscopic information is summarized in Table 3.2. The entire system has admittedly been designed to resemble HF and DF, for reasons that will become apparent as this work progresses.

3.5.3 (d.2) Model Hamiltonians and Synthetic Spectra

Herein, the model molecular systems are defined mathematically. The $X^1\Sigma^+$ valence ground state for the hydride HX has been represented by a Morse potential function, Eq. (2.101), the relevant parameters given in Table 3.3. The potential function of the deuteride has been constructed by adding the simple polynomial form,

$$\Delta U_X^H(R) = \sum_{i=1}^6 h_i (R - R_e)^i, \quad (3.51)$$

to the hydride Morse function. The h_i are listed in Table 3.3. The rotational perturbations from $A^1\Pi$ are described by the nuclear-mass-independent part of the $g(R)$ function, Eq. (3.37), as

$$(\hbar^2/2) \frac{m_e \tilde{R}_H^X(R)}{R^2} = a_2 (R - R_e)^2 + a_3 (R - R_e)^3 + a_4 (R - R_e)^4, \quad (3.52)$$

constructed by considering the theoretical scenario described above. Parameters a_i are listed in Table 3.3. It is assumed that the same functional form (*i.e.* the isotopically invariant part) of $g(R)$ applies to both

TABLE 3.2

Synthetic Spectroscopic Data Base for the Model Calculations

HF	DF
Fourier Transform Infrared Spectra	
Bands: 1-0, 2-0	Bands: 1-0, 2-0
Precision: 0.0002 cm ⁻¹	Precision: 0.0002 cm ⁻¹
Infrared Flame Emission Spectra	
Bands: 1-0, 2-1, 3-2, 4-3, 5-4, 4-2, 5-3, 6-4, 7-4, 8-4, 8-5	Bands: 1-0, 2-1, 3-2, 4-3, <u>5-4</u> , <u>6-5</u> , <u>7-4</u> , <u>8-5</u> , <u>9-5</u> , <u>9-6</u> , <u>10-6</u> , <u>11-6</u> , <u>12-7</u>
Precision: 0.05 cm ⁻¹	Precision: 0.05 cm ⁻¹
<i>B</i> → <i>X</i> Electronic Emission Spectra	
Bands: 0-12, 0-13, 0-14, 0-16, 1-11, 1-15, 1-16, 2-10, 2-14, 2-17, 3-15, 3-17, 3-18, 3-19, 4- 9, 4-10, 4-18, 4-19, 5- 9, 5-13, 6-11, 6-12	Bands: 0-20, 0-21, 0-22, 1-17, 1-18, 1-19, <u>2-12</u> , 2-16, 2-17, <u>3-14</u> , 3-15, 3-16, <u>4-12</u> , <u>4-13</u> , <u>4-14</u> , 5-23, 5-24, 5-25, 6-22, 6-26, <u>7-12</u> , <u>7-13</u> , 8-24, 8-26
Precision: 0.030 cm ⁻¹	Precision: 0.035 cm ⁻¹

Underlined data subsets were excluded in fit II (see text).

TABLE 3.3

Parameters of Hamiltonian Operators for the
Model Calculations^a

Potential Functions	
HF($X^1\Sigma^+$) Eq. (2.101)	HF($B^1\Sigma^+$) Eq. (2.105)
$\mathcal{D}_e = 49\,380\text{ cm}^{-1}$	$\mathcal{D}_e = 45\,000\text{ cm}^{-1}$
$R_e = 0.9168\text{ \AA}$	$R_e = 2.1000\text{ \AA}$
$\beta = 2.382\,704\,898\,3\text{ \AA}^{-1}$	
Radial Range: 0.40 - 4.00 \AA	Radial Range: 1.20 - 4.20 \AA
Number of Points: 2001	Number of Points: 1201
$\Delta U_X^H(R)$ Function, Eq. (3.51)	
$h_1 = -4.20$	$h_4 = 6.02$
$h_2 = 10.16$	$h_5 = -1.47$
$h_3 = -11.60$	$h_6 = 0.14$
$(\hbar^2/2)m_e \tilde{R}_X^H(R)/R^2$ Function, Eq. (3.52)	
$a_2 = -4.0 \times 10^{-3}$	$a_3 = 4.0 \times 10^{-3}$ $a_4 = -2.0 \times 10^{-3}$

^a h_i are in $\text{cm}^{-1}\text{\AA}^{-i}$ units and a_i in units of $\text{amu}^2\text{cm}^{-1}\text{\AA}^{-i}$.

isotopomers. This implies that only contributions from $\tilde{R}_H^X(R)$ in Eq. (3.30) are considered spectroscopically significant.

$B^1\Sigma^+$ is assumed to be a Born-Oppenheimer state. Its representation has been chosen to reflect the ionic nature of the interaction, and is given by a Fues-Kratzer potential, Eq. (2.105), with R_e and \mathcal{D}_e given in Table 3.3.

Following the construction of model operators, the point spectra (eigenvalues) were obtained. The ground state rovibrational eigenvalues for the two isotopomers were obtained through numerical solution of the radial wave equation, whereas the eigenvalues for the $B^1\Sigma^+$ state were obtained directly from Eq. (2.106). The spectra described briefly above were then calculated from the true eigenvalues, normally distributed zero-mean random errors were generated using the Box-Muller method (125) and added onto the synthetic line positions. These errors are known precisely and facilitate a later comparison with the fitted values.

3.5.3 (d.3) Trial Operators and Least-Squares Fit

Although trial operators for a real data set are normally found from least-squares estimates of the molecular constants, this was not required for the model calculations; it sufficed to identify the quantum mechanical definitions of the traditionally derived rotational constants and vibrational term values. In defining properly the true rotational constant of the ground state, it is helpful to write,

$$E_w = G_v + B_v[J(J + 1)] - D_v[J(J + 1)]^2 + H_v[J(J + 1)]^3 + \dots, \quad (3.53)$$

so that the partial derivative

$$\frac{\partial E_{vJ}}{\partial [J(J+1)]} = B_v - 2D_v[J(J+1)] + 3H_v[J(J+1)]^2 + \dots, \quad (3.54)$$

evaluated at $J = 0$, gives precisely the rotational constant B_v . This partial derivative may be estimated by applying the Hellmann-Feynman theorem with $\lambda = J(J+1)$ to yield,

$$B_v = \left[\frac{\partial E_{vJ}}{\partial [J(J+1)]} \right]_{J=0} = \langle \psi_v | \left[\frac{\partial U_J(R)}{\partial [J(J+1)]} \right]_{J=0} | \psi_v \rangle, \quad (3.55)$$

where, as a result of the heterogeneous mixing,

$$U_J(R) = U_0(R) + \beta^2 J(J+1)[1 + q(R)]/R^2. \quad (3.56)$$

Evaluation of the partial derivative on the right-hand side of Eq. (3.55), gives

$$B_v = \beta^2 \langle \psi_v | [1 + q(R)]/R^2 | \psi_v \rangle, \quad (3.57)$$

which is composed of the usual mechanical R^{-2} expectation value, and a nonmechanical contribution, $\beta^2 \langle q(R)/R^2 \rangle_v$. Identical results are obtained by applying the first-order Rayleigh-Schrödinger perturbation expression, showing once again the intimate relationship between the HFT and ordinary perturbation theory. It is important to realize that a conventional Dunham-style rotational analysis would estimate precisely these constants, as the energy levels, however parametrized, reflect fully the L -uncoupling effects. The constants of Eq. (3.57) can then be safely regarded as the experimental constants, demonstrating the futility of performing time consuming band-by-band and merge fits. However, it is only fair to comment that constants obtained traditionally would be slightly different than these quantum mechanical constants owing to interparameter correlations and truncation of the series in the least-squares procedure. At the same time,

for the lowest-order constants B_v , these should be of the order of the uncertainties. The true rotational constants were thus calculated and the vibrational terms, G_v , were obtained by numerical integration of the radial wave equation with $U_0(R)$, the true rotationless potential. The G_v , B_v pairs were employed to calculate first-order RKR curves which serve as the trial potentials.

In order to introduce uncertainty in the RKR calculations, the rotational constants and the vibrational term values were truncated at the fourth and second decimal places, respectively. Additional error arises from the use of a simple first-order RKR procedure, although for the Morse potential this would be very small, as there exists an exact quantization condition for this oscillator, which resembles that of Bohr and Sommerfeld (126). This can be expected also by calculating the Dunham Y_{00} correction, which turns out to be zero, suggesting that the third-order JWKB contributions are small, at least near the minimum. The eight-point interpolation of Lagrange introduces yet more error, and finally, the RKR potential for $X^1\Sigma^+$ was purposely extrapolated to a false dissociation limit, 20 cm^{-1} lower than the true value. This might be a common problem for hydride molecules, as the dissociation energy is rarely known with more certainty, chiefly due to the relatively sparse distribution of vibrational levels near dissociation. With the pointwise trial potential known, it is possible to calculate exactly what correction is required to give back the model potential. The main objective of the model testing is to examine to what extent the least-squares procedure employed here can recover the model functions. RKR calculations were also carried out for the $B^1\Sigma^+$ state employing rotational constants which were simple expectation values of R^{-2} .

For the $B^1\Sigma^+$ state, a dissociation energy 2000 cm^{-1} lower than the true limit was assumed.

In order to set up the least-squares problem to take into account data for two isotopomers simultaneously, the rotationless potential functions for $X^1\Sigma^+$ resulting from such an analysis are written as,

$$U_X^{\text{eff}}(R)_{\text{HX}} = U_X^0(R)_{\text{HX}} + \Delta U_X(R), \quad (3.58)$$

$$U_X^{\text{eff}}(R)_{\text{DX}} = U_X^{\text{eff}}(R)_{\text{HX}} + \Delta U_X^{\text{H}}(R), \quad (3.59)$$

where $\Delta U_X^{\text{H}}(R)$ relates the hydride and deuteride effective functions. For the Born-Oppenheimer $B^1\Sigma^+$ state,

$$U_B^{\text{eff}}(R)_{\text{HX,DX}} = U_B^0(R)_{\text{HX}} + \Delta U_B(R), \quad (3.60)$$

for both isotopomers. The ground state rotational perturbations can be handled simultaneously for both HX and DX, having already made the approximation that the halogenic contribution to $q(R)$ is spectroscopically insignificant. Thus, the relationship

$$q_X^{\text{HX}}(R) = (M_{\text{D}}/M_{\text{H}})q_X^{\text{DX}}(R), \quad (3.61)$$

is built into the fit.

The mathematical model employed in the representation of correction functions is given by Eq. (3.40). Table 3.4 lists the basis functions that represented correction functions in the least-squares fit. Initial fits were concerned with finding an adequate representation for the basic correction functions, $\Delta U_X(R)$ and $\Delta U_B(R)$, as well as for the function $g_X(R)$, by employing a small representative hydridic data base. This was accomplished by numerous trial and error fits. Once satisfactory representations of these functions were obtained, a partial representative data base for both isotopomers was set

TABLE 3.4
Basis Functions for Model Calculations

$X^1\Sigma^+$ State	
$\Delta U_X(R)$	$\Delta U_X^H(R)$
$G_{v=0}^{\text{inn}}$ and $G_{v=3}^{\text{inn}}$	F_{X11} and F_{X31}
F_{X42} , F_{X62} and F_{X82}	F_{X12} , F_{X32} , F_{X52} , F_{X72} ,
$G_{v=0-13}^{\text{out}}$	and F_{X92}
S_X	S_X^H
$g_X(R)$	$\Delta U_B(R)$
H_{X4} , H_{X5} and H_{X6}	F_{B41} , F_{B61} and F_{B81}
	F_{B32} , F_{B52} , F_{B72} , F_{B92}

The functions are defined in the text by Eqs. (3.42, 3.44, 3.45, 3.46, and 3.48). The superscripts ^{inn/out} refer to Gaussian functions centered on inner/outer turning points of the vibrational levels denoted as subscripts. The subscripts X/B for functions F identify the electronic state.

up. Numerous subsequent fits optimized the additional functions required to take the effective hydride functions to those of the deuteride. Finally, the entire data set was included in a two-isotopomer fit.

Before a comprehensive discussion is made of the results, it is helpful to summarize briefly the final findings. The reduced standard deviation, which is defined as,

$$\hat{\sigma}_{red} = (1/f) \sum_i \left\{ \frac{(\nu_{obs}^i - \nu_{fit}^i)^2}{\epsilon_i^2} \right\}^{1/2}, \quad (3.62)$$

with f being the degrees of freedom and ϵ_i the measurement error of the i^{th} line position, is ideally $\hat{\sigma}_{red} = 1$, for a model representing the data within the precision of the measurements, on average. The value obtained here in fit A (complete data base) was $\hat{\sigma}_{red} = 1.07$, which is considered satisfactory. Some numerical results of interest are summarized in Table 3.5; with a full data set, the ability of the method to extract the model electronic term value is excellent. However, the fact that the final equilibrium bond lengths are, for the ground state, further away from the model values than the trial estimates is somewhat disconcerting. It can be noted, however, that the fitted difference, $R_e^{\text{HX}} - R_e^{\text{DX}}$, was obtained very accurately.

A second data base was collected, excluding all spectroscopic information for the deuteride in the region $\nu = 5-14$ of the ground electronic state. This simulates the situation which is found for the spectral data base of the diatomic DF, considered later in this thesis. A subsequent least-squares fit (B), gave a reduced standard deviation identical to that of fit A. Moreover, it was found (Table 3.5) that the electronic term values of the $B^1\Sigma^+$ state were obtained in very good agreement with the model parameters, despite the gap of several thousand wavenumbers in $\text{DX}(X^1\Sigma^+)$. The interpolated data were

TABLE 3.5

Results of the Model Calculations: Radial Functions

Quantity	HF	DF
$R_e^{\text{mod}}(X^1\Sigma^+)$	0.916 800 0 Å	0.916 807 5(1) Å
$R_e^{\text{fit}}(X^1\Sigma^+)$	0.916 791 7(1) Å	0.916 799 3(1) Å
$R_e^{\text{mod}}(B^1\Sigma^+)$	2.100 0 Å	
$R_e^{\text{fit}}(B^1\Sigma^+)$	2.099 999 5(5) Å	
$T_e^{\text{mod}}(B^1\Sigma^+)$	84 780.00 cm ⁻¹	84 800.00 cm ⁻¹
	FIT I	
$T_e^{\text{fit}}(B^1\Sigma^+)$	84 780.01(2) cm ⁻¹	84 799.98(2) cm ⁻¹
	FIT II	
$T_e^{\text{fit}}(B^1\Sigma^+)$	84 779.98(3) cm ⁻¹	84 799.88(6) cm ⁻¹

Quantities X^{mod} and X^{fit} are associated with the model and fitted operators, respectively. R_e is the equilibrium bond length and T_e is the term value of $B^1\Sigma^+$.

typically within two to three standard measurement errors.

Results for selected J for a representative model band, the 4-14 electronic band of DX, are shown in Table 3.6. The random normally distributed errors $\Delta\bar{\nu}_{\text{err}}$ added onto the synthetic line positions are shown to be in better than expected agreement with the fitted residuals, $\Delta\bar{\nu}_{\text{fit}}$. This situation is typical of the vast majority of line positions and is indicative of the large flexibility of the mathematical model. This shows the ability of the procedure in representing accurately spectroscopic line positions subject to random error. From the application of the procedure to real data, later in this work, it is found that systematic error is also readily detected.

The ability of the procedure to predict energies and widths of quasibound states is shown by the results given in Table 3.7. It is particularly interesting to note that for the levels $(v, J) = (24, 29)$ and $(v, J) = (25, 26)$ of DX, which were not sampled by the least-squares fit, the agreement in the widths is nevertheless satisfactory. It should be mentioned, however, that several line positions associated with high-lying orbiting resonances, could not be fitted by the model and had to be excluded from consideration. There does not appear to be any distinguishing characteristic linking these levels together. While they all have fairly short lifetimes, levels with even shorter lifetimes were included in the fit and represented satisfactorily. Perhaps these problems are associated with local discrepancies between the true and fitted correction functions.

3.5.3 (d.4) *Radial Functions and Discussion*

Substantial effort with trial and error optimization was required to provide the success described above for the model calculations. During the

TABLE 3.6

Results of Least-Squares Fit for the Model DF 4-14 ($B \rightarrow X$) Band

J	P -Branch (cm^{-1})			R -Branch (cm^{-1})		
	$\bar{\nu}_{\text{mod}} + \Delta\bar{\nu}_{\text{err}}$	$\Delta\bar{\nu}_{\text{err}}$	$\Delta\bar{\nu}_{\text{fit}}$	$\bar{\nu}_{\text{mod}} + \Delta\bar{\nu}_{\text{err}}$	$\Delta\bar{\nu}_{\text{err}}$	$\Delta\bar{\nu}_{\text{fit}}$
0				51780.361	0.065	0.072
4	51662.825	0.027	0.033	51697.194	-0.041	-0.035
8	51393.582	-0.037	-0.033	51458.358	-0.002	0.002
12	50973.535	-0.082	-0.081	51068.081	-0.020	-0.020
16	50410.245	-0.004	-0.007	50533.660	-0.010	-0.013
20	49713.670	-0.037	-0.042	49864.980	-0.043	-0.049
24	48896.913	0.024	0.016	49074.877	0.024	0.015
28	47975.435	-0.014	-0.027	48178.587	-0.042	-0.055
32	46967.943	0.016	-0.002	47194.756	0.023	0.006
36	45896.094	0.004	-0.013	46144.908	0.103	0.086
40	44785.619	-0.010	-0.018	45054.435	-0.006	-0.012
44	43667.558	-0.036	-0.038	43954.653	0.031	0.031
48	42581.491	-0.034	-0.039	42884.820	-0.032	-0.034
52	41583.730	0.065	0.071	41901.408	0.047	0.056

$\bar{\nu}_{\text{mod}}$ are line positions synthesized from the eigenvalues of the model operators. $\Delta\bar{\nu}_{\text{err}}$ are the random normally distributed errors and $\Delta\bar{\nu}_{\text{fit}}$ represent the fitted residuals.

TABLE 3.7

Results of the Model Calculations: Energies and Widths
of Selected Quasibound Levels

v	J	E^{mod}	$\Gamma_{\text{fwhm}}^{\text{mod}}$	E^{fit}	$\Gamma_{\text{fwhm}}^{\text{fit}}$
HF($X^1\Sigma^+$)					
10	40	51 617.77	0.30	51 617.76	0.30
11	38	51 390.69	1.71	51 390.70	1.73
12	35	50 831.06	0.11	50 831.07	0.12
13	33	50 704.76	1.49	50 704.77	1.55
14	30	50 318.86	0.27	50 318.86	0.30
15	27	50 023.86	0.08	50 023.85	0.06
16	24	49 812.24	0.06	49 812.22	0.04
17	21	49 671.96	0.15	49 671.76	0.11
18	17	49 463.07	0.09	49 463.00	0.08
19	14	49 454.01	1.46	49 454.09	1.33
v	J	E^{mod}	$\Gamma_{\text{fwhm}}^{\text{mod}}$	E^{fit}	$\Gamma_{\text{fwhm}}^{\text{fit}}$
DF($X^1\Sigma^+$)					
*24	29	49 746.69	0.30	49 746.81	0.19
*25	26	49 667.91	1.02	49 668.69	0.81
26	21	49 478.25	0.13	49 478.24	0.11

Quantities X^{mod} and X^{fit} are associated with the model and fitted operators, respectively. E (cm^{-1}) are the eigenenergies and Γ_{fwhm} (cm^{-1}) are the full widths at half intensity maximum. Levels marked with an asterisk (*) were not represented in the least-squares fits.

course of this intermediate phase of the analysis it was possible to identify some interesting aspects of the physical problem which deserve some discussion.

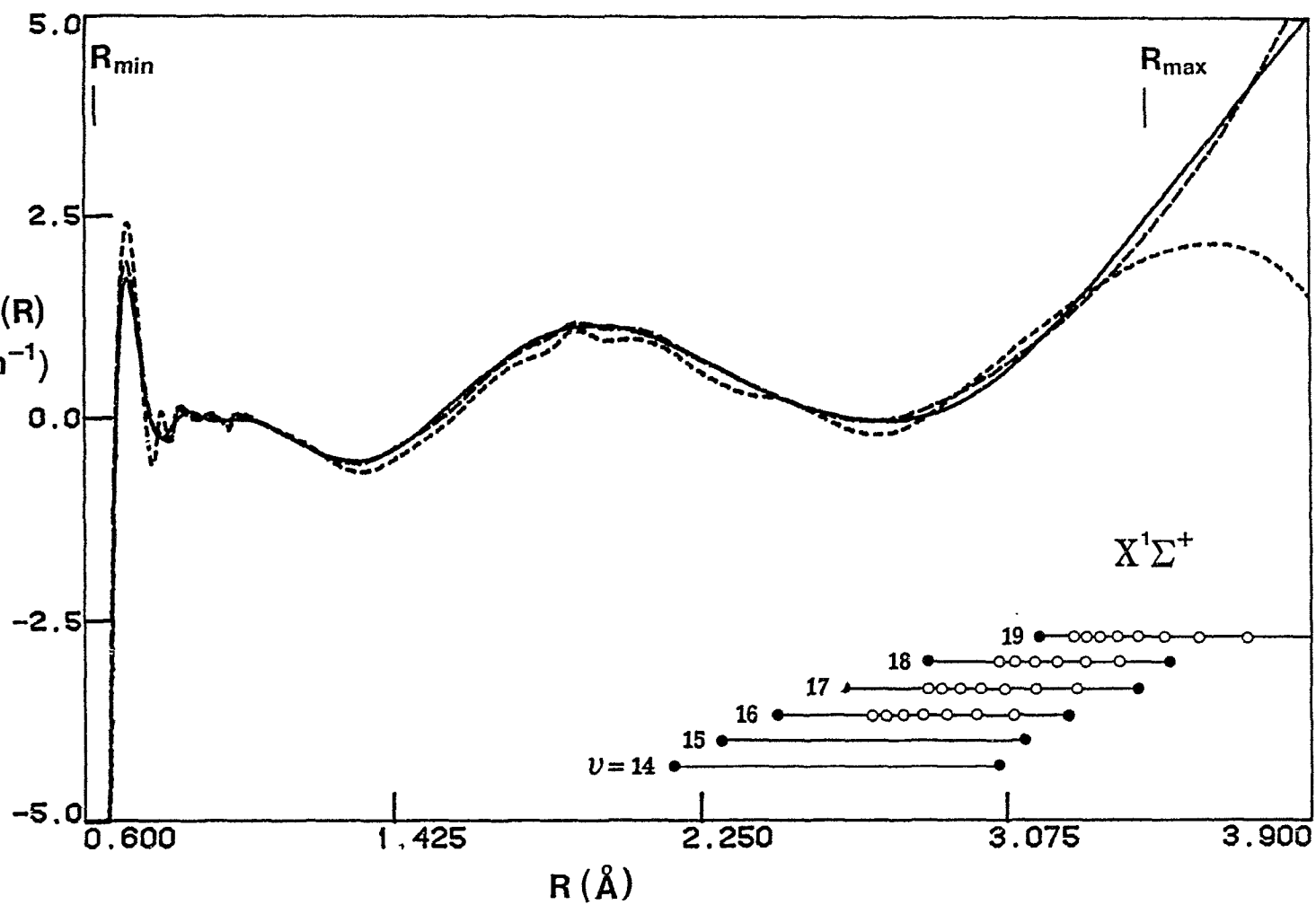
Since information pertaining to energy is employed to determine the radial variation of elements of the Hamiltonian operators, it seemed natural to consider a mapping of the vibrational-rotational energy eigenvalues onto the radial domain. This can be achieved by linking the energy levels to the classical turning points of motion for the outer limb, or to the internuclear separations at which the probability function $\psi_{v,J}^2(R)$ has decreased to a small percentage (*e.g.* 10%) of the outermost peak magnitude. The resulting distribution peaks at mid- v,J and finds the highest vibrational-rotational levels relatively isolated and sparsely distributed. Determining a correction function at large- R then places a large burden on these few implicitly outweighed levels. While low- v,J levels near the potential minimum are also somewhat similarly distributed, these are often more precisely studied. The total weighting, then, derives explicitly from the precision of the data and the frequency of observation, and implicitly from the distribution of levels along the radial coordinate.

A number of correction functions were obtained in various fits, differing only slightly from the true correction at short/large- R , while providing equally satisfactory representation of the data. This demonstrates the expected difficulties in obtaining a unique solution of the radial functions in regions of lower weights. Fortunately, it was also noted that as statistical correlations among fit parameters were reduced, by careful choice of basis functions, the fitted corrections reproduced the true functions essentially exactly. The nonuniqueness problem is depicted in Figure 3.2,

Figure 3.2

The correction function $\Delta U_X(R)$ for the model calculations. The solid line represents the model correction function and the broken lines are functions obtained in two independent fits (see text). R_{\min} and R_{\max} are the innermost and outermost turning points respectively, obtained by considering all the fitted E_{vJ} . Filled circles represent the radial distances where the probability function $\psi_{vJ}^2(R)$ declines to 10% of its value at the outermost maxima for $J = 0$ and $J = J_{\max}$ of given v . For HF vibrational levels $v = 16-19$, the open circles indicate the analogous positions for other high- J rotational levels, with J decreasing in steps of unity from J_{\max} .

Figure 3.2



which shows two fitted $\Delta U_X(R)$ functions, both representing the line positions equally well, but with only one being a good representation of the true radial correction functions, also shown in the figure. Some indication is given of the distribution of the higher rovibronic levels along the radial coordinate, which helps in rationalizing the onset of nonuniqueness with a sharp decline in the distribution. The range defined by R_{\min} and R_{\max} in Fig. 3.2, is that of the innermost and outermost turning points obtained by considering all the fitted E_{vJ} .

The agreement between the fitted and model $g(R)$ functions is also very good, as shown in Fig. 3.3. The systematic disagreement at large- R is due to the rapidly diminishing implicit weighting in this region. For the functions $\Delta U_B(R)$ and $\Delta U_X^H(R)$, Figures 3.4 and 3.5 show excellent agreement in regions of ample weighting, but exhibit clear disagreement at both extremities of the function, where only a relatively few (implicitly outweighed) line positions influence the determination of the functions. It is interesting to note, however, that the disagreement for the two limbs is of opposite sign; it is hence found that the model *eigenvalues* are predicted considerably better, despite the nonuniqueness in the determination of the radial functions at small/large- R .

Although it is essential to choose radial ranges for the generation of first-order perturbation expectation values (Hellmann-Feynman/least-squares partial derivatives) which sample the rovibrational eigenfunctions adequately, it is not expected that the fitted corrections will be physically meaningful in this entire range of R . While this would be the case for a perfect model, the collective results of the model testing indicate clearly that the true functions fall within the 95% confidence intervals of the fitted functions in

Figure 3.3

The isotopically invariant component of the ground state $g(R)$ function for the model calculations. The solid curve represents the model function and the two broken curves give the 95% confidence limits of the fitted function. For the definitions of R_{\min} and R_{\max} and the filled circles see the legend to Figure 3.2.

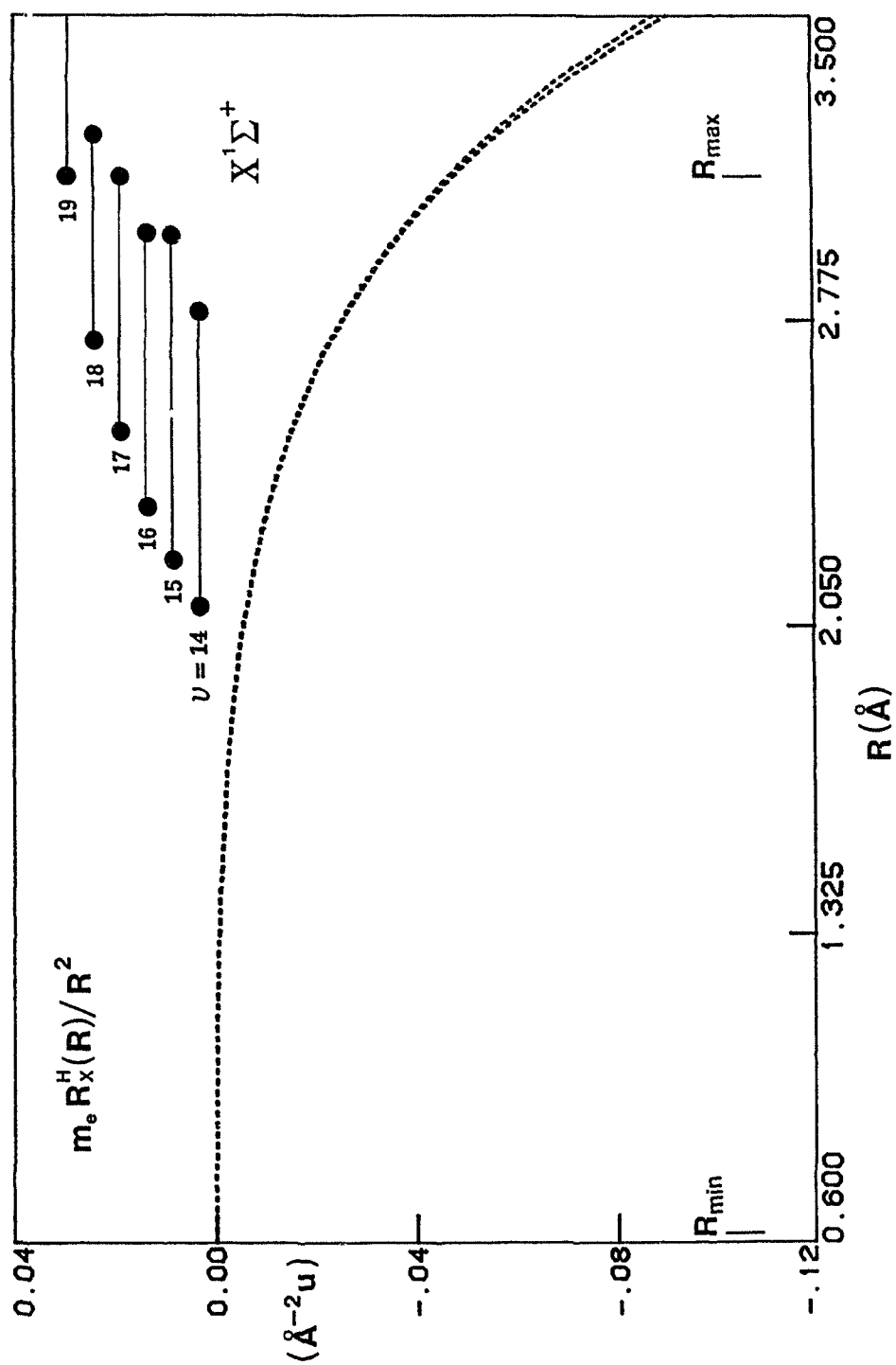


Figure 3.3

Figure 3.4

The function $\Delta U_{\text{B}}(R)$ for the model calculations. The solid curve represents the model correction and the two broken curves represent the 95% confidence limits of the fitted function. For the definitions of R_{min} and R_{max} and the filled circles see the legend to Figure 3.2.

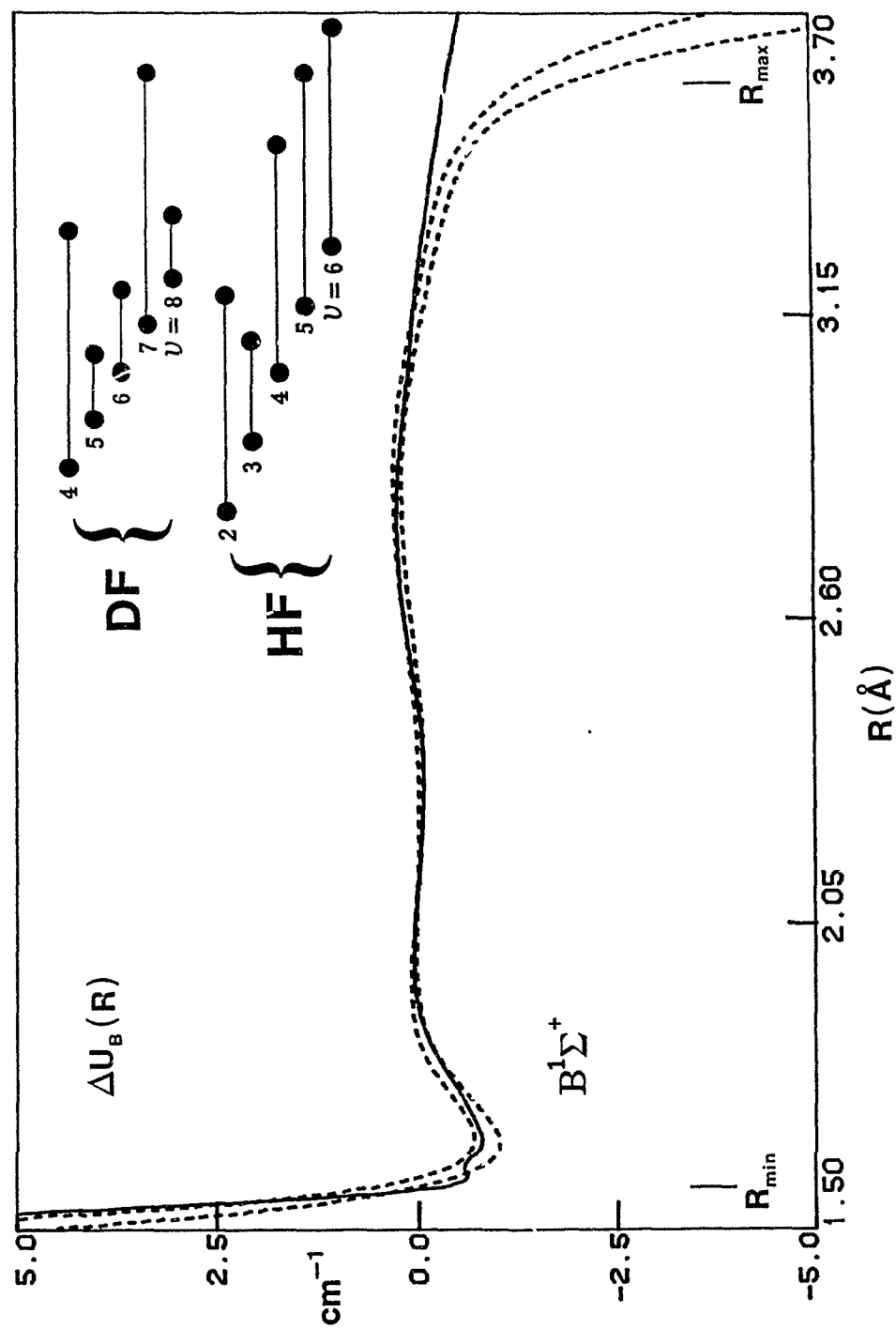


Figure 3.4

Figure 3.5

The function $\Delta U_X^H(R)$ for the model calculations. The solid curve represents the model correction and the two broken curves represent the 95% confidence limits of the fitted function. For the definition of R_{\min} and R_{\max} and the filled circles see the legend to Figure 3.2.

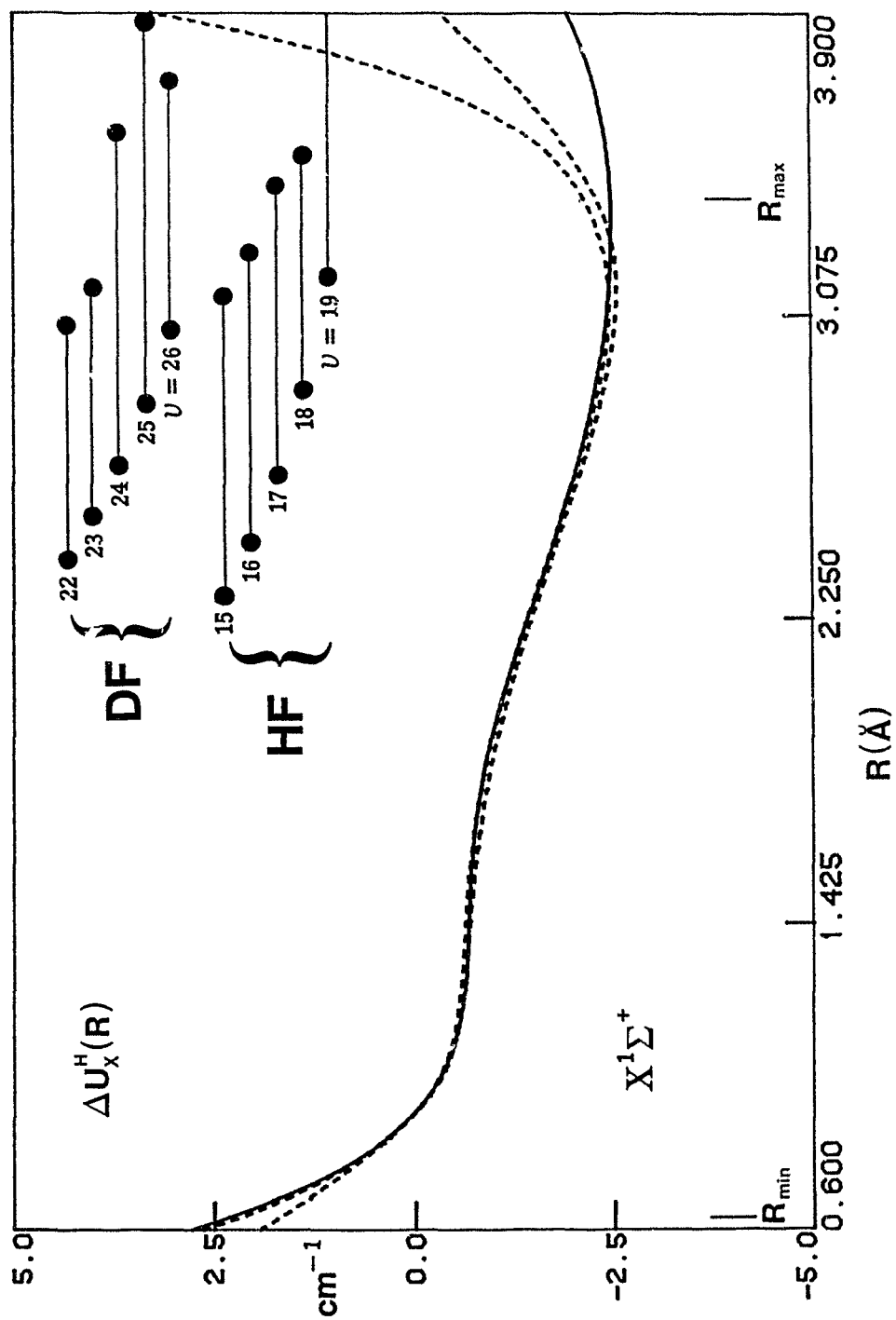


Figure 3.5

a slightly less extensive range of R . It is found that the innermost and outermost classical turning points (R_{\min} and R_{\max}), obtained by considering all the fitted eigenvalues, define a more realistic range of R for a statistically meaningful determination of the correction functions. It is evident that outside this range, the calculated statistical confidence limits have little significance.

In summary, the overall results of the model testing are very satisfactory and quite enlightening. While the intermediate regions of the fitted corrections are trustworthy, the extreme inner and outer sections of the derived potential functions are less reliable and should be regarded with caution. This is partly due to the inherent nonuniqueness of the central field problem, which unavoidably correlates the corrections on the inner and outer limbs, and also due to a slight inadequacy of the mathematical correction model. In regions of low weighting, the procedure is more committed to the determination of a unique set of eigenvalues than unique determinations of the radial variations of the Hamiltonian operator elements. The uniqueness in the determination of radial functions can be improved by careful choice of basis functions as to decrease interparameter correlations, and hence also by the careful choice of trial operators.

CHAPTER 4

ROTATIONAL ANALYSIS OF THE $B^1\Sigma^+ - X^1\Sigma^+$

EMISSION BANDS OF $D^{35}\text{Cl}$

4.1 Introduction

The $X^1\Sigma^+$ state of HCl/DCl is not a pure covalent state. While it does yield neutral products upon dissociation, its chemical properties in the ground vibronic level reflect some degree of ionicity. This is due to an avoided crossing with the excited $B^1\Sigma^+$ state, as a recent *ab initio* study has shown (127). The ground state is mainly ionic, $4\sigma^2 2\pi^4 5\sigma^2$, at small (≤ 3.5 bohr) internuclear separations while at larger bond lengths (≥ 5.2 bohr) the $4\sigma^2 2\pi^4 5\sigma 6\sigma$ valence configuration is dominant. Contributing in the intermediate internuclear separation region is yet a third configuration, $4\sigma^2 2\pi^4 6\sigma^2$, peaking at about 15% of the total contribution at approximately 4.8 bohr. The valence contribution increases rapidly at large R leading to the neutral dissociation products $\text{Cl}(^2P) + \text{H}(^2S)$. Correspondingly, the $B^1\Sigma^+$ interaction is valence at small separations, becoming increasingly ionic at long-range and yielding the products $\text{Cl}^-(^1S) + \text{H}^+$. Also, at very small (≈ 1.5 bohr) internuclear distances, the B state intersects a set of tightly bound Rydberg states which converge gradually to, and resemble, the $\text{HCl}^+(X^2\Pi)$ core in character.

A single electron ($\pi \rightarrow \sigma^*$) excitation gives rise to the $A^1\Pi$ repulsive state, lying between $X^1\Sigma^+$ and $B^1\Sigma^+$ and sharing neutral dissociation products with $X^1\Sigma^+$. This state contributes heterogeneously to the energy level manifold of the ground state in a rotationally dependent fashion. The smooth

vibrational dependence of this effect makes it impossible to detect the $A - X$ interaction from a spectroscopic analysis based on molecular constants for a single isotopomer. Figure 4.1 shows some of the low-lying electronic states of HCl(DCl) . The experimental spectrum (128) displays severe local perturbations beginning approximately above $v = 9(13)$ for HCl(DCl) of the $B^1\Sigma^+$ state due to interactions with the neighbouring Rydberg states.

The ground electronic state of hydrogen chloride has been the subject of numerous spectroscopic studies. Very precise molecular constants are available for the lowest vibronic level (129). Far-infrared transitions in $v'' = 0$ have been studied by tunable laser techniques and serve as reliable spectral standards. The first eight vibrational levels are known well from experiment and the higher vibrational levels ($7 \leq v'' \leq 17$) have been characterized by the rotational analysis of Coxon and Roychowdhury (130). These authors observed emission from the lower ($0 \leq v' \leq 6$) levels of the B state. The $B^1\Sigma^+$ state has also been detected in absorption from $v'' = 0$ of the ground state by Douglas and Greening (128). The higher vibrational levels accessed in this study were found to be highly perturbed so that the quoted molecular constants must be viewed with caution. This study also reported fragmentary structure attributed to several high-lying Rydberg states.

The spectroscopic characterization of the $X^1\Sigma^+$ state of DCl is less well established. Only levels with $v'' = 0-5$ have been studied experimentally and no information is available for the higher vibrational levels, the emission from $B^1\Sigma^+$ not having been hitherto observed. A principal aim of the present work is therefore to provide an analysis of the $B - X$ system of DCl in emission to complement the information already available for the hydride (130). A combined treatment of HCl and DCl line positions will result

Figure 4.1

Arrangement of low-lying electronic states of HCl(DCl). The potentials for $X^1\Sigma^+$ and $B^1\Sigma^+$ are RKR curves (130). All other potentials were taken from an *ab initio* study (127).

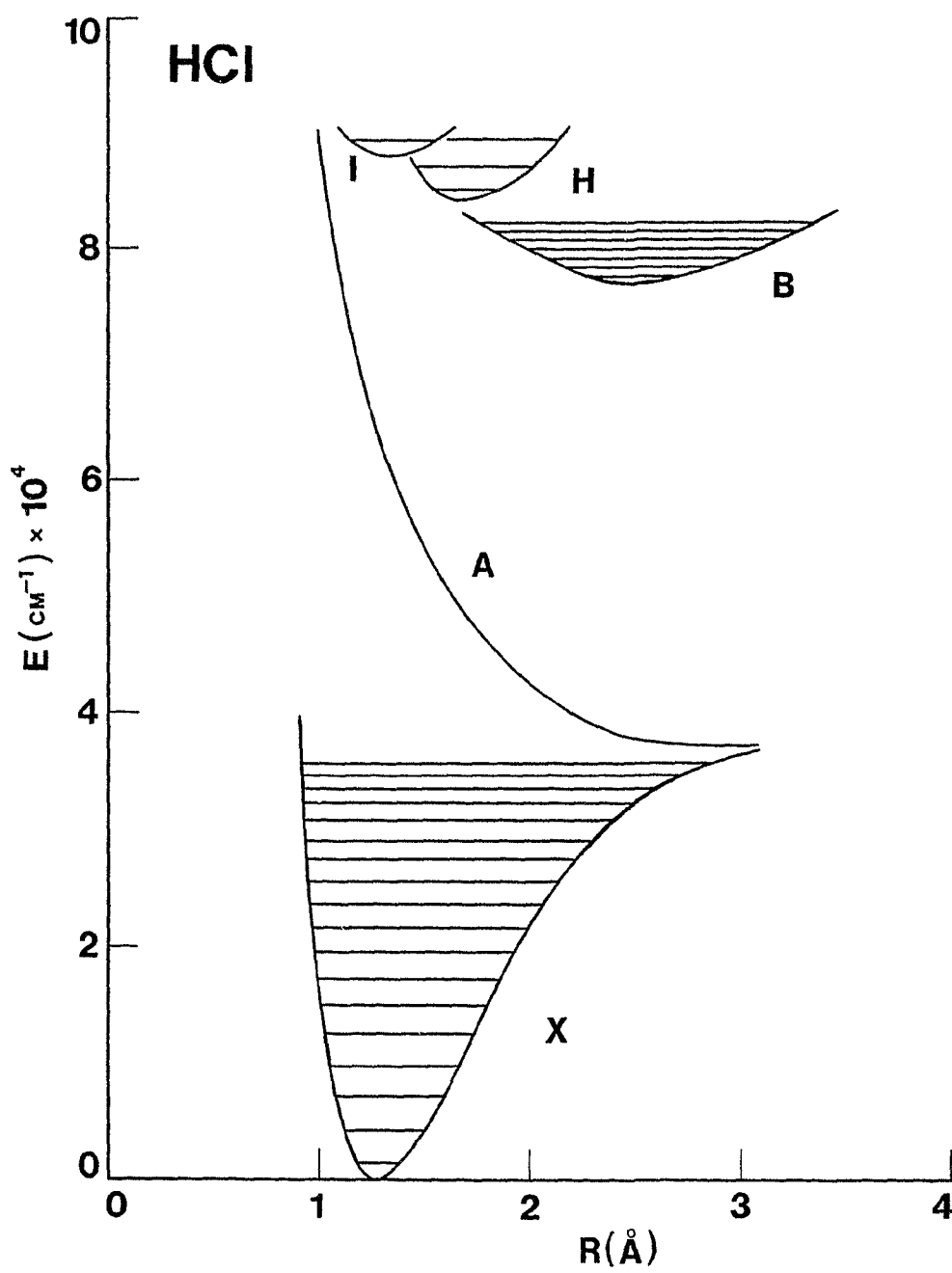


Figure 4.1

in radial Hamiltonian operators for each isotopomer and will allow for a reliable extrapolation to the energy levels of tritium chloride, as well as providing an improved understanding of the electronic structures of HCl/DCI.

4.2 *Experimental Details*

Experimental spectroscopy in the ultraviolet region is faced with special problems. The strongly absorbing $B^3\Sigma_u^- - X^3\Sigma_g^-$ (Schumann-Runge) band system of atmospheric oxygen in the 1950-1759 Å region interferes even if air is present at very low concentrations. Carbon dioxide and water vapour absorb below 1750 Å and molecular nitrogen poses problems below 1450 Å (131). Thus for meaningful spectroscopic work below 2000 Å, it is necessary to evacuate the chamber containing the dispersive element and the detector.

The pioneering work of Victor Schumann (131) was instrumental in establishing a sound understanding of the special problems of vacuum ultraviolet (VUV) spectroscopy. Schumann recognized that ordinary quartz optics become opaque below 1850 Å and employed fluorite prisms instead. Since the gelatin based emulsions employed traditionally also become opaque around 1850 Å, Schumann developed photographic plates which were essentially free of gelatin. Having established methodology with respect to optics, medium and detectors, Schumann can be regarded as the founder of VUV spectroscopy.

The emission spectrum of DCI in the ultraviolet has been recorded with the 10.7-m vacuum spectrograph at the Herzberg Institute of Astrophysics. A detailed account of the construction and operation of this instrument has been published (132). It is useful, however, to review briefly some important features. The general layout of the spectrograph is shown in Figure 4.2. The entrance slit, diffraction grating, and photographic plate holder all lie

Figure 4.2

Schematic of the 10.7-m concave grating vacuum spectrograph.

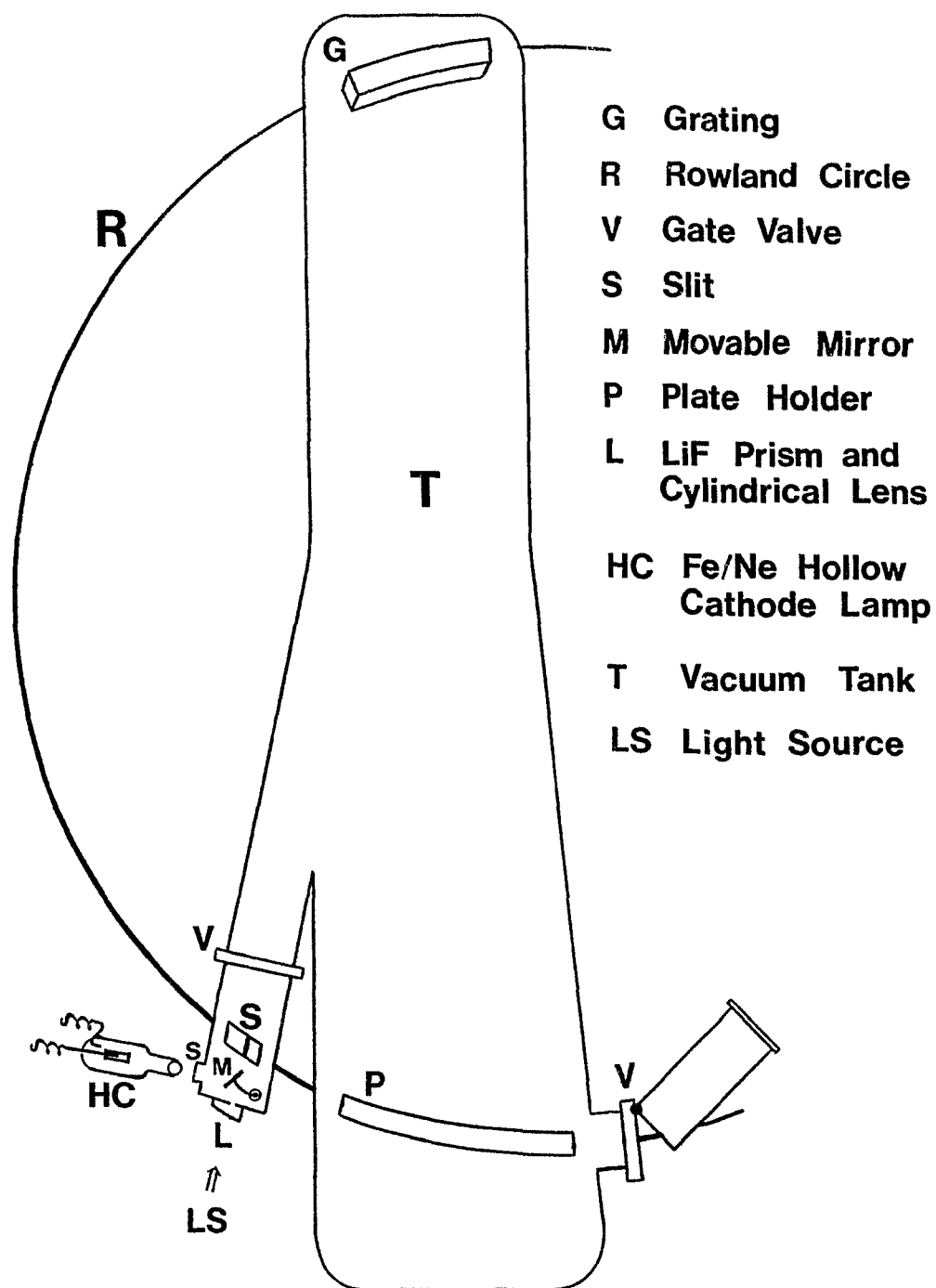


Figure 4.2

along the perimeter of what is known as a Rowland circle (131). The radius of curvature of the concave dispersion element is 10.685-m and its ruled area is 198×100 mm. The slightly curved plate holder is 93-cm long and can hold two 5×45 cm photographic plates. The entire assembly is contained within a vacuum tank a little over 11-m in length and equipped with a powerful pumping system composed of a parallel arrangement of a 22-cm Edwards 1500 L/s oil diffusion pump and a 52 L/s Kinney mechanical pump. In addition to this "fast system", there is a "stand-by system" consisting of a 15-cm National Research Corp. fractionating pump backed by a 5-cm Edwards diffusion pump and a 0.9 L/s Kinney mechanical pump. The plate holder assembly can be isolated from the rest of the tank by means of a gate valve, so that changing photographic plates can be accomplished without subjecting large parts of the tank surface to the atmosphere.

The slit is also associated with a gate valve so that changes to its height and width can be made without breaking the vacuum in the tank; it is thus possible to operate the spectrograph for months without significant contamination from atmospheric gases. Since inert gases are transparent far into the ultraviolet (131), for certain studies it is possible to "flush" the surface of the grating with a steady stream of argon or helium. Two gratings were employed for the present study. The first is a 600 line/mm grating blazed at $11\,600 \text{ \AA}$. Blazing is a process whereby the shape of the ruled groove is adjusted to cause the incident intensity to diffract with the highest possible efficiency at a particular angle (133). This grating has been coated with MgF_2 in order to increase its reflectivity at approximately 1200 \AA . A 1200 line/mm platinum coated grating blazed at 1200 \AA was employed in its first-order for lower resolution exploratory work. This grating is

particularly helpful for the vacuum ultraviolet region owing to the high reflectivity of platinum at such wavelengths, and was used by Di Lonardo and Douglas in recording the electronic absorption spectrum of HF (87).

The $B^1\Sigma^+$ state was populated by flowing DCl (Matheson, 99.9% purity) and helium (Matheson, 99.995%) through a 2450 MHz microwave discharge, at total pressures of about 5 Torr. Order separation was attempted by predispersing and refocussing the emission onto the 20- μ m slit of the 10.7-m concave grating vacuum spectrograph. Spectra were recorded in the wavelength region 1660 to 2400 Å in the fourth to sixth orders of the 600 line/mm grating. Kodak SWR and 103a-0 as well as Ilford Q2 photographic plates were used with exposure times ranging from 7 min to 2½ hr and reciprocal dispersions of 0.018 to 0.035 nm/mm. The exposed plates were subsequently developed and photographic prints of all the spectra were obtained.

Measurement of the plates was made with the aid of a comparator accompanied by an oscilloscope display of the spectral line profiles. Atomic calibration lines were measured during the same sessions as the molecular lines to avoid any systematic shifts in the vacuum wavenumbers from different plates. Each plate required three separate measuring sessions and care was exercised to obtain slightly overlapped measurement regions between sessions so that any systematic shifts could be readily detected. The position of the plate along the platform was automatically punched onto a card after a conversion of the (analog) comparator translation wheel position into a digital signal. Additional information, relating to the relative intensity and shape characteristics of spectral line contours were manually punched onto cards. The cards were assembled and the information was transferred onto magnetic tape so it could be more easily manipulated.

4.3 Wavelength Calibration

The first step of the analysis involved wavelength calibration of the molecular line positions. Initial efforts were concerned with the identification of atomic lines from the measurements with the vacuum wavelengths of Crosswhite (134). Here, the photographic prints were very useful, but it was found that the job of identifying manually lines recorded in overlapping orders was very time consuming, with an average processing time of several hours for the results of each measuring session. Thus, the task of identifying atomic line measurements with standards, the least-squares construction of a dispersion curve relating the distance along the plate with the vacuum wavelength, and the generation of vacuum wavenumbers for molecular line measurements, were combined into an automated computer program.

Program SPECTRUM (Appendix A-1) accomplishes the same tasks as the preliminary manual analysis in a matter of a few minutes. A brief description follows here, and is extended by comment statements in the source listing. The spectral order containing most assignments was selected (*e.g.* 3rd) and approximate dispersion curve coefficients were used to make additional identifications and improve the preliminary dispersion curve. This iterative increase of identifications was carried out in an interactive fashion as the desired convergence was in a few cases not immediately realized, with fits latching-on to false dispersion curves. In such cases, the program was halted and a manual least-squares fit provided better trial coefficients. In all cases the desired convergence was achieved eventually. Following this, lines not identified previously were calculated in all other expected orders (2nd, 4th, 5th) and a search was performed to make the remaining identifications.

Finally, a least-squares fit employing all identified lines was carried out, excluding lines involved in coincidences between different orders. The fitted dispersion curve was then transformed to the order of the molecular emission spectrum. This made possible the rapid estimation of vacuum wavenumbers for the $\text{DCl}(B - X)$ measurements.

Small adjustments ($\leq 0.10 \text{ cm}^{-1}$) were made to the wavenumbers of a small portion of the data to establish internal consistency, and multiple measurements of the same transition were averaged to produce a unique set of measurements.

4.4 *Analysis of Molecular Spectrum*

The high rotational temperature of $\text{DCl}(B^1\Sigma^+)$ formed in the discharge leads to severe overlapping between different vibronic bands, yielding spectra which lack any apparent regularity. In addition, the presence of two predominant nuclides of chlorine lends further complexity to the spectrum. A feature that is often helpful in initiating the process of assigning quantum numbers to spectral line positions is a well-defined band head. In this case, however, the rapidly diminishing line intensities toward low- J make the visual identification of bandheads an almost impossible task. An appreciation for these problems can be gained by examining Figure 4.3 which shows a small partially assigned portion of the spectrum.

A modern technique that could be employed to simplify the appearance of complex spectra involves a supersonic jet expansion apparatus, leading to spectra with a "cold" rotational distribution. However, this technique is useful for absorption spectroscopy only. Initial efforts at making assignments consisted of drawing "stick-spectra" from approximate term values

Figure 4.3

A small portion of the $B^1\Sigma^+ \rightarrow X^1\Sigma^+$ emission band system of DCl. Assignments are shown for the $D^{35}\text{Cl}$ isotopomer.

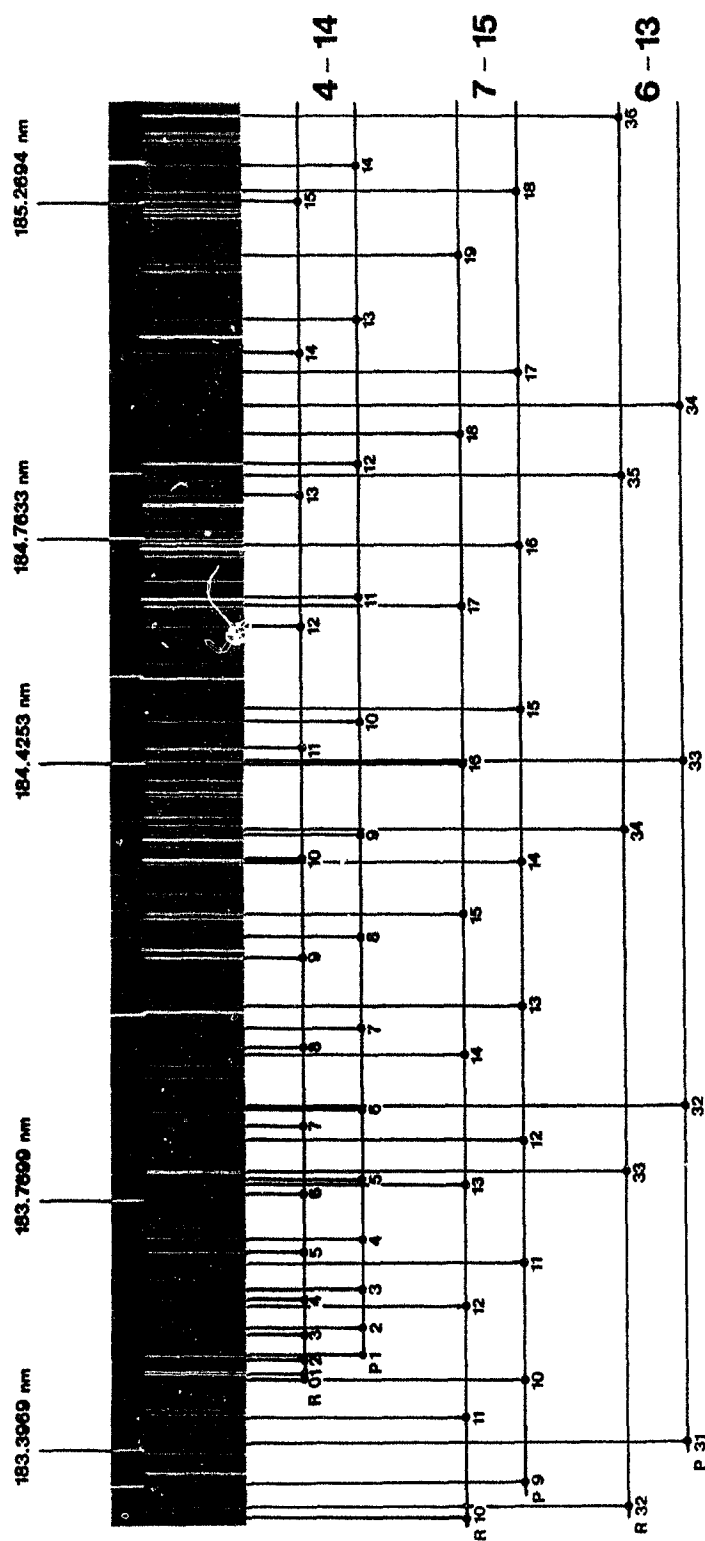


Figure 4.3

obtained by solving the radial wave equation with the H^{35}Cl potentials (130). Shifting these along the appropriate photographic prints led to visual matches. Although some success was realized, it was decided to abandon such traditional methodology and devise a computer-aided search procedure for obtaining quick and reliable rotational assignments.

The computer search was developed on the basis of the conventional combination relations. These can be written as,

$$\Delta_2 F''_v(J) = R(J - 1) - P(J + 1) = F''_v(J + 1) - F''_v(J - 1), \quad (4.1)$$

$$\Delta_2 F'_v(J) = R(J) - P(J) = F'_v(J + 1) - F'_v(J - 1), \quad (4.2)$$

for the lower and upper states, respectively. In past years, analyses of moderately resolved spectra employed these expressions in a graphical fashion to yield estimates of molecular constants. However, with better resolved spectra now available, and with the wide availability of computers and software, the role of combination differences in spectroscopic analyses has been somewhat diminished. These were found to be very helpful in the present work mainly for their rather low sensitivity to small smooth changes to the internuclear potentials. In preliminary efforts towards the development of molecular line search software, it was found that term values for D^{35}Cl obtained by employing the H^{35}Cl RKR potentials of Coxon and Roychowdhury (130), gave synthetic line positions that deviated from the observed values by several wavenumbers. At the same time, however, the synthetic *combination differences* were in remarkably good agreement with those observed. This provided for a stable and trustworthy means of obtaining quick and reliable rotational assignments.

As the analysis progressed, better potentials and combination differences

became available. Two separate computer search programs were written, one each for the upper and lower combination differences. The algorithms were designed to search $\Delta\nu_c$ wavenumber units on either side of the calculated combination difference, and $\Delta\nu_R$ wavenumbers on either side of the calculated $R(J)$ lines; thus, the amount of output could be controlled. From the several possibilities provided, it was quite straightforward to recognize a nonrandom J -dependent pattern in the residuals between observed and calculated frequencies, signifying the discovery of a vibronic band.

Using the progressively improved potentials for both states, it was possible to decide which bands to search for, on the basis of calculated Franck-Condon factors (FCF). These are defined as,

$$q_{v'J'v''J''} = \left[\int_0^\infty \psi'_{vJ'}(R) \psi''_{vJ''}(R) dR \right]^2, \quad (4.3)$$

the square of the overlap integral between rovibronic wavefunctions involved in a transition. The FCF for DCl were found to be highly J -dependent, and a simple $J = 0$ calculation did not offer an accurate prediction of the observations. Table 4.1 shows FCF calculated for various values of J , on the basis of the final RKR potential functions given below. These were extremely useful in rationalizing observed intensity patterns and in avoiding futile searches for structure with predicted low transition probabilities. Even with this insight in hand, however, the poor extrapolation properties of a power series in $J(J + 1)$ often precluded the identification of structure which commenced or resumed at higher J .

Assignments were made for 56 bands of $D^{35}\text{Cl}$ with $0 \leq v' \leq 7$ and $11 \leq v'' \leq 23$. Rotational lines belonging to a vibronic transition were fitted to a band origin and rotational parameters for both electronic states, in

TABLE 4.1

Franck-Condon Factors^a for the $B^1\Sigma^+ - X^1\Sigma^+$ Band System of $D^{35}\text{Cl}$
for Selected Values of J^b

v''	J	$v' = 0$	$v' = 1$	$v' = 2$	$v' = 3$	$v' = 4$	$v' = 5$	$v' = 6$	$v' = 7$
11	0	1.48-5	2.14-4	1.47-3	6.35-3	1.89-2	4.01-2	6.04-2	6.25-2
	15	1.56-5	2.16-4	1.44-3	6.07-3	1.78-2	3.79-2	5.82-2	6.28-2
	30	2.08-5	2.58-4	1.56-3	6.06-3	1.68-2	3.47-2	5.38-2	6.17-2
	45	5.27-5	5.27-4	2.63-3	8.64-3	2.07-2	3.80-2	5.40-2	5.91-2
	60	4.33-4	2.95-3	1.03-2	2.45-2	4.31-2	5.82-2	6.17-2	5.30-2
12	0	7.23-5	8.64-4	4.87-3	1.69-2	3.95-2	6.28-2	6.53-2	3.87-2
	15	7.82-5	9.01-4	4.92-3	1.67-2	3.85-2	6.14-2	6.58-2	4.20-2
	30	1.13-4	1.16-3	5.68-3	1.77-2	3.85-2	6.00-2	6.60-2	4.71-2
	45	3.15-4	2.53-3	1.01-2	2.60-2	4.80-2	6.52-2	6.43-2	4.37-2
	60	2.78-3	1.41-2	3.64-2	6.26-2	7.69-2	6.82-2	4.23-2	1.64-2
13	0	3.18-4	3.08-3	1.39-2	3.74-2	6.47-2	6.99-2	4.00-2	5.40-3
	15	3.53-4	3.29-3	1.43-2	3.76-2	6.44-2	7.03-2	4.24-2	7.32-3
	30	5.46-4	4.46-3	1.73-2	4.14-2	6.63-2	7.06-2	4.47-2	1.06-2
	45	1.63-3	1.01-2	3.06-2	5.85-2	7.61-2	6.63-2	3.40-2	5.85-3
	60	1.48-2	5.04-2	8.68-2	9.34-2	6.32-2	2.20-2	9.37-4	4.98-3
14	0	1.26-3	9.59-3	3.31-2	6.56-2	7.64-2	4.48-2	5.25-3	6.92-3
	15	1.43-3	1.04-2	3.47-2	6.67-2	7.67-2	4.57-2	6.27-3	5.46-3
	30	2.32-3	1.46-2	4.24-2	7.30-2	7.68-2	4.34-2	6.17-3	4.21-3
	45	7.24-3	3.26-2	6.97-2	8.84-2	6.66-2	2.32-2	2.14-4	1.13-2
15	0	4.41-3	2.55-2	6.41-2	8.47-2	5.35-2	6.66-3	8.18-3	3.71-2
	15	5.09-3	2.80-2	6.71-2	8.55-2	5.26-2	6.56-3	7.69-3	3.62-2
	30	8.56-3	3.93-2	7.97-2	8.65-2	4.47-2	3.42-3	9.90-3	3.61-2
	45	2.69-2	8.02-2	1.05-1	6.87-2	1.38-2	2.35-3	2.80-2	3.90-2
16	0	1.36-2	5.65-2	9.38-2	6.79-2	1.03-2	8.17-3	4.08-2	2.87-2
	15	1.59-2	6.19-2	9.65-2	6.54-2	8.67-3	9.12-3	4.11-2	2.89-2
	30	2.71-2	8.34-2	1.03-1	5.12-2	2.09-3	1.67-2	4.36-2	2.54-2
	45	8.10-2	1.34-1	7.89-2	7.47-3	1.19-2	4.50-2	3.55-2	5.71-3
17	0	3.66-2	9.92-2	9.13-2	1.90-2	6.65-3	4.48-2	2.89-2	3.69-5
	15	4.28-2	1.06-1	8.84-2	1.47-2	9.20-3	4.62-2	2.76-2	9.11-6
	30	7.16-2	1.28-1	6.91-2	2.15-3	2.40-2	4.96-2	1.81-2	9.04-4
	45	1.88-1	1.17-1	5.13-3	2.75-2	5.75-2	2.16-2	3.53-4	2.08-2
18	0	8.33-2	1.26-1	4.03-2	3.29-3	4.90-2	3.16-2	9.46-5	2.74-2
	15	9.65-2	1.28-1	3.17-2	6.92-3	5.24-2	2.80-2	5.10-4	2.87-2
	30	1.53-1	1.16-1	5.60-3	3.06-2	5.62-2	1.12-2	7.33-3	3.42-2
	45	3.05-1	1.08-2	4.82-2	6.52-2	6.04-3	1.43-2	3.77-2	1.63-2

TABLE 4.1 (Cont'd)
Franck-Condon Factors^a for the $B^1\Sigma^+$ - $X^1\Sigma^+$ Band System of $D^{35}\text{Cl}$
for Selected Values of J^b

v''	J	$v' = 0$	$v' = 1$	$v' = 2$	$v' = 3$	$v' = 4$	$v' = 5$	$v' = 6$	$v' = 7$
19	0	1.56-1	9.51-2	6.47-7	5.25-2	3.86-2	3.17-4	3.37-2	2.35-2
	15	1.76-1	8.30-2	1.70-3	6.00-2	3.18-2	1.85-3	3.64-2	2.04-2
	30	2.47-1	2.94-2	3.37-2	6.74-2	6.16-3	1.90-2	3.91-2	6.69-3
	45	2.90-1	1.08-1	6.63-2	4.31-5	4.30-2	3.04-2	1.53-4	1.64-2
20	0	2.29-1	1.79-2	4.98-2	5.41-2	2.42-4	4.07-2	2.03-2	3.40-3
	15	2.46-1	6.27-3	6.61-2	4.35-2	3.17-3	4.46-2	1.45-2	6.40-3
	30	2.75-1	2.33-2	9.34-2	3.80-3	3.52-2	3.68-2	6.34-5	2.34-2
	40	2.08-1	2.34-1	1.08-2	3.11-2	4.74-2	4.01-4	2.22-2	2.61-2
21	0	2.45-1	2.29-2	8.90-2	5.85-5	4.98-2	1.84-2	9.63-3	3.40-2
	15	2.42-1	5.32-2	7.69-2	2.99-3	5.56-2	9.31-3	1.68-2	3.10-2
	30	1.75-1	2.31-1	3.30-3	5.42-2	2.97-2	6.15-3	3.68-2	8.18-3
	35	1.13-1	3.24-1	2.67-2	5.73-2	4.66-3	2.80-2	2.70-2	6.86-5
22	0	1.69-1	1.83-1	6.39-3	6.25-2	1.95-2	1.88-2	3.38-2	3.30-5
	15	1.41-1	2.37-1	6.56-4	7.27-2	6.03-3	3.16-2	2.47-2	2.45-3
	30	3.83-2	2.82-1	2.09-1	4.81-3	1.90-2	3.74-2	7.86-4	2.45-2
	35	5.63-3	1.64-1	3.87-1	5.95-2	1.26-2	1.53-2	2.51-2	1.54-2
23	0	5.71-2	2.61-1	1.18-1	2.24-2	2.91-2	3.19-2	5.52-3	3.24-2
	15	3.22-2	2.37-1	2.15-1	4.80-4	4.26-2	1.55-2	1.73-2	2.56-2
	20	1.71-2	1.98-1	2.93-1	1.19-2	4.02-2	5.10-3	2.86-2	1.64-2

^a1.48-5 reads as 1.48×10^{-5} .

^b $J = J' = J''$.

accord with the model,

$$\nu(v', v'', J', J'') = \nu_0(v', v'') + F'(v', J') - F''(v'', J'') + \epsilon_i, \quad (4.4)$$

where

$$\nu_0(v', v'') = T_e' + G_v' - G_v'', \quad (4.5)$$

and

$$F(v, J) = \sum_n X_v^{(n)} [J(J+1)]^n, \quad (4.6)$$

and ϵ_i are the associated measurement errors. This individual band fitting approach of 2784 lines led to a set of 560 parameters, most of which were redundant estimates. The results for individual band fits are given in Table 4.2. These results were merged to a set of single-valued estimates composed of 32 upper state and 65 lower state rotational parameters (Table 4.3) and 56 band origins (Table 4.2). The standard deviation of this merge was $\hat{\sigma}_M = 1.70$, dictating that reported standard error estimates for the parameters should be multiplied by this factor. A subsequent merge in which the 56 band origins were reduced to a set of vibronic term values relative to the energy of the lowest observed level, $v'' = 11$, gave a standard deviation of $\hat{\sigma}_M = 1.81$, indicating that there is little relative systematic error in the data across the extensive band system. The relative vibronic terms are listed in Table 4.4.

4.5 RKR Potentials and Electronic Isotope Shift

Since energy data are not available for ground state levels with $v'' = 6-10$, the energy of $v'' = 11$ relative to the energy of $v'' = 0$ can only be obtained by interpolating vibrational intervals above $v'' = 5$ and below

TABLE 4.2

Least-Squares Fits^a for Individual Bands of the
 $B^1\Sigma^+ - X^1\Sigma^+$ Band System of $D^{35}\text{Cl}$.

v'	v''	ν_0	$\hat{\sigma}$	N	J_P	J_R
0	16	49529.90(2)	0.030	49	22-58	27-54
0	17	48316.34(2)	0.032	58	11-52	9-52
0	18	47167.78(2)	0.030	72	7-49	8-50
0	19	46085.99(2)	0.032	65	6-48	5-48
0	20	45075.07(3)	0.031	50	3-31	6-37
0	21	44139.38(2)	0.031	47	4-38	0-39
0	22	43284.35(2)	0.033	23	3-28	3-30
1	15	51417.28(2)	0.026	56	24-56	22-56
1	16	50142.48(2)	0.030	82	7-55	7-56
1	17	48929.40(2)	0.026	72	2-51	5-50
1	18	47780.34(1)	0.026	58	4-38	4-38
1	19	46698.58(3)	0.030	23	12-22	11-31
1	21	44751.96(3)	0.036	36	16-40	17-40
1	22	43896.94(2)	0.029	47	5-37	4-37
2	14	53347.83(2)	0.034	82	3-60	3-59
2	15	52013.35(2)	0.030	85	6-56	6-56
2	16	50738.56(1)	0.032	73	7-50	4-50
2	17	49525.48(1)	0.030	58	2-38	2-40
2	18	48376.41(2)	0.035	27	3-23	3-24
2	19	47294.63(3)	0.041	24	32-47	33-47
2	20	46283.75(4)	0.034	33	16-38	16-37
2	21	45348.04(3)	0.029	31	13-40	16-41
2	22	44493.05(3)	0.027	15	24-37	24-37
2	23	43725.28(2)	0.026	19	6-22	7-19
3	13	55320.20(1)	0.027	87	4-64	8-63
3	14	53927.88(1)	0.024	82	6-55	5-54
3	15	52593.40(1)	0.027	73	3-49	3-49
3	16	51318.58(1)	0.030	45	5-35	4-35
3	18	48956.52(2)	0.030	36	24-48	23-49
3	19	47874.73(2)	0.033	40	6-32	3-31
3	21	45928.09(3)	0.037	19	28-39	25-38
3	22	45073.11(3)	0.025	29	7-30	7-28
4	12	57333.89(1)	0.028	79	4-62	2-59
4	13	55884.83(1)	0.029	79	2-52	3-53
4	14	54492.51(1)	0.032	80	1-58	0-56
4	15	53158.02(1)	0.032	66	2-47	1-49
4	17	50670.19(2)	0.039	34	27-50	27-49
4	18	49521.12(1)	0.028	52	3-40	0-38
4	19	48439.33(3)	0.036	17	7-24	9-26
4	21	46492.76(3)	0.037	21	14-32	13-30

TABLE 4.2 (Cont'd)

Least-Squares Fits^a for Individual Bands of the
 $B^1\Sigma^+ - X^1\Sigma^+$ System of $D^{35}\text{Cl}$.

v'	v''	ν_0	$\hat{\sigma}$	N	J_P	J_R
5	11	59388.12(2)	0.030	64	8-53	7-47
5	12	57883.70(1)	0.027	67	5-48	4-41
5	13	56434.65(2)	0.030	63	7-47	6-38
5	14	55042.31(1)	0.030	45	3-37	1-36
5	17	51219.96(2)	0.033	42	8-40	9-38
5	20	47978.23(3)	0.032	24	7-29	9-31
6	11	59923.86(2)	0.025	56	9-48	8-42
6	12	58419.46(2)	0.030	47	4-41	3-40
6	13	56970.39(2)	0.036	56	7-51	10-53
6	16	52968.79(2)	0.035	45	6-37	2-40
6	19	49524.94(3)	0.036	30	8-31	9-31
7	11	60446.45(3)	0.031	67	13-55	15-55
7	12	58942.04(3)	0.032	55	9-48	7-54
7	15	54766.16(2)	0.036	40	6-37	8-35
7	16	53491.34(2)	0.043	33	7-41	3-33
7	18	51129.25(3)	0.039	26	12-41	12-41

^aThe merged band origins (ν_0) and standard deviations ($\hat{\sigma}$) are in cm^{-1} ; N is the number of lines fitted; J_P and J_R indicate the ranges of fitted lines in the P and R branches. Standard errors (in parentheses) are given in units of the last quoted decimal place.

TABLE 43

Merged Parameters^a (cm⁻¹) for the $X^1\Sigma^+$ and $B^1\Sigma^+$ States of D³⁵Cl

v''	$X_{v''}^{(1)}$	$-10^4 X_{v''}^{(2)}$	$10^8 X_{v''}^{(3)}$	$10^{11} X_{v''}^{(4)}$	$10^{15} X_{v''}^{(5)}$
11	4.1692 ₅₆ (2)	1.312 ₅₈ (3)	-0.05 ₇₈₃ (3)	0.04 ₈₇₇ (1)	-0.09 ₀₇₂ (1)
12	4.0554 ₁₈ (1)	1.325 ₂₂ (2)	-0.04 ₈₆₈ (1)	0.033 ₉₆ (4)	-0.078 ₆₇ (4)
13	3.9389 ₂₃ (1)	1.329 ₃₇ (2)	-0.136 ₉₂ (9)	0.047 ₆₄ (3)	-0.103 ₈₈ (3)
14	3.8210 ₀₇ (1)	1.354 ₁₁ (2)	-0.14 ₃₃₉ (1)	0.038 ₄₁ (4)	-0.116 ₄₆ (4)
15	3.6994 ₇₅ (1)	1.376 ₇₅ (2)	-0.22 ₂₃₇ (2)	0.048 ₉₁ (6)	-0.164 ₀₁ (7)
16	3.5741 ₈₅ (1)	1.403 ₄₈ (2)	-0.38 ₄₀₇ (2)	0.092 ₈₀ (5)	-0.284 ₀₂ (7)
17	3.4449 ₉₆ (2)	1.452 ₂₃ (3)	-0.47 ₅₈₈ (3)	0.10 ₇₀₇ (1)	-0.40 ₅₂₃ (2)
18	3.3085 ₀₅ (2)	1.497 ₀₉ (3)	-0.76 ₉₆₅ (4)	0.19 ₉₀₆ (2)	-0.71 ₇₄₃ (3)
19	3.1653 ₇₀ (2)	1.558 ₅₆ (5)	-1.21 ₅₄₀ (6)	0.38 ₁₀₄ (3)	-1.36 ₃₇₂ (5)
20	3.0145 ₅₂ (4)	1.70 ₆₄₄ (2)	-0.8 ₃₄₉ (3)	0.0 ₃₂₃₄ (2)	-1.1 ₁₉₃ (7)
21	2.8504 ₈₄ (3)	1.79 ₉₅₈ (1)	-2.1 ₄₅₉ (2)	0.8 ₂₈₃₉ (1)	-4.3 ₃₇₂ (2)
22	2.6716 ₁₂ (4)	1.95 ₉₈₆ (2)	-3.4 ₄₁₈ (3)	1.6 ₆₅₆ (2)	-9.7 ₉₇₆ (7)
23	2.470 ₀₇ (6)	1.8 ₈₄₆ (6)	-30. ₉₄₃ (27)	92. ₈₅₁ (55)	-1087(411)
v'	$X_{v'}^{(1)}$	$-10^5 X_{v'}^{(2)}$	$10^9 X_{v'}^{(3)}$	$10^{13} X_{v'}^{(4)}$	
0	1.4082 ₁₇ (1)	2.95 ₄₆₇ (1)	1.27 ₂₇ (7)	-0.59 ₆₅ (11)	
1	1.4165 ₄₇ (1)	3.37 ₅₉₆ (1)	1.80 ₃₆ (5)	-0.97 ₇₉ (8)	
2	1.4263 ₈₉ (1)	3.83 ₀₁₁ (1)	2.32 ₆₄ (5)	-1.28 ₃₀ (7)	
3	1.4381 ₃₉ (1)	4.36 ₇₂₉ (1)	3.05 ₁₂ (4)	-1.79 ₂₃ (5)	
4	1.4517 ₄₁ (1)	5.00 ₅₈₉ (1)	4.14 ₇₂ (5)	-2.87 ₆₀ (7)	
5	1.4670 ₂₈ (1)	5.70 ₄₀₇ (2)	5.26 ₉₀ (9)	-3.75 ₅₈ (17)	
6	1.4838 ₀₃ (1)	6.48 ₅₅₂ (2)	6.70 ₅₄ (8)	-5.16 ₅₁ (15)	
7	1.5011 ₃₈ (1)	7.23 ₈₂₀ (2)	7.84 ₄₀ (8)	-5.99 ₄₇ (14)	

^aThe standard errors (in parentheses) are given in units of the last decimal place preceding the subscript figures which have been added to reproduce the original data.

TABLE 4.4
Merged Vibronic Energies (cm^{-1}) for the $B^1\Sigma^+$ and $X^1\Sigma^+$
States of $\text{D}^{35}\text{Cl}^{a,b}$

v'	$T_{v'}$	v''	$T_{v''}$
0	56484.95 ₅ (3)	11	0.0
1	57097.53 ₄ (3)	12	1504.41 ₂ (3)
2	57693.61 ₉ (3)	13	2953.47 ₁ (3)
3	58273.67 ₆ (3)	14	4345.79 ₄ (3)
4	58838.30 ₁ (3)	15	5680.27 ₆ (3)
5	59388.11 ₁ (3)	16	6955.07 ₅ (3)
6	59923.86 ₈ (3)	17	8168.13 ₄ (3)
7	60446.42 ₅ (3)	18	9317.18 ₇ (3)
		19	10398.95 ₂ (3)
		20	11409.88 ₄ (4)
		21	12345.57 ₀ (4)
		22	13200.59 ₉ (4)
		23	13968.3 ₄ (2)

^aSee footnote ^a of Table 4.3.

^bThe term values in the table refer to $v = 11$ of the ground state. They may be referred to $v = 0$ by adding $20077.0 \pm 1.0 \text{ cm}^{-1}$ (see text).

$v'' = 11$. This procedure gave $G(v'' = 11) - G(v'' = 0) = 20\,077.0\text{ cm}^{-1}$ with a rather conservative error estimate of $\pm 1.0\text{ cm}^{-1}$. Following a similar interpolation of the missing rotational constants, through a fit to a power series in $(v + \frac{1}{2})$, a first-order RKR potential was constructed. The turning points and energies for the $X^1\Sigma^+$ and $B^1\Sigma^+$ states are listed in Table 4.5.

With an absolute energy scale for the ground state levels established, it was possible to estimate the electronic term of the $B^1\Sigma^+$ state of D^{35}Cl and hence any isotopic shift from H^{35}Cl . The value obtained here was $T_e(\text{DCI}) = 77\,318 \pm 1.0\text{ cm}^{-1}$, which, when compared to the value of $T_e(\text{HCl}) = 77\,307.13\text{ cm}^{-1}$ (119), gave an electronic isotope shift of $\Delta T_e = -11 \pm 1.0\text{ cm}^{-1}$. The approximate equation of Bunker (135),

$$\begin{aligned} \Delta T_e = & 0.000068[T_e] + [B_e(\text{HCl}) - B_e(\text{DCI})]_B \langle L^2 \rangle_B \\ & - [B_e(\text{HCl}) - B_e(\text{DCI})]_X \langle L^2 \rangle_X, \end{aligned} \quad (4.7)$$

where $\langle L^2 \rangle$ was approximated by the sum of the values of $L(L + 1)$ for the dissociation products for each electronic state, gave a value of $\Delta T_e = -5.0\text{ cm}^{-1}$, in only approximate agreement with the experimental value.

4.6 Rydberg \approx non-Rydberg Interactions

The inner limb of the ionic $B^1\Sigma^+$ state intersects the 0^+ components of a set of high-lying Rydberg states which are derived from the ground $^2\Pi$ state of the ion. This gives rise to marked irregularities in large portions of the $B^1\Sigma^+ \leftarrow X^1\Sigma^+(v = 0)$ absorption spectrum (136-139), which samples higher vibrational levels of the B state. A deperturbation of these primarily local interactions has yet to be attempted; nor has an unequivocal vibrational numbering been established for the levels of $B^1\Sigma^+$ involved in the absorption

TABLE 4.5

RKR V Turning Points^a for the $X^1\Sigma^+$ and $B^1\Sigma^+$ States of $D^{35}\text{Cl}$

v	$X^1\Sigma^+$			$B^1\Sigma^+$		
	$G_v + Y_{00}$	R_{\min}	R_{\max}	$G_v + Y_{00}$	R_{\min}	R_{\max}
0	1066.60	1.19091	1.37364	310.59	2.34579	2.68207
1	3157.66	1.13797	1.45779	923.17	2.22567	2.81597
2	5195.03	1.10512	1.52250	1519.26	2.14205	2.91318
3	7179.05	1.08041	1.57976	2099.31	2.07266	2.99563
4	9109.99	1.06041	1.63305	2663.94	2.01118	3.06964
5	10988.03	1.04356	1.68397	3213.75	1.95486	3.13814
6	12813.25*	1.02899	1.73347	3749.51	1.90229	3.20267
7	14585.68*	1.01619	1.78214	4272.06	1.85275	3.26435
8	16305.20*	1.00479	1.83042			
9	17971.62*	0.99454	1.87866			
10	19584.59*	0.98526	1.92716			
11	21143.62	0.97681	1.97618			
12	22648.05	0.96908	2.02601			
13	24097.07	0.96199	2.07692			
14	25489.41	0.95546	2.12929			
15	26823.89	0.94946	2.18335			
16	28098.70	0.94393	2.23971			
17	29311.77	0.93885	2.29874			
18	30460.84	0.93421	2.36115			
19	31542.57	0.92995	2.42798			
20	32553.63	0.92609	2.50001			
21	33489.22	0.92255	2.57944			
22	34344.20	0.91940	2.66797			
23	35111.95	0.91676	2.77001			

^aBoth R_{\min} and R_{\max} are given in Ångstrom units; $G_v + Y_{00}$ is in cm^{-1} .

* Interpolated energies.

$$Y_{00}(X^1\Sigma^+) = 0.82 \text{ cm}^{-1}; Y_{00}(B^1\Sigma^+) = -1.97 \text{ cm}^{-1}.$$

spectrum of DCl. Progress in the latter had been curtailed due to the total absence of $B - X$ emission data prior to the present work.

Douglas and Greening (128) reported the vibrational numbering of $B^1\Sigma^+$ on a relative basis and proposed that the vibrational quantum number corresponding to the lowest level observed on their plates was $v = 12$. On the basis of the vibronic term values presented earlier in this chapter and the current T_e value, it has been possible to confirm this prediction. A graphical display of the determination of the absolute vibrational numbering of the $B^1\Sigma^+$ state of DCl is given in Figure 4.4. Also shown are the positions of $B^1\Sigma^+$ vibrational levels reported in the more recent resonance enhanced multiphoton ionization (REMPI) study of Callaghan *et al.* (139). These authors reported an additional level $B^1\Sigma^+(v = 11)$, as shown in Fig. 4.4. The position of $v = 11$ is predicted in the present work to lie approximately 100 cm^{-1} from the value reported in Ref. (139). In view of the absence of a perturbation in $\text{HCl}(B^1\Sigma^+)$ at similar energy, the assignment of $B^1\Sigma^+(v = 11)$ (139), which was supported by fragmentary data only, is clearly erroneous.

The lowest energy interaction of $B^1\Sigma^+$ has been identified (138) as that with the $H^1\Sigma^+$ Rydberg electronic state. The sequence of $B^1\Sigma^+$ vibrational levels proceeds in a smooth fashion up to an energy of approximately $84\,000\text{ cm}^{-1}$. Above this energy, the vibronic structure begins to display anomalous behaviour. It is possible to gain a qualitative understanding of these local perturbations quite effectively in a graphical manner. Figures 4.5 and 4.6, for HCl and DCl respectively, show clearly that discontinuities in the behaviour of rotational constants of $B^1\Sigma^+$ occur precisely at the reported energies for the vibrational levels of $H^1\Sigma^+$. It is interesting to note that the positions of $B^1\Sigma^+$ levels can be rationalized qualitatively from the

Figure 4.4

Determination of the absolute vibrational numbering for the $B^1\Sigma^+$ state of DCl. Column A contains levels involved in the emission spectrum from the present study, as solid lines; the dashed lines are levels obtained by extrapolation on the basis of the smooth behaviour of levels observed in emission. Levels in column B are from the work of Douglas and Greening (128). The levels in column C are from Ref. (139). N is found to be 12.

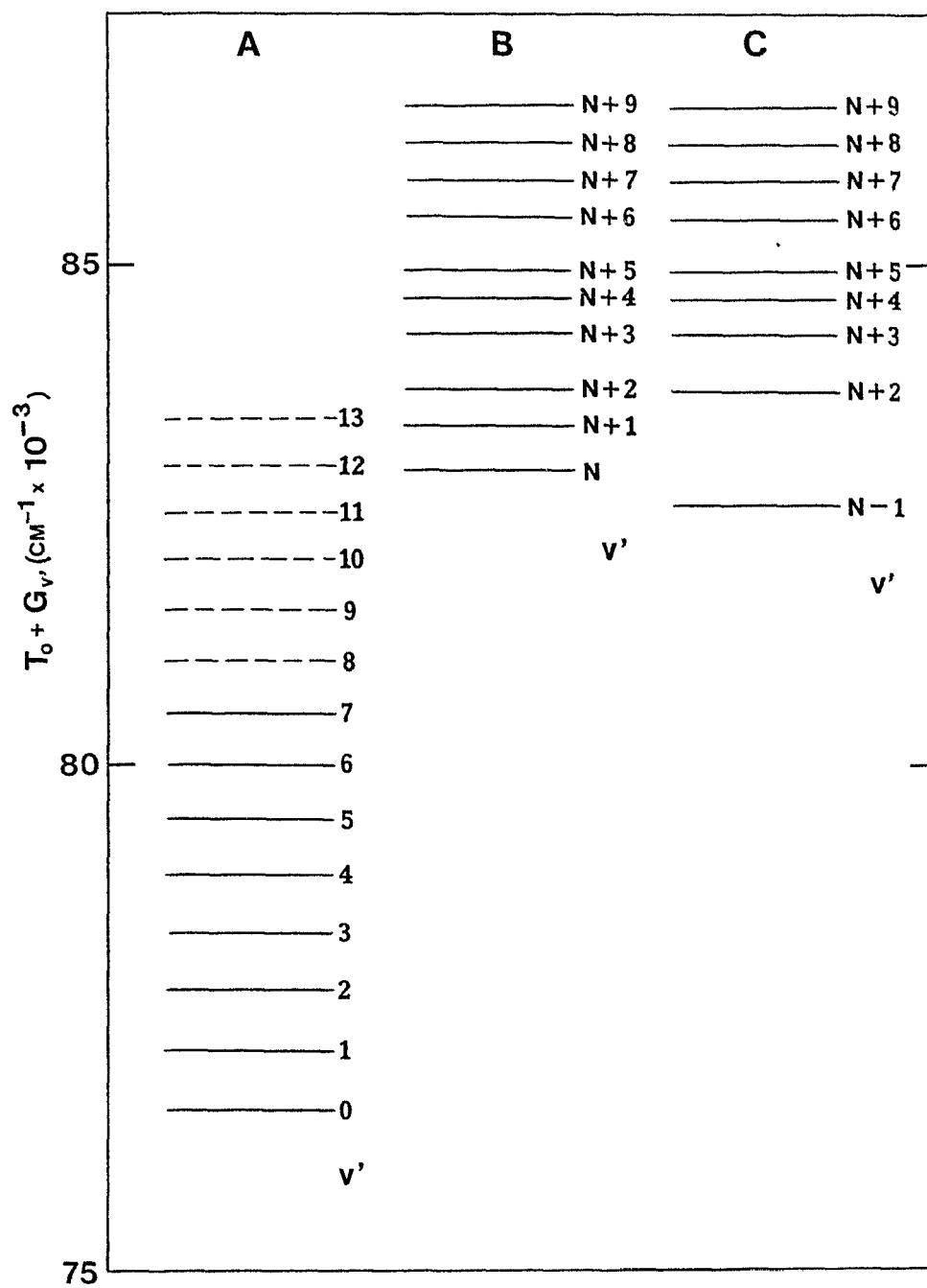


Figure 4.4

Figure 4.5

Perturbations in the $B^1\Sigma^+$ state of HCl. The discontinuities in the vibrational dependence of the rotational constant, B_v , on the lower part of the figure, correspond to local interactions with the $H(0^+)$ Rydberg state's vibrational levels. The upper part of the figure displays the potential energy curves of $B^1\Sigma^+$ and $H(0^+)$, as well as the $I(1)$ Rydberg state. The plot predicts an additional vibronic level $v = 2$ of the $H(0^+)$ state which is responsible for the local interaction near an energy of 89500 cm^{-1} . The $B^1\Sigma^+$ state potential is from an RKR calculation (130) and the Rydberg state potentials are Morse functions chosen to give eigenvalues corresponding to the observed vibronic energies (128).

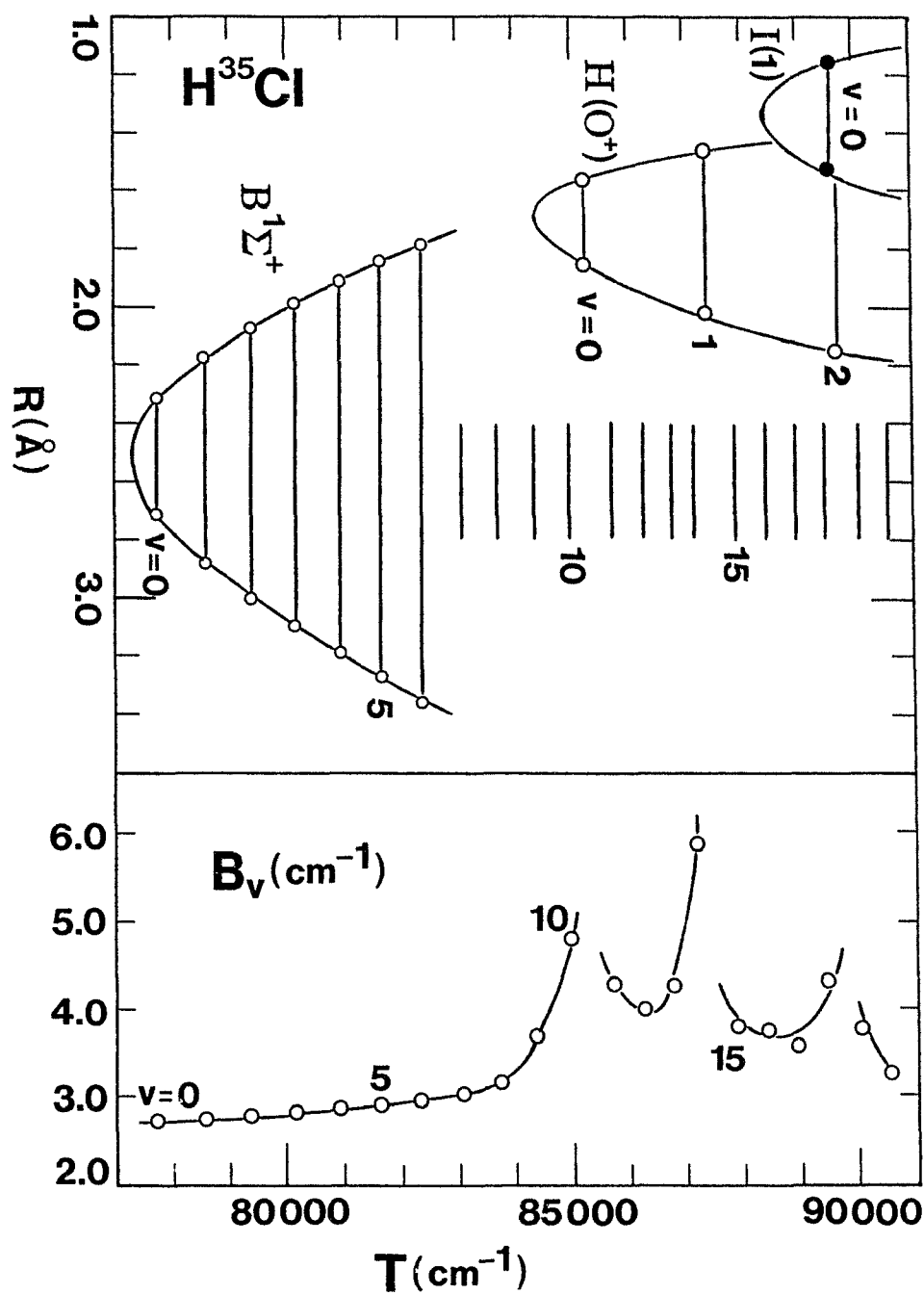


Figure 4.5

Figure 4.6

Perturbations in the $B^1\Sigma^+$ state of DCl. The discontinuities in the vibrational dependence of the rotational constant, B_v , shown in the lower part of the figure, are due to local interactions with the $H(0^+)$ Rydberg state's vibrational levels $v = 0$ and 1. The upper part of the figure displays the potential energy curves of $B^1\Sigma^+$ and $H(0^+)$. A diabatic crossing of $B^1\Sigma^+$ and $H(0^+)$ is anticipated near $v = 0$ of the Rydberg state.

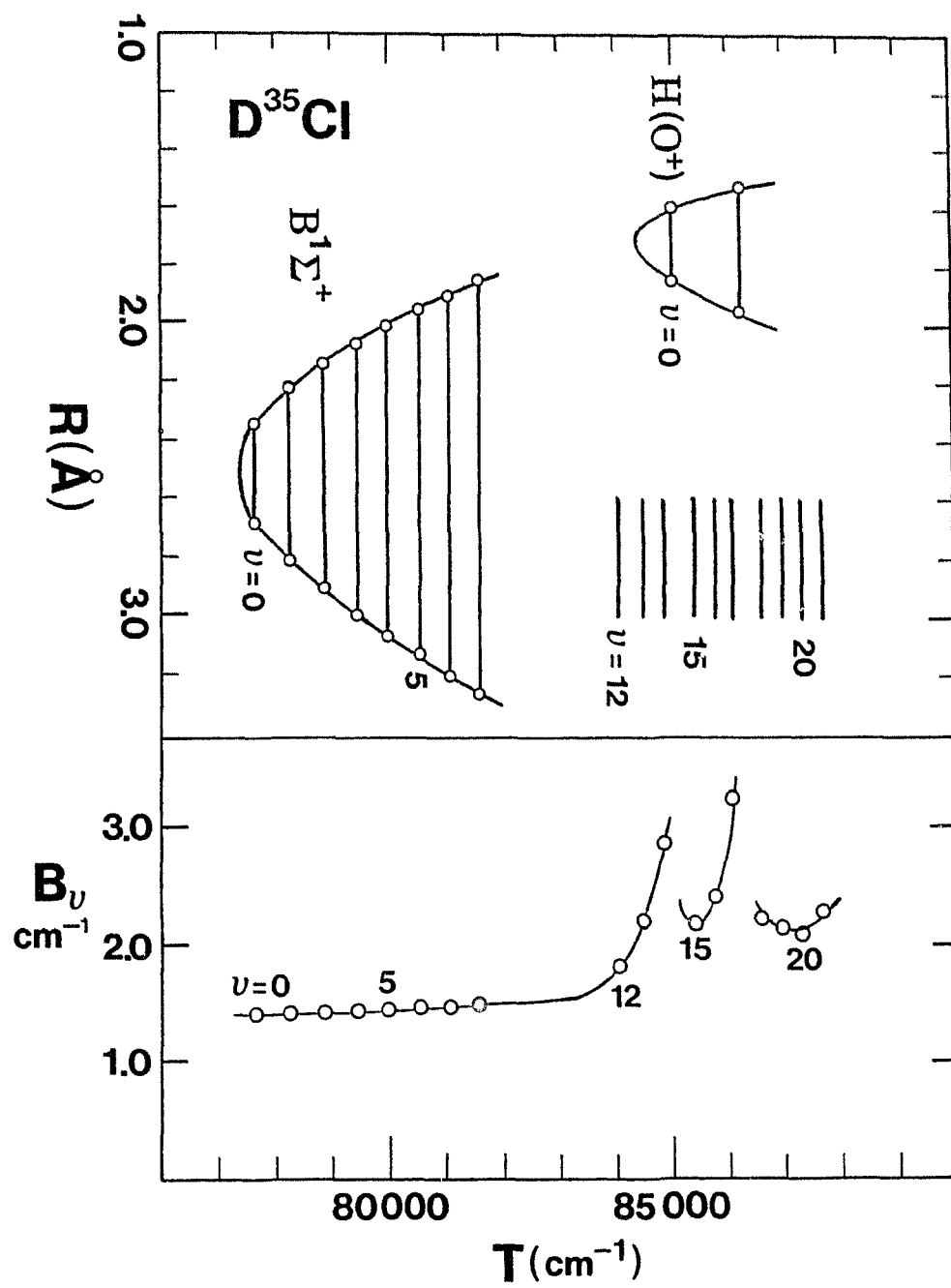


Figure 4.6

diagrams, given the positions of the perturbing $H^1\Sigma^+$ vibrational levels. It is evident in Fig. 4.5 from the slightly larger than average gap between $B^1\Sigma^+$ vibrational levels $v = 18$ and $v = 19$ that an additional local interaction occurs between $B^1\Sigma^+$ and another electronic state. This interaction is likely due to the experimentally unobserved $v = 2$ level of $H^1\Sigma^+$ and not due to the ground vibronic level of $I(1)$, also shown in the figure. The latter level is too close to the $v = 18$ vibronic level of $B^1\Sigma^+$ and hence cannot be the local perturber.

An additional conclusion that can be made on the basis of the diagrams is that the $B^1\Sigma^+$ state potential is not characterized by a well-defined double minimum, in contrast to the results of a recent theoretical work (127). Instead, the two curves are shown to interact in a diabatic fashion near an energy of $84\,500\text{ cm}^{-1}$. However, a satisfactory quantitative interpretation of the experimental observations will probably not be achieved by employing solely diabatic electronic wavefunctions. Neither will a model constructed on the basis of purely adiabatic eigenvectors succeed in rationalizing the data. Unfortunately, it is not a simple matter to predict which formulation might achieve the best description of the data.

A comprehensive interpretation of the $B^1\Sigma^+ \approx H^1\Sigma^+$ interaction is complicated further by the observation that perturbing $H^1\Sigma^+$ levels are not of pure $^1\Sigma^+$ character. These acquire partial spin and orbital momentum through interactions with $^3\Pi(0^+)$ and $^3\Sigma^-(0^+)$ states which also derive from the same Rydberg l complex.

CHAPTER 5
SPECTROSCOPIC INVESTIGATIONS OF DEUTERIUM FLUORIDE
PART A: FOURIER TRANSFORM SPECTROSCOPY OF DF

5.1 Basic Principles of Fourier Transform Spectroscopy

Experimental spectroscopists concerned primarily with the infrared region benefitted tremendously from the advent of Fourier transform spectrometric instruments. Fourier transform spectroscopy (140) has a profitable advantage over more conventional methods. For most of the latter, it is necessary to record portions of a spectrum in a consecutive fashion so that each wavelength must be sampled individually for a selected period of time. Photographic studies, on the other hand, often involve long exposure times over which a source or experimental conditions must be sustained. Interferometric techniques have improved the quality of spectroscopic information and reduced significantly the time required for data acquisition.

Consider a hypothetical spectral transition in emission with frequency ν_1 and of infinitely small line width. The radiation associated with this emission is characterized by a pure sine wave of constant frequency ν_1 . If an additional transition of frequency ν_2 is also considered from the same source, the radiation will now be described by a linear combination of these two sine waves. The two waves may combine constructively or destructively at each point in time yielding a complex waveform known as an interferogram. The pattern is still easily decomposed into the individual sine waves. The process of decomposing the waveform into individual frequencies ν_1 and ν_2 and

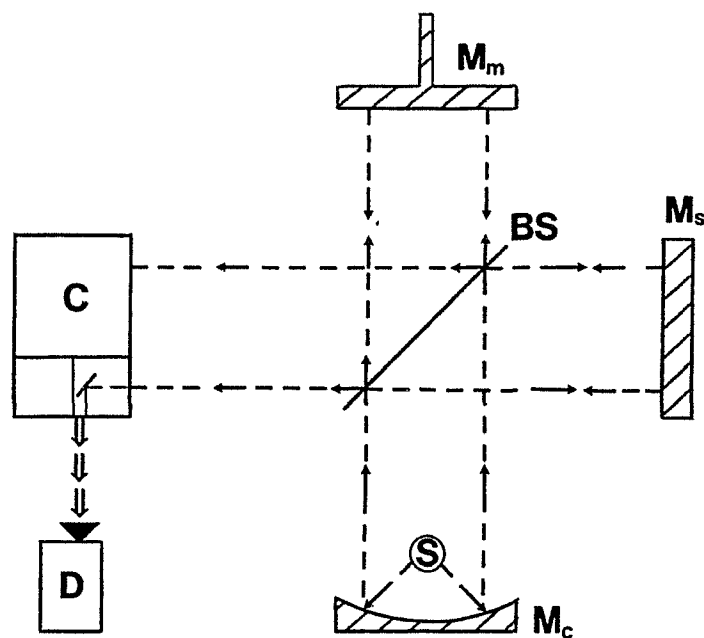
intensities I_1 and I_2 is a well-known mathematical operation known as Fourier transformation (141). Essentially, this corresponds to an integration of the complex waveform from the time domain to the frequency domain. For a real emitting source composed of many spectral transitions that now also possess finite line widths, it is easy to appreciate the complexity of the waveform in the time domain. However, the Fourier transform operation can be performed quite efficiently by a computer; in practice this poses little difficulty.

A Fourier transform spectrometer operating in emission consists of a detector which considers the incoming radiation as a function of time. The signal is stored as an interferogram and the computer carries out a Fourier transformation to resolve the individual components of the waveform. A familiar frequency domain spectrum is the result. What is important to realize is that the radiation, or the interferogram, with all its disguised frequency information, can be recorded almost instantaneously, leading to significant improvement in the time required for an experiment. The transformation also requires short periods of time, so that the total time for an experiment is still sharply reduced over conventional methods.

Most of the Fourier transform work in the infrared and far-infrared is performed in absorption. The arrangement here is different than in emission and is similar to that employed by Michelson earlier in this century to measure the speed of light. Figure 5.1 shows the basic components of the interferometer unit in a Michelson-type Fourier transform spectrometer. The "white" reference source, which emits a broad range of spectral frequencies, is directed to a beam splitter; 50% of the emission is directed onto two mirrors, M_s and M_m . M_s is stationary while M_m is moved smoothly over a specified distance. The combined reflected signal from the two mirrors, which

Figure 5.1

Interferometer unit of a Fourier transform spectrometer.



- M_m** Movable Mirror
M_s Stationary Mirror
M_c Concave Mirror
S Light Source
C Sample Cell
D Detector
BS Beam Splitter

Figure 5.1

constitutes an interferogram, is then directed into the sample. Upon exiting the cell, carrying now information about the absorbing resonances of the species under investigation, it is guided into a detector and the output stored into computer memory. A Fourier transform of this waveform will result in the familiar absorption pattern, since the absorptions in the sample correspond to gaps in the frequency distribution of the original interferogram.

It is found that a series of n scans increases the level of the noise in the recorded spectrum as $n^{1/2}$. Thus, the signal to noise ratio is $n/n^{1/2}$ or $n^{1/2}$. This is known as the multiplex advantage (133). Normally, then, many scans of a sample are performed to average out the random noise, resulting in spectra with high S/N ratios.

5.2 *Experimental*

A far-infrared spectrum of deuterium fluoride involving pure rotational transitions with $J'' = 1-8$ has been obtained. DF gas was introduced into the 11-cm cell of a Bomem DA3.002 Fourier transform spectrometer at total pressures of approximately 100 mTorr. The detector was a Ge bolometer cooled to less than 1 K by a liquid helium cryostat. A bolometer is a background-limited thermal detector measuring the rise in temperature in the sample from absorption of radiation as a change in electrical resistance (133). Cooling is required to reduce the surrounding thermal noise and thus increase the sensitivity. The bolometer was very sensitive and could detect low-level external microphonic noise such as conversation near the instrument. A spectral resolution of approximately 0.002 cm^{-1} was employed and several scans were performed, usually overnight. The calibration was

based on HF pure rotational transitions which are known extremely precisely from laser heterodyne measurements (142); HF is conveniently an impurity in the DF sample. Unfortunately, so is H_2O , eliminating the use of one HF line ($\approx 123 \text{ cm}^{-1}$) due to an overlap with a water line.

A trace of a small portion of the Fourier transform spectrum of DF containing the $J = 3 \leftarrow J = 2$ pure rotational transition is shown in Fig. 5.2.

5.3 Analysis

Calibration of the Fourier transformed spectrum was not achieved in the normal fashion. First, measurements of the spectral features were obtained automatically by the computer from the intersections on the abscissa of the spectrum first derivative. The differences between the measured and standard HF frequencies were then plotted against frequency, giving a fairly linear plot (Fig. 5.3). The raw DF measurements were corrected using the relationship between calibrant error and frequency. A final, corrected, set of DF pure rotational transitions is listed in Table 5.1. Dr. J. W. Johns at the Herzberg Institute of Astrophysics recorded the fundamental band of DF subsequent to the far-infrared work and provided the set of wavenumbers also listed in Table 5.1.

These new data were combined with the laser emission transitions of Sengupta *et al.* (143) in a simultaneous merge fit to Dunham coefficients for $0 \leq v'' \leq 4$. The results are presented in Table 5.2.

The main reason for conducting this research was to make available data of high precision to complement similarly precise data on HF in this range of v'' so that an extrapolation to the energy levels and transitions of TF could be achieved with comparable precision.

Figure 5.2

A small portion of the far-infrared spectrum of DF. The $J = 3 \leftarrow J = 2$ pure rotational transition near 65 cm^{-1} is shown.

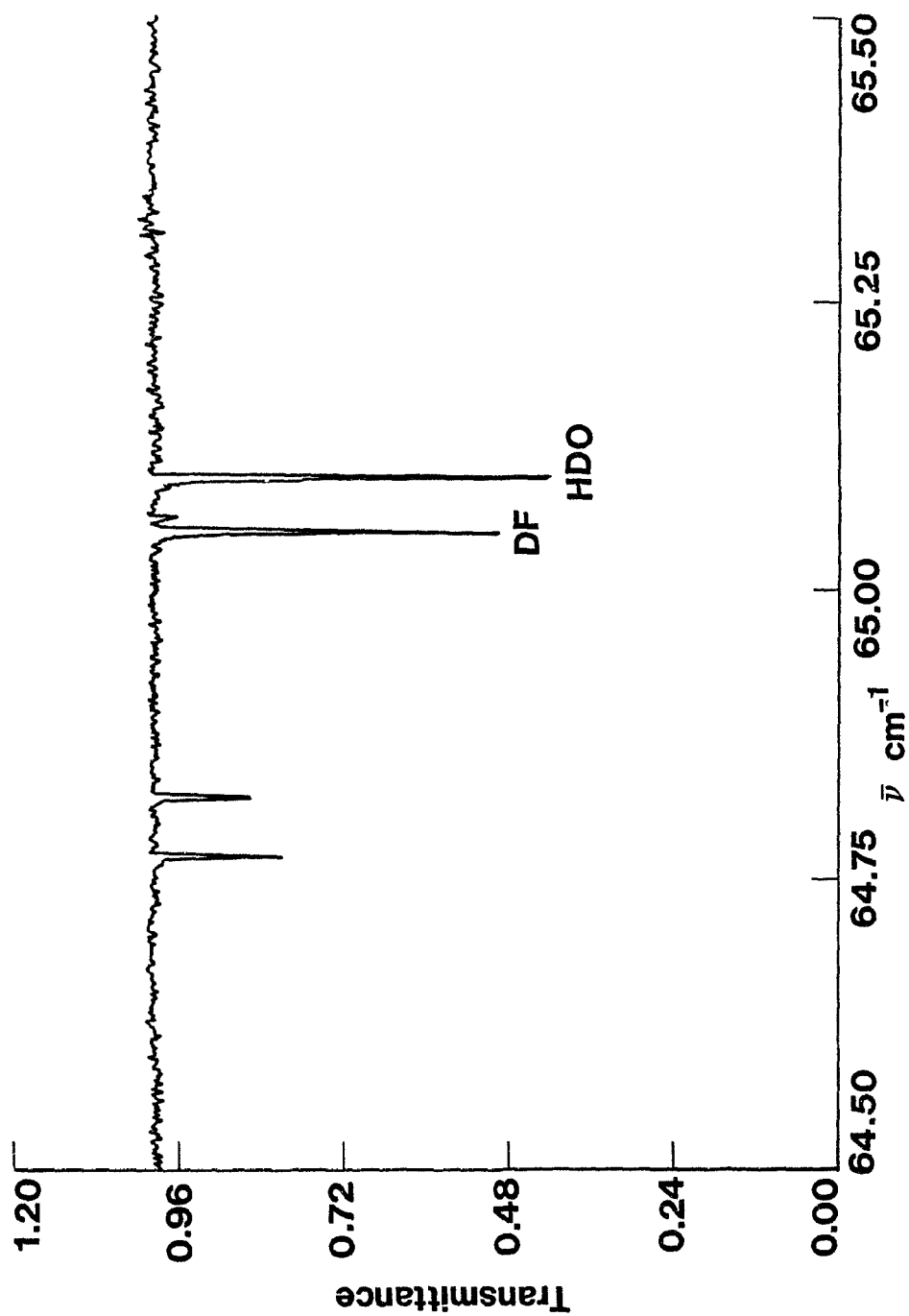


Figure 5.2

Figure 5.3

A plot of calibrant error versus frequency. The calibration was achieved with heterodyne measurements (129) of HF pure rotational transitions in $v'' = 0$. The HF line near 123 cm^{-1} is overlapped by a transition of HDO and is hence excluded from consideration in the construction of the solid line.

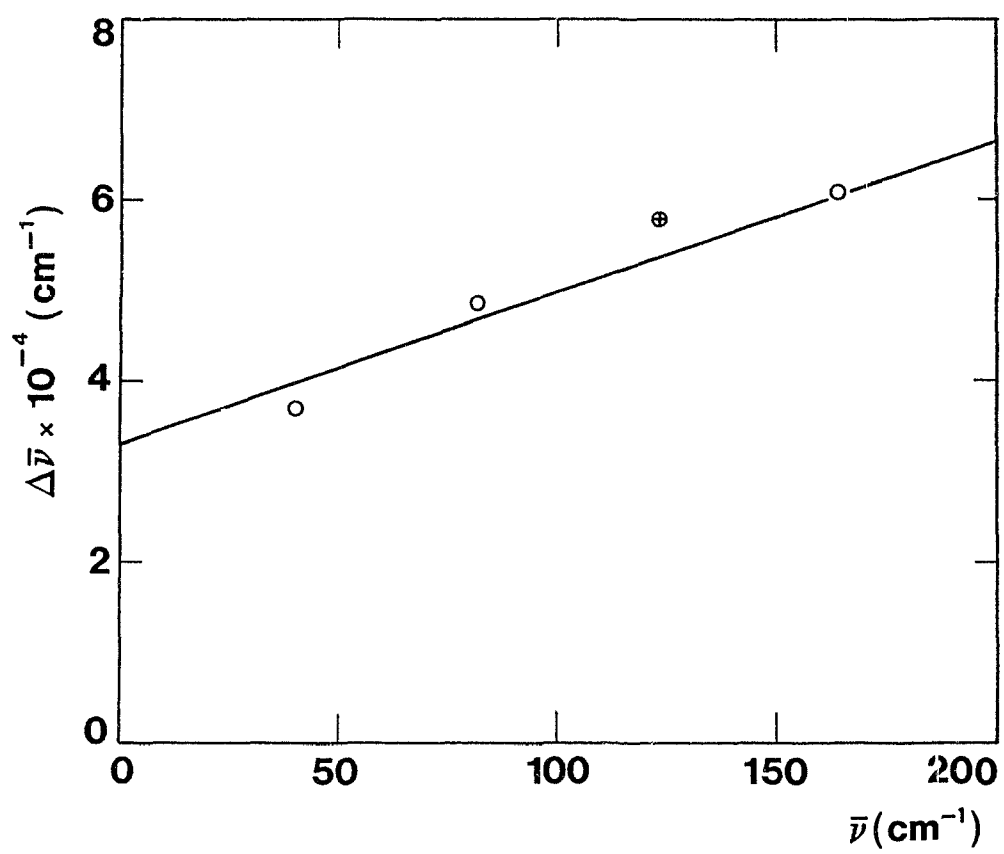


Figure 5.3

TABLE 5.1
Fourier Transform Line Positions of $\text{DF}(X^1\Sigma^+)$

Pure Rotational Transitions in $v = 0$			
J''	$\bar{\nu}(\text{cm}^{-1})$	J''	$\bar{\nu}(\text{cm}^{-1})$
1	43.42268(40)	5	129.81770(20)
2	65.09863(20)	6	151.24126(20)
3	86.73251(20)	7	172.56709(20)
4	108.31021(20)	8	193.78167(40)

Fundamental Band		
J''	$P(J)(\text{cm}^{-1})$	$R(J)(\text{cm}^{-1})$
0		2927.78725
1	2884.94325	2948.30660
2	2862.64640	2968.20599
3	2839.78537	2987.47230
4	2816.37489	3006.09249
5	2792.42963	3024.05393
6	2767.96456	3041.34460
7	2742.99505	3057.95269
8	2717.53624	3073.86638
9	2691.60400	3089.07498
10	2665.21349	3103.56756
11	2638.38085	3117.33405
12	2611.12169	3130.36458

The experimental error estimate for the fundamental band line positions is $\epsilon = 5 \times 10^{-5} \text{ cm}^{-1}$.

TABLE 5.2
Dunham Coefficients (cm^{-1}) for $\text{DF}(X^1\Sigma^+)$

Y_{kl}	Estimate	$2\hat{\sigma}$	Y_{kl}	Estimate	$2\hat{\sigma}$
Y_{10}	3000.09251	7.83×10^{-3}	Y_{02}	-5.93259×10^{-4}	5.11×10^{-8}
Y_{20}	-47.283395	6.59×10^{-3}	Y_{12}	1.17476×10^{-5}	1.24×10^{-7}
Y_{30}	0.357898	1.96×10^{-3}	Y_{22}	-1.874×10^{-7}	6.12×10^{-8}
Y_{40}	-5.4702×10^{-3}	1.92×10^{-4}			
Y_{01}	11.0106910	1.88×10^{-5}	Y_{03}	2.375×10^{-8}	1.30×10^{-10}
Y_{11}	-0.3021884	5.33×10^{-5}	Y_{13}	-5.188×10^{-10}	1.01×10^{-10}
Y_{21}	3.01066×10^{-3}	3.39×10^{-5}			
Y_{31}	-4.5930×10^{-5}	4.69×10^{-6}			

**PART B: SPECTROGRAPHIC STUDY OF THE DF $B^1\Sigma^+$ - $X^1\Sigma^+$
EMISSION BAND SYSTEM IN THE ULTRAVIOLET**

5.4 Introduction

Hydrogen fluoride has been investigated extensively in its ground electronic state by experimental as well as theoretical methods. The pioneering efforts of Deutsch (144) showed HF to be a viable chemical laser medium based on vibrational-rotational transitions. For this reason, the lower vibrational levels of the ground state have been the subject of numerous spectroscopic studies (86, 143, 145, 146); the pure rotational transitions in the lowest vibrational level have been examined (129, 142, 147) by a variety of techniques and very precise molecular constants are available. These pure-rotational transitions have established HF as a frequency standard in the infrared and far-infrared regions of the spectrum.

The $X^1\Sigma^+$ state is also interesting because of its unusually high degree of ionicity (148). This observation has been explained in terms of a strongly avoided crossing with the $B^1\Sigma^+$ state in the rigorous *ab initio* study of Bettendorff *et al.* (149). The ground electronic state is primarily ionic, $(1\sigma)^2(2\sigma)^2(3\sigma)^2(1\pi)^4$, at small (≤ 2.5 bohr) internuclear separations. At approximately 3.0 bohr, it is approximately 50% ionic and 50% valence, $(1\sigma)^2(2\sigma)^2(3\sigma)^1(1\pi)^4(4\sigma)^1$. The valence contribution increases rapidly leading to the neutral dissociation products $F(^2P) + H(^2S)$. The calculated (149) nonadiabatic coupling matrix element $\langle X^1\Sigma^+ | \partial/\partial R | B^1\Sigma^+ \rangle$ reaches its maximum value at approximately 3.5 bohr. Correspondingly, the $B^1\Sigma^+$ state has valence character at small separations, becomes increasingly ionic at long-range and yields the dissociation products $F(^1S) + H^+$. Also, at very small (≈ 1.5

bohr) internuclear distances, the B state mixes with high-energy Rydberg states which arise from the $\text{HF}^+(X^2\Pi)$ core. Figure 5.4 displays some of the low-lying electronic states of $\text{HF}(\text{DF})$. The main difference with the analogous diagram for HCl (Fig. 4.1) is that the Rydberg \approx non-Rydberg interactions on the inner limb of the $B^1\Sigma^+$ state occur at relatively lower energies for hydrogen chloride.

The low-lying repulsive $(1\sigma)^2(2\sigma)^2(3\sigma)^2(1\pi)^3(4\sigma)-A^1\Pi$ state of HF , which approaches the $X^1\Sigma^+$ state dissociation limit asymptotically, has been observed in continuous absorption by Safary *et al.* (150). This state is shown later in this work to be responsible for rotational energy shifts in the ground state that become especially noticeable at high vibrational energies. The quantum mechanical description of such significant nonadiabatic coupling can be given by the Hamiltonian operator Eq. (3.29).

Past spectroscopic investigations of the excited electronic states of HF were limited to the $B - X$ emission and absorption band systems (87) and the vacuum ultraviolet absorption (128) from $X(v'' = 0)$ to several excited states. The observations are much less complete for deuterium fluoride. The $B - X$ bands of the deuteride were first detected in emission by Johns and Barrow (151); rotational analysis provided molecular constants for $15 \leq v'' \leq 24$ and $0 \leq v' \leq 3$. The $C^1\Pi$ state was detected in absorption by Douglas and Greening (128) and more recently in the resonance enhanced multiphoton ionization study of Tashiro *et al.* (152).

The present work reports a reinvestigation of the ultraviolet $B^1\Sigma^+ - X^1\Sigma^+$ emission bands of DF . The higher dispersions afforded by the 10.7-m vacuum spectrograph employed here give significantly better resolved spectra than obtained previously (151). This has a twofold advantage. First, it provides

Figure 5.4

Low-lying electronic states of hydrogen fluoride. The $X^1\Sigma^+$ and $B^1\Sigma^+$ potentials are from RKR calculations (87). The repulsive $A^1\Pi$ state was modelled on the basis of *ab initio* calculations (127). The Rydberg states were constructed with the aid of experimental results (128).

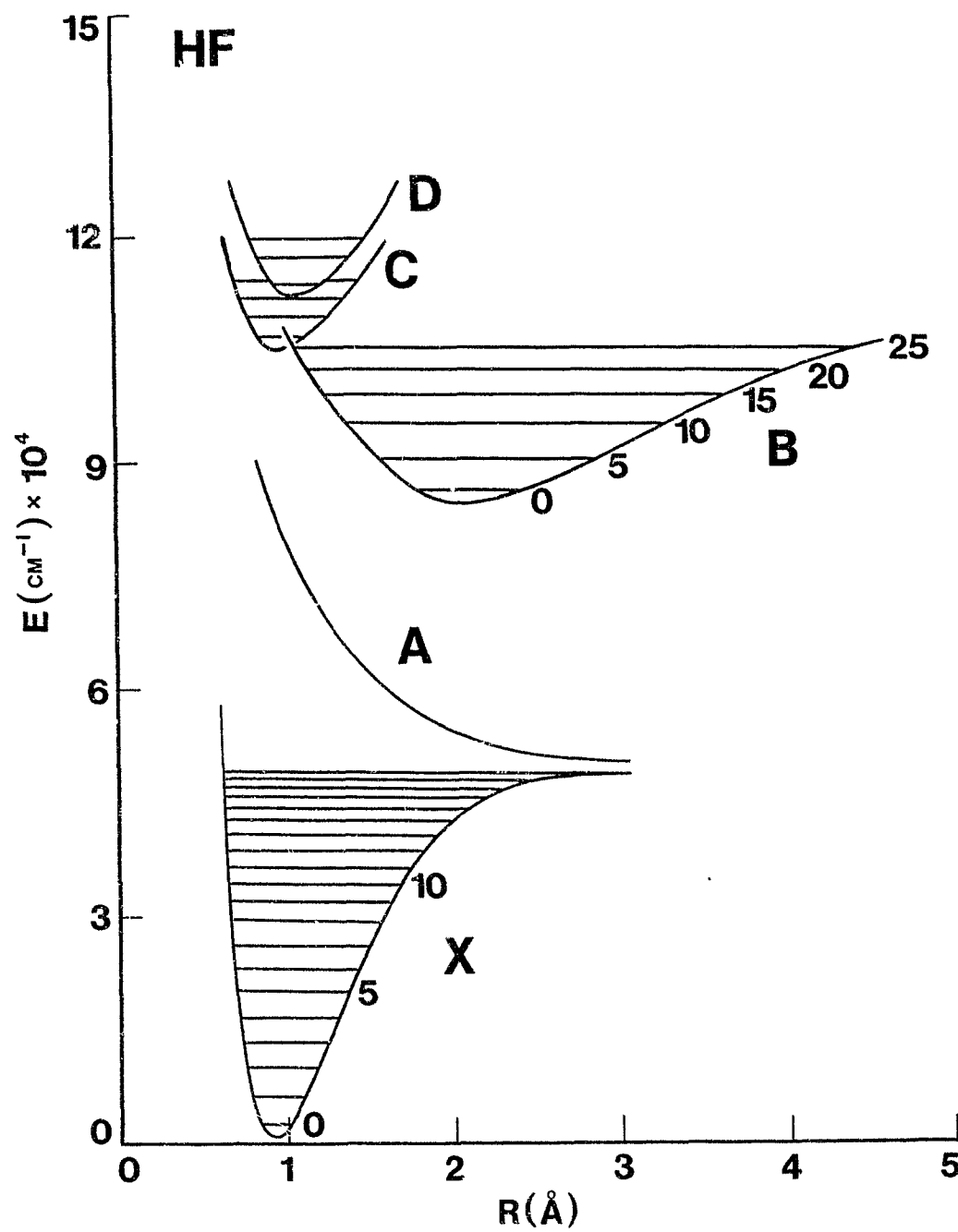


Figure 5.4

a general improvement in the precision of the measurements which gives in turn more precise estimates of the molecular constants. Second, it resolves the congested rotational structure associated with very high v . Precise estimates of the positions of these levels are important in giving an improved value for the dissociation energy and a more reliable estimation of the significant nonadiabatic mixing shifts. The present study also extends the information on the $B^1\Sigma^+$ state to higher vibrational levels and gives better estimates for the electronic term value of $B^1\Sigma^+$ and the electronic isotope shift from HF. In addition, an improved data set for DF, used in association with the similarly precise HF data of Di Lonardo and Douglas (87), enables a reliable prediction of the energy levels of tritium fluoride.

5.5 *Experimental Details*

The ultraviolet emission spectrum of DF was recorded with the 10.7-m spectrograph at the Herzberg Institute of Astrophysics. Emission of ultraviolet photons follows the population of lower vibrational levels of the $B^1\Sigma^+$ state. Electronic excitation was accomplished by flowing 99.2% isotopically pure DF gas (Matheson 99.9%) and helium (Matheson 99.995%), at pressures near 5 Torr, through a hollow cathode discharge operating at 300-500 mA. Spectra were recorded in the wavelength range 2050-2750 Å in the fourth and fifth orders of a 600 line/mm grating, with reciprocal dispersions of 0.18-0.35 Å/mm. Lower resolution exploratory spectra were also recorded in the first-order of a 1200 line/mm grating blazed at 1200 Å. Emission from an Fe/Ne hollow cathode lamp (125 mA, 220 V), in overlapping orders, was recorded separately (onto the same plates but at different times) to calibrate the molecular spectra. The emitted radiation was predispersed and refocussed in

an attempt to minimize the overlap between different spectral orders. It then entered the 10.7-m spectrograph through a 20- μm wide slit and was diffracted by the concave grating. The dispersed light was then projected onto the focal plane containing the photographic plates. Exposure times varied from 10 min to 1 hr on ultraviolet sensitive Ilford Q2, Kodak SWR and 103-a0 plates.

A small portion of the $B^1\Sigma^+ \rightarrow X^1\Sigma^+$ emission spectrum of DF is shown in Fig. 5.5. Assignments are shown for three vibronic bands.

The measurements were made with the comparator described previously and the spectra were calibrated against iron/neon standards (134). Standard deviations of calibration line fits were typically 0.0008 \AA , which corresponds to 0.015 cm^{-1} at 2350 \AA . Since the molecular lines were broader than the atomic lines, their measurement error should be slightly higher, approximately 0.020-0.025 cm^{-1} for sharp, strong, unblended lines. Such is not the case for most of the lines measured here. Owing to the high rotational temperature in the discharge, extensive overlapping of different vibronic bands occurs. The concomitant blending, complicated further by the observation that some hydride impurity spectrum was identified on the plates, makes the average measurement error approximately 0.030-0.035 cm^{-1} . This, however, does not take into account any relative systematic error in the data across the entire band system.

In order to detect any systematic shifts from plate-to-plate that are often encountered in spectrographic work, careful computer-aided comparisons were made of slightly overlapped regions from independent measuring sessions, and larger overlapped regions from plate-to-plate. The session-to-session measurements were in excellent agreement, any systematic shifts being wavelength independent and less than the measurement errors ($\leq 0.02 \text{ cm}^{-1}$).

Figure 5.5

A small portion of the $DF(B^1\Sigma^+ - X^1\Sigma^+)$ emission spectrum.
Rotational assignments are shown for three vibronic bands.

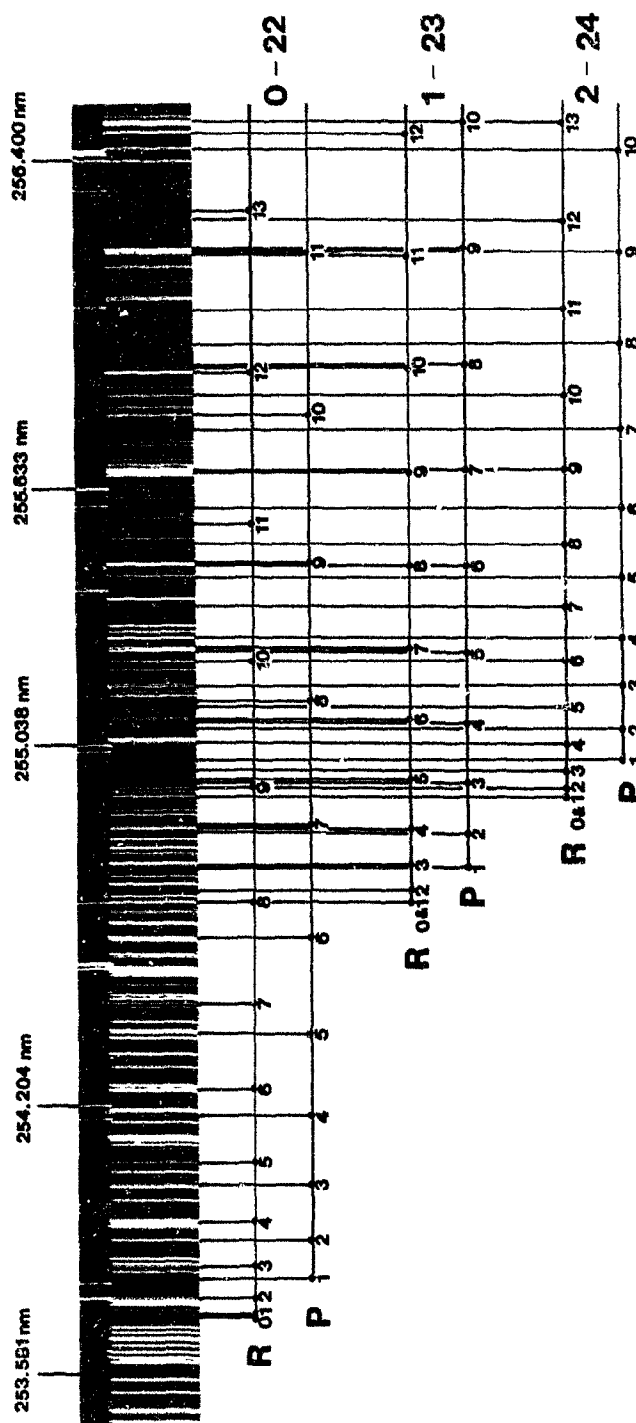


Figure 5.5

The plate-to-plate comparisons revealed slightly larger inconsistencies, for the most part $\leq 0.04 \text{ cm}^{-1}$ in magnitude, and wavelength independent. In one case, the shift was approximately 0.15 cm^{-1} , consistently, for that plate alone. Following a careful computer evaluation of the shifts, all measurements were made mutually consistent by adjustment to a common reference, chosen by observing that the vast majority of the measurements were already well-consistent with each other. The adjusted lines were then averaged where multiple measurements of the same transition existed, resulting in a set of precise unique vacuum wavenumbers. It should be clear, however, that because of the need to make adjustments in the first place, the *absolute* error in the wavenumbers could be as high as the largest observed systematic shift, 0.15 cm^{-1} . In a reduction of line positions to molecular constants, this will only affect estimates of the band origins.

As mentioned above, the causes for the presence of such shifts are often not well-understood, calling for intuitive speculation. A first possibility has to do with the fact that calibration spectra were recorded at separate times. While small time intervals were spanned between the recording of atomic and molecular spectra, it is entirely possible that small vibrations moved the plate very slightly during this time period. Vibrations due to "nearby construction projects" caused rather significant shifts in the HF(B - X) plates of Di Lonardo and Douglas (87). Another possibility deals with small temperature variations in the tank during recording sessions. The shift in the position of a spectral line due to changes in the index of refraction of the grating has been estimated (131) at approximately 0.5 \AA per degree Celsius for a flint glass spectrograph. Assuming a similar temperature coefficient for the index of refraction of the 10.7-m spectrograph concave

grating, a 0.02°C temperature fluctuation would be quite sufficient in causing a shift of 0.15 cm^{-1} . While this is not inconceivable, it would necessarily cause an accompanying serious loss in definition of spectral features, resulting in "fuzzy", badly focussed spectra. This was not found to be the case for the plate with the 0.15 cm^{-1} shift, therefore making the temperature shift theory unlikely. Other possibilities include small pressure variations in the vacuum tank, a mechanical imperfection of the slit, or small defects in the plate holder curvature; nevertheless, the most probable cause appears to be small vibrations between recordings of calibration and molecular spectra.

5.6 Rotational Assignments

Rotational assignments were facilitated in part by the availability of approximate term values for the $B^1\Sigma^+$ and $X^1\Sigma^+$ states from the previous rotational analysis (151). Additional assignments, particularly those involving vibrational levels not observed previously, were achieved by employing the molecular line search computer program described in the previous chapter. A helpful guide to the search was the preliminary and periodically improved set of Franck-Condon factors over a range of J . An extensive calculation of the rotationally dependent FCF is found in Table 7.18. Some very interesting intensity patterns were predicted by the FCF, as for example for the 2-22, 3-23, and 1-20 bands. For these bands, the calculated low- J intensities are quite high, in accord with observations, but decline with increasing J to reach a minimum at mid- J , where no rotational structure was in fact observed, and pick-up again at higher J . Without the rotationally dependent FCF, the search for rotational structure may have been abandoned prematurely at mid- J , at the onset of a noticeable decrease in intensity.

5.7 Molecular Parameters

Initial assignments were obtained with the computer search program described previously. They were extended, where possible, by performing fits to the linear least-squares model Eqs. (4.4-4.6) with the summation index taken to $n = 3$ and 4 for the excited and ground states, respectively, a model which represents adequately the vast majority of assigned line positions. For some high- J lines of high- ν'' , the model is clearly not adequate, requiring additional $X_v^{(n)}$. Inclusion of such parameters for bands which did not require them resulted in poorly determined estimates for the lower-order constants, chiefly due to high correlations between parameters. It is important to make the definitions of parameters as consistent as possible by employing the same model throughout, even at the expense of a few transitions. In analyzing the highly rotationally excited $B - X$ emission bands of HF, Di Lonardo and Douglas (87) encountered a similar problem. In their work, this was rectified by reducing the line positions directly to relative rovibrational term values using the method of Åslund (153). Estimates for the rotational parameters were then obtained by least-squares fits to Eq. (4.6), employing low- and mid- J energies only.

Assignments were made for 41 bands in the present conventional analysis, covering $0 \leq \nu' \leq 5$ and $16 \leq \nu'' \leq 26$. The results of individual band least-squares fits are listed in Table 5.3. The table contains the estimated standard deviations ($\hat{\sigma}$) of such "free" fits, the total number of lines fitted (N), the range of J fitted for each branch (J_P and J_R), and estimates of the band origins (ν_0), obtained by merging the entire collection of bands. A total of 1240 line positions was fitted and the root-mean square of the

TABLE 5.3

Least-Squares Fits^a for Individual Bands of the $B \rightarrow X$ Band
System of DF

v' v''	ν_0	$\hat{\sigma}$	N	J_P	J_R
0 - 16	47426.32(6)	0.035	19	29 - 42	30 - 43
0 - 17	45857.35(2)	0.027	26	22 - 36	21 - 36
0 - 18	44376.29(2)	0.027	43	6 - 33	5 - 34
0 - 19	42986.01(2)	0.031	49	2 - 30	2 - 31
0 - 20	41691.07(1)	0.029	55	2 - 32	1 - 32
0 - 21	40496.77(2)	0.039	36	2 - 31	0 - 31
0 - 22	39410.32(1)	0.031	47	1 - 27	0 - 28
0 - 23	38440.32(2)	0.028	26	2 - 20	3 - 21
1 - 17	46679.02(2)	0.027	49	5 - 35	1 - 37
1 - 18	45198.03(2)	0.024	47	4 - 31	6 - 32
1 - 19	43807.74(1)	0.025	45	3 - 29	0 - 30
1 - 20	42512.84(2)	0.039	19	4 - 17	2 - 17
1 - 22	40232.08(2)	0.032	41	3 - 27	1 - 25
1 - 23	39262.06(2)	0.029	41	2 - 27	2 - 27
1 - 24	38419.43(2)	0.025	27	5 - 19	2 - 17
2 - 16	49051.29(7)	0.034	52	11 - 42	13 - 41
2 - 17	47482.43(2)	0.032	57	6 - 37	2 - 39
2 - 18	46001.47(2)	0.036	38	2 - 23	1 - 22
2 - 20	43316.26(2)	0.036	31	14 - 34	15 - 35
2 - 21	42122.02(2)	0.027	35	4 - 25	2 - 24
2 - 22	41035.54(2)	0.040	16	3 - 10	2 - 16
2 - 23	40065.48(2)	0.025	20	13 - 25	11 - 25
2 - 24	39222.83(2)	0.031	27	6 - 22	1 - 22
2 - 25	38521.23(3)	0.034	26	2 - 19	2 - 19
3 - 16	49836.81(8)	0.033	28	17 - 34	18 - 36
3 - 17	48267.94(2)	0.032	42	2 - 28	3 - 30
3 - 20	44101.75(2)	0.035	33	7 - 27	5 - 28
3 - 24	40008.38(3)	0.019	15	10 - 18	9 - 19
3 - 25	39306.75(3)	0.029	21	5 - 18	4 - 18
4 - 19	46164.80(3)	0.034	33	9 - 30	7 - 30
4 - 22	42589.14(3)	0.032	20	7 - 19	7 - 19
4 - 24	40776.52(2)	0.027	14	3 - 10	1 - 12
4 - 25	40074.85(4)	0.032	20	4 - 19	5 - 19
5 - 18	48306.09(4)	0.035	14	13 - 22	14 - 24
5 - 19	46915.78(3)	0.032	15	4 - 14	6 - 14
5 - 21	44426.59(4)	0.031	21	7 - 20	7 - 21
5 - 26	40283.42(6)	0.027	14	2 - 14	10 - 13

^aThe merged band origins (ν_0) and standard deviations ($\hat{\sigma}$) are in units of cm^{-1} ; N is the number of lines fitted; J_P and J_R are the J ranges of the fitted lines for the P and R branches.

individual $\hat{\sigma}$ in Table 5.3 was approximately 0.035 cm^{-1} , in agreement with the estimate given above. This serves as a rough indicator of the precision of the data, but does not take into account any relative systematic error.

In order to reduce the 328 parameters obtained from individual least-squares fits, many of which are multiple estimates, to a set of 103 single-valued parameter estimates, the method of correlated least-squares (merging) was applied in a stepwise fashion. Of these 103 values, 41 are the band origin estimates given in Table 5.3; the remaining parameters consist of the 18 $X_{v'}^{(n)}$ and 44 $X_{v''}^{(n)}$ rotational parameter estimates given in Table 5.4. The standard deviation of this merge fit was $\hat{\sigma}_M = 1.30$ with $f_M = 225$ degrees of freedom. A subsequent merge was carried out to reduce the 41 band origin estimates to a set of relative vibronic terms for both electronic states. The results are given in Table 5.5. The standard deviation of this merge was $\hat{\sigma}_M = 1.44$ with $f_M = 250$ degrees of freedom, indicating a small degree of systematic error across the entire band system. In view of this, $0.035 \times (1.44/1.30) \text{ cm}^{-1}$, or $\approx 0.040 \text{ cm}^{-1}$, might be a more honest estimate of the precision of the measurements. Two additional merge fits furnished the equilibrium vibrational-rotational parameters presented in Table 5.6.

5.8 RKR Potential Curves for DF

Past spectroscopic investigations in the far-infrared (154, 155) and infrared (143, 145) have characterized vibrational levels with $0 \leq v'' \leq 4$ of the ground state of DF. The electronic emission from $P^1\Sigma^+$ involved levels with $15 \leq v'' \leq 26$, leaving a significant $20\,000 \text{ cm}^{-1}$ gap in the range $v'' = 5-14$ where no spectroscopic information exists. The chemical laser work of Sileo and Cool (156) was aimed at rationalizing intensities. Though bands

TABLE 5.4

Merged Parameters^a (cm⁻¹) for the $X^1\Sigma^+$ and $B^1\Sigma^+$ States of DF

v''	$X_v^{(1)}$	$-10^4 X_v^{(2)}$	$10^8 X_v^{(3)}$	$10^{11} X_v^{(4)}$
16	6.5467 ₀₀ (5)	4.963 ₀₅ (9)	1.30 ₅₅₆ (7)	-0.64 ₂₅₀ (2)
17	6.2699 ₁₃ (2)	4.964 ₄₆ (5)	0.20 ₄₁₆ (5)	-0.52 ₄₆₃ (2)
18	5.9881 ₁₉ (2)	5.113 ₈₂ (8)	0.0 ₂₀₄₂ (1)	-0.82 ₁₉₅ (5)
19	5.6927 ₄₃ (2)	5.28 ₃₅₇ (1)	-0.6 ₁₉₅₂ (2)	-1.1 ₃₇₁₀ (1)
20	5.3832 ₇₂ (2)	5.61 ₄₄₂ (1)	0. ₃₀₆₁ (1)	-2.53 ₆₇ (5)
21	5.0510 ₇₆ (3)	5.96 ₆₇₂ (1)	-0.8 ₂₄₅ (2)	-3.8 ₆₈₈ (1)
22	4.6917 ₅₉ (3)	6.46 ₁₇₀ (2)	-2.2 ₈₂₇ (4)	-6.0 ₅₀₅ (2)
23	4.2971 ₄₄ (4)	7.26 ₉₆₉ (2)	-1.2 ₈₆₆ (4)	-13.4 ₉₁ (3)
24	3.8531 ₅₅ (5)	8.27 ₉₃₆ (4)	-5. ₆₁₆₇ (1)	-24. ₇₆₆ (2)
25	3.343 ₀₄₆ (1)	10.2 ₁₈₆ (1)	4. ₀₆₃₇ (5)	-91. ₅₅₈ (6)
26	2.717 ₃₁₉ (3)	11.9 ₈₄₁ (6)	-100. ₀₁ (45)	-128. ₃₁ (104)
v'	$X_{v'}^{(1)}$	$-10^5 X_{v'}^{(2)}$	$10^9 X_{v'}^{(3)}$	
0	2.1154 ₀₃ (1)	5.60 ₅₄₂ (3)	2.4 ₁₀₁ (2)	
1	2.1079 ₉₄ (1)	5.97 ₀₀₈ (2)	2.5 ₈₉₆ (1)	
2	2.1001 ₅₁ (1)	6.33 ₀₃₆ (2)	2.7 ₅₂₂ (1)	
3	2.0922 ₃₆ (2)	6.76 ₆₁₉ (3)	3.3 ₃₈₇ (1)	
4	2.0840 ₄₂ (2)	7.24 ₄₀₇ (6)	4.2 ₂₁₇ (4)	
5	2.0758 ₅₈ (4)	7.7 ₅₉₆₉ (2)	5. ₃₀₅₂ (2)	

^aTo reproduce the original data, entries are quoted with more significant figures (as subscripts) than the associated standard errors (in parentheses) require.

TABLE 5.5

Merged Vibronic Terms^a (cm⁻¹) for the
 $B^1\Sigma^+$ and $X^1\Sigma^+$ States of DF^b

v'	$T_{v'}$	v''	$T_{v''}$
0	47426.10 ₄ (7)	16	0.0
1	48247.85 ₄ (7)	17	1568.84 ₄ (7)
2	49051.12 ₈ (7)	18	3049.81 ₇ (7)
3	49836.79 ₅ (7)	19	4440.10 ₆ (8)
4	50604.93 ₉ (8)	20	5735.03 ₁ (8)
5	51355.87 ₉ (8)	21	6929.26 ₂ (8)
		22	8015.77 ₇ (8)
		23	8985.79 ₂ (8)
		24	9828.42 ₅ (8)
		25	10530.05 ₁ (8)
		26	11072.4 ₆₃ (1)

^aSee footnote ^a of Table 5.4.

^bThe term values in this table refer to $v = 16$ of the ground state. They may be referred to the minimum of the $X^1\Sigma^+$ state potential by adding $G''_{16} = 37792 \pm 5$ cm⁻¹.

TABLE 5.6
Equilibrium Vibrational-Rotational Parameters
for the $B^1\Sigma^+$ State of DF^a

ω_e	$840.45_{\pm 3}(3)$
$\omega_e x_e$	$9.47_{\pm 34}(1)$
$\omega_e y_e$	$7.0_{\pm 42}(2) \times 10^{-2}$
B_e	$2.1191_{\pm 01}(2)$
α_e	$7.28_{\pm 08}(12) \times 10^{-3}$
γ_e	$-1.21_{\pm 84}(24) \times 10^{-4}$

^aAll quantities are in cm^{-1} units. Numbers in parentheses are the 95% confidence limits.

with v'' up to 12 were observed, no band origin estimates were reported. The resolution of the spectra was too poor to give reliable energy estimates and these authors resorted to the molecular constants of Johns and Barrow (151) to construct the RKR curves required for evaluation of Einstein coefficients.

Since more precise estimates of the molecular constants became available in this work, it was decided to repeat the interpolation of the missing data. Precise $\Delta G(v'' + \frac{1}{2})$ estimates for $v'' = 0-3$ were derived by merging the laser data of Sengupta *et al.* (143). These were fitted to a power series in $(v'' + \frac{1}{2})$, along with the $\Delta G''(16\frac{1}{2}) - \Delta G''(25\frac{1}{2})$ values obtained in this work and the intermediate $\Delta G''$ values were interpolated. This procedure gave $G''_{16} + Y''_{00} = 37\,796 \pm 5 \text{ cm}^{-1}$, for the lowest observed level in this work. This serves as a reference for the vibronic terms in Table 5.5. After interpolating the rotational constants in an analogous fashion, first-order RKR turning points were calculated and are presented in Table 5.7, along with those of the $B^1\Sigma^+$ state. These potentials can be regarded as approximate initial descriptions of the $X^1\Sigma^+$ and $B^1\Sigma^+$ radial operators.

5.9 Dissociation Energy of $DF(X^1\Sigma^+)$

The results of the conventional rotational analysis presented above can be used to obtain an estimate for the dissociation energy of the ground state. For the levels $v'' = 23-26$ an abrupt breaking-off of rotational structure at high- J has been observed. Although there was no indication of noticeable broadening for the last observed line positions, this phenomenon can still be attributed to a predissociation mechanism. The tunnelling for the deuteride is not as efficient as that for the hydride, for which measurable broadening was reported (87) in predissociated levels.

TABLE 5.7
RKRV Turning Points^a for the $X^1\Sigma^+$ and $B^1\Sigma^+$ States of DF

ν	$X^1\Sigma^+$			$B^1\Sigma^+$		
	$G_\nu + Y_{00}$	R_{\min}	R_{\max}	$G_\nu + Y_{00}$	R_{\min}	R_{\max}
0	1490.34	0.84540	1.00365	416.14	1.94778	2.24550
1	4397.00	0.80112	1.07876	1237.89	1.84934	2.37044
2	7212.15	0.77406	1.13728	2041.32	1.78399	2.46327
3	9937.69	0.75394	1.18953	2826.83	1.73206	2.54345
4	12575.38	0.73782	1.23851	3594.97	1.68792	2.61662
5	15126.99*	0.72435	1.28556	4345.91	1.64894	2.68547
6	17594.08*	0.71275	1.33144			
7	19978.05*	0.70262	1.37669			
8	22280.03*	0.69363	1.42167			
9	24500.91*	0.68559	1.46670			
10	26641.30*	0.67834	1.51204			
11	28701.57*	0.67177	1.55792			
12	30681.76*	0.66580	1.60461			
13	32581.63*	0.66035	1.65235			
14	34400.65*	0.65538	1.70141			
15	36137.79*	0.65082	1.75213			
16	37791.75*	0.64665	1.80487			
17	39360.60	0.64284	1.86014			
18	40841.58	0.63933	1.91856			
19	42231.87	0.63613	1.98074			
20	43526.80	0.63321	2.04819			
21	44721.03	0.63058	2.12208			
22	45807.55	0.62825	2.20515			
23	46777.57	0.62620	2.30081			
24	47620.20	0.62445	2.41527			
25	48321.83	0.62304	2.55985			
26	48864.24	0.62211	2.76072			

^a $G_\nu + Y_{00}$ are given in cm^{-1} ; R_{\min} and R_{\max} are in Ångstrom units. Energies marked with an asterisk (*) were obtained by interpolation (see text).

$$Y_{00}(X^1\Sigma^+) = 2.03 \text{ cm}^{-1}; \quad Y_{00}(B^1\Sigma^+) = -1.57 \text{ cm}^{-1}.$$

The independence of this effect from excited state vibrational levels signifies a predissociation in the ground electronic state. This can also be expected from a purely theoretical argument. The behaviour of the $B^1\Sigma^+$ state potential of HF(DF) at large- R has been shown from experimental results (87), to follow primarily an $1/R$ (ionic) dependence. For this type of interaction, the rotationless potential approaches the dissociation limit at a slower rate than the centrifugal $1/R^2$ term, precluding the formation of a potential barrier.

Büttenbender and Herzberg (157) have shown how these observations can be utilized to furnish an estimate of the dissociation energy, \mathscr{D}_e . By plotting the energies of ground state levels associated with the abrupt breaking-off of rotational structure versus $J(J + 1)$, as well as the estimated energies of first unobserved levels, and extrapolating a curve drawn between the two sets of energies to $J = 0$, an estimate for the dissociation limit is given directly. This type of plot was termed the limiting curve of dissociation (LCD). Soon afterwards, Schmid and Gerö (158) showed that the slope of the LCD could be related to the R value corresponding to the rotational barrier maximum.

One problem with the LCD method is that the last observed levels need not correspond to the last bound levels, particularly when no significant broadening of lines has been detected. It is possible that bound levels above the last observed exist but have lifetimes which make them difficult to detect experimentally. This is especially true for light molecules. It was shown in Chapter 2 that the tunnelling efficiency through a centrifugal barrier increases for systems with smaller reduced masses. Thus, \mathscr{D}_e estimates obtained from the LCD method are usually lower than the true limit.

In order to gain a better appreciation of the quantitative behaviour of the LCD method, model calculations were carried out using a Morse potential with $\mathscr{D}_e = 50000 \text{ cm}^{-1}$, $R_e = 1.00 \text{ \AA}$, $\omega_e x_e = 100.0 \text{ cm}^{-1}$ and $\mu = 2.000 \text{ amu}$. A nonadiabatic $g(R)$ function need not be considered; its inclusion serves only to alter the *slope* of an LCD plot and has no effect on the intercept (\mathscr{D}_e), as the pure centrifugal and nonadiabatic rotational contributions both tend to zero, albeit at different rates, as $J \rightarrow 0$.

The wave equation was then solved for all quasibound levels of vibrational levels with $v'' = 16\text{--}20$ to obtain estimates for their positions and widths. The results are listed in Table 5.8. In the lower solid curve of Figure 5.6, levels which had widths of less than 1 cm^{-1} were included. This plot allows for the estimation of the error that might arise where large widths preclude the experimental observation of levels which still lie below the barrier maximum. A second solid curve was plotted on Fig. 5.6 including all levels below the barrier maximum. It is evident from the plots that the LCD method provides slight overestimates of \mathscr{D}_e when all bound levels are considered. Theoretically, the slope of the LCD at $J = 0$ should be zero, yet as can be seen from the true LCD points on Fig. 5.6 this does not occur for the range of J considered. The tendency to "flatten" the LCD towards $J = 0$ in order to satisfy the theoretical behaviour is the reason that experimental LCD's give slightly higher estimates of \mathscr{D}_e . When levels with $\Gamma_{\text{fwhm}} \leq 1 \text{ cm}^{-1}$ are considered, the \mathscr{D}_e estimate is understandably lower, which implies that for light molecules the LCD method may be somewhat self-compensating. It is also obvious that \mathscr{D}_e estimates obtained through the LCD method are associated with a large uncertainty due to the large extrapolation to $J = 0$.

A second method was therefore explored. If a numerical potential is

TABLE 5.8

A Test of the LCD Method: Energies and Widths of
Model Potential Quasibound Levels^a

v	J	E_{vJ}^{QM}	Γ_{fwhm}	ΔE_1	ΔE_2
16	31	50017.179	b	864.988	847.809
16	32	50211.494	b	936.360	724.867
16	33	50407.148	b	1011.394	604.246
16	34	50603.288	b	1090.178	486.890
16	35	50798.823	b	1172.805	373.982
16	36	50992.239	0.016	1259.369	267.130
16	37	51181.054	0.505	1349.966	168.912
16	38	51361.275	5.558	1444.689	83.415
17	27	50012.396	b	614.305	601.909
17	28	50166.301	b	671.931	505.630
17	29	50321.487	b	732.862	411.374
17	30	50477.069	b	797.185	320.116
17	31	50631.850	0.006	864.988	233.139
17	32	50783.941	0.242	936.360	152.419
17	33	50930.181	3.328	1011.394	81.213
18	23	50038.479	b	415.132	376.653
18	24	50154.619	b	460.396	305.776
18	25	50271.752	b	508.623	236.870
18	26	50388.840	0.007	559.898	171.058
18	27	50504.204	0.312	614.305	110.101
18	28	50615.236	3.761	671.931	56.695
19	19	50074.864	b	262.044	187.179
19	20	50156.017	0.004	296.286	140.270
19	21	50237.360	0.057	333.160	95.801
19	22	50316.988	1.279	372.748	55.759
19	23	50393.772	8.733	415.132	21.360
20	13	50002.003	0.019	107.256	105.254
20	14	50049.548	0.072	127.432	77.885
20	15	50097.894	0.292	149.747	51.853
20	16	50145.703	1.770	174.284	28.581
20	17	50193.067	11.994	201.125	8.058

^aEnergies and Widths are given in units of cm^{-1} .

ΔE_1 is the energy from the dissociation limit to the barrier maximum.

ΔE_2 is the energy from E_{vJ} to the barrier maximum.

^b $\Gamma_{\text{fwhm}} \leq 0.0005 \text{ cm}^{-1}$.

$\mathcal{D}_e^{\text{true}} = 50000 \text{ cm}^{-1}$.

Figure 5.6

Limiting curve of dissociation (LCD) plots of model data. The points represented by open triangles fall along the true LCD plot found by numerical determination of the barrier height for various values of J . The lower solid curve represents an LCD plot for levels with widths of $\Gamma \leq 1 \text{ cm}^{-1}$; the upper solid curve represents an LCD plot in which all bound vibrational levels were considered. The data employed in the construction of this figure are listed in Table 5.8. The filled circles represent the last "observed" levels. The open circles represent extrapolated levels with J one unit higher than those of the last "observed" levels. The model dissociation limit is denoted by D_e^{true} and corresponds to an energy of 50000 cm^{-1} .

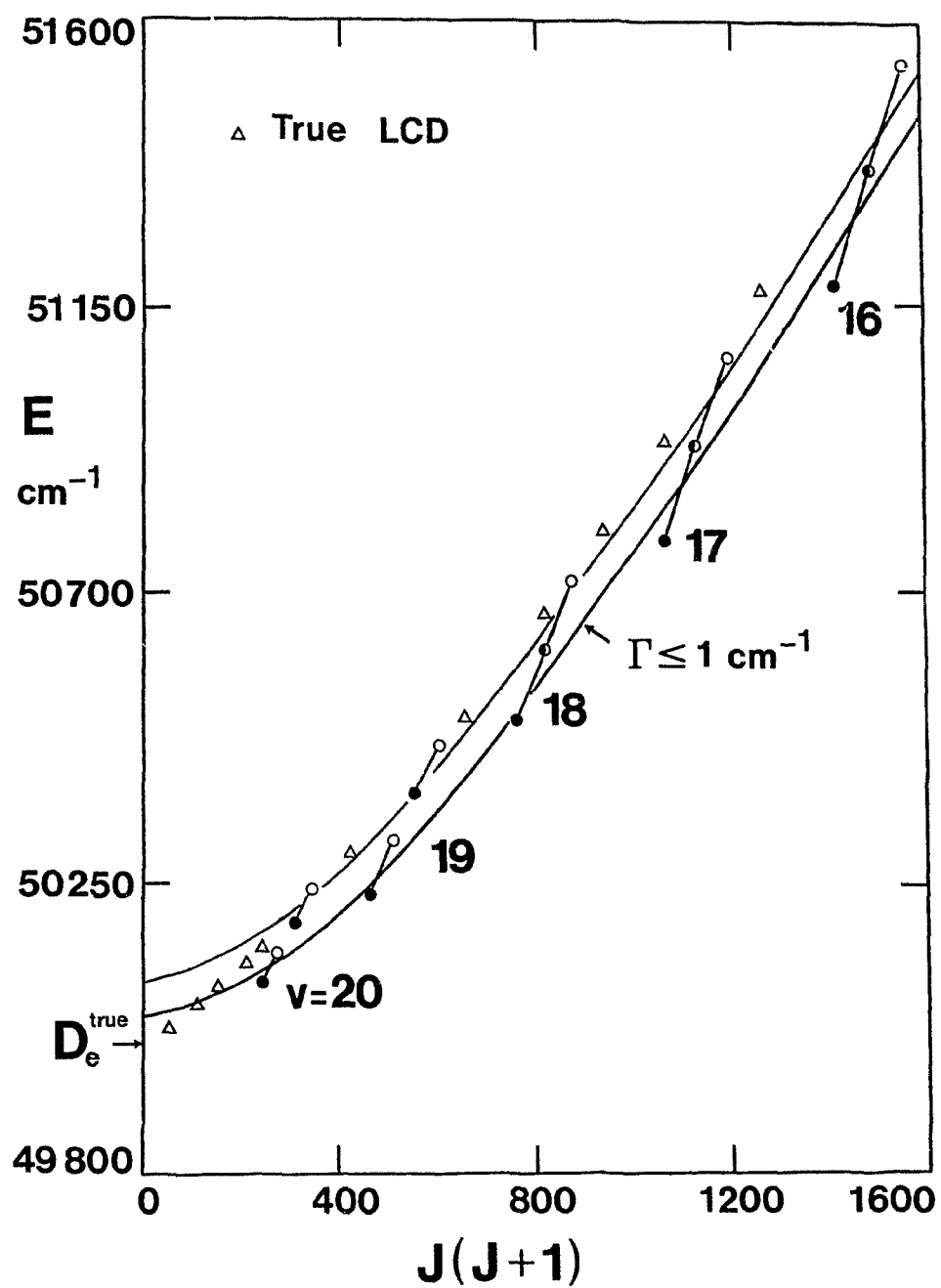


Figure 5.6

available, it is possible to find the position of the barrier maximum using numerical methods. Moreover, it has been found here that these energies can be represented very well by,

$$E_J^\ddagger = e_0 + e_1 \mathcal{J} + e_2 \mathcal{J}^2 + e_3 \mathcal{J}^3 + \dots, \quad (5.1)$$

where $\mathcal{J} = \sqrt{J(J+1)}$, and e_0 is the dissociation limit, \mathcal{D}_e . Use of the variable \mathcal{J} in Eq. (5.1) is not supported theoretically but was suggested by the analytical LCD expression of Waech and Bernstein (159). The E_J^\ddagger values for the rotational barrier maxima with $10 \leq J \leq 20$ were found numerically and fitted to Eq. (5.1). The value of \mathcal{D}_e was slightly model dependent but for a satisfactory fit, without systematic error in the residuals, it was always a few wavenumbers higher than the true limit.

With a quantitative appreciation for the errors expected in the LCD estimates, a plot was constructed for the real DF data. Table 5.9 gives term values for the last observed rotational levels for $v'' = 23-26$, as well as estimates of the energies for the first unobserved levels. The experimental LCD plot is shown in Figure 5.7. Extrapolation to $J = 0$ with the constraint of a zero slope at the intercept, gave the estimate $\mathcal{D}_e = 49400 \pm 55 \text{ cm}^{-1}$. The uncertainty not only considers the extrapolation to $J = 0$; on the basis of the model calculations an additional error estimate is included to consider the possible exclusion of quasibound levels that cannot be detected by spectrographic methods. Finally, the uncertainty in the absolute energies is also included. In comparison with the most recent estimate for HF, $\mathcal{D}_e = 49380 \pm 60 \text{ cm}^{-1}$ (87), there does not appear to be a significant difference between the \mathcal{D}_e values for the two isotopomers.

TABLE 5.9

Rotational Predissociation in the $X^1\Sigma^+$ State of DF:Determination of the Dissociation Energy^a

v	J	$E(v, J) \text{ (cm}^{-1}\text{)}$	$J + 1$	$E(v, J+1) \text{ (cm}^{-1}\text{)}$
23	29	49879	30	50026
24	25	49715	26	49831
25	20	49522	21	49606
26	15	49433	16	49489

^a J is the value of the rotational quantum number for the last observed level of vibrational state v .

Figure 5.7

Limiting curve of dissociation (LCD) plot for $\text{DF}(X^1\Sigma^+)$. The filled circles represent the last observed levels and the open circles represent extrapolated levels with J one unit higher than those of the last observed levels. An LCD estimate of $\mathscr{D}_e = 49\,400 \pm 50 \text{ cm}^{-1}$ is obtained.

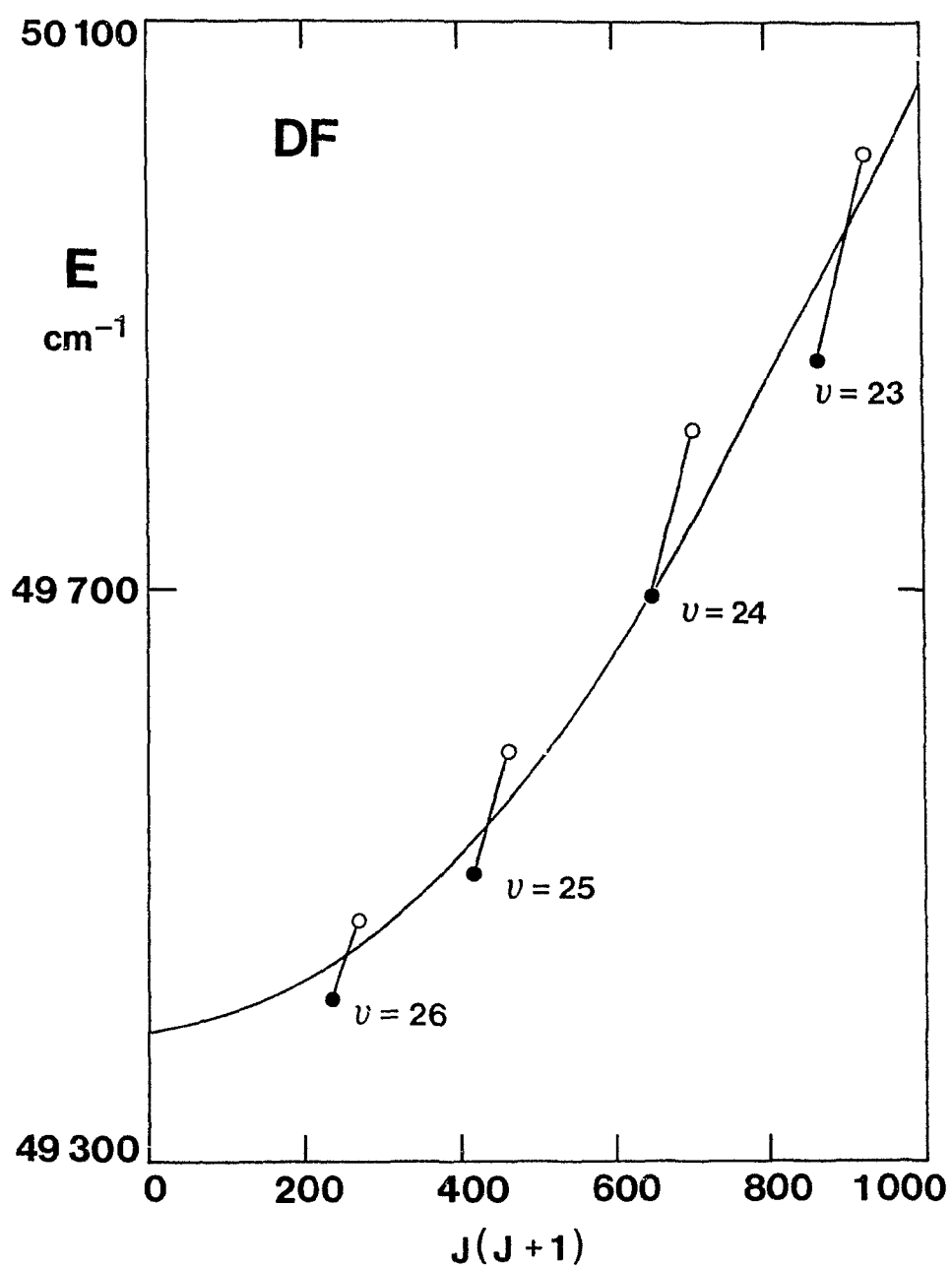


Figure 5.7

5.10 Electronic Isotope Shift

Since an absolute energy scale for the ground state has been established, it is now possible to obtain an estimate for the electronic isotope shift of the $B^1\Sigma^+$ state. This shift represents the difference in the term values, T_e , for HF and DF. The presence of a significant electronic isotope shift would occur because of breakdown of the Born-Oppenheimer approximation. Van Vleck (37) indicates that this shift arises because the centre of mass of the bare dinuclear framework is not the same as that of the diatomic molecule, including the motions of the electrons. In reality, one wobbles about the other, in a nuclear-mass-dependent fashion, so that electronic term energies for excited states are not exactly the same upon isotopic substitution of the constituent nuclides.

Di Lonardo and Douglas (87) obtained a value $T_e = 84783 \text{ cm}^{-1}$ for the B state of HF. In the present work, the corresponding value for DF was found to be $T_e = 84806 \pm 5 \text{ cm}^{-1}$. If the electronic isotope shift is defined as the difference $T_e(\text{HF}) - T_e(\text{DF})$, then a value $\Delta T_e = -23 \pm 5 \text{ cm}^{-1}$ is obtained. The uncertainty reflects primarily the error in the interpolation of ΔG values to obtain absolute energy estimates for the missing ground state levels. This experimental value may be compared with a theoretical estimate obtained by Bunker's (135) equation,

$$\begin{aligned} \Delta T_e = & 0.000068[T_e] + [B_e(\text{HF}) - B_e(\text{DF})]_B \langle L^2 \rangle_B \\ & - [B_e(\text{HF}) - B_e(\text{DF})]_X \langle L^2 \rangle_X \end{aligned} \quad (5.2)$$

where $\langle L^2 \rangle$ is approximated by the sum of the values of $L(L + 1)$ for the dissociation products, for each electronic state. The ground state dissociation products, $\text{F}(^2P) + \text{H}(^2S)$, give a value for $\langle L^2 \rangle_X = 2$, whereas the

corresponding value for the excited state ionic products is $\langle L^2 \rangle_B = 0$. Eq. (5.2), which gives an approximate description only, furnishes a value $\Delta T_e = -14.1 \text{ cm}^{-1}$. This is in reasonable agreement with the value derived experimentally.

CHAPTER 6

ISOTOPIC BEHAVIOUR OF BORN-OPPENHEIMER BREAKDOWN: THE $B^1\Sigma^+$ AND $X^1\Sigma^+$ STATES OF HCl AND DCl

6.1 Introduction

The interpretation of spectroscopic frequencies in terms of theoretical models involving internuclear potentials and functions describing electronic state interactions, forms an important theme of contemporary chemical physics. The thrust of this chapter is to achieve an interpretation of spectral line positions within the framework of an effective radial Schrödinger equation that considers both adiabatic and nonadiabatic corrections.

In Chapter 3, a modern method for reducing experimentally measured line positions to elements of the radial operators was described. Also, an application was made to a set of model data, giving insight into the effectiveness of the procedure. Here, the procedure is applied to experimental line positions of the $X^1\Sigma^+$ and $B^1\Sigma^+$ electronic states of the four isotopically related diatomics, $H^{35}Cl$, $H^{37}Cl$, $D^{35}Cl$, and $D^{37}Cl$.

Before the analysis is described, it is useful to review, briefly, previous works in which the molecular potentials for the HCl isotopomers were calculated. First, we consider the work of Coxon and Ogilvie (46). This analysis was based on the Watson-Dunham analytical expression for E_{vJ} , Eq. (2.47), which makes corrections for omission of higher-order JWKB terms and breakdown of the Born-Oppenheimer approximation. Ground state spectral data for four isotopomers were considered, namely, $H^{35}Cl$ ($v'' = 0-7$), $H^{37}Cl$

($v'' = 0-7$), $D^{35}\text{Cl}$ ($v'' = 0-5$), and $D^{37}\text{Cl}$ ($v'' = 0-4$). It was also possible to determine the Born-Oppenheimer potential for $X^1\Sigma^+$ over a limited range of R . It must be noted, however, that the quoted (46) range of $R = 0.987 - 1.920 \text{ \AA}$, which defines $U^{\text{BO}}(R)$ up to 52% of \mathcal{D}_e , is unduly optimistic. Rather, the smaller range $R = 1.03 - 1.70 \text{ \AA}$, which accounts for the fact that data for DCl up to 30% of the dissociation limit were employed, gives a more realistic indication of the physically significant range for the Born-Oppenheimer potential curve.

In later work by Coxon and Roychowdhury (130), the electronic emission bands of the $B^1\Sigma^+ \rightarrow X^1\Sigma^+$ system of H^{35}Cl were analyzed rotationally, providing reliable and extensive information on the higher vibrational levels of the ground state. The quantum mechanical eigenvalues of a first-order RKR potential constructed for the ground state did not succeed in recovering the experimentally derived vibrational spacings; furthermore, it was demonstrated convincingly that the failure of experimentally derived rotational constants, B_v , to correspond to the RKR averages $\langle R^{-2} \rangle_v$, was accompanied by significant breakdown of the Born-Oppenheimer approximation. In short, this work was important in bringing to light the difficulties encountered in a conventional rotational analysis of high quality spectral data for a hydride.

Improved understanding of the nature of these problems was demonstrated in subsequent work by Coxon (119). Here, the principles of IPA were at the heart of an improved numerical procedure that was superior in its theoretical interpretation of J -dependent nonadiabatic corrections. It was possible for the first time to incorporate systematically the entire spectroscopic information for a hydride over a wide range of vibrational levels, spanning from the potential minimum to near dissociation and taking full account of

adiabatic breakdown. The method was applied to the $X^1\Sigma^+$ ($v'' = 0-17$) and $B^1\Sigma^+$ ($v' = 0-6$) states of H^{35}Cl , and the rather limited ground state data on H^{37}Cl , D^{35}Cl , and D^{37}Cl .

A significantly enhanced procedure, containing improvements to the mathematical correction model, was reported in further work by Coxon (120). Using this more reliable predictor, Coxon was able to extend the assignments for the $B \rightarrow X$ system of H^{35}Cl , particularly to higher J , and made the first extensive rotational assignments for the corresponding band system of H^{37}Cl . The J -dependent nonadiabatic contributions from $q(R)$ (cf. Eq. (3.29)) to the higher rovibrational levels of $X^1\Sigma^+$ were explained in terms of a significant heterogeneous interaction with the repulsive $A^1\Pi$ state. Previously, Mulliken (160) had implicated the $A^1\Pi$ state as the likely single-perturber of the rotational level manifold near the $X^1\Sigma^+$ potential minimum. The small effects encountered in $v'' = 0$ are relatively unimportant in comparison with the rapidly increasing energy shifts experienced by high- v'' , J'' levels, the latter shown (119) to be of the order of several wavenumbers.

The unavailability of spectroscopic data for the higher vibrational levels of deuterium chloride hitherto precluded verification of the predicted (42) theoretical isotopic dependence of $q(R)$. This limitation served as the primary motivation for the spectrographic study reported in Chapter 4. With information on the ground states of HCl and DCl nearly complete, it is now possible to examine reliably the isotopic dependence of Born-Oppenheimer breakdown in $X^1\Sigma^+$ over a large range of R . The analysis also allows for a sound estimation of the Born-Oppenheimer potentials for the $X^1\Sigma^+$ and $B^1\Sigma^+$ electronic states of HCl , and thus a reliable extrapolation to the energy levels of the tritium chloride isotopomer.

6.2 The Multi-Isotopomer Problem

The analysis furnishes effective rotationless potentials for electronic states n that can be expressed as,

$$U_n^{\text{eff}}(R) = U_n^{\text{BO}}(R) + U_n^{\text{A}}(R)/M_{\text{A}} + U_n^{\text{B}}(R)/M_{\text{B}}. \quad (6.1)$$

The inverse dependence on the atomic masses in this expression is theoretically incomplete; smaller terms $\mathcal{O}(1/M^2)$ also predicted, are omitted. The $1/M$ dependence accounts fully for adiabatic corrections and largely for homogeneous nonadiabatic contributions to the rotationless curve. Bunker and Moss (40) have shown that secondary (homogeneous) nonadiabatic terms which are inversely dependent on the square of mass also contribute to $U_n^{\text{eff}}(R)$ if the contact transformation of the exact Hamiltonian is carried out to sufficiently high order. Fortunately, these are predicted to be much smaller than the primary homogeneous contributions; this is confirmed experimentally (46), for even the most highly precise data.

Even if data are available for only a single isotopomer, the present method of analysis can yield direct information on the J -dependent shifts arising from heterogeneous coupling of two nearby electronic states. This is not possible with the approach of molecular constants. The isotopic dependence of $q(R)$ has been given previously, with regard to the model calculations, but is written here also in slightly different notation, as

$$q_n(R) = \mathfrak{q}_n^{\text{A}}(R)/M_{\text{A}} + \mathfrak{q}_n^{\text{B}}(R)/M_{\text{B}}. \quad (6.2)$$

For the multi-isotopomer problem, it is reasoned that, for $\mathfrak{q}_n^{\text{A}}(R)$ and $\mathfrak{q}_n^{\text{B}}(R)$ of comparable magnitude, and M_{A} usually much smaller than M_{B} , the J -dependent

shifts can be explained adequately in terms of $\varphi_n^A(R)$ alone. It is stressed that this is not a necessary condition for the simultaneous consideration of data for many isotopomers. This can be achieved without difficulty, albeit with reduced compactness; the validity of using $\varphi_n^A(R)$ alone in all work was tested critically at intermediate stages of the analysis. A determination of separate $q(R)$ functions for different isotopomers does not improve the quality of the fits significantly. It is found that, within the precision of the data, such an approximation is absorbed at negligible cost to the physical significance of $\varphi_n^A(R)$.

The aim of incorporating spectroscopic line positions for different isotopomers in a least-squares fit to radial functions is to determine functions $U_n^{\text{BO}}(R)$, $U_n^A(R)$, $U_n^B(R)$, and $\varphi_n^A(R)$. The determination of $U_n^{\text{BO}}(R)$ requires isotopic substitution at both atomic centres and can thus be achieved in the present analysis of HCl/DCl data. The four-isotopomer problem is setup as,

$$U_n^{\text{eff}}(R, \text{H}^{35}\text{Cl}) = U_n^{(0)}(R) + \Delta U_n(R), \quad (6.3)$$

$$U_n^{\text{eff}}(R, \text{H}^{37}\text{Cl}) = U_n^{\text{eff}}(R, \text{H}^{35}\text{Cl}) + \Delta U_n^{\text{Cl}}(R), \quad (6.4)$$

$$U_n^{\text{eff}}(R, \text{D}^{35}\text{Cl}) = U_n^{\text{eff}}(R, \text{H}^{35}\text{Cl}) + \Delta U_n^{\text{H}}(R), \quad (6.5)$$

$$U_n^{\text{eff}}(R, \text{D}^{37}\text{Cl}) = U_n^{\text{eff}}(R, \text{H}^{35}\text{Cl}) + \Delta U_n^{\text{H}}(R) + \Delta U_n^{\text{Cl}}(R), \quad (6.6)$$

where $U_n^{(0)}(R)$ is a trial potential for the predominant isotopomer, H^{35}Cl . There are simple mass relationships between the correction functions $\Delta U_n^{\text{Cl}}(R)$ and $\Delta U_n^{\text{H}}(R)$, and the isotopically invariant functions $U_n^{\text{Cl}}(R)$ and $U_n^{\text{H}}(R)$ (cf. Eq. (6.1)).

A $q(R)$ function is determined significantly for the ground electronic

state only. The individual functions for H^{35}Cl and D^{35}Cl can be written as,

$$q_X(\text{H}^{35}\text{Cl}) = m_e [\tilde{R}_X^{\text{H}}(R)/M_{\text{H}} + \tilde{R}_X^{\text{Cl}}(R)/M_{^{35}\text{Cl}}], \quad (6.7)$$

$$q_X(\text{D}^{35}\text{Cl}) = m_e [\tilde{R}_X^{\text{H}}(R)/M_{\text{D}} + \tilde{R}_X^{\text{Cl}}(R)/M_{^{35}\text{Cl}}]. \quad (6.8)$$

Since it has already been established that the $\tilde{R}_X^{\text{Cl}}(R)/M_{\text{Cl}}$ term is not significant to the precision of the data, the multi-isotopomer problem can be cast as,

$$q_X(\text{DCl}) = (M_{\text{H}}/M_{\text{D}})q_X(\text{HCl}). \quad (6.9)$$

The simultaneous incorporation of data for the four isotopomers thus leads to the isotopically invariant function $(\hbar^2/2)m_e \tilde{R}_X^{\text{H}}(R)/R^2$.

The results of the present analysis make it possible to extrapolate to the energy levels of tritium chloride. The calculation of numerical Hamiltonian operators for T^{35}Cl and T^{37}Cl is quite straightforward; from these functions, quantum mechanical eigenvalues can be obtained and synthetic spectra constructed. These can then be compared to available experimental spectra giving an indication of the isotopic self-consistency of the model.

6.3 Determination of Effective Hamiltonian Operators

6.3.1 Selection of Data

The vibrational-rotational spectrum of hydrogen chloride has been known since the pioneering days of infrared absorption spectroscopy. The spectroscopic characterization of the ground electronic state has since been well-established. Here, a brief discussion is given of the data base employed in the least-squares fit to Hamiltonian operators. The information is summarized in Table 6.1, which refers to the ground state HCl/DCl data. The

TABLE 6.1

Summary of Vibrational-Rotational Data for HCl/DCI^a

$\text{H}^{35}\text{Cl}(X^1\Sigma^+)$					
$v'-v''$	Reference	$\epsilon(\text{cm}^{-1})$	N	P_J	R_J
$v = 0$	163	3.3×10^{-6}	1	$J = 1 \leftarrow J = 0$	
$v = 0$	129	6.67×10^{-6}	6	$J'' = 1-6$	
$v = 0$	129	1.17×10^{-5}	3	$J'' = 7-9$	
$v = 0$	166	0.0197	16	$J'' = 18-40$	
$v = 1$	166	0.016	8	$J'' = 19-26$	
$v = 2$	166	0.016	2	$J'' = 21-25$	
1-0	162	0.001	15	1- 2	0-13
1-0	163	0.0022	31	2-29	5-34
1-0	164	0.0045	51	1-30	0-31
2-0	86	0.0002	25	1-12	0-12
2-0	164	0.004	50	1-26	0-25
2-1	163	0.0019	45	1-26	0-29
3-0	162	0.0025	18	1- 9	0- 8
3-0	164	0.007	15	1- 8	0-11
3-1	164	0.0055	21	2-16	0-16
3-2	163	0.0022	44	1-24	0-29
4-2	164	0.0048	11	3-10	4-15
5-3	164	0.007	3	5- 7	
5-4	163	0.0025	21	3-15	1-17
6-5	163	0.006	3		2- 9
$\text{H}^{37}\text{Cl}(X^1\Sigma^+)$					
$v'-v''$	Reference	$\epsilon(\text{cm}^{-1})$	N	P_J	R_J
$v = 0$	161	3.3×10^{-6}	1	$J = 1 \leftarrow J = 0$	
$v = 0$	129	6.7×10^{-6}	6	$J'' = 1-6$	
$v = 0$	129	1.15×10^{-5}	3	$J'' = 7-9$	
$v = 1$	166	0.008	1	$J'' = 20$	

TABLE 6.1 (Cont'd)

Summary of Vibrational-Rotational Data for HCl/DCI^a

$\text{H}^{37}\text{Cl}(X^1\Sigma^+)$					
$v'-v''$	Reference	$\epsilon(\text{cm}^{-1})$	N	P_J	R_J
1-0	162	0.0006	13	1- 2	0-12
1-0	167	0.0085	24	3-19	13-22
2-0	86	0.0002	22	1-11	0-11
2-0	168	0.0093	21	1-13	0-13
3-0	162	0.0028	12	2- 7	0- 5
3-0	169	0.0039	17	1- 8	0- 9
$\text{D}^{35}\text{Cl}(X^1\Sigma^+)$					
$v'-v''$	Reference	$\epsilon(\text{cm}^{-1})$	N	P_J	R_J
$v = 0$	161	1.0×10^{-6}	1	$J = 1 \leftarrow J = 0$	
$v = 0$	161	3.7×10^{-6}	1	$J = 2 \leftarrow J = 1$	
1-0	164	0.0021	13	1- 8	0- 7
1-0	164	0.005	5		12-16
2-0	162	0.00024	26	1-15	0-16
2-0	164	0.002	27	1-15	0-14
3-0	162	0.00054	22	1-11	0-11
3-0	170	0.0034	9	12-16	12-16
$\text{D}^{37}\text{Cl}(X^1\Sigma^+)$					
$v'-v''$	Reference	$\epsilon(\text{cm}^{-1})$	N	P_J	R_J
$v = 0$	161	1.1×10^{-6}	1	$J = 1 \leftarrow J = 0$	
$v = 0$	161	1.0×10^{-5}	1	$J = 2 \leftarrow J = 1$	
1-0	167	0.0125	29	1-15	0-17
2-0	162	0.0005	29	1-14	0-15
2-0	168	0.0082	25	1-13	0-15

TABLE 6.1 (Cont'd)

Summary of Vibrational-Rotational Data for HCl/DCI^a

$D^{37}\text{Cl}(X^1\Sigma^+)$					
$v'-v''$	Reference	$\epsilon(\text{cm}^{-1})$	N	P_J	R_J
3-0	162	0.0013	12	2- 8	1- 0
3-0	170	0.0044	15	1-15	0-14

^a ϵ is the estimated precision of the data; N is the number of lines fitted; P_J and R_J are the ranges of J fitted for the P and R branches, respectively.

weights of individual line positions were calculated as the inverse squares of the precision estimates.

The ground state $v'' = 0$ pure rotational transitions of H^{35}Cl and H^{37}Cl have been studied by CO_2 -laser heterodyning techniques, resulting in very precise molecular constants (129). Although there has not been an analogous study for DCl, the $J = 0, 1$ microwave transitions are known (161) with comparable precision. There have been many investigations (86, 162-171) of the infrared vibrational-rotational bands, involving levels $v'' = 0-6$ in H^{35}Cl , and $v'' = 0-3$ in H^{37}Cl , D^{35}Cl , and D^{37}Cl . A variety of spectroscopic techniques has been employed, including absorption Fourier transform, laser emission, and classical spectrographic absorption methods.

Information on the higher vibrational levels of the ground states of HCl and DCl has become available by analyzing the complex emission rotational structure of $B^1\Sigma^+ - X^1\Sigma^+$ bands (130, 172, 173). For HCl, vibrational levels $v'' = 7-17$ have been studied (130); for DCl the levels $v'' = 10-24$ are involved in emission from the lower vibrational levels of $B^1\Sigma^+$ (173). It is obvious, then, that there is still a significant gap in the information on the ground state of DCl, involving levels $v = 4-9$. Although Deutsch (166) obtained data on levels $v = 4$ and 5, these were found to be contaminated with significant systematic error and were not included in the final least-squares fit. Systematic error in these data has also been detected by Coxon and Ogilvie (46). Similarly, Zughal's (165) data, which were obtained in a study of the pressure broadening of spectral lines, were found to contain systematic error, possibly due to pressure shift effects, and were also excluded from the global fit.

6.3.2 Assignment of $D^{37}\text{Cl } B^1\Sigma^+ - X^1\Sigma^+$ Bands

In the conventional rotational analyses of emission spectra of HCl and DCl, no effort was made to assign lines associated with the ^{37}Cl nuclide; the traditional mass-transformation of molecular constants is simply unreliable. The assignments for H^{37}Cl and D^{37}Cl were thus accomplished by obtaining effective Hamiltonian operators for these isotopomers from the assigned ^{35}Cl isotopomer data. Coxon (120) fitted H^{35}Cl line positions to obtain operators for the $X^1\Sigma^+$ and $B^1\Sigma^+$ states of this isotopomer, and mass-transformed them to obtain approximate operators for H^{37}Cl . The eigenvalues of such functions predicted the $B - X$ emission band structure to within two standard measurement errors. This enabled a reliable assignment of the rotational line positions of H^{37}Cl . A similar analysis of D^{35}Cl data in this work yielded quick and unequivocal assignments for D^{37}Cl through a computer search program.

The $B^1\Sigma^+ \rightarrow X^1\Sigma^+$ line positions were assigned labels describing the spectral line contours (*e.g.* asymmetric, broad, shoulder, diffuse, etc.) as they appeared on the oscilloscope display during the plate-measuring process. It was thus possible to gain a better understanding of the blending problem and justify the exclusion of certain line positions from the global fits. As expected, the blending was worse for the deuteride, as there are more vibrational and rotational levels involved in observed transitions.

6.3.3 Initial Operators and Hamiltonian Correction Model

The most accurate potential functions for the majority of diatomic molecules are available through RKR calculations. However, there are two distinct disadvantages associated with these potentials.

First, experimentally derived molecular constants are used as input. The associated uncertainties have been demonstrated (174) to give rise to an inner limb ripple, despite the "buffering" action that is inherent on account of the structure of the RKR_V equations. Such ripple may be reduced somewhat by smoothing input values through fitting power series in $(v + \frac{1}{2})$.

This, however, does not address the second problem. It is simply not sufficient to report the coefficients of such power series to define the potentials uniquely; many procedures have been proposed to evaluate the RKR_V integrals and the slight nonuniqueness would probably result in differences large enough to cause problems in the description of highly precise pure rotational lines. In addition, and as others have pointed out (95, 175), the extensive multi-digit numerical information required to define the RKR_V potentials is a somewhat undesirable feature.

It was decided therefore to explore the possibility of representing RKR_V turning points entirely by analytic functions. However, in anticipation of a potential lack of smoothness on the inner limb, a method was devised for the smoothing of raw turning points before any attempt was made to represent the potentials by flexible functions. Some time ago, it was found by Coxon (176) that the Morse β parameter (*cf.* Eq. (2.101)) obtained locally for the inner limb turning points as,

$$\beta = \ln[1 + (U^{\text{RKR}_V}(R)/\mathcal{D}_e)^{1/2}]/(R_e - R), \quad (6.10)$$

displayed a linear dependence on the square root of energy, for the higher vibrational levels of diatomic halogen and interhalogen ground states. For the hydrogen halide molecules considered here, it was found that local values of β could be represented very well by,

$$\beta(U) = \sum_{n=0}^N b_n u^n, \quad (6.11)$$

where

$$u = \ln[1 + (U^{\text{RKRV}}(R)/\mathcal{D}_e)^{1/2}]. \quad (6.12)$$

After imposing small corrections on the inner limb, corresponding adjustments were made to the outer limb turning points. This method then assumes that there is essentially no error in the vibrational terms and makes corrections for any lack of smoothness introduced from error in the rotational constants. Although this is not strictly correct, the major source of ripple is expected from error in the g integral (174).

Following the smoothing of the raw RKR V turning points and the generation of extrapolated points in accord with the theoretically expected behaviour of the potential beyond the innermost and outermost points, an attempt was made to find a simple, yet flexible, analytical function for representing the numerical information. Many functions were tested, and it was concluded that no single expression was uniformly successful for all diatomic molecules considered in the tests. For HCl, the function,

$$U(R) = \mathcal{D}_e \left[1 - e^{-\beta(R)[R - R_e]} \right]^2, \quad (6.13)$$

with

$$\beta(R) = \beta_0 + \beta_1(R - R_e) + \beta_2(R - R_e)^2 + \dots + \beta_m(R - R_e)^m, \quad (6.14)$$

was successful at describing the smoothed numerical information. Both electronic states were represented by Eqs. (6.13, 6.14). The weighted nonlinear least-squares analysis gave the fitted parameters listed in Table 6.2. The residuals between the smoothed and fitted functions do not exceed

TABLE 6.2

Trial Potential Functions^a for the $X^1\Sigma^+$ and $B^1\Sigma^+$

States of HCl

Parameter	$X^1\Sigma^+$	$B^1\Sigma^+$
R_e	1.274 558 3 Å	2.511 547 2 Å
β_0	1.867 940 8	0.863 721 98
β_1	$1.401\ 745\ 1 \times 10^{-2}$	0.275 610 08
β_2	0.239 770 33	-0.123 991 54
β_3	$-1.350\ 400\ 0 \times 10^{-2}$	$-3.351\ 652\ 7 \times 10^{-2}$
β_4	$4.566\ 623\ 4 \times 10^{-2}$	$8\ 137\ 865\ 9 \times 10^{-2}$
β_5	$-3.574\ 987\ 1 \times 10^{-2}$	$1.284\ 928\ 8 \times 10^{-2}$
β_6	$-1.242\ 920\ 1 \times 10^{-3}$	$-1.718\ 832\ 9 \times 10^{-2}$
β_7	$2.510\ 519\ 2 \times 10^{-3}$	
D_e	37 243 cm ⁻¹	15 000 cm ⁻¹
R_{min}	0.70 Å	1.40 Å
R_{max}	4.20 Å	3.90 Å
h	0.0025 Å	0.0025 Å
R_{inner}	0.90 Å	1.75 Å
R_{outer}	3.30 Å	3.55
\mathcal{R}	0.90 Å	

^aPotentials constructed from Eqs. (6.13, 6.14) (see text); units of β_m are Å^{-(m+1)}. R_e is the equilibrium internuclear separation, D_e is the dissociation limit and the functions are defined from R_{min} to R_{max} in a mesh of h . R_{inner} , R_{outer} and \mathcal{R} are defined in the text.

2 cm^{-1} on the outer limb, with a root-mean square deviation of approximately 0.7 cm^{-1} .

There are several advantages in representing the potential functions by analytical models. First, the trial functions are defined unequivocally, eliminating any error from interpolation. Smooth initial functions also lead to increased economy in the representation of correction functions in the fitting procedure. Of equal importance is the avoidance of discontinuities associated with potential functions that have been constructed by splicing together different analytic forms with little regard for derivative continuity. This latter concern should be of importance in the numerical integration of the radial wave equation. Finally, the analytical representation approach leads to compact functions, an undeniable advantage over the alternative of long lists of multi-digit RKR_V energies and classical turning points.

A trial $q(R)$ function was not considered. This is not found to affect the ability of first-order perturbation theory to describe properly the rotational shifts after just one iteration. Omitting $q(R)$ in the trial operator is not a matter of necessity but of expedience, and it is shown here how to estimate such a trial function. As demonstrated previously, the experimentally derived rotational constants contain a nonmechanical contribution from $q(R)$. If one calculates the expectation values,

$$B_v^{\text{RKR}_V} = \beta_{\text{at}}^2 \langle \psi_v^{\text{RKR}_V} | R^{-2} | \psi_v^{\text{RKR}_V} \rangle, \quad (6.15)$$

then a *first-order* approximation to $q(R)$ may be obtained from the differences,

$$\Delta B_v = B_v^{\text{exp}} - B_v^{\text{RKR}_V} = \beta_{\text{at}}^2 \langle \psi_v^{\text{RKR}_V} | q(R)/R^2 | \psi_v^{\text{RKR}_V} \rangle. \quad (6.16)$$

$q(R)$ could be expressed in terms of some radial power series expansion and the unknown coefficients determined in accord with the principles of IPA. Normally, however, there is too much noise in the experimentally determined rotational constants to give reliable results. Also, this procedure requires initial potentials (and hence rovibronic wavefunctions) which form close approximations for the effective functions that would be obtained by a full analysis.

Nonetheless, anomalously large *systematic* ΔB_v differences should, at the very least, signal the need to consider inclusion of a $q(R)$ function in the effective Hamiltonian. The ΔB_v residuals were plotted for the ground state by Coxon and Roychowdhury (130) for H^{35}Cl in the rotational analysis of the $B \rightarrow X$ transition. These were found to increase with v and were several times greater than their estimated statistical uncertainties.

A least-squares fit to spectroscopic line positions of the four HCl isotopomers was performed to determine the functions $\Delta U_X(R)$, $\Delta U_X^{\text{H}}(R)$, $\Delta U_X^{\text{Cl}}(R)$, $\Delta U_B(R)$, $\Delta U_B^{\text{H}}(R)$, and the mass-invariant part of $q(R)$, that is, the function $(\hbar^2/2)m_e \tilde{R}_X^{\text{H}}(R)/R^2$. The correction functions $\Delta U_X(R)$ and $\Delta U_B(R)$, were modelled as linear combinations of types of functions appearing in Eq. (3.40).

6.3.4 Least-Squares Fit and Radial Operators

A total of 73 parameters was required to describe 8497 line positions with a reduced standard deviation of $\hat{\sigma}_{red} = 0.961$. The only marginal increase in the value of $\hat{\sigma}_{red}$ from that obtained in a similar analysis of $\text{H}^{35}\text{Cl}/\text{H}^{37}\text{Cl}$ spectroscopic data by Coxon (120) ($\hat{\sigma}_{red} = 0.945$), indicates that the constraint Eq. (6.9) is valid within the precision of the bulk of the data. Tables 6.3 and 6.4 describe the final fitted $B^1\Sigma^+ - X^1\Sigma^+$ data sets for HCl and

TABLE 6.3

Final Assignments for $\text{HCl}(B - X)^a$

Band	H^{35}Cl				H^{37}Cl			
	P_J	R_J	N	rms	P_J	R_J	N	rms
0 - 11	12 - 40	11 - 41	51	0.021				
0 - 12	6 - 42	5 - 42	67	0.021	21 - 41	21 - 42	37	0.022
0 - 13	3 - 38	3 - 38	67	0.019	12 - 37	11 - 38	46	0.024
0 - 14	2 - 35	1 - 35	66	0.021	6 - 34	5 - 34	51	0.023
0 - 15	5 - 30	2 - 30	47	0.018	9 - 30	7 - 30	39	0.027
0 - 16	5 - 22	2 - 24	39	0.025	5 - 19	6 - 19	20	0.023
1 - 10	10 - 45	10 - 43	58	0.029	25 - 44	24 - 44	34	0.019
1 - 11	5 - 44	5 - 42	72	0.027				
1 - 12	4 - 38	0 - 39	71	0.016	4 - 36	3 - 37	57	0.017
1 - 13	3 - 29	5 - 31	49	0.021	18 - 27	15 - 29	20	0.023
1 - 14	26 - 34	26 - 34	18	0.021				
1 - 15	10 - 30	11 - 29	33	0.020	20 - 30	23 - 30	18	0.023
1 - 16	4 - 25	1 - 25	42	0.019	14 - 25	10 - 25	24	0.031
1 - 17	3 - 19	2 - 19	29	0.016	7 - 17	7 - 17	17	0.023
2 - 8	8 - 34	10 - 35	44	0.032				
2 - 9	3 - 45	2 - 42	74	0.027	10 - 27	8 - 25	26	0.030
2 - 10	2 - 44	1 - 43	78	0.024	7 - 38	4 - 39	56	0.028
2 - 11	6 - 38	4 - 38	64	0.022	15 - 34	15 - 33	36	0.030
2 - 12	3 - 28	3 - 29	45	0.018	10 - 22	9 - 22	23	0.016
2 - 14	13 - 32	14 - 32	36	0.015	20 - 30	22 - 30	19	0.016
2 - 15	3 - 22	3 - 23	35	0.019	11 - 16	12 - 20	14	0.019
2 - 16	17 - 25	17 - 24	16	0.028	18 - 25	20 - 25	11	0.027
2 - 17	5 - 19	3 - 19	29	0.026	14 - 19	11 - 18	13	0.029
3 - 7	11 - 35	11 - 33	34	0.033				
3 - 8	4 - 36	5 - 38	64	0.024	11 - 33	10 - 33	33	0.033
3 - 9	3 - 40	1 - 39	68	0.022	6 - 32	7 - 31	46	0.027
3 - 10	2 - 40	2 - 39	71	0.026	7 - 37	7 - 37	52	0.027
3 - 11	5 - 32	3 - 33	53	0.026	26 - 31	25 - 33	14	0.026
3 - 12	32 - 39	35 - 38	11	0.024				
3 - 13	8 - 35	6 - 34	51	0.018				
3 - 14	7 - 21	8 - 24	29	0.016				
3 - 15	22 - 29	23 - 28	12	0.027				
3 - 16	7 - 21	5 - 21	27	0.019				
4 - 7	6 - 35	8 - 34	50	0.024	23 - 33	28 - 32	11	0.028
4 - 8	2 - 37	2 - 38	68	0.027	15 - 35	14 - 36	38	0.027
4 - 9	3 - 36	3 - 35	66	0.023	10 - 33	7 - 34	47	0.026
4 - 10	6 - 27	1 - 28	45	0.017	12 - 22	15 - 24	18	0.021
4 - 12	19 - 34	21 - 34	27	0.017				

TABLE 6.3 (Cont'd)

Final Assignments for $\text{HCl}(B-X)^a$

Band	H^{35}Cl				H^{37}Cl			
	P_J	R_J	N	rms	P_J	R_J	N	rms
4 - 13	4 - 25	5 - 27	39	0.022	10 - 22	13 - 23	20	0.020
4 - 15	12 - 26	14 - 25	25	0.018				
5 - 7	5 - 29	2 - 28	48	0.029				
5 - 8	4 - 32	2 - 31	55	0.028	10 - 26	10 - 25	30	0.032
5 - 9	4 - 30	4 - 29	44	0.037	13 - 27	11 - 25	23	0.036
5 - 12	20 - 30	19 - 29	19	0.020				
6 - 7	11 - 20	10 - 21	19	0.030				
6 - 8	11 - 22	10 - 20	23	0.037				
6 - 11	13 - 23	9 - 22	21	0.020				

^a P_J and R_J define the ranges of J fitted for the P and R branches, respectively. N are the number of lines fitted and the quantity rms is the root-mean-square of the residuals (cm^{-1}) between observed and calculated line positions.

TABLE 6.4

Final Assignments for $\text{DCl}(B - X)^a$

Band	D^{35}Cl				D^{37}Cl			
	P_J	R_J	N	rms	P_J	R_J	N	rms
0 - 16	25 - 60	25 - 62	51	0.036	35 - 59	35 - 61	26	0.042
0 - 17	12 - 59	9 - 59	71	0.032	39 - 56	39 - 56	26	0.041
0 - 18	8 - 55	8 - 54	80	0.036	27 - 54	27 - 54	38	0.041
0 - 19	6 - 51	5 - 51	65	0.037	22 - 51	22 - 51	43	0.041
0 - 20	3 - 46	6 - 45	62	0.036	11 - 46	10 - 46	38	0.048
0 - 21	4 - 38	0 - 39	44	0.032	7 - 28	7 - 26	21	0.031
1 - 14	36 - 45	36 - 45	11	0.042	39 - 44	39 - 44	10	0.056
1 - 15	24 - 63	22 - 63	69	0.035	28 - 63	24 - 61	30	0.039
1 - 16	7 - 57	7 - 58	82	0.034	18 - 55	16 - 58	54	0.042
1 - 17	2 - 51	5 - 50	73	0.033	4 - 50	3 - 49	54	0.041
1 - 18	7 - 38	4 - 38	52	0.032	2 - 40	2 - 38	39	0.041
1 - 19	12 - 50	11 - 50	37	0.036				
1 - 20	30 - 47	30 - 47	32	0.036	34 - 46	34 - 44	13	0.044
1 - 21	16 - 42	17 - 42	43	0.041	22 - 42	19 - 39	26	0.036
1 - 22	4 - 37	4 - 37	50	0.033	18 - 36	15 - 36	15	0.050
1 - 23	12 - 28	11 - 28	29	0.040				
2 - 12	31 - 59	31 - 59	24	0.051				
2 - 13	16 - 54	16 - 54	47	0.040				
2 - 14	10 - 64	3 - 63	84	0.037	13 - 64	13 - 64	40	0.055
2 - 15	6 - 57	7 - 57	87	0.039	18 - 48	21 - 49	33	0.043
2 - 16	7 - 62	2 - 63	81	0.037	15 - 40	14 - 38	30	0.042
2 - 17	2 - 57	2 - 57	61	0.033	13 - 33	12 - 33	32	0.044
2 - 18	6 - 53	5 - 55	39	0.040				
2 - 19	32 - 47	33 - 47	23	0.040	40 - 45	39 - 45	12	0.043
2 - 20	16 - 38	17 - 39	33	0.039				
2 - 21	13 - 41	16 - 42	30	0.043				
2 - 22	24 - 37	24 - 37	17	0.030	28 - 36	26 - 36	13	0.046
2 - 23	7 - 30	9 - 31	29	0.040				
2 - 24	8 - 22	8 - 22	13	0.051				
3 - 12	10 - 60	8 - 60	58	0.042	20 - 40	22 - 40	19	0.049
3 - 13	4 - 64	8 - 64	94	0.042	6 - 60	9 - 60	57	0.048
3 - 14	6 - 59	5 - 58	90	0.035	8 - 55	7 - 53	60	0.048
3 - 15	3 - 49	4 - 51	78	0.035	11 - 50	12 - 50	48	0.045
3 - 16	5 - 35	4 - 37	48	0.043	11 - 38	11 - 39	29	0.048
3 - 17	8 - 55	8 - 55	25	0.044				
3 - 18	24 - 48	24 - 50	35	0.033				
3 - 21	23 - 39	25 - 40	24	0.046				
3 - 22	11 - 26	10 - 28	26	0.047				
3 - 23	24 - 31	24 - 30	12	0.046				
3 - 24	15 - 21	13 - 22	11	0.049				

TABLE 6.4 (Cont'd)
Final Assignments for DCl(*B* - *X*)^a

Band	D ³⁵ Cl				D ³⁷ Cl			
	<i>P_J</i>	<i>R_J</i>	<i>N</i>	rms	<i>P_J</i>	<i>R_J</i>	<i>N</i>	rms
4 - 11	5 - 48	5 - 51	59	0.044	27 - 48	29 - 50	18	0.045
4 - 12	4 - 64	2 - 64	90	0.036	7 - 43	8 - 42	36	0.054
4 - 13	2 - 59	0 - 59	91	0.036	8 - 60	9 - 59	56	0.043
4 - 14	4 - 56	2 - 55	82	0.038	5 - 41	7 - 45	51	0.041
4 - 15	2 - 46	1 - 49	67	0.038				
4 - 17	27 - 50	27 - 49	35	0.042				
4 - 18	3 - 40	0 - 40	56	0.040				
4 - 19	10 - 24	9 - 26	15	0.042				
4 - 21	17 - 26	14 - 26	11	0.023				
5 - 10	23 - 46	23 - 46	29	0.042				
5 - 11	7 - 55	7 - 57	79	0.043	17 - 47	16 - 48	28	0.046
5 - 12	3 - 58	2 - 59	97	0.045	5 - 49	5 - 48	52	0.046
5 - 13	7 - 53	6 - 51	78	0.036	4 - 47	4 - 47	47	0.041
5 - 14	1 - 43	1 - 44	57	0.038	14 - 28	15 - 32	21	0.041
5 - 16	34 - 50	35 - 50	22	0.037				
5 - 17	8 - 45	9 - 46	52	0.040	19 - 43	19 - 39	17	0.049
5 - 19	26 - 41	28 - 41	14	0.045				
5 - 20	8 - 29	9 - 31	21	0.041				
6 - 10	26 - 57	26 - 55	35	0.045				
6 - 11	9 - 57	9 - 57	73	0.041	15 - 48	15 - 48	37	0.047
6 - 12	4 - 54	3 - 53	69	0.049	9 - 42	9 - 42	38	0.050
6 - 13	7 - 49	10 - 53	61	0.042	18 - 42	18 - 41	27	0.045
6 - 16	6 - 43	2 - 44	50	0.045				
6 - 17	14 - 38	17 - 35	17	0.042				
6 - 19	11 - 35	11 - 36	27	0.040				
7 - 10	27 - 49	27 - 49	29	0.040				
7 - 11	13 - 52	15 - 50	60	0.056	21 - 48	18 - 48	31	0.050
7 - 12	15 - 47	15 - 47	39	0.048				
7 - 15	11 - 46	8 - 46	43	0.050				
7 - 16	11 - 37	4 - 39	27	0.056				
7 - 18	18 - 43	12 - 43	24	0.045				

^a*P_J* and *R_J* define the ranges of *J* fitted for the *P* and *R* branches, respectively. *N* are the number of lines fitted and the quantity rms is the root-mean-square of the residuals (cm⁻¹) between observed and calculated line positions.

DCI, respectively.

A calculation of the line positions from the eigenvalues of the corrected operators gave a reduced standard deviation of $\hat{\sigma}_{red} = 0.979$. This slight increase from the value obtained in the fit can be interpreted in terms of breakdown of first-order perturbation theory. The breakdown is insignificant however, and the data are still described within the measurement precisions. Also in view of the fact that the increase in $\hat{\sigma}_{red}$ was global and not restricted to individual line positions, an iteration was considered unwarranted.

The fitted values of the 73 parameters required to reconstruct the correction functions are given in Table 6.5. No uncertainties are given here, but the determinations were typically ten to one. Watson's prescription (177) for rounding-off least-squares parameter estimates has been followed. The trial and error method of constraining systematically individual parameters proposed recently by Tellinghuisen (178), would clearly be impractical for this work.

It is realized that a fair amount of labour is required to reconstruct the functions from the coefficients. Such is the price that must be paid, however, for achieving accuracy in the rotational spacings of $\approx 10^{-6} \text{ cm}^{-1}$ near the potential minimum. For some purposes it is sufficient to consult the RKR_V-type of listings given in Tables 6.6-6.9. An 8-point Lagrangian interpolation of the function $R^2U(R)$ has been recommended (111, 179) to keep the associated errors small, and its use is also suggested here. A more complete numerical listing of the fundamental functions $U^{BO}(R)$, $U^H(R)$, $U^{Cl}(R)$ and $\tilde{R}_X^H(R)$ is given in Appendix A-2.

The quantum mechanical eigenvalues of the eight operators obtained in

TABLE 6.5

Fitted Coefficients (p_k) for Correction Functions^a

k	Function	p_k
<i>Ground State $\Delta U_X(R)$ function</i>		
1	F_{X41}	$3.118\ 25 \times 10^4$
2	F_{X51}	$6.004\ 643 \times 10^5$
3	F_{X61}	$5.019\ 099 \times 10^6$
4	F_{X71}	$2.118\ 461\ 1 \times 10^7$
5	F_{X81}	$4.391\ 117\ 9 \times 10^7$
6	F_{X91}	$3.599\ 082 \times 10^7$
7	$G_{X1}\ (1.2725/1.37364)$	$2.099\ 8 \times 10^{-2}$
8	$G_{X2}\ (1.45779)$	$-1.429\ 01 \times 10^{-1}$
9	$G_{X3}\ (1.49729)$	$-9.803\ 5 \times 10^{-2}$
10	$G_{X4}\ (1.57897)$	$-3.907\ 0 \times 10^{-1}$
11	$G_{X5}\ (1.65262)$	$-9.107\ 5 \times 10^{-2}$
12	$G_{X6}\ (1.72238)$	-3.357×10^{-1}
13	$G_{X7}\ (1.79028)$	2.436×10^{-1}
14	$G_{X8}\ (1.85752)$	4.397×10^{-1}
15	$G_{X9}\ (1.92500)$	1.086 9
16	$G_{X10}\ (1.99348)$	1.669 3
17	$G_{X11}\ (2.06377)$	2.144 2
18	$G_{X12}\ (2.13663)$	2.646 9
19	$G_{X13}\ (2.21300)$	3.115 9
20	$G_{X14}\ (2.29430)$	3.199 0
21	$G_{X15}\ (2.38202)$	2.886 9
22	$G_{X16}\ (2.47880)$	2.244 1
23	$G_{X17}\ (2.58849)$	9.272 9
24	$G_{X18}\ (2.71724)$	1.799 4
25	$G_{X19}\ (2.87796)$	1.040 3
26	$G_{X20}\ (2.97300)$	$1.024\ 3 \times 10^1$
27	$G_{X21}\ (3.183/3.40)$	-8.630
28	S_X	$1.219\ 225 \times 10^{-5}$

TABLE 6.5 (Cont'd)
 Fitted Coefficients (p_k) for Correction Functions^a

k	Function	p_k
<i>Ground State $g_X(R)$ function</i>		
29	H_{X2}	$3.807 \ 1 \times 10^{-4}$
30	H_{X3}	$-3.188 \ 4 \times 10^{-3}$
31	H_{X4}	$2.312 \ 6 \times 10^{-3}$
32	H_{X5}	$-6.441 \ 0 \times 10^{-4}$
<i>Ground State $\Delta U_X^{Cl}(R)$ function</i>		
33	F_{X21}	6.349
34	F_{X31}	$7.760 \ 8 \times 10^1$
35	F_{X41}	$2.252 \ 2 \times 10^2$
36	F_{X32}	5.880×10^{-2}
37	F_{X42}	-3.906×10^{-2}
38	$S_{X,Cl}$	1.96×10^{-7}
<i>Ground State $\Delta U_X^H(R)$ function</i>		
39	F_{X41}	$-2.225 \ 35 \times 10^3$
40	F_{X51}	$-2.648 \ 27 \times 10^4$
41	F_{X61}	$-1.061 \ 16 \times 10^5$
42	F_{X71}	$-1.387 \ 53 \times 10^5$
43	F_{X22}	3.989 59
44	F_{X32}	$-2.118 \ 331 \times 10^1$
45	F_{X42}	$1.494 \ 713 \times 10^1$
46	F_{X52}	-1.506 01
47	F_{X62}	$-7.938 \ 1 \times 10^{-1}$
48	$S_{X,H}$	$-3.022 \ 3 \times 10^{-5}$
<i>Excited State $\Delta U_B(R)$ function</i>		
49	F_{B31}	$-3.980 \ 60 \times 10^2$
50	F_{B41}	$1.173 \ 982 \times 10^4$
51	F_{B51}	$8.291 \ 192 \times 10^3$

TABLE 6.5 (Cont'd)
Fitted Coefficients (p_k) for Correction Functions^a

k	Function	p_k
52	F_{X61}	$1.144\ 334 \times 10^4$
53	F_{X71}	$4.567\ 71 \times 10^3$
54	$G_{B1}(2.50/2.68207)$	-1.019 0
55	$G_{B2}(2.81597)$	-4.045 2
56	$G_{B3}(2.87585)$	-4.484 2
57	$G_{B4}(2.99438)$	-8.579 4
58	$G_{B5}(3.09621)$	-4.437 0
59	$G_{B6}(3.18869)$	-7.021 1
60	$G_{B7}(3.27476)$	1.419 6
61	$G_{B8}(3.35686/3.45)$	-2.360
62	S_B	$4.001\ 0 \times 10^{-4}$
<i>Excited State $\Delta U_B^H(R)$ function</i>		
63	F_{B11}	-1.884 4
64	F_{B21}	$-1.441\ 4 \times 10^1$
65	F_{B31}	$1.785\ 2 \times 10^1$
66	F_{B42}	$-2.688\ 31 \times 10^2$
67	F_{B52}	$1.513\ 62 \times 10^3$
68	F_{B62}	$-3.181\ 49 \times 10^3$
69	F_{B72}	$2.956\ 45 \times 10^3$
70	F_{B82}	$-1.020\ 568 \times 10^3$
71	$S_{B,H}$	$7.753\ 1 \times 10^{-4}$
<i>Excited State T_e Corrections</i>		
72	$\Delta T_e(\text{HCl})$	-3.318
73	$\Delta T_e(\text{DCI})$	7.791

^aThe internuclear distances used for the generation of expectation values are $R_e^X = 1.27455363\ \text{\AA}$ and $R_e^B = 2.5104848\ \text{\AA}$. For the G_{ni} , the values in parentheses are the R_{ni} ; for G_{X1} and G_{B1} the values given are the R_{n0} and R_{n1} ; similarly, for G_{X21} and G_{B8} , the second values in parentheses are the pivot points for the α_{ni2} .

TABLE 6.6

Internuclear Potentials for the $X^1\Sigma^+$ States of H^{35}Cl and H^{37}Cl^a

v	$\text{H}^{35}\text{Cl}(X^1\Sigma^+)$			$\text{H}^{37}\text{Cl}(X^1\Sigma^+)$		
	G_v	R_{\min}	R_{\max}	G_v	R_{\min}	R_{\max}
0	1483.880	1.177176	1.393424	1482.768	1.177209	1.393374
1	4369.857	1.117191	1.497280	4366.639	1.117241	1.497179
2	7151.864	1.080690	1.578958	7146.695	1.080748	1.578813
3	9830.658	1.053654	1.652589	9823.697	1.053717	1.652400
4	12406.715	1.032069	1.722353	12398.117	1.032136	1.722119
5	14880.158	1.014122	1.790229	14870.080	1.014191	1.789948
6	17250.770	0.998818	1.857456	17239.370	0.998888	1.857125
7	19517.840	0.985546	1.924922	19505.281	0.985617	1.924537
8	21680.085	0.973901	1.993401	21666.533	0.973973	1.992956
9	23735.620	0.963604	2.063649	23721.253	0.963675	2.063136
10	25681.690	0.954452	2.136476	25666.696	0.954523	2.135885
11	27514.689	0.946298	2.212857	27499.271	0.946367	2.212174
12	29229.726	0.939033	2.294050	29214.111	0.939100	2.293255
13	30820.375	0.932579	2.381762	30804.819	0.932644	2.380826
14	32278.243	0.926885	2.478470	32263.044	0.926946	2.477350
15	33592.316	0.921918	2.588014	33577.829	0.921975	2.586636
16	34747.970	0.917673	2.716789	34734.628	0.917725	2.715024
17	35725.102	0.914168	2.877233	35713.469	0.914212	2.874839

^aEnergies are in units of cm^{-1} and internuclear separations in \AA .

TABLE 6.7

Internuclear Potentials for the $X^1\Sigma^+$ States of $D^{35}\text{Cl}$ and $D^{37}\text{Cl}^a$

v	$D^{35}\text{Cl}(X^1\Sigma^+)$			$D^{37}\text{Cl}(X^1\Sigma^+)$		
	G_v	R_{\min}	R_{\max}	G_v	R_{\min}	R_{\max}
0	1066.603	1.190909	1.373633	1065.044	1.190965	1.373553
1	3157.663	1.137970	1.457786	3153.105	1.138057	1.457630
2	5195.034	1.105120	1.522496	5187.633	1.105222	1.522275
3	7179.055	1.080413	1.579754	7168.967	1.080526	1.579471
4	9109.984	1.060410	1.633036	9097.365	1.060531	1.632692
5	10988.018	1.043554	1.683963	10973.024	1.043680	1.683557
6	12813.238	1.028984	1.733454	12796.026	1.029115	1.732985
7	14585.653	1.016170	1.782105	14566.378	1.016304	1.781571
8	16305.222	1.004756	1.830367	16284.041	1.004892	1.829764
9	17971.695	0.994493	1.878585	17948.769	0.994631	1.877909
10	19584.715	0.985199	1.927055	19560.208	0.985337	1.926303
11	21143.818	0.976733	1.976062	21117.896	0.976872	1.975226
12	22648.301	0.968991	2.025880	22621.139	0.969129	2.024954
13	24097.277	0.961889	2.076794	24069.056	0.962025	2.075769
14	25489.663	0.955358	2.129116	25460.573	0.955494	2.127982
15	26824.102	0.949347	2.183208	26794.345	0.949481	2.181952
16	28098.921	0.943813	2.239502	28068.715	0.943944	2.238106
17	29312.064	0.938720	2.298526	29281.645	0.938848	2.296967
18	30461.041	0.934043	2.360945	30430.667	0.934167	2.359195
19	31542.848	0.929761	2.427633	31512.806	0.929881	2.425651
20	32553.829	0.925860	2.499769	32524.441	0.925975	2.497500
21	33489.525	0.922332	2.578988	33461.160	0.922441	2.576353
22	34344.501	0.919174	2.667652	34317.584	0.919275	2.664533
23	35111.924	0.916390	2.769687	35086.966	0.916483	2.765877
24	35782.945	0.913995	2.891090	35760.567	0.914077	2.886313

^aEnergies are in cm^{-1} and internuclear distances in \AA .

TABLE 6.8

Internuclear Potentials for the $B^1\Sigma^+$ States of H^{35}Cl and H^{37}Cl^a

v	$\text{H}^{35}\text{Cl}(B^1\Sigma^+)$			$\text{H}^{37}\text{Cl}(B^1\Sigma^+)$		
	G_v	R_{\min}	R_{\max}	G_v	R_{\min}	R_{\max}
0	430.936	2.317497	2.714873	430.616	2.317569	2.714794
1	1276.358	2.175088	2.876472	1275.421	2.175217	2.876323
2	2090.344	2.074589	2.995175	2088.838	2.074760	2.994970
3	2874.378	1.990216	3.096697	2872.343	1.990425	3.096442
4	3630.282	1.914810	3.189113	3627.756	1.915055	3.188811
5	4359.904	1.845365	3.274896	4356.921	1.845644	3.274548
6	5065.210	1.780419	3.357174	5061.800	1.780729	3.356778

^aEnergies are given in cm^{-1} units and internuclear distances in Å.

TABLE 6.9

210

Internuclear Potentials for the $B^1\Sigma^+$ States of $D^{35}\text{Cl}$ and $D^{37}\text{Cl}$

v	$D^{35}\text{Cl}(B^1\Sigma^+)$			$D^{37}\text{Cl}(B^1\Sigma^+)$		
	G_v	R_{\min}	R_{\max}	G_v	R_{\min}	R_{\max}
0	310.570	2.345892	2.682145	310.119	2.346011	2.682016
1	923.148	2.225790	2.816166	921.820	2.226000	2.815926
2	1519.189	2.141985	2.913145	1517.030	2.142261	2.912821
3	2099.183	2.072417	2.995614	2096.239	2.072751	2.995216
4	2663.796	2.010812	3.069400	2660.109	2.011201	3.068932
5	3213.602	1.954403	3.137904	3209.211	1.954843	3.137366
6	3749.364	1.901710	3.202499	3744.305	1.902199	3.201898
7	4271.750	1.851890	3.263793	4266.056	1.852426	3.263129

^aEnergies are in units of cm^{-1} and internuclear distances in \AA .

this work are listed in Appendix A-3. From these eigenvalues, the fitted line positions were calculated and the residuals from the observed frequencies formed. These are listed in Appendix A-4.

The functions $U_X^H(R)$, $U_X^{Cl}(R)$, and $U_B^H(R)$ are plotted in Figures 6.1, 6.2, and 6.3, respectively. Also shown in these plots are the innermost and outermost turning points obtained by considering all the fitted E_{wJ} , and some indication of the radial distribution of rotational levels for the highest vibrational levels. The function $\tilde{R}_X^H(R)$ is plotted in Figure 6.4. Shown in all plots of radial functions are the 95% confidence limits as obtained by standard methods (57).

According to the theory of Watson (42), the function $\tilde{R}_X^H(R)$ can be expressed as,

$$\tilde{R}_X^H(R) = R_X^H(R) - R^{-1} \int_{R_0}^R Q_X^H(R) dR, \quad (6.17)$$

where the function $Q_X^H(R)$ accounts for homogeneous coupling of $X^1\Sigma^+$ to excited $1\Sigma^+$ electronic states, and $R_X^H(R)$ signifies pure heterogeneous mixing. In regions where $R_X^H(R) \gg Q_X^H(R)$, the coupling can be thought of as purely heterogeneous, and the radial variation of the matrix element $\langle A^1\Pi | L_{xH} | X^1\Sigma^+ \rangle$ can be examined. The function $R_X^H(R)$ ($\approx \tilde{R}_X^H(R)$) can be written as,

$$R_X^H(R) = \left[\frac{1}{m_e R^2} \right] \sum_n \left\{ |\langle n | L_{xH} | X^1\Sigma^+ \rangle|^2 + |\langle n | L_{yH} | X^1\Sigma^+ \rangle|^2 \right\} / \{U_X(R) - U_n(R)\} + Z_H, \quad (6.18)$$

where Z_H is the charge of the hydrogen nucleus and the summation is taken over all excited 1Π states. It is assumed that $A^1\Pi - X^1\Sigma^+$ is the predominant

Figure 6.1

The estimated function $U_X^H(R)$ for $\text{HCl/DCI}(X^1\Sigma^+)$. The dotted and broken curves represent the 95% confidence limits of the fitted function. R_{\min} and R_{\max} represent the innermost and outermost classical turning points respectively, obtained by considering all the fitted E_{vJ} .

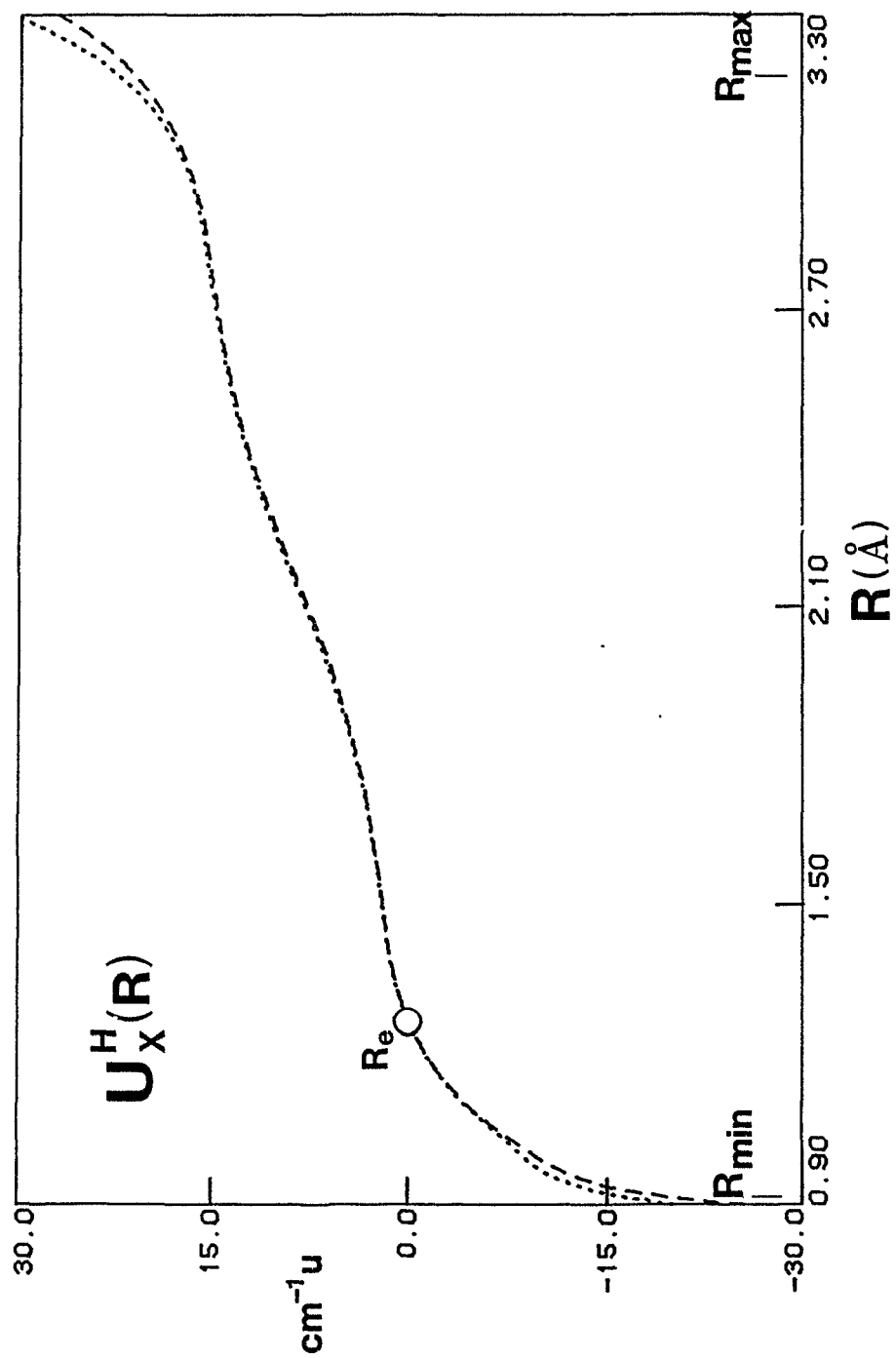


Figure 6.1

Figure 6.2

The estimated function $U_X^{\text{Cl}}(R)$ for $\text{HCl/DCI}(X^1\Sigma^+)$. The dotted and broken curves represent the 95% confidence limits of the fitted function. R_{min} and R_{max} represent the innermost and outermost classical turning points respectively, obtained by considering all the fitted E_v .

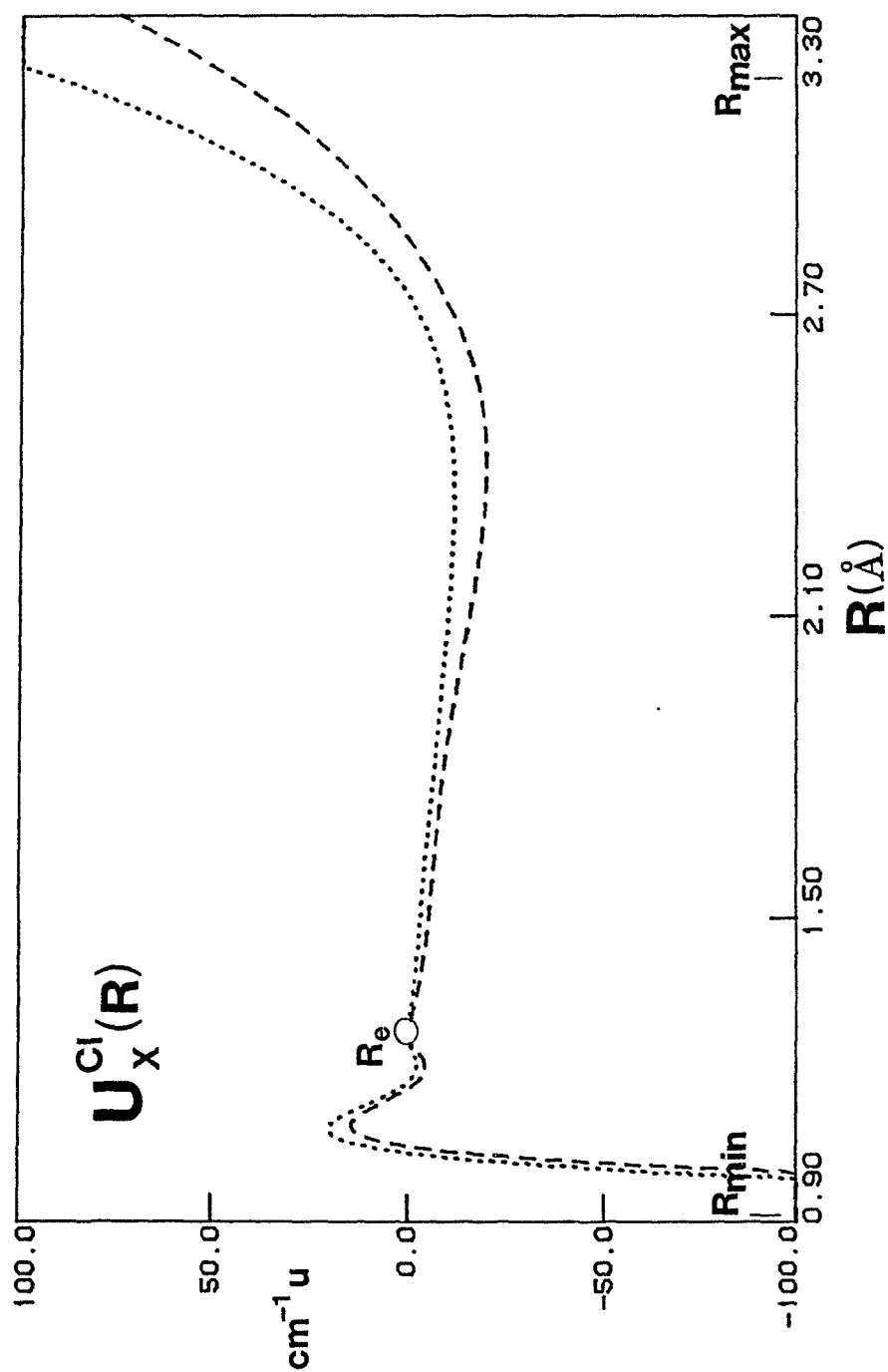


Figure 6.2

Figure 6.3

The estimated function $U_B^H(R)$ for $\text{HCl/DCI}(B^1\Sigma^+)$. The dotted and broken curves represent the 95% confidence limits of the fitted function. R_{\min} and R_{\max} represent the innermost and outermost classical turning points respectively, obtained by considering all the fitted E_{vJ} .

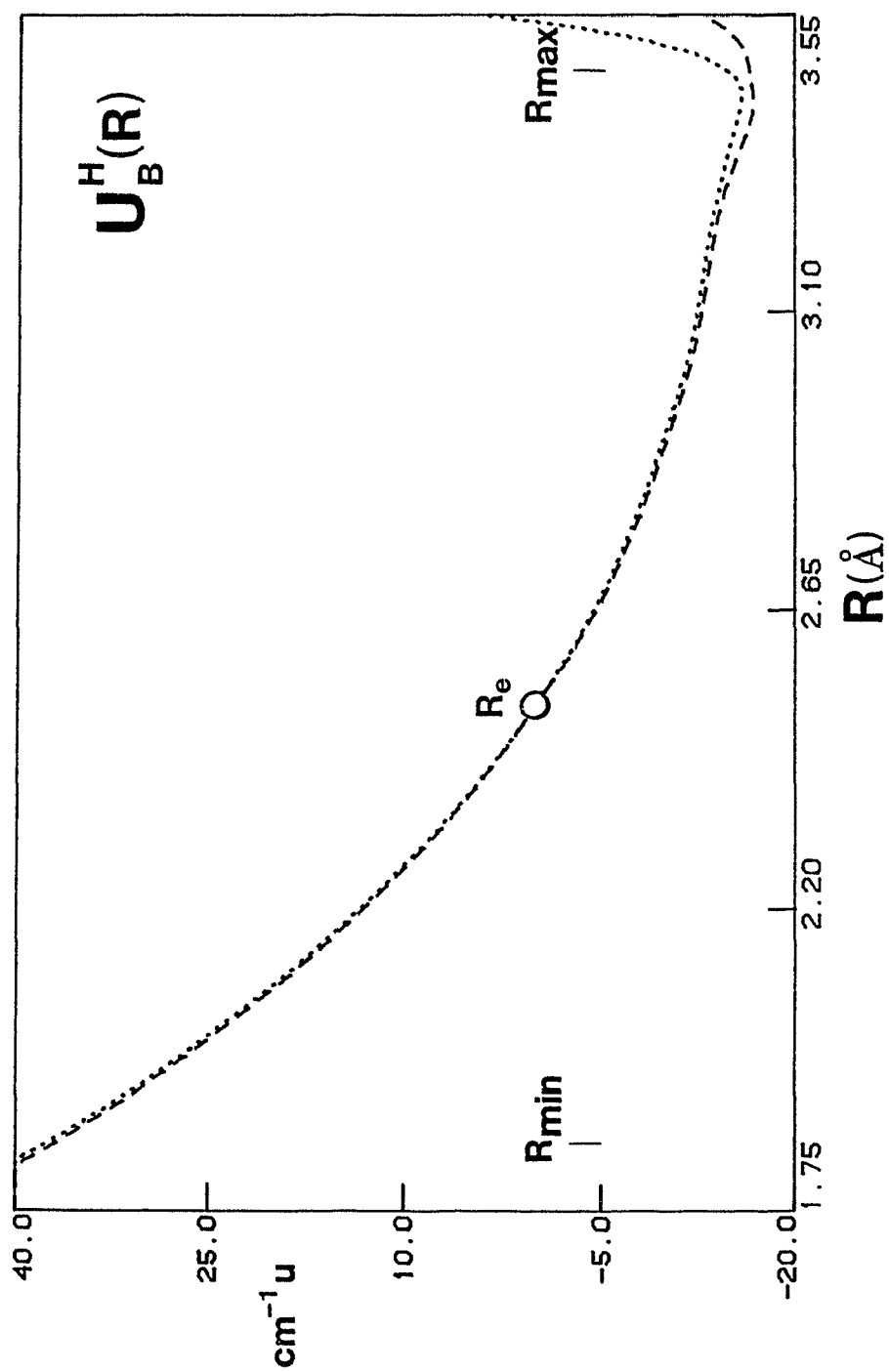


Figure 6.3

Figure 6.4

The estimated function $\tilde{R}_X^H(R)$ for $\text{HCl/DCI}(X^1\Sigma^+)$. The two solid lines represent the 95% confidence limits of the fitted function.

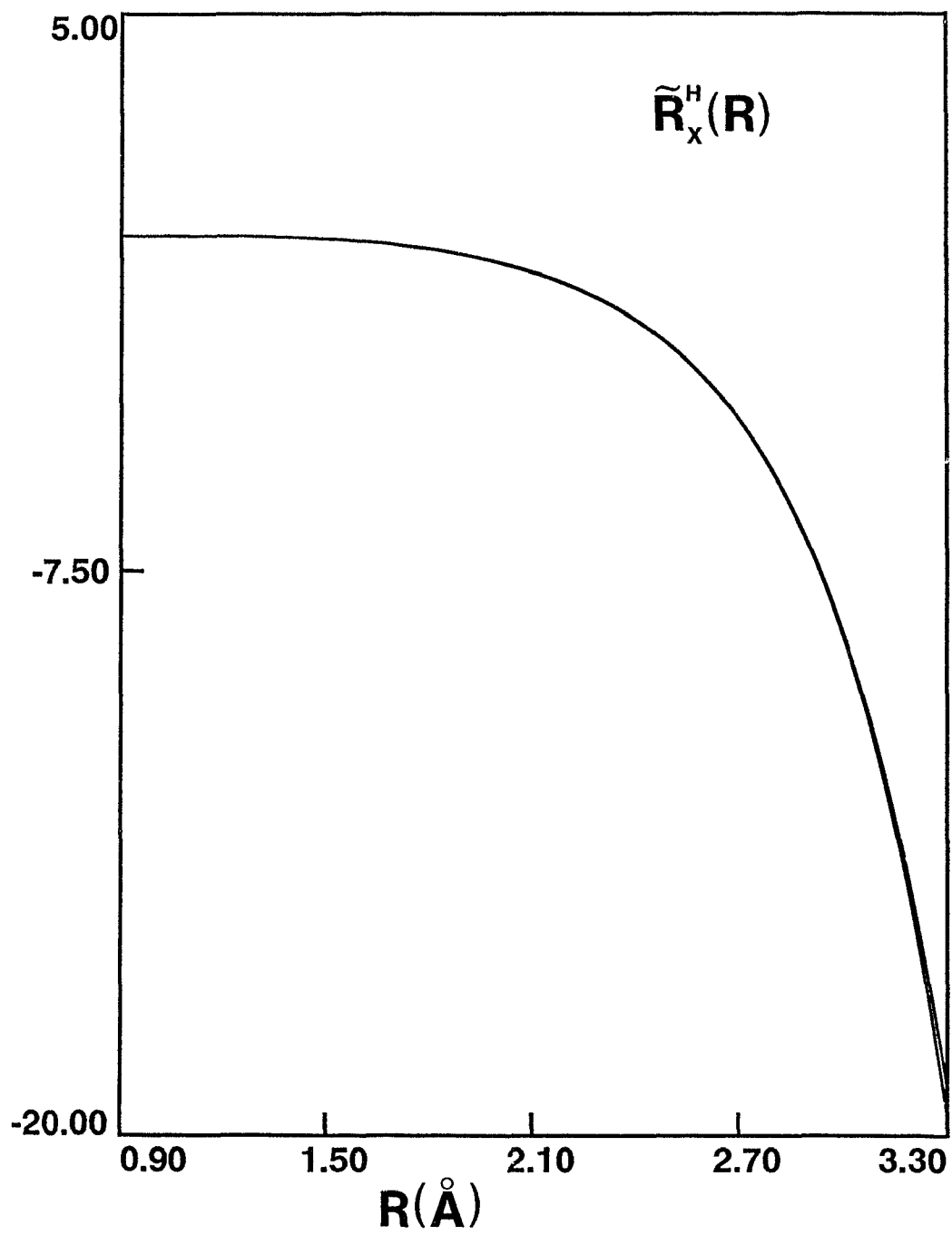


Figure 6.4

heterogeneous interaction in regions where homogeneous coupling is small. From the results of *ab initio* calculations (127), this range has been chosen as 1.80 - 3.20 Å for HCl/DCl. Based on this single heterogeneous perturber hypothesis, the matrix element $\langle A^1\Pi | L_{xH} | X^1\Sigma^+ \rangle$ can be found from,

$$|\langle A^1\Pi | L_{xH} | X^1\Sigma^+ \rangle| = \left[(\tilde{R}_X^H(R) - Z_H)(m_e R^2/4)[U_X(R) - U_A(R)] \right]^{1/2}, \quad (6.19)$$

having assumed $\langle L_{xH} \rangle^2 = \langle L_{yH} \rangle^2$. The potential for the repulsive $A^1\Pi$ state was represented by the analytical expression,

$$U_A(R) = \mathcal{D}_e(X^1\Sigma^+) + \mathcal{A} e^{-R^n}, \quad (6.20)$$

obtained by fitting parameters \mathcal{A} and n to the *ab initio* potential (127); the fitted parameters are $\mathcal{A} = 140\,998\text{ cm}^{-1}$ and $n = 1.745\,390\,5$, and the dissociation limit $\mathcal{D}_e(X^1\Sigma^+)$ was constrained to the thermochemical value of $37\,243\text{ cm}^{-1}$ (119). Values of the matrix element obtained in this fashion are presented in Table 6.10. This restricted type of calculation shows the matrix element to possess a smooth radial variation with increasing R , reaching a fairly constant value in the range $2.8 \leq R \leq 3.2\text{ Å}$. Beyond this internuclear separation the function $q(R)$ (and hence $\tilde{R}_X^H(R)$) is not known with certainty. Also, as $A^1\Pi$ continues to approach $X^1\Sigma^+$ towards larger R , there is an expected breakdown of the Van Vleck transformation, which is essentially a second-order *nondegenerate* perturbation description.

6.4 Isotopic Variation of Equilibrium Bond Lengths

The isotopic dependence of equilibrium rotational constants has received considerable attention. Fortunately, the spectroscopic characterization of the low- v, J levels of the isotopomers of HCl has been accomplished through

TABLE 6.10

Radial Variation of Matrix Element $\langle A^1\Pi | L_x | X^1\Sigma^+ \rangle$ for HCl^a

R	$\Delta U(R)$	\tilde{R}_X^H	$ \langle A^1\Pi L_x X^1\Sigma^+ \rangle $
2.2	-12711	-1.09	0.44
2.4	-7529	-1.88	1.14
2.6	-4230	-3.16	1.46
2.8	-2271	-5.28	1.62(8)
3.0	-1184	-8.86	1.69(9)
3.2	-620	-14.89	1.74(8)

^a R are in Å units and $\Delta U(R)$ in units of cm^{-1} . For the last three entries, the numbers in parentheses signify estimated errors.

techniques which provide very precise results; the isotopic variation of R_e for HCl can therefore also be described with comparable certainty.

The work of Kaiser (93) dealt primarily with the hyperfine structure and parameters of $v'' = 0-2$, $J'' = 1-2$ in H^{35}Cl , and $v'' = 0-1$, $J'' = 1-3$ in D^{35}Cl , as well as with the influence of the electric dipole moment on the moment of inertia. The rotational g factor was determined as $g_J = 0.47 \pm 0.03$ for $v'', J'' = 0, 1$ of H^{35}Cl from a measurement of the rotational magnetic moment of the perturbed ground state. Kaiser also reported estimates of R_e for H^{35}Cl and D^{35}Cl ; these appear to be the adiabatic values, even though they were not explicitly identified as such. They were obtained by considering the effect on the moment of inertia of the nonspherical electron distribution around the two atoms.

Shortly thereafter, improved measurements of submillimeter-wave transitions were made for several hydrogen halides (161). These included the first reliable measurements on the H^{37}Cl and D^{37}Cl isotopomers. A detailed theoretical interpretation of these frequencies was made to obtain R_e^{BO} , the equilibrium bond length in the Born-Oppenheimer approximation. This result was in slight error because an assumption was made that g_J is proportional to μ^{-1} ; g_J has a more complicated mass dependence. This oversight led to slightly erroneous estimates of the correction for the nonspherical electron distribution.

A rigorous theoretical investigation into the isotopic variation of R_e was made by Watson (180). An important result of this work was the expression,

$$R_e(Y_{01}) = R_e^{\text{BO}} \{1 + m_e(d_{\text{H}}/M_{\text{H}} + d_{\text{Cl}}/M_{\text{Cl}})\}, \quad (6.21)$$

which enables the estimation of the Born-Oppenheimer equilibrium bond length by considering R_e values obtained from uncorrected estimates of Y_{01} . The parameters d_i comprise adiabatic, nonadiabatic and semiclassical corrections. Collectively, they describe the small difference between B_e and Y_{01} .

Another important expression in Watson's article (180) relates the adiabatic equilibrium bond length to that obtained in the clamped nuclei approximation, as

$$R_e^{\text{ad}} = R_e^{\text{BO}} \{1 + m_e(d_{\text{H}}^{\text{ad}}/M_{\text{H}} + d_{\text{Cl}}^{\text{ad}}/M_{\text{Cl}})\}. \quad (6.22)$$

The parameters d_i^{ad} refer to adiabatic corrections exclusively. A solution of the electronic wave equation in spaced-fixed coordinates gives these as,

$$d_i^{\text{ad}} = -(1/2m_e k^{\text{BO}} R_e^{\text{BO}}) \left[\frac{d}{dR} \langle X^1 \Sigma^+ | \mathbf{p}_i^2 | X^1 \Sigma^+ \rangle \right]_{R_e^{\text{BO}}}, \quad (6.23)$$

where \mathbf{p}_i are the momenta of the nuclei relative to space-fixed axes. A space-fixed coordinate system was employed (180) as it leads to a simpler expression for the adiabatic correction, the expectation value in Eq. (6.23). k^{BO} is the Born-Oppenheimer harmonic force constant, or $d^2 U^{\text{BO}}(R)/dR^2$ evaluated at R_e^{BO} . The relation between R_e^{ad} and R_e^{BO} can also be written as (180),

$$R_e^{\text{ad}} = R_e^{\text{BO}} - (1/k^{\text{BO}}) \left[\frac{d\Delta U^{\text{ad}}(R)}{dR} \right]_{R_e^{\text{BO}}}, \quad (6.24)$$

where $\Delta U^{\text{ad}}(R)$ is the adiabatic correction.

Improved atomic masses (181) and fundamental constants (182) have become available since the analysis of Watson (180); his analysis was therefore repeated here for the isotopomers of HCl. Table 6.11 lists estimates of $R_e(Y_{01})$ obtained by using the conversion factor, $B(\text{MHz}) = 505\,379.075/\mu R_e^2$, for μ in amu and R_e in Å, where μ is calculated from improved estimates of the

TABLE 6.11

Isotopic Dependence of Equilibrium Internuclear Separations for HCl^a

Isotopomer	$R_e(Y_{01})$	$R_e(U_X^{\text{eff}})$	R_e^{ad}
H ³⁵ Cl	1.274 556 710(40)	1.274 545 903(18)	1.274 709 86
H ³⁷ Cl	1.274 556 631(40)	1.274 545 797(10)	1.274 709 73
D ³⁵ Cl	1.274 579 071(55)	1.274 576 083(20)	1.274 656 13
D ³⁷ Cl	1.274 578 989(60)	1.274 575 964(12)	1.274 656 01
T ³⁵ Cl	1.274 587 254(1140)	1.274 585 960(55)	1.274 638 25
T ³⁷ Cl	1.274 586 171(1140)	1.274 585 935(47)	1.274 638 13

$$R_{Xe}^{\text{BO}} = 1.274\ 604\ 3(1) \text{ from } U_X^{\text{BO}}(R).$$

$$R_e^{\text{BO}} = 1.274\ 600\ 0(6) \text{ from Eq. (6.21) and } R_e(Y_{01}) \text{ above.}$$

^aAll quantities are in Ångstrom units.

atomic masses. The atomic masses and reduced molecular masses employed in this work are listed in Table 6.12. Table 6.11 also contains the R_e^{eff} values corresponding to the minima of the numerical functions $U^{\text{eff}}(R)$ determined in the present analysis. The quantal values, R_e^{eff} , differ from the semiclassical $R_e(Y_{01})$ values in a clearly mass-dependent way. A weighted least-squares fit of Eq. (6.21) to the semiclassical estimates gave $R_e^{\text{BO}} = 1.274\,600\,0(6) \text{ \AA}$, $d_{\text{H}} = -0.06451(12)$, and $d_{\text{Cl}} = 0.075(34)$.

The Born-Oppenheimer potential for $X^1\Sigma^+$ has also been obtained from the individual isotopically dependent potential functions. Its minimum has been found numerically at $R_e^{\text{BO}} = 1.274\,604\,3(1) \text{ \AA}$, in good agreement with the value given above, considering that the errors on these quantities do not reflect the uncertainties in the fundamental constants. In particular, the uncertainty in Planck's constant would introduce a corresponding uncertainty in the R_e^{BO} value of approximately $1 \times 10^{-6} \text{ \AA}$. This alone does not explain the observed discrepancy; nor is it clear why a deviation of such magnitude is found. One may speculate that, while the potentials obtained in this work inextricably contain radiative and relativistic corrections, Eq. (6.21) may not be capable of extracting such effects in a theoretically proper fashion. Along the similar theme of a deficiency in Eq. (6.21), a separate fit found the coefficient of $(m_e/M_{\text{H}})^2$ to be marginally supported; this indicates that R_e^{BO} and d_i determined in accord with Eq. (6.21) are slightly contaminated. On the other hand, since the correction functions determined in this work are expanded about a *trial* R_e estimate and hence forced to assume zero values at the trial potential minimum, it may not be unreasonable to expect a *model-dependent* error on the R_e^{eff} estimates which would also display isotopic dependence; this could lead to a slightly ($\approx 10^{-6} \text{ \AA}$) erroneous R_e^{BO} estimate.

TABLE 6.12

Atomic and Reduced Molecular Masses^a

<i>Atomic Masses</i>	
$M(^1\text{H})$	1.007 825 037
$M(^2\text{H})$	2.014 101 787
$M(^3\text{H})$	3.016 049 286
$M(^{35}\text{Cl})$	34.968 852 729
$M(^{37}\text{Cl})$	36.965 902 624
<i>Reduced Molecular Masses</i>	
$\mu(^1\text{H}^{35}\text{Cl})$	0.979 592 544
$\mu(^1\text{H}^{37}\text{Cl})$	0.981 077 299
$\mu(^2\text{H}^{35}\text{Cl})$	1.904 413 254
$\mu(^2\text{H}^{37}\text{Cl})$	1.910 032 891
$\mu(^3\text{H}^{35}\text{Cl})$	2.776 571 155
$\mu(^3\text{H}^{37}\text{Cl})$	2.788 532 798

^aAtomic masses taken from Ref. (181).

With R_e^{BO} and d_i now available, it was possible to obtain new estimates of the adiabatic parameters d_i^{ad} from the expressions (180),

$$d_{\text{H}} = d_{\text{H}}^{\text{ad}} - \frac{\mu \Delta Y_{01}}{2m_e B_e} - \frac{(\mu g_J)_{\text{Cl}}}{2m_p}, \quad (6.25)$$

$$d_{\text{Cl}} = d_{\text{Cl}}^{\text{ad}} - \frac{\mu \Delta Y_{01}}{2m_e B_e} - \frac{(\mu g_J)_{\text{H}}}{2m_p}, \quad (6.26)$$

where m_p is the protonic mass and ΔY_{01} the Dunham correction. The isotopically independent values $(\mu g_J)_i$ are given by (180),

$$(\mu g_J)_{\text{H}} = \mu g_J + 2c_{\text{Cl}} m_p M_{\text{Cl}} / (M_{\text{H}} + M_{\text{Cl}}), \quad (6.27)$$

and

$$(\mu g_J)_{\text{Cl}} = \mu g_J + 2c_{\text{H}} m_p M_{\text{H}} / (M_{\text{H}} + M_{\text{Cl}}), \quad (6.28)$$

so that

$$g_J = (\mu g_J)_{\text{Cl}} / M_{\text{H}} + (\mu g_J)_{\text{H}} / M_{\text{Cl}}, \quad (6.29)$$

showing clearly that g_J is not simply dependent on μ^{-1} . Eqs. (6.27, 6.28) introduce the formal charges c_{H} and c_{Cl} , discussed further below. The Dunham correction in Eqs. (6.25, 6.26) is given in terms of the anharmonic potential derivatives, a_n , as

$$\Delta Y_{01} = (B_e^3 / 4\omega_e^2) (30 + 28a_1 + 21a_1^2 + 21a_1^3 - 18a_2 - 46a_1 a_2 + 30a_3). \quad (6.30)$$

Precise a_n for $\text{HCl}(X^1\Sigma^+)$ have been reported by Coxon and Ogilvie (46). Despite these improved estimates, we do not obtain a significant difference in the estimates of d_i^{ad} from those of Watson (180). Using $d_{\text{H}}^{\text{ad}} = 0.155$ and $d_{\text{Cl}}^{\text{ad}} = 0.116$ (180), estimates of R_e^{ad} are also presented in Table 6.11. It is interesting to note that, given the expression for d_i^{ad} , Eq. (6.23) above, the

adiabatic matrix elements $\langle X^1\Sigma^+ | \mathbf{P}_i^2 | X^1\Sigma^+ \rangle$ must possess *negative* slopes near the equilibrium configuration of the Born-Oppenheimer curve. Hence, the total adiabatic correction must similarly be associated with a negative slope near R_e^{BO} .

According to Watson (180), there exists a relationship between d_i and d_i^{ad} and c_i , the formal charges associated with each atom. It is given by

$$d_{\text{H}} - d_{\text{Cl}} = d_{\text{H}}^{\text{ad}} - d_{\text{Cl}}^{\text{ad}} - c_{\text{H}} = d_{\text{H}}^{\text{ad}} - d_{\text{Cl}}^{\text{ad}} + c_{\text{Cl}}, \quad (6.31)$$

where $|c_i| = |D/eR_e|$, D being the equilibrium dipole moment and e the electronic charge. From the d_i and d_i^{ad} obtained in this work, we calculate $c_{\text{H}} = 0.1786$ and $c_{\text{Cl}} = -0.1786$. Using Kaiser's (93) equilibrium dipole moment, $M_e = 1.0933$ D and $R_e = 1.27456$ Å, we also obtain $|c_i| = 0.1786$, indicative of the consistency in the theory. The small formal charges on atoms H and Cl imply a H^+Cl^- distribution of electronic charge, in accord with chemical intuition. This slight imbalance of charge is related to a finite dipole moment, and is also linked to the small degree of ionicity in the ground electronic state. For HF, the significantly higher degree of ionicity in the ground state is reflected in the formal charges $c_{\text{H}} = 0.4083$, and $c_{\text{F}} = -0.4083$ obtained by using a dipole moment of 1.7982 D (183). Ultimately, these observations reflect the orbital composition of the electronic wavefunctions for HCl and HF ground states, shown by *ab initio* calculations (127, 149) to be admixtures of ionic with valence configurations.

It is clear that the equilibrium bond lengths in the adiabatic approximation follow a mass-dependent trend which is opposite to that of both the $R_e(Y_{01})$ and R_e^{eff} . As indicated by Eq. (6.24), above, in order for the adiabatic R_e^{ad} values to be larger than R_e^{BO} , it is necessary for the adiabatic

correction, $\Delta U^{\text{ad}}(R)$, to possess a negative slope at R_e^{BO} . An examination of Fig. 6.1 of $U_X^{\text{H}}(R)$ obtained in this work reveals a *positive* slope near the potential minimum; hence the opposite isotopic trend is observed in R_e^{eff} . This observation is important. It implies that the function $U_X^{\text{H}}(R)$ is considerably different from the true adiabatic correction, $\Delta U_X^{\text{ad}}(R)$. Therefore, the experimentally derived function $U_X^{\text{H}}(R)$ must contain significant homogeneous nonadiabatic contributions, most likely due to interactions between $X^1\Sigma^+$ and the lowest excited bound electronic state, $B^1\Sigma^+$, which has a vertical excitation energy of approximately 10.9 eV (173), and the Rydberg $H^1\Sigma^+(0^+)$ state, which undergoes a diabatic curve crossing with $B^1\Sigma^+$ at approximately the same energy.

6.5 Perturbation Calculation of Centrifugal Distortion

A nonuniqueness has been discussed previously regarding the potential energy functions for individual isotopomers. Coxon (120) has demonstrated numerically that the nonuniqueness parameter λ has negligible effect on the quantum mechanical eigenvalues, when applied in the prescription suggested by Watson (42). This is discussed further in Section 6.8. Any parametrization of energy must also be independent of λ . Hence, the rotational energy expression,

$$F_w = B_v^{\text{eff}}[J(J + 1)] - D_v^{\text{eff}}[J(J + 1)]^2 + H_v^{\text{eff}}[J(J + 1)]^3 + \dots, \quad (6.32)$$

will also be affected only slightly by use of different λ as prescribed by Watson (42). B_v^{eff} , D_v^{eff} , H_v^{eff} , etc., are rotational and centrifugal distortion constants contaminated with nonmechanical effects. They are the perturbed constants determined through a fit of experimental line positions to

a power series in $J(J + 1)$. The theoretically correct expression for B_v^{eff} has been given previously as Eq. (3.57). The centrifugal distortion constants can be calculated most efficiently through the methodology laid out by Hutson (53). The computer code of Hutson was modified, however, to account for the effects of $q(R)$. Constants were calculated in this fashion for the $B^1\Sigma^+$ and $X^1\Sigma^+$ states of all four isotopomers and are listed in Tables 6.13-6.16.

A particularly rigid test of the physical significance of such constants was carried out for $v'' = 0$ of H^{35}Cl and H^{37}Cl , by comparing synthetic pure rotational line positions for $J'' = 0-9$ with those obtained very precisely through tunable far-infrared laser spectroscopy (129). The comparison is shown in Table 6.17. Also shown is a comparison of rotational and centrifugal constants obtained from perturbation theory and experimentally. The agreement is found to be exceptional. These observations provide strong support for the physical significance of the calculated constants and hence also the derived operators.

There is a twofold benefit in obtaining molecular constants through perturbation theory. First, the physical significance of the results derived from a Hamiltonian correction analysis may be evaluated. In some cases it is even possible to diagnose the progressive lack of physical meaning of rotational parameters obtained traditionally; this problem is of particular concern for the coefficients of increasing powers of $J(J + 1)$. Second, the availability of constants which are quantum mechanically consistent with the derived operators offers the possibility of representing the eigenvalues compactly.

This latter potential benefit was investigated further. The calculated

TABLE 6.13

Quantum Mechanical Molecular Constants for $\text{HCl}(X^1\Sigma^+)^a$

$\text{H}^{35}\text{Cl}(X^1\Sigma^+)$						
v	G_v	B_v	D_v	H_v	L_v	M_v
0	1483.8803	10.4401982	5.280772-4	1.672182-8	-8.64924-13	3.086-17
	1483.8803	10.4402186	5.280302-4	1.673014-8	-8.64250-13	3.091-17
1	4369.8569	10.1361830	5.214313-4	1.61678-8	-8.963-13	2.698-17
	4369.8569	10.1362482	5.213716-4	1.61775-8	-8.955-13	2.704-17
2	7151.8635	9.8345962	5.154519-4	1.55218-8	-9.418-13	2.37-17
	7151.8635	9.8347122	5.153782-4	1.55330-8	-9.408-13	2.38-17
3	9830.6584	9.5347866	5.102765-4	1.47755-8	-1.0107-12	1.22-17
	9830.6584	9.5349600	5.101873-4	1.47885-8	-1.0095-12	1.23-17
4	12406.7146	9.236010	5.061039-4	1.3866-8	-1.088-12	8.78-18
	12406.7146	9.236248	5.059975-4	1.3881-8	-1.087-12	8.99-18
5	14880.1579	8.937344	5.03084-4	1.2828-8	-1.20-12	-6.2-17
	14880.1579	8.937655	5.02957-4	1.2846-8	-1.19-12	-6.2-17
6	17250.770	8.63780	5.0155-4	1.13-8		
	17250.770	8.63820	5.0140-4	1.13-8		
7	19517.840	8.33580	5.01924-4	9.7025-9	-1.560-12	-1.699-16
	19517.840	8.33629	5.01749-4	9.7301-9	-1.556-12	-1.690-16
8	21680.085	8.02993	5.04502-4	7.273-9	-2.076-12	-1.01-16
	21680.085	8.03052	5.04294-4	7.309-9	-2.069-12	-9.91-17
9	23735.620	7.717943	5.10297-4	4.438-9	-2.4018-12	-3.507-16
	23735.620	7.718651	5.10048-4	4.484-9	-2.3919-12	-3.481-16
10	25681.690	7.397450	5.19730-4	4.233-10	-3.4461-12	-5.812-16
	25681.690	7.398296	5.19429-4	4.869-10	-3.4298-12	-5.764-16
11	27514.689	7.065210	5.34621-4	-5.286-9	-4.630-12	-9.420-16
	27514.689	7.066220	5.34250-4	-5.195-9	-4.603-12	-9.328-16
12	29229.726	6.716843	5.56686-4	-1.3414-8	-6.969-12	-1.6540-15
	29229.726	6.718049	5.56217-4	-1.3278-8	-6.921-12	-1.6350-15
13	30820.375	6.34665	5.88966-4	-2.5465-8	-1.0929-11	-3.469-15
	30820.375	6.34810	5.88351-4	-2.5247-8	-1.0835-11	-3.424-15
14	32278.243	5.94685	6.3632-4	-4.4865-8	-1.8549-11	-6.784-15
	32278.243	5.94861	6.3547-4	-4.4487-8	-1.8348-11	-6.670-15
15	33592.316	5.50610	7.0716-4	-7.757-8	-3.493-11	-1.675-14
	33592.316	5.50829	7.0591-4	-7.684-8	-3.444-11	-1.640-14

TABLE 6.13 (Cont'd)

Quantum Mechanical Molecular Constants for $\text{HCl}(X^1\Sigma^+)^a$

$\text{H}^{35}\text{Cl}(X^1\Sigma^+)$						
v	G_v	B_v	D_v	H_v	L_v	M_v
16	34747.970	5.00723	8.1828-4	-1.4130-7	-7.738-11	-4.81-14
	34747.970	5.01007	8.1621-4	-1.3965-7	-7.587-11	-4.66-14
17	35725.102	4.42018	1.0097-3	-2.901-7	-2.259-10	-2.25-13
	35725.102	4.42411	1.0057-3	-2.853-7	-2.196-10	-2.16-13
$\text{H}^{37}\text{Cl}(X^1\Sigma^+)$						
v	G_v	B_v	D_v	H_v	L_v	M_v
0	1482.7679	9.4245153	5.264830-4	1.664659-8	-8.5975-13	3.058-17
	1482.7679	9.4245357	5.264361-4	1.665487-8	-8.5908-13	3.063-17
1	4366.6391	10.121190	5.19863-4	1.6095-8	-8.9-13	2.7-17
	4366.6391	10.121256	5.19804-4	1.6104-8	-8.9-13	2.7-17
2	7146.6954	9.820285	5.1390-4	1.54-8	-9.4-13	2.4-17
	7146.6954	9.820401	5.1383-4	1.55-8	-9.3-13	2.4-17
3	9823.697	9.521148	5.0874-4	1.47-8	-1.0-12	1.2-17
	9823.697	9.521321	5.0865-4	1.47-8	-1.0-12	1.2-17
4	12398.117	9.223043	5.0458-4	1.38-8	-1.1-12	8.5-18
	12398.117	9.223280	5.0447-4	1.38-8	-1.1-12	8.7-18
5	14870.080	8.925051	5.0156-4	1.28-8	-1.2-12	-6.2-17
	14870.080	8.925361	5.0144-4	1.28-8	-1.2-12	-6.1-17
6	17239.370	8.62619	5.0002-4	1.124-8	-1.390-12	1.035-17
	17239.370	8.62659	4.9988-4	1.126-8	-1.387-12	1.086-17
7	19505.281	8.32489	5.0039-4	9.666-9	-1.5482-12	-1.678-16
	19505.281	8.32537	5.0021-4	9.694-9	-1.5439-12	-1.669-16
8	21666.533	8.01974	5.0293-4	7.256-9	-2.0615-12	-1.003-16
	21666.533	8.02032	5.0273-4	7.291-9	-2.0549-12	-9.886-17
9	23721.253	7.70850	5.0869-4	4.438-9	-2.3822-12	-3.447-16
	23721.253	7.70921	5.0844-4	4.484-9	-2.3723-12	-3.421-16
10	25666.696	7.38881	5.1805-4	4.578-10	-3.4175-12	-5.750-16
	25666.696	7.38965	5.1775-4	5.210-10	-3.4015-12	-5.703-16

TABLE 6.13 (Cont'd)

Quantum Mechanical Molecular Constants for $\text{HCl}(X^1\Sigma^+)^a$

$\text{H}^{37}\text{Cl}(X^1\Sigma^+)$						
v	G_v	B_v	D_v	H_v	L_v	M_v
11	27499.271	7.05744	5.3283-4	-5.206-9	-4.5895-12	-9.280-16
	27499.271	7.05844	5.3246-4	-5.116-9	-4.5626-12	-9.189-16
12	29214.111	6.71003	5.5474-4	-1.326-8	-6.9031-12	-1.633-15
	29214.111	6.71123	5.5427-4	-1.313-8	-6.8550-12	-1.614-15
13	30804.819	6.34092	5.8678-4	-2.520-8	-1.0808-11	-3.419-15
	30804.819	6.34237	5.8616-4	-2.498-8	-1.0715-11	-3.375-15
14	32263.044	5.94239	6.3376-4	-4.440-8	-1.8326-11	-6.674-15
	32263.044	5.94415	6.3292-4	-4.402-8	-1.8128-11	-6.562-15
15	33577.829	5.50319	7.0400-4	-7.672-8	-3.4440-11	-1.644-14
	33577.829	5.50537	7.0275-4	-7.600-8	-3.3955-11	-1.609-14
16	34734.628	5.00629	8.1405-4	-1.396-7	-7.6103-11	-4.701-14
	34734.628	5.00911	8.1200-4	-1.379-7	-7.4629-11	-4.560-14
17	35713.469	4.42197	1.0033-3	-2.856-7	-2.2075-10	-2.181-13
	35713.469	4.42587	9.9930-4	-2.809-7	-2.1458-10	-2.100-13

^aAll quantities are in units of cm^{-1} . For each vibrational level, the top and bottom entries represent perturbed and deperturbed values, respectively. 5.280772-4 reads as 5.280772×10^{-4} .

TABLE 6.14

Quantum Mechanical Molecular Constants for $\text{HCl}(B^1\Sigma^+)^a$

$\text{H}^{35}\text{Cl}(B^1\Sigma^+)$						
v	G_v	B_v	D_v	H_v	L_v	M_v
0	430.936	2.73990	1.1614-4	1.2638-8	-2.836-12	7.866-16
1	1276.358	2.76407	1.4032-4	2.0484-8	-5.753-12	1.980-15
2	2090.344	2.79491	1.6994-4	3.1703-8	-1.059-11	4.298-15
3	2874.378	2.83232	2.0529-4	4.6962-8	-1.829-11	8.601-15
4	3630.282	2.87564	2.4691-4	6.7482-8	-2.985-11	1.578-14
5	4359.904	2.92435	2.9469-4	9.3524-8	-4.642-11	2.688-14
6	5065.210	2.97732	3.4872-4	1.2576-7	-6.561-11	3.453-14
$\text{H}^{37}\text{Cl}(B^1\Sigma^+)$						
v	G_v	B_v	D_v	H_v	L_v	M_v
0	430.616	2.73574	1.1578-4	1.2578-8	-2.818-12	7.803-16
1	1275.421	2.75985	1.3986-4	2.0381-8	-5.714-12	1.963-15
2	2088.838	2.79061	1.6936-4	3.1534-8	-1.052-11	4.259-15
3	2872.343	2.82793	2.0457-4	4.6702-8	-1.815-11	8.521-15
4	3627.756	2.87113	2.4601-4	6.7097-8	-2.962-11	1.563-14
5	4356.921	2.91971	2.9359-4	9.2979-8	-4.606-11	2.665-14
6	5061.798	2.97254	3.4740-4	1.2504-7	-6.517-11	3.435-14

^aAll quantities are in units of cm^{-1} . 1.1614-4 reads as 1.1614×10^{-4} .

TABLE 6.15

Quantum Mechanical Molecular Constants for $\text{DCl}(X^1\Sigma^+)^a$

$\text{D}^{35}\text{Cl}(X^1\Sigma^+)$						
v	G_v	B_v	D_v	H_v	L_v	M_v
0	1066.6029 1066.6029	5.3922719 5.3922756	1.39956-4 1.39950-4	2.286-9 2.286-9	-6.0-14 -6.0-14	
1	3157.6629 3157.6629	5.2798470 5.2798587	1.38663-4 1.38656-4	2.233-9 2.234-9	-6.1-14 -6.1-14	
2	5195.0340 5195.0340	5.1681217 5.1681422	1.37451-4 1.37443-4	2.175-9 2.176-9	-6.4-14 -6.4-14	
3	7179.0550 7179.0550	5.0569848 5.0570148	1.36338-4 1.36328-4	2.111-9 2.112-9	-6.6-14 -6.6-14	
4	9109.984 9109.984	4.946317 4.946358	1.3533-4 1.3532-4	2.046-9 2.046-9	-7.1-14 -7.1-14	
5	10988.018 10988.018	4.836002 4.836053	1.3447-4 1.3446-4	1.955-9 1.956-9	-7.3-14 -7.3-14	
6	12813.24 12813.24	4.72582 4.72589	1.337-4 1.337-4	1.88-9 1.88-9	-7-14 -7-14	
7	14585.65 14585.65	4.61568 4.61576	1.331-4 1.331-4	1.76-9 1.76-9	-9-14 -9-14	
8	16305.22 16305.22	4.50533 4.50542	1.328-4 1.328-4	1.62-9 1.62-9		
9	17971.69 17971.69	4.39446 4.39457	1.327-4 1.326-4	1.49-9 1.49-9	-9.5-14 -9.5-14	
10	19584.715 19584.715	4.28289 4.28301	1.32754-4 1.32730-4	1.3069-9 1.3088-9	-1.239-13 -1.237-13	-6.12-18 -6.10-18
11	21143.818 21143.818	4.17026 4.17041	1.33226-4 1.33199-4	1.0716-9 1.0739-9	-1.280-13 -1.278-13	-2.35-19 -2.14-19
12	22648.301 22648.301	4.05615 4.05631	1.34063-4 1.34034-4	8.3554-10 8.3825-10	-1.522-13 -1.520-13	-9.43-18 -9.39-18
13	24097.277 24097.278	3.94017 3.94036	1.35335-4 1.35301-4	5.2349-10 5.2682-10	-1.890-13 -1.886-13	-1.39-17 -1.39-17
14	25489.663 25489.663	3.82182 3.82204	1.37176-4 1.37137-4	1.2495-10 1.2913-10	-2.256-13 -2.250-13	-1.85-17 -1.84-17
15	26824.102 26824.102	3.70047 3.70071	1.39706-4 1.39661-4	-3.8342-10 -3.7807-10	-2.943-13 -2.935-13	-2.54-17 -2.52-17

TABLE 6.15 (Cont'd)

Quantum Mechanical Molecular Constants for $\text{DCI}(X^1\Sigma^+)^a$

$\text{D}^{35}\text{Cl}(X^1\Sigma^+)$						
v	G_v	B_v	D_v	H_v	L_v	M_v
16	28098.921	3.57533	1.43119-4	-1.0286-9	-3.728-13	-4.30-17
	28098.921	3.57561	1.43066-4	-1.0216-9	-3.717-13	-4.28-17
17	29312.064	3.44549	1.47618-4	-1.8675-9	-4.896-13	-6.75-17
	29312.064	3.44581	1.47556-4	-1.8580-9	-4.879-13	-6.71-17
18	30461.041	3.30983	1.53505-4	-3.0010-9	-6.792-13	-1.03-16
	30461.041	3.31018	1.53429-4	-2.9878-9	-6.764-13	-1.03-16
19	31542.848	3.16690	1.61244-4	-4.5743-9	-9.817-13	-1.640-16
	31542.848	3.16731	1.61150-4	-4.5552-9	-9.771-13	-1.628-16
20	32553.829	3.01486	1.71494-4	-6.7729-9	-1.435-12	-2.878-16
	32553.829	3.01534	1.71374-4	-6.7440-9	-1.426-12	-2.853-16
21	33489.525	2.85132	1.85153-4	-1.0003-8	-2.278-12	-5.713-16
	33489.525	2.85187	1.84993-4	-9.9563-9	-2.262-12	-5.657-16
22	34344.501	2.67303	2.03930-4	-1.5309-8	-4.052-12	-1.161-15
	34344.501	2.67369	2.03706-4	-1.5229-8	-4.018-12	-1.146-15
23	35111.924	2.47496	2.31046-4	-2.4092-8	-6.929-12	-2.288-15
	35111.924	2.47576	2.30710-4	-2.3937-8	-6.849-12	-2.245-15
24	35782.945	2.24989	2.71069-4	-4.1184-8	-1.875-11	-1.218-14
	35782.945	2.25092	2.70509-4	-4.0832-8	-1.850-11	-1.198-14
$\text{D}^{37}\text{Cl}(X^1\Sigma^+)$						
v	G_v	B_v	D_v	H_v	L_v	M_v
0	1065.0435	5.376490	1.39134-4	2.266-9	-5.96-14	
	1065.0435	5.376494	1.39128-4	2.266-9	-5.96-14	
1	3153.1050	5.264562	1.37852-4	2.214-9	-6.07-14	
	3153.1050	5.264573	1.37845-4	2.214-9	-6.07-14	
2	5187.6325	5.153328	1.36648-4	2.156-9	-6.28-14	
	5187.6325	5.153349	1.36639-4	2.156-9	-6.28-14	
3	7168.9668	5.042678	1.35541-4	2.093-9	-6.54-14	
	7168.9668	5.042708	1.35532-4	2.093-9	-6.53-14	

TABLE 6.15 (Cont'd)

Quantum Mechanical Molecular Constants for $\text{DCl}(X^1\Sigma^+)^a$

$\text{D}^{37}\text{Cl}(X^1\Sigma^+)$						
v	G_v	B_v	D_v	H_v	L_v	M_v
4	9097.365 9097.365	4.93249 4.93253	1.3454-4 1.3453-4	2.028-9 2.029-9	-6.98-14 -6.98-14	
5	10973.024 10973.024	4.82266 4.82271	1.3368-4 1.3367-4	1.938-9 1.939-9	-7.18-14 -7.17-14	
6	12796.026 12796.026	4.71297 4.71303	1.3296-4 1.3295-4	1.8599-9 1.8610-9	-7.02-14 -7.02-14	
7	14566.378 14566.378	4.60331 4.60339	1.3236-4 1.3235-4	1.7439-9 1.7451-9	-8.93-14 -8.92-14	
8	16284.041 16284.041	4.49345 4.49354	1.3202-4 1.3200-4	1.6046-9 1.6060-9	-8.65-14 -8.64-14	
9	17948.769 17948.769	4.38308 4.38318	1.3188-4 1.3186-4	1.4738-9 1.4754-9	-9.33-14 -9.32-14	
10	19560.208 19560.208	4.27200 4.27213	1.31966-4 1.31943-4	1.2984-9 1.3003-9	-1.221-13 -1.219-13	-6.144-18 -6.127-18
11	21117.896 21117.896	4.159893 4.160036	1.32428-4 1.32402-4	1.0656-9 1.0678-9	-1.264-13 -1.262-13	-1.40-19 -1.19-19
12	22621.139 22621.139	4.046311 4.046475	1.33253-4 1.33223-4	8.3269-10 8.3538-10	-1.498-13 -1.496-13	-9.179-18 -9.145-18
13	24069.056 24069.056	3.930885 3.931072	1.34505-4 1.34471-4	5.2550-10 5.2879-10	-1.861-13 -1.857-13	-1.365-17 -1.360-17
14	25460.573 25460.573	3.813111 3.813324	1.36320-4 1.36282-4	1.3277-10 1.3689-10	-2.219-13 -2.214-13	-1.786-17 -1.779-17
15	26794.345 26794.345	3.692363 3.692605	1.38814-4 1.38769-4	-3.6722-10 -3.6195-10	-2.894-13 -2.887-13	-2.488-17 -2.476-17
16	28068.715 28068.715	3.567880 3.568154	1.42180-4 1.42127-4	-1.0021-9 -9.9521-10	-3.661-13 -3.650-13	-4.193-17 -4.173-17
17	29281.645 29281.645	3.438742 3.439053	1.46616-4 1.46554-4	-1.8267-9 -1.8174-9	-4.801-13 -4.784-13	-6.557-17 -6.523-17
18	30430.667 30430.667	3.303843 3.304198	1.52418-4 1.52343-4	-2.9392-9 -2.9263-9	-6.652-13 -6.625-13	-1.001-16 -9.947-17
19	31512.806 31512.806	3.161776 3.162182	1.60041-4 1.59948-4	-4.4814-9 -4.4627-9	-9.606-13 -9.560-13	-1.596-16 -1.585-16

TABLE 6.15 (Cont'd)

Quantum Mechanical Molecular Constants for $\text{DCI}(X^1\Sigma^+)^a$

$\text{D}^{37}\text{Cl}(X^1\Sigma^+)$						
v	G_v	B_v	D_v	H_v	L_v	M_v
20	32524.441	3.010703	1.70132-4	-6.6355-9	-1.400-12	-2.785-16
	32524.441	3.011173	1.70013-4	-6.6073-9	-1.392-12	-2.761-16
21	33461.160	2.848275	1.83567-4	-9.7900-9	-2.214-12	-5.491-16
	33461.160	2.848825	1.83410-4	-9.7448-9	-2.199-12	-5.437-16
22	34317.584	2.671313	2.02000-4	-1.4951-8	-3.930-12	-1.124-15
	34317.584	2.671968	2.01781-4	-1.4873-8	-3.897-12	-1.110-15
23	35086.966	2.47488	2.28584-4	-2.3516-8	-6.712-12	-2.158-15
	35086.966	2.47568	2.28255-4	-2.3365-8	-6.635-12	-2.117-15
24	35760.567	2.25191	2.67676-4	-3.9802-8	-1.768-11	-1.142-14
	35760.567	2.25293	2.67131-4	-3.9464-8	-1.744-11	-1.123-14

^aAll quantities are in units of cm^{-1} . For each vibrational level, the top and bottom entries represent perturbed and deperturbed values, respectively. 1.39956-4 reads as 1.39956×10^{-4} .

TABLE 6.16

Quantum Mechanical Molecular Constants for $\text{DCI}(B^1\Sigma^+)^a$

$\text{D}^{35}\text{Cl}(B^1\Sigma^+)$						
v	G_v	B_v	D_v	H_v	L_v	M_v
0	310.570	1.40843	2.9958-5	1.6002-9	-1.774-13	2.421-17
1	923.148	1.41680	3.4313-5	2.2925-9	-3.034-13	4.934-17
2	1519.189	1.42695	3.9391-5	3.2069-9	-4.873-13	9.017-17
3	2099.183	1.43894	4.5198-5	4.3541-9	-7.559-13	1.587-16
4	2663.796	1.45264	5.1871-5	5.8182-9	-1.115-12	2.608-16
5	3213.602	1.46798	5.9310-5	7.6400-9	-1.633-12	4.100-16
6	3749.364	1.48495	6.7683-5	9.7565-9	-2.283-12	6.561-16
7	4271.750	1.50312	7.6932-5	1.2508-8	-3.118-12	9.434-16
$\text{D}^{37}\text{Cl}(B^1\Sigma^+)$						
v	G_v	B_v	D_v	H_v	L_v	M_v
0	310.119	1.40428	2.9779-5	1.5856-9	-1.752-13	2.384-17
1	921.820	1.41261	3.4101-5	2.2706-9	-2.995-13	4.855-17
2	1517.030	1.42271	3.9139-5	3.1749-9	-4.808-13	8.866-17
3	2096.239	1.43464	4.4900-5	4.3092-9	-7.454-13	1.559-16
4	2660.109	1.44827	5.1520-5	5.7562-9	-1.099-12	2.562-16
5	3209.211	1.46353	5.8898-5	7.5579-9	-1.609-12	4.025-16
6	3744.305	1.48041	6.7201-5	9.6476-9	-2.250-12	6.439-16
7	4266.056	1.49849	7.6376-5	1.2366-8	-3.069-12	9.252-16

^aAll quantities are in units of cm^{-1} . 2.9958-5 reads as 2.9958×10^{-5} .

TABLE 6.17

Rotational and Centrifugal Distortion Constants for HCl:
Calculation of Far-Infrared Transitions for H^{35}Cl and H^{37}Cl^a

H^{35}Cl					H^{37}Cl		
$B_0(\text{calc})$	10.440 198 2(23)				10.424 515 3(23)		
(exp)	10.440 197 4(5)				10.424 514 9(5)		
$10^4 D_0(\text{calc})$	5.280 771 8(74)				5.264 829 7(73)		
(exp)	5.280 49(11)				5.264 75(9)		
$10^8 H_0(\text{calc})$	1.672 182(72)				1.664 659(72)		
(exp)	1.644 8(63)				1.650 1(54)		
$-10^{13} L_0(\text{calc})$	8.649 24(65)				8.597 54(65)		
$10^{17} M_0(\text{calc})$	3.086 4(47)				3.058 2(47)		
J	$\bar{\nu}_{\text{obs}}$	Res.	R		$\bar{\nu}_{\text{obs}}$	Res.	R
0	20.878 284	0.000 000	0.0		20.846 923	-0.000 002	-0.3
1	41.743 895	-0.000 003	-0.4		41.681 215	-0.000 002	-0.3
2	62.584 183	0.000 001	0.1		62.490 255	-0.000 002	-0.3
3	83.386 501	-0.000 002	-0.3		83.261 445	-0.000 002	-0.3
4	104.138 260	0.000 000	0.0		103.982 226	-0.000 001	-0.1
5	124.826 909	0.000 004	0.6		124.640 084	0.000 000	0.0
6	145.439 949	0.000 004	0.6		145.222 562	-0.000 002	-0.3
7	165.964 971	0.000 011	0.9		165.717 277	-0.000 006	-0.5
8	186.389 616	0.000 007	0.6		186.111 934	-0.000 006	-0.5
9	206.701 655	0.000 002	0.2		206.394 337	0.000 011	0.9

^aRotational parameters and line positions are in cm^{-1} . The column labelled 'Res.' contains the residuals of observed—calculated line positions and the R are ratios of the residuals and the experimental uncertainty. The experimentally derived constants and the observed line positions are from Ref. (129).

constants were employed to calculate the positions of $B^1\Sigma^+ - X^1\Sigma^+$ rovibronic transitions. The agreement was within the experimental errors for low- and mid- J but deteriorated rather significantly for the high- J lines, particularly for bands involving high vibrational levels of the ground state. It appears that as the dissociation limit is approached, constants beyond the available $B_v - M_v$ are required. This is supported by order-of-magnitude estimates of the missing higher-order constants and their expected contribution with increasing J , as well as by the obvious inability of the fifth-order rotational energy expression to reproduce the precisely known quantum mechanical eigenvalues. In order to estimate the number of additional constants required for given v , the quantum mechanical eigenvalues were fitted to a power series in $J(J + 1)$ while constants $B_v - M_v$ were constrained to the calculated values. This test was not fully conclusive on account of the relatively high statistical correlations that exist between adjacent higher-order parameters. It was possible nevertheless to determine that the perturbation in the wavefunction needs to be calculated to fourth or fifth order; in other words, terms up to $[J(J + 1)]^{11}$ may in fact be required to describe the experimental observations within the uncertainties of the measurements. It is clear, then, from these results that the parameters $X^{(i)}$ presented in Tables 4.3 and 5.4 for $D^{35}\text{Cl}$ and DF , respectively, lack any strict physical significance; they are parameters aimed simply at representing the data within the experimental errors.

Despite the failure of a fifth-order rotational energy expression in representing spectroscopic information satisfactorily, the constants given in Tables 6.13-6.16 are the true perturbation expansion coefficients, obeying identical boundary conditions as the associated radial operators and having

proper theoretical meanings, free from the contamination of interparameter statistical correlations.

Currently, all methods available for calculating centrifugal distortion constants for diatomic molecules are set up to evaluate constants up to M_v . Tellinghuisen (54) recently improved on Hutson's (53) algorithm by eliminating instabilities in the nonclassical region, and remarked that the method could now be extended to higher orders of perturbation theory. This would be highly desirable in view of the results presented in this work.

It is not entirely clear whether there is full convergence of the perturbation expansion for the rotational energy, given the relatively large magnitude of the perturbation for the diatomic hydrides considered here. This might be of special concern for the higher vibrational levels of the ground state, for despite the rapid decrease in the rotational constant, the distortion constants become increasingly singular and dominant. For the ionic $B^1\Sigma^+$ state, the perturbation expansion appears to converge at a slower rate than that of the ground state.

6.6 Tritium Chloride

An appealing test of the isotopic self-consistency of the model consists of evaluating the accuracy of purely synthetic operators for tritium chloride. The Born-Oppenheimer potential for HCl is given by,

$$U^{\text{BO}}(R) = (1 - \mathcal{M}_H - \mathcal{M}_{\text{Cl}})U^{\text{H}^{35}\text{Cl}}(R) + \mathcal{M}_H U^{\text{D}^{35}\text{Cl}}(R) + \mathcal{M}_{\text{Cl}} U^{\text{H}^{37}\text{Cl}}(R) \quad (6.33)$$

where

$$\mathcal{M}_H = \frac{M_D}{M_D - M_H}, \quad (6.34)$$

and

$$\mathcal{M}_{\text{Cl}} = \frac{M_{37\text{Cl}}}{M_{37\text{Cl}} - M_{35\text{Cl}}} . \quad (6.35)$$

The rotationless potential functions for TCl are given by,

$$U^{\text{T}^{35}\text{Cl}}(R) = (1 + \mathcal{M})U^{\text{H}^{35}\text{Cl}}(R) - \mathcal{M}U^{\text{D}^{35}\text{Cl}}(R), \quad (6.36)$$

$$U^{\text{T}^{37}\text{Cl}}(R) = (1 + \mathcal{M})U^{\text{H}^{37}\text{Cl}}(R) - \mathcal{M}U^{\text{D}^{37}\text{Cl}}(R), \quad (6.37)$$

where

$$\mathcal{M} = \frac{M_{\text{D}}}{M_{\text{H}}} \left[\frac{M_{\text{H}} - M_{\text{T}}}{M_{\text{D}} - M_{\text{H}}} \right], \quad (6.38)$$

defined with the atomic masses. The $q(R)$ function for TCl is calculated from,

$$q^{\text{TCl}}(R) = (M_{\text{H}}/M_{\text{T}})q^{\text{HCl}}(R). \quad (6.39)$$

A calculation of the eigenvalues was carried out for $X^1\Sigma^+$ of T^{35}Cl and T^{37}Cl , and the precisely known (184) microwave $J = 1 \leftarrow J = 0$ transitions were constructed. The comparison with the experimental lines is shown in Table 6.18 to be excellent, the residuals between observed and calculated transitions lying well within the experimental uncertainties. It is interesting to note that the TCl energy levels $v'', J'' = 0, 0$ and $0, 1$ lie below the $v'', J'' = 0, 0$ levels of HCl and DCl so that, in a sense, their prediction amounts to an extrapolation.

Also listed in Table 6.18 are rotationless eigenvalues, and rotational and centrifugal distortion constants for the lowest four levels of $\text{TCl}(X^1\Sigma^+)$. Only B_0 and D_0 have been reported in the literature (161) from analyses of experimental data; these are shown to be in reasonable agreement with the

TABLE 6.18

Calculated Eigenvalues and Rotational Constants^a for TCl: Comparison
of Observed and Calculated Microwave Transitions^b

v	G_v	B_v	$10^5 D_v$	$10^{10} H_v$	$-10^{14} L_v$
0	884.192 867 882.305 310	3.705 093 3 3.689 268 9	6.589 038 6.532 684	7.389 4 7.295 2	1.331 7 1.309 5
1	2 623.648 7 2 618.106 5	3.641 162 3.625 749	6.538 20 6.482 43	7.250 0 7.157 9	1.348 0 1.325 3
2	4 326.212 1 4 317.170 5	3.577 570 3.562 565	6.489 75 6.434 46	7.099 5 7.008 4	1.382 5 1.357 2
3	5 992.091 7 5 979.707 6	3.514 279 3.499 678	6.444 25 6.389 38	6.931 2 6.842 8	1.446 3 1.422 0

$v'' = 0 \quad J = 1 \leftarrow J = 0$ Microwave Transition of T³⁵Cl (MHz)

Calculated	Experimental	Residual	Uncertainty	Ratio
222 143.90	222 143.78	-0.12	0.40	-0.30

$v'' = 0 \quad J = 0 \leftarrow J = 1$ Microwave Transition of T³⁷Cl (MHz)

Calculated	Experimental	Residual	Uncertainty	Ratio
222 195.16	221 195.40	0.24	0.40	0.60

^aTop and bottom entries correspond to T³⁵Cl and T³⁷Cl, respectively.

^bExperimental frequencies are from Ref. (184). Eigenvalues and rotational parameters are in units of cm⁻¹. Ratio = Residual/Uncertainty.

calculated constants. The infrared TCl measurements (185) appear to be in systematic discrepancy with the wavenumbers calculated from the constants in Table 6.18. Systematic error in these measurements has also been discussed by Guelachvili *et al.* (162), as well as by Coxon and Ogilvie (46), the latter attributing such discrepancy to unreliable DBr calibration standards (186).

The eigenvalues of $B^1\Sigma^+$ and $X^1\Sigma^+$ for $T^{35}\text{Cl}$ and $T^{37}\text{Cl}$ have been calculated and are listed in Appendix A-5. The prediction of the TCl ($B \rightarrow X$) emission band spectrum from these energies should provide a rather stringent test of the isotopic self-consistency of the method. An estimate of the electronic term value for $B^1\Sigma^+$ is required to predict the absolute positions of the expected rotational lines. The chlorine independent estimates for T_e obtained in this work for HCl and DCl have been employed to construct the empirical relationship,

$$T_e^i = t_e^\infty + t_e^H/M_i, \quad (6.40)$$

with $t_e^\infty = 77\,329.477\text{ cm}^{-1}$, the separation between the minima of the Born-Oppenheimer curves, and $t_e^H = -22.409\text{ cm}^{-1}\text{ amu}$. This expression predicts $T_e^{\text{TCl}} = 77\,322.05\text{ cm}^{-1}$. An expression similar to Eq. (6.40) but employing molecular reduced masses gives the same result.

6.7 Higher-Order JWKB Effects in the RKR Procedure

It is possible to use the results from the present analysis to estimate the effects of neglected higher-order JWKB integrals in the RKR procedure. Using quantum mechanical rotational constants which have had the effect of $q(R)$ subtracted from them, and the quantal rotationless eigenvalues, a first-order RKR potential is constructed. This was then compared with the

numerical potential obtained from the Hamiltonian correction analysis; the difference between the quantal and semiclassical potentials gives the higher-order JWKB corrections.

A set of deperturbed B_v , obtained simply by setting $q(R) = 0$, and the corresponding eigenvalues for $J = 0$ are listed in Tables 6.13 and 6.15 for the $X^1\Sigma^+$ state of H^{35}Cl , and D^{35}Cl . From these, first-order RKR curves were constructed and the difference functions from the quantal potentials were obtained. These were multiplied by μ_i and plotted in Figure 6.5. It is clear that the discrepancies scale in accord with expected mass behaviour (89). The small undulations in the difference functions are due to lack of smoothness in the semiclassical turning points.

6.8 Nonuniqueness in the Hamiltonian Operators: Further Comments.

As discussed previously, Watson (42) predicts that addition of $(\lambda/2)\partial U/\partial R$ onto the rotationless potential with a corresponding modification of $q(R)$ by $-\lambda/R$, for any real λ , should have no effect on the rovibrational eigenvalues. This appeared to be confirmed numerically by Coxon (120). Under closer scrutiny, however, this was found to be true for small ($\leq 10^{-4}$) values of λ only. For greater values of λ , noticeable discrepancies begin to appear.

It was decided to investigate this apparently puzzling behaviour of the radial Hamiltonian operator mathematically, in order to find a prescription that gives an *exact* agreement for any value of λ . The results presented below indicate that it is not possible to obtain exact agreement for all values of λ , but the range of λ that can be employed is significantly enlarged. Also, the results shed more light on the physical significance of Watson's (42) prescription.

Figure 6.5

Mass-scaled higher-order JWKB corrections for the $X^1\Sigma^+$ state of $\text{H}^{35}\text{Cl}/\text{D}^{35}\text{Cl}$. The raw JWKB corrections for each isotopomer are multiplied by the respective reduced masses and the two plots are found to be virtually superimposed in the entire range of R with the exception of the point at $R = 0.95 \text{ \AA}$.

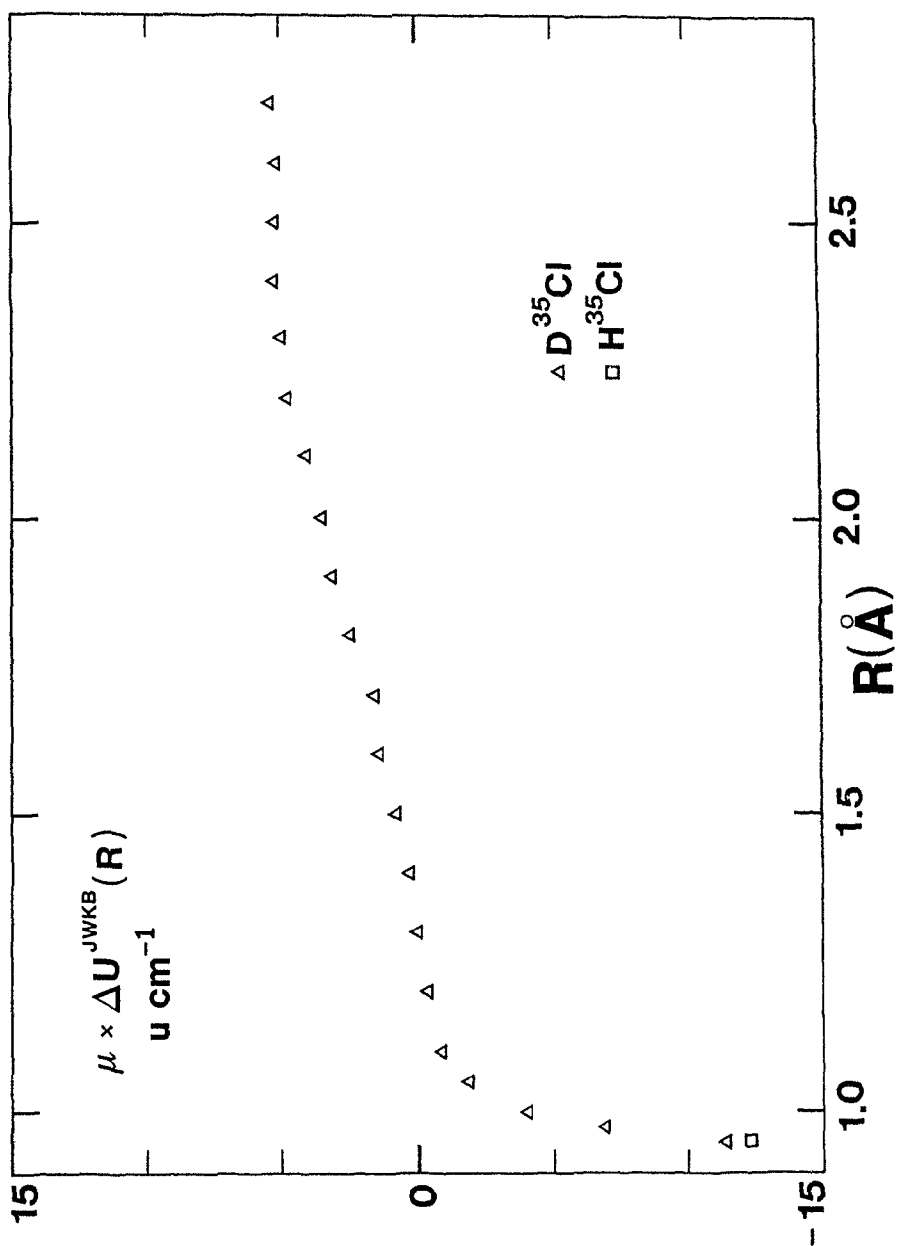


Figure 6.5

We begin with a general, nonadiabatically perturbed rotational potential energy function,

$$U_J(R) = U_0(R) + \beta^2[J(J+1)][1 + q(R)]/R^2. \quad (6.41)$$

We then proceed to transform this expression into the increment form of a Taylor series (122), as

$$\begin{aligned} U_J(R + \lambda) = & U_J(R) + \lambda(\partial U_J/\partial R) + (\lambda^2/2!)(\partial^2 U_J/\partial R^2) + (\lambda^3/3!)(\partial^3 U_J/\partial R^3) \\ & + (\lambda^4/4!)(\partial^4 U_J/\partial R^4) + \dots, \end{aligned} \quad (6.42)$$

which can then be considered as a lateral translation of the rotational potential by λ units along the R axis. After considerable algebra and some simplification, it is useful to consider a translation operator \hat{T} ,

$$\hat{T} = \hat{T}_0 + \hat{T}_J, \quad (6.43)$$

where \hat{T}_0 , which modifies the rotationless potential by

$$U_0^{\lambda}(R) = U_0^0(R) + \hat{T}_0, \quad (6.44)$$

is defined as

$$\hat{T}_0^{(N)} = \sum_{n=1}^N \frac{\lambda^n}{n!} \hat{D}^{(n)} U_0^0(R), \quad (6.45)$$

where

$$\hat{D}^{(n)} = d^n/dR^n, \quad (6.46)$$

is a differentiation operator. The effect of \hat{T}_J is shown by the difference,

$$U_J^{\lambda}(R) - U_0^{\lambda}(R) = \frac{\beta^2 J(J+1)}{R^2} \left\{ 1 + q(R) + \hat{T}_J \right\}, \quad (6.47)$$

with

$$\hat{T}_J^{(M)} = \sum_{n=1}^M \frac{\lambda^n}{n!} (-1)^n (\hat{F}/R - \hat{D})^n q(R) + \sum_{n=1}^M \frac{\lambda^n}{n!} (-1)^n (\hat{F})^n R^{-n}, \quad (6.48)$$

which can be written more succinctly as,

$$\hat{T}_J^{(M)} = \sum_{n=1}^M \frac{\lambda^n}{n!} (-1)^n \left\{ (\hat{F}/R - \hat{D})^n q(R) + (\hat{F})^n R^{-n} \right\}, \quad (6.49)$$

where the factorial operator \hat{F} is assigned the property,

$$(\hat{F})^n = \hat{F}^{(n)} = (n + 1)!, \quad (6.50)$$

and the operators \hat{D} and \hat{F} *do not* commute. The first term in curly brackets in Eq. (6.49) represents a shift along the internuclear axis of the perturbation due to $q(R)$ and the second term gives the shift of the usual kinetic energy of rotation.

It is helpful to write the first few terms of these operators explicitly to give an appreciation for their effects. The rotationless part \hat{T}_0 has been given previously in this thesis, as Eq. (3.43), and corresponds simply to a radial shift of the rotationless function by λ units. The first few terms of \hat{T}_J are quite interesting; these are

$$\hat{T}_J^{(1)} = \lambda \{ dq(R)/dR - 2[1 + q(R)]/R \}, \quad (6.51)$$

$$\hat{T}_J^{(2)} = \frac{\lambda^2}{2!} \{ d^2 q(R)/dR^2 - (4/R) dq(R)/dR + 6[1 + q(R)]/R^2 \}, \quad (6.52)$$

$$\begin{aligned} \hat{T}_J^{(3)} = \frac{\lambda^3}{3!} \{ d^3 q(R)/dR^3 - (6/R) d^2 q(R)/dR^2 + (18/R^2) dq(R)/dR - \\ 24[1 + q(R)]/R^3 \}. \end{aligned} \quad (6.53)$$

Now, for small values of $q(R)$ we can write the first term as

$$\hat{T}_J^{(1)} \approx -2\lambda/R. \quad (6.54)$$

If we write the *shifted* rotational potential, including the effects of $\hat{T}_0^{(1)}$

and $\hat{T}_J^{(1)}$ only, we find

$$U_J(R + \lambda) \simeq \{U_0^0(R) + \lambda dU_0^0(R)/dR\} + \beta^2 J(J + 1)[1 + \{q(R) - 2\lambda/R\}/R^2], \quad (6.55)$$

which is exactly Watson's (42) mathematical description of nonuniqueness in the radial operators; that is, modification of the rotationless potential by addition of a constant k multiplied by the potential first derivative should be accompanied by addition of $-2k/R$ to the function $q(R)$. This also illustrates why Watson's procedure fails for larger values of λ ; simply, more terms of \hat{T} are required. However, convergence in Eq. (6.42) is not guaranteed for all values of λ . The determination of the radius of convergence of this expression is not a trivial undertaking; neither is it of particular value when the physical meaning of λ is examined.

From Eqs. (2.42, 2.43) and Eq. (6.55) above, it is easy to see that

$$\lambda_e = \int_{R_0}^{R_e} Q_i^{(n)}(R) dR, \quad (R_e > R_0), \quad (6.56)$$

where λ_e is a special value of λ . Essentially, this is a small amount of homogeneous mixing that is neglected. This neglect is made inadvertently when $q(R)$ is constrained to vanish at R_e (42). For small values of λ_e the contribution from $Q_i^{(n)}(R)$, or the homogeneous mixing of electronic states, for arbitrary values of R_0 , corresponds to a shift of the rotational potential energy along the internuclear coordinate. The value of λ_e increases in proportion to the total homogeneous perturbation experienced by the electronic state in question. Since it is assumed to be zero, finite values of λ_e would lead to small discrepancies in the derived R_e^{eff} values.

Consider a hypothetical situation where the first bound excited ($B^1\Sigma^+$)

state of HCl is lowered in energy. According to Eq. (6.42), this would affect the inertial properties of the ground $X^1\Sigma^+$ state by causing a radial shift of its potential. As the $B^1\Sigma^+$ state is continuously brought closer to $X^1\Sigma^+$, an apparent contradiction begins to form. Will the ground state shift endlessly along R ? Of course not! The ground state will shift by a certain amount, but as the excited state continues its approach, the wave equation which describes $X^1\Sigma^+$ will become progressively inapplicable due to a increasing breakdown of the perturbation theory on which it is based. It will then be necessary to apply degenerate perturbation theory to describe the system, and the nondegenerate perturbation parameter λ_e has little physical meaning.

6.9 The Adiabatic Correction at the Potential Minimum

Homogeneous nonadiabatic coupling of $X^1\Sigma^+$ shifts the adiabatic curve by a negative amount along R , requiring that the perturbation function possess a positive slope near the equilibrium configuration. Since the isotopic trend of equilibrium bond lengths found from Y_{01} requires a positive slope for $U_X^H(R_e)$, and since the adiabatic correction is found to have a negative slope near R_e , the homogeneous perturbation must be of greater magnitude than the adiabatic function near the potential minimum. This can also be seen from the relation,

$$\tilde{S}_X^H(R) = S_X^H(R) + \frac{1}{2} \frac{\partial U(R)}{\partial R} \int_{R_0}^R Q_X^H(R) dR, \quad (6.57)$$

where $S_X^H(R)$ is the pure adiabatic correction and the second term corresponds to the homogeneous nonadiabatic contribution to the rotationless potential. Since $Q_X^H(R)$ is of the order of the number of valence electrons (42) and thus

positive, and since the slope of the potential derivative is similarly always positive near R_e , the effect of the second term on R_e is contrary to that of the pure adiabatic correction. Since the $U_X^H(R)$ function, which is related directly to the composite function $\tilde{S}_X^H(R)$, has a net positive slope near R_e , the homogeneous coupling must overtake the adiabatic contribution in this region.

This can be seen yet more clearly by differentiating Eq. (6.57), above, and evaluating the derivatives at $R = R_e$. Assuming that $Q_X^H(R)$ is fairly constant near the potential minimum we can write,

$$\left[\frac{\partial \tilde{S}_X^H(R)}{\partial R} \right]_{R=R_e} = \left[\frac{\partial S_X^H(R)}{\partial R} \right]_{R=R_e} + (\lambda_e/2) \left[\frac{\partial \left[\frac{\partial U(R)}{\partial R} \right]}{\partial R} \right]_{R=R_e}, \quad (6.58)$$

It is obvious that there is a competing slope mechanism here and that the second term on the RHS dominates. This occurs mainly because of the large potential derivative term. The net slope is responsible for the observed trend in the $R_e(Y_{01})$ values.

Given the adiabatic bond lengths in Table 6.11 and Eq. (6.24), it is possible to obtain an estimate of the slope of the *pure* adiabatic correction at R_e^{BO} . Expanding $\Delta U^{\text{ad}}(R)$ as,

$$\Delta U^{\text{ad}}(R) = (1/\mu) \{ c_1(R - R_e^{\text{BO}}) + c_2(R - R_e^{\text{BO}})^2 + \dots \}, \quad (6.59)$$

near the equilibrium configuration, the first derivative evaluated at $R_e = R_e^{\text{BO}}$ yields,

$$\left[\frac{d\Delta U^{\text{ad}}(R)}{dR} \right]_{R_e^{\text{BO}}} = c_1/\mu. \quad (6.60)$$

For H^{35}Cl and D^{35}Cl , Eq. (6.24) may now be written as,

$$R_e^{\text{ad}}(\text{H}^{35}\text{Cl}) = R_e^{\text{BO}} - c_1/[k^{\text{BO}}\mu(\text{H}^{35}\text{Cl})], \quad (6.61)$$

and

$$R_e^{\text{ad}}(\text{D}^{35}\text{Cl}) = R_e^{\text{BO}} - c_1/[k^{\text{BO}}\mu(\text{D}^{35}\text{Cl})]. \quad (6.62)$$

Obtaining c_1 separately for each isotopomer and averaging, gives a predicted value of $c_1 = -28 \pm 2 \text{ cm}^{-1} \text{ \AA}^{-1}$ for the slope of the adiabatic correction of $X^1\Sigma^+$ at R_e^{BO} . The adiabatic corrections for HCl and DCl have been computed by *ab initio* methods (187) and clearly possess negative slopes near the equilibrium configuration. The average mass-adjusted theoretical slope obtained from Fig. 3 of Ref. (187) is $c_1 = -29 \text{ cm}^{-1} \text{ \AA}^{-1}$, in gratifying agreement with the present estimate.

The overall results here infer that the adiabatic equilibrium bond length in well-isolated ground states is always displaced at larger equilibrium separations from the Born-Oppenheimer potential minima; in other words, the adiabatic parameters d_i^{ad} are always positive. Watson (180) found this to be the case for the molecules CO, HCl, and LiCl. Further confirmation is found in Figs. 1 and 2 of Kołos' (24) article, from explicit calculations of the diagonal motion corrections for the various states of H_2^+ and H_2 ; these have negative slopes at R_e . Additional support is found from Saykally's laboratory for the cations $\text{ArH}^+/\text{ArD}^+$ and OH^+/OD^+ (188), where it is found that the quantity R_e^{BO} occurs at smaller internuclear separations than R_e^{ad} . Negative d_i^{ad} values should serve as an indication of anomalies arising from significant breakdown of the adiabatic approximation.

CHAPTER 7
ISOTOPIC BEHAVIOUR OF BORN-OPPENHEIMER BREAKDOWN:
THE $B^1\Sigma^+$ AND $X^1\Sigma^+$ STATES OF HF AND DF

7.1 Introduction

Hydrogen fluoride has been the subject of numerous theoretical and experimental investigations dealing with electronic effects on isotopic exchange equilibria (189), the electronic potential energy curves (108, 149, 190), the electric dipole moment (156, 183), and Einstein coefficients (108, 156). Consisting of only two nuclei and ten electrons, HF is a particularly attractive candidate for *ab initio* studies.

Although the excited electronic states are not known in great detail from experiment, the ground state has been characterized rather well. The analyses of the $B^1\Sigma^+ - X^1\Sigma^+$ emission band systems of HF and DF by Johns and Barrow (151) resulted in rotational parameters and vibrational energies. These were employed later by Alvarino *et al.* (191) to construct RKR curves for the two states. The potentials were in turn used to calculate Franck-Condon factors for the $B \rightarrow X$ transition. The $B^1\Sigma^+ - X^1\Sigma^+$ emission band system of HF was reinvestigated by Di Lonardo and Douglas (87) under higher resolution. The rotational analysis yielded precise vibrational terms and rotational parameters on the vibrational levels with $v'' = 7-19$ and $v' = 0-10$. Analysis of the electronic absorption spectrum (87) gave information on B state levels with $v' = 14-73$. Vibrational levels with $v' \geq 26$ were found to be highly perturbed. RKR potentials were reported for

both electronic states.

The accuracy of the RKR_V function for HF($X^1\Sigma^+$) has been tested in the present work. The Schrödinger equation was solved with this potential to yield rotationless eigenvalues, $E_v^{\text{RKR}_V}$, and vibrational wavefunctions, $\psi_v^{\text{RKR}_V}(R)$, which were then employed to calculate expectation values of R^{-2} , and thus mechanical rotational constants. The differences between these quantities and those derived experimentally are plotted in Figure 7.1. The unsmooth behaviour of these differences is due to a corresponding lack of smoothness in the potential function; experimental uncertainties in G_v and B_v are much smaller than the scatter. This shows clearly that the RKR_V function is quite inconsistent with the experimental information from which it was derived. The reasons for this lack of agreement have been discussed previously; briefly, one must consider higher-order JWKB effects and breakdown of the Born-Oppenheimer approximation.

Such considerations were taken into account in the recent work of Coxon and Ogilvie (190). The rotationless potential was modelled as

$$U(z) = c_0 z^2 (1 + \sum_{n=1} c_n z^n), \quad (7.1)$$

where the reduced internuclear coordinate is given by

$$z = 2(R - R_e)/(R + R_e). \quad (7.2)$$

A further hydrogenic radial function $K^H(z)$

$$K^H(z) = \sum_{n=1} h_n^H z^n, \quad (7.3)$$

was determined from experimental data on HF and DF and together with $U(z)$ account for adiabatic, nonadiabatic, semiclassical, radiative and relativistic

Figure 7.1

Quantum mechanical inconsistency of an RKR potential for the $X^1\Sigma^+$ state of HF. The potential was constructed from the results of Ref. (87). The upper half of the figure shows a plot of the differences $\Delta B_v = B_v^{\text{exp}} - B_v^{\text{RKR}}$. The lower half of the figure gives a plot of the differences $\Delta G_v = G_v^{\text{exp}} - G_v^{\text{RKR}}$.

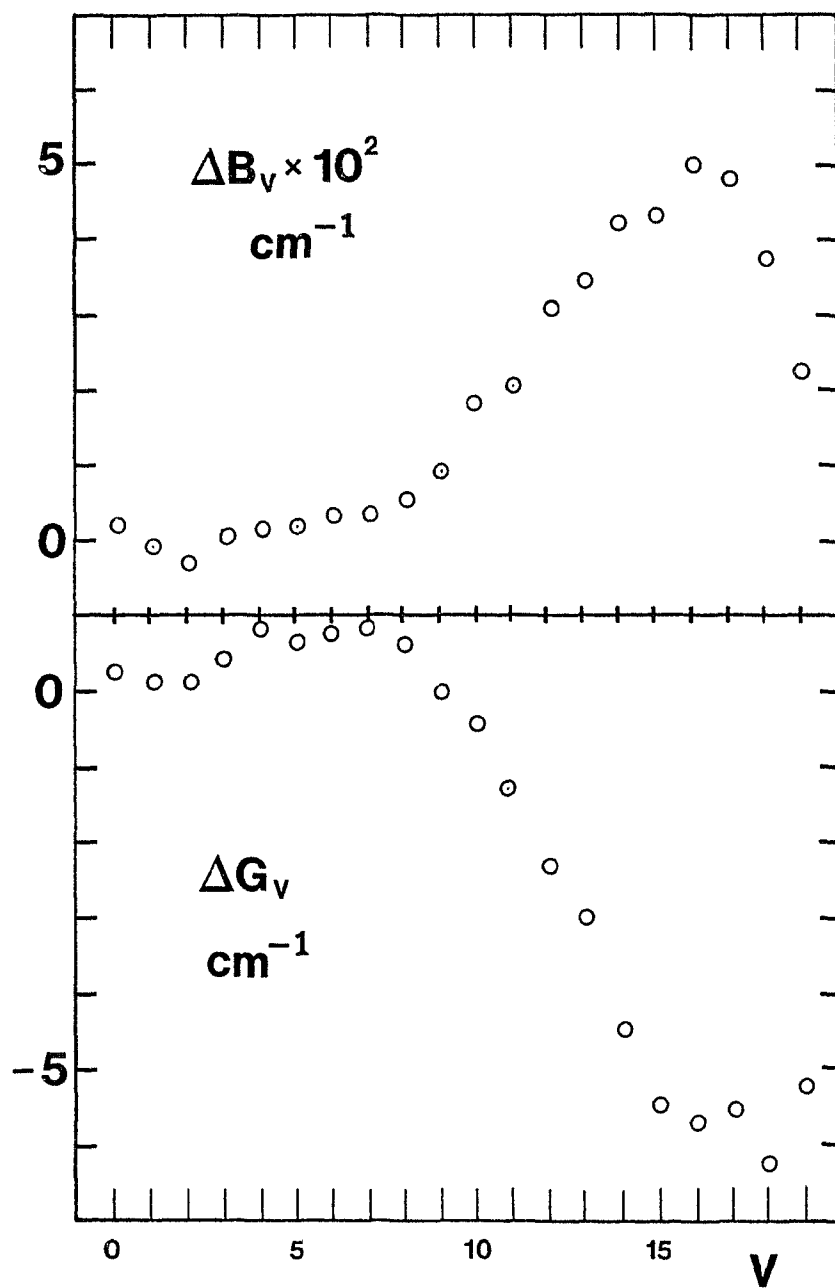


Figure 7.1

effects. The coefficients c_n and h_n^H were found by an analytical inversion of the Dunham U_{kl} and Δ_{kl}^H coefficients in Eq. (2.47). Radial functions were determined up to 65% of the well depth.

There are two problems with this work. First and foremost, the effect of $q(R)$ was neglected in the generation of analytical relationships linking U_{kl} and Δ_{kl} with the coefficients c_n and h_n . Thus, heterogeneous contributions to the rotational energy levels were inverted onto the $J = 0$ potential functions. The theory supports homogeneous but not heterogeneous nonadiabatic adjustment of the rotationless potential. Although $q(R)$ is of small magnitude near the potential minimum, its effect on the eigenvalues can be quite significant in relation to the high precision with which low- v levels are studied spectroscopically. The second problem is similar to that discussed in Chapter 6 for HCl/DCl. A fifth-order rotational energy expansion in $J(J + 1)$ is found to be inadequate in representing some of the energy levels within their spectroscopic precision. This is especially true for low- v levels known very accurately from heterodyne measurements and for high- v, J levels even though these might be known with only moderate precision. The estimates of U_{kl} and Δ_{kl} obtained by Coxon and Ogilvie (190) do not therefore retain their proper quantum mechanical identities but contain contributions from missing constants and interparameter statistical correlations; this in turn contaminates the functions $U(z)$ and $K^H(z)$. This is a general problem with the reduction of spectroscopic line positions to "molecular constants".

In the recent work of Huffaker (108), the RKR potential of Di Lonardo and Douglas (87) for the ground state of HF was represented analytically by a Perturbed Morse Oscillator/Extended Geometric Series (PMO/EGS) model. Huffaker claimed the $J = 0$ representation to correspond to the adiabatic

potential. This was derived by considering not only the RKR turning points but also the rotational and centrifugal distortion constants B_v and D_v . A chief criticism of this work is that effective rotational constants, which are perturbed significantly by excited $^1\Pi$ states, are employed to determine the $J = 0$ potential while the rotational Hamiltonian operator is constrained to the kinetic energy of rotation expression. It is thus not surprising that considerable problems were encountered (108) in finding a satisfactory representation for *all* vibrational levels, forcing Huffaker to consider two separate fits, one for $v'' \leq 16$ and another for $v'' \leq 19$. A smaller problem is associated with the fact that the HF($X^1\Sigma^+$) RKR potential of Di Lonardo and Douglas (87) is not particularly smooth. There was no indication in Huffaker's paper (108) that it had been smoothed prior to the fit to the PMO/EGS model. Although the fit itself can be considered a smoothing of the raw turning points, lack of smoothness can require more terms in the model and hence increase interparameter correlations and instability. Another criticism of the PMO/EGS study of HF (108) is the apparent need to fit the residual "nonadiabatic" eigenvalue corrections to a sinusoidal function, which in Huffaker's opinion is an indication of a true physical effect. This conclusion was made on the basis of previous results on $H_2(X^1\Sigma^+)$ (109). It seems likely, however, that for HF all that is being fitted is the residual inadequacy of the PMO/EGS model in fitting the adiabatic/homogeneously nonadiabatic potential, as *it is impossible* to extract the nonadiabatic component of the rotationless eigenvalues from the results of first-order spectroscopic experiments.

In summary, no investigation has previously taken into account the contributions from $q(R)$ to the rotational energies. Franck-Condon factors,

Einstein coefficients, and other intensity related information continue to be reported in the literature in complete ignorance of this potentially important effect. The purpose of this chapter is to undertake a rotational analysis of all $X^1\Sigma^+$ and the low- v' $B^1\Sigma^+$ spectroscopic line position data on the basis of an effective Hamiltonian operator. The effect of $q(R)$ on intensity calculations will be examined.

7.2 Analysis

7.2.1 Selection of Data

There have been several studies of the pure rotational transitions of $\text{HF}(X^1\Sigma^+)$ in vibrational levels $v'' = 0-5$. Akitt and Yardley (192) observed HF pure rotational transitions in $v'' = 0-3$ by examining laser emission in pulsed discharges through BF_3 , apparently without the presence of any intentional hydrogen source. Cuellar and Pimentel (193) observed pure rotational transitions of HF ($v'' = 0-2$) in a ClF-H_2 chemical laser. Mason and Neilsen (194) studied pure rotational transitions of HF in $v'' = 0$ using a simple absorption setup and atmospheric vapour lines to calibrate their spectrum. Revich and Stankevich (195), Sengupta *et al.* (143), and Rothschild (196) also examined the pure rotational spectrum of HF. More recently, highly precise heterodyne measurements of $\text{HF}(v'' = 0)$ were reported by Jennings *et al.* (142).

The vibrational-rotational spectrum of HF has been similarly well studied in various laboratories (143-146). The most extensive and significant study is that of Mann *et al.* (146); here, the H_2/F_2 flame emission spectrum was analyzed spectrographically to yield information on vibrational levels $v'' = 0-9$. This work is important because it connects the lower- v'' data in the

infrared region to the vacuum ultraviolet $B \rightarrow X$ emission data.

The spectroscopic information available for deuterium fluoride is much less complete, consisting of only 9 far-infrared transitions (154, 156) and 101 vibrational-rotational transitions (143, 145). Improved $v'' = 0$ pure rotational measurements and a Fourier transform spectrum of the fundamental band in the infrared were presented in Chapter 5. Sengupta *et al.* (143) obtained spectroscopic measurements from DF chemical laser emission for the 1-0, 2-1, 3-2 and 4-3 bands. The rotational analysis of the $B^1\Sigma^+ \rightarrow X^1\Sigma^+$ band system presented in Chapter 5 provides information on levels $v'' = 16-26$ in the ground state and $v' = 0-5$ in $B^1\Sigma^+$. The emission measurements are interpreted further in this chapter to yield information on levels $v'' = 9-26$ in $X^1\Sigma^+$ and $v' = 0-7$ in $B^1\Sigma^+$. For most of the bands presented in Chapter 5, it was possible to extend the rotational assignments to higher and/or lower J .

The individual spectroscopic line positions have been assigned weights which are inversely proportional to the square of their precision estimates. Precision estimates for line positions obtained previously in other studies were obtained by reference to the original papers, or by performing new fits to power series in $J(J + 1)$. A summary of the HF/DF ground state pure rotational and vibrational-rotational information employed in this work is given in Table 7.1.

7.2.2 Trial Operators

The initial radial operator for the ground state was modelled after the RKR potential of Di Lonardo and Douglas (87); however, instead of working with the turning points provided in Table 9 of Ref. (87), which were only quoted to four decimal points, the molecular constants given in Table 5 of

TABLE 7.1
Summary of Experimental Data Base for HF/DF^a

HF Pure Rotational Data in $X^1\Sigma^+$					
v	Reference	$\epsilon(\text{cm}^{-1})$	N	J -Range	
0	142	7.5×10^{-6}	4	0- 3	
0	142	0.0003	3	4- 6	
0	142	0.0018	3	17-19	
0	142	0.01	5	20-21, 26-28	
0	192	0.70	8	13-24	
0	193	0.20	12	21-32	
0	194	0.05	10	0- 9	
0	195	0.50	32	9-40	
0	143	0.0037	5	17-21	
0	196	0.20	11	0-10	
1	192	0.20	4	14-23	
1	193	0.20	7	22-28	
1	195	0.575	23	10-34	
1	143	0.01	6	18-23	
2	192	0.20	1	15	
2	193	0.10	2	23-24	
2	195	0.50	16	10-28	
2	143	0.014	6	14-23	
3	192	0.20	1	16	
3	143	0.013	3	14-22	
4	195	0.20	2	16-24	
5	195	0.50	2	16-18	
HF Vibrational-Rotational Data in $X^1\Sigma^+$					
$v'-v''$	Reference	$\epsilon(\text{cm}^{-1})$	N	J_P	J_R
1 0	<i>b</i>	0.03	19	1- 9	0- 9
1-0	144	0.10	5	6-10	
1-0	86	0.0005	22	1-10	0-11
1-0	146	0.014	32	5-15	7-27
1-0	143	0.009	10	6-15	
1-0	<i>c</i>	0.10	11	1- 6	0- 5
1-0	168	0.02	29	1-15	0-14

TABLE 7.1 (Cont'd)

Summary of Experimental Data Base for HF/DF^a

HF Vibrational-Rotational Data in $X^1\Sigma^+$					
$v'-v''$	Reference	$\epsilon(\text{cm}^{-1})$	N	J_P	J_R
2-0	<i>b</i>	0.04	16	1- 7	0- 8
2-0	86	0.0008	17	1- 8	0- 8
2-0	146	0.22	52	1-28	2-26
2-0	168	0.016	15	1- 9	0- 7
2-1	144	0.10	13	2-14	
2-1	146	0.12	36	1-12	0-24
2-1	143	0.012	12	2-13	
3-0	<i>d</i>	0.025	16	1- 7	0- 8
3-2	146	0.075	29	1- 9	0-22
3-2	143	0.025	9	3-13	
4-0	146	0.10	41	1-19	0-21
4-2	146	0.23	47	1-22	0-24
4-3	143	0.012	9	3-14	
5-0	146	0.12	16	4-14	1-13
5-1	146	0.05	44	1-22	0-23
5-2	146	0.05	28	1- 8	0-20
5-3	146	0.12	35	1-18	0-19
6-1	146	0.12	29	2-16	1-16
6-2	146	0.045	41	1-20	0-21
6-3	146	0.03	12		1-13
6-4	146	0.03	32	1-14	0-18
6-5	143	0.04	3	4- 9	
7-2	146	0.055	34	2-18	2-18
7-3	146	0.034	35	2-16	0-19
8-3	146	0.058	34	1-15	0-21
8-4	146	0.058	24	2-11	1-16
9-4	146	0.06	18	2- 8	0-15
DF Ground State Data					
	Reference	$\epsilon(\text{cm}^{-1})$	N	J_P	J_R
$v = 0$	161	3.3×10^{-7}	1	$J = 1 \leftarrow J = 0$	

TABLE 7.1 (Cont'd)
 Summary of Experimental Data Base for HF/DF^a

DF Ground State Data					
$v'-v''$	Reference	$\epsilon(\text{cm}^{-1})$	N	J_P	J_R
$v = 0$	Present Work	0.0002	6		2- 7
$v = 0$	Present Work	0.0004	2		1 and 8
1-0	<i>e</i>	0.00005	25	1-12	1-12
1-0	143	0.005	29	2-17	0-14
2-0	154	0.01	19	1- 8	0-10
2-1	143	0.003	12	3-16	
3-2	143	0.003	11	3-14	
4-3	143	0.01	5	4- 8	

^a ϵ is the estimated precision; N is the number of lines fitted;

J_P and J_R are the ranges of J fitted for the P and R branches.

^bW. F. Herget, W. E. Deeds, N. M. Gailar, R. J. Lovell, and A. H. Neilsen, *J. Opt. Soc. Am.* **52**, 1113 (1962).

^cR. M. Talley, H. M. Kaylor, and A. H. Neilsen, *Phys. Rev.* **77**, 529 (1950).

^dE. S. Fishburne and K. N. Rao *J. Mol. Spectrosc.* **19**, 290 (1966).

^eDF fundamental band data obtained by J. W. Johns (see Chapter 5).

TABLE 7.1 (Cont'd)

Summary of Experimental Data Base for HF/DF^a

Assigned Lines and Least-Squares Results for Bands of DF ($B \rightarrow X$)									
Band	P_J	R_J	N	rms	Band	P_J	R_J	N	rms
0-12	55-60	57-61	10	0.041	2-21	3-22	2-25	35	0.041
0-14	42-57	39-57	24	0.045	2-22	3-25	2-24	20	0.036
0-15	36-55	39-55	26	0.045	2-23	11-29	11-28	27	0.050
0-16	29-52	30-51	36	0.046	2-24	6-22	1-22	27	0.049
0-17	22-49	21-49	48	0.038	2-25	2-19	2-19	23	0.034
0-18	7-46	7-46	54	0.034	2-26	10-13	10-14	7	0.055
0-19	2-43	2-43	59	0.042					
0-20	2-38	3-38	62	0.049	3- 9	63-67	-	4	0.046
0-21	1-34	0-36	45	0.039	3-10	59-65	59-66	12	0.054
0-22	1-33	0-27	45	0.026	3-11	51-65	52-63	20	0.048
0-23	3-20	3-21	29	0.039	3-12	45-60	47-60	26	0.049
					3-13	39-56	40-55	28	0.030
1- 9	68-69	68	3	0.044	3-14	32-48	33-47	24	0.040
1-10	61-66	65-66	6	0.041	3-15	25-43	27-43	33	0.030
1-11	59-63	60-65	9	0.039	3-16	17-34	18-36	30	0.039
1-12	51-60	53-59	12	0.047	3-17	2-41	3-48	55	0.040
1-13	39-59	40-60	28	0.036	3-18	5-38	6-38	25	0.043
1-14	32-55	34-55	30	0.043	3-19	20-35	21-36	23	0.050
1-15	20-50	22-53	48	0.040	3-20	7-27	5-28	35	0.042
1-16	12-52	13-52	54	0.045	3-22	12-26	16-25	20	0.049
1-17	5-42	1-40	62	0.043	3-23	2-28	4-28	29	0.052
1-18	4-45	3-45	57	0.040	3-24	10-23	9-25	24	0.042
1-19	3-36	0-42	52	0.031	3-25	5-18	4-18	21	0.052
1-20	4-39	2-39	35	0.045					
1-21	15-35	18-36	29	0.036	4- 9	67-69	-	3	0.024
1-22	3-31	1-31	44	0.039	4-11	50-62	53-63	17	0.045
1-23	3-26	2-26	34	0.054	4-12	46-54	47-57	13	0.051
1-24	6-19	2-13	23	0.047	4-13	39-50	40-52	19	0.043
					4-14	35-44	36-47	22	0.028
2- 9	60-70	67	8	0.030	4-15	29-42	30-40	19	0.040
2-10	51-66	57-63	12	0.027	4-16	22-49	23-50	28	0.049
2-11	57-65	60-64	12	0.040	4-17	36-43	40-43	9	0.038
2-12	44-62	47-58	19	0.046	4-18	19-34	20-36	24	0.032
2-13	40-57	40-56	29	0.041	4-19	9-30	7-30	31	0.034
2-14	32-54	32-55	37	0.044	4-20	27-34	32-37	12	0.049
2-15	23-50	24-47	40	0.031	4-21	18-29	16-32	18	0.042
2-16	11-41	12-40	52	0.039	4-22	7-19	7-20	22	0.045
2-17	6-35	0-34	57	0.034	4-24	3-10	1-10	10	0.045
2-18	2-43	1-45	54	0.044	4-25	4-19	5-19	21	0.042
2-19	29-38	30-39	14	0.052					
2-20	16-33	14-31	26	0.043	5-10	54-67	56-65	14	0.046

TABLE 7.1 (Cont'd)

Summary of Experimental Data Base for HF/DF^a

Assigned Lines and Least-Squares Results for Bands of DF ($B \rightarrow X$)									
Band	P_J	R_J	N	rms	Band	P_J	R_J	N	rms
5-11	52-58	51-61	15	0.041	5-26	3-14	10-14	14	0.041
5-12	48-54	47-53	11	0.051					
5-13	42-48	43-48	10	0.028	6- 9	60-68	60-67	13	0.058
5-16	36-45	38-47	14	0.054	6-15	39-46	42-51	9	0.040
5-18	13-21	14-26	14	0.034	6-19	25-32	21-37	15	0.051
5-19	4-37	6-41	24	0.034					
5-20	18-30	25-32	13	0.036	7- 9	62-66	62-64	6	0.031
5-21	7-20	10-21	18	0.034	7-14	45-52	47-52	7	0.026
5-22	23-30	24-27	8	0.044	7-18	30-36	32-39	10	0.038
5-23	8-16	4-18	16	0.036	7-25	10-18	8-19	13	0.048

^aFor each band, the table shows the J -ranges of fitted lines in the P and R branches, the number of fitted lines (N), and the root mean square residual (rms) between the observed line positions and those calculated from the fitted B and X Hamiltonian operators.

Ref. (87) were employed to generate RKR potentials with the computer program developed in this laboratory by Coxon and Foster (197). Furthermore, the turning points were smoothed with the variable- β Morse procedure described previously in section 6.3.3.

Following the smoothing of the inner limb and the corresponding adjustments to the outer turning points, an attempt was made to fit the RKR curve to the analytical potential given by Eq. (6.13). Initial efforts met with considerable difficulty in achieving such a description for the ground state; above approximately 80% of the potential well depth, the analytic representation obtained herein deviated from the numerical RKR function in an oscillatory fashion, with average peak deviations on the outer limb of several wavenumbers. Slight improvement was realized by resorting to the representation,

$$\beta(R) = \sum_m \beta_m (1 - R_e/R)^m, \quad (7.4)$$

which has an improved radius of convergence (17) over Eq. (6.14), but the final representations obtained even with this model were not satisfactory. It is clearly not desirable to introduce additional, artificial, error for the fitting procedure to have to reproduce, particularly at larger- R (higher energy), where the model calculations presented in Chapter 3 have shown a slightly reduced effectiveness. It was decided therefore to employ the smoothed interpolated RKR potentials as the trial operators, for both electronic states. Extrapolated points were obtained by applying the smoothing computer program *locally* to the innermost and outermost regions of the potential.

7.2.3 Least-Squares Fitting

It is important to plan wisely the choice of correction functions in the long- R region. Clearly, Gaussian correction functions would not be appropriate in representing a *systematic* error in the extrapolation. Local basis functions are inappropriate in this region for another reason. It was found in preliminary model fits that these functions were extremely sensitive to the magnitudes of local weights; in many cases the determination of Gaussian functions at large- R became unstable, giving correction functions with large oscillatory structure.

It was thus decided to distribute Gaussian functions locally on the outer limb up to the last rotationless turning point and combine them with a few higher-order global radial functions, $F_{nij}(R)$. In this fashion, the Gaussian functions looked after *local* structure and the radial functions represented smooth *systematic* corrections, as well as systematic extrapolation corrections that may be required at large R .

In preliminary work, a small representative data set for HF was employed to determine linear combinations of terms for $\Delta U_X(R)$, $\Delta U_B(R)$, and $q_X(R)$. A $q_B(R)$ function could not be significantly determined for the $B^1\Sigma^+$ state. A representative data set for DF was then added and initial descriptions of the additional corrections $\Delta U_X^H(R)$ and $\Delta U_B^H(R)$ were obtained. The least-squares fit was organized on the basis of the relations,

$$U_{\text{HF}}^{\text{eff}}(R) = U_{\text{HF}}^{(0)}(R) + \Delta U(R), \quad (7.5)$$

$$U_{\text{DF}}^{\text{eff}}(R) = U_{\text{HF}}^{\text{eff}}(R) + \Delta U^H(R), \quad (7.6)$$

$$q_{\text{DF}}(R) = (M_{\text{H}}/M_{\text{D}})q_{\text{HF}}(R), \quad (7.7)$$

so that the determination of functions $\Delta U(R)$, $\Delta U^H(\tilde{R})$ and $q(R)$ depends on data for *both* isotopomers. After initial linear combinations for the correction functions were obtained, the entire set of 3939 spectral line positions was included in a final fit (A) and a total of 60 parameters was fitted with a reduced standard deviation of $\hat{\sigma}_{red} = 0.961$.

This is considered satisfactory. A reduced standard deviation near unity indicates that the data, on average, are being represented by the fitted parameters in accord with the experimental error within a first-order perturbation model. However, an attempt to calculate these same line positions from the quantum mechanical eigenvalues of the corrected Hamiltonian operators failed to give corresponding agreement. Some line positions at high- v, J and very highly precise data for $v'' = 0$ could not be represented by the calculated eigenvalues within the precision of the measurements. This observation has a twofold interpretation. It can be seen as a breakdown of first-order perturbation theory, or it may mean that, within the pseudolinearized problem framework, the trial potential was not uniformly a close enough approximation to the final solution. In any case, the results signalled a necessity to iterate.

Before the iteration was carried out, however, a search was made for additional assignments in the electronic spectrum of DF, using the corrected eigenvalues. The assignment of the measured frequencies was until this point less than half-complete. A search for additional rotational structure on the basis of traditional methods was neither a realistic nor a desirable option. The structure predicted on the basis of intensity calculations occurs at very high- J and the approach of constants is not reliable for such extrapolations. A significant number of previously unassigned measurements were identified as

newly discovered band structure. Rotational lines associated with quasibound levels at very high- J ($J \geq 60$) were found, involving new ground state vibrational levels $v'' = 9-15$.

Since the isotopic constraints, Eqs. (7.6-7.7) were employed, the iteration (fit B) proceeded in the following manner. Smaller, secondary corrections were determined to improve further on $U_{X/B}^{\text{eff}}(R)$, and the functions $\Delta U_{X/B}^{\text{H}}(R)$ and $q_X(R)$ were redetermined. These latter functions were found to differ insignificantly from those determined in fit A. This is indicative of the stability of the procedure in determining functions from different initial choices for the potentials and also shows the relatively small correlations between the functions $\Delta U^{\text{H}}(R)$ and $\Delta U(R)$. The reduced standard deviation of fit B was raised slightly to $\hat{\sigma}_{\text{red}} = 0.997$, chiefly due to the inclusion of the new DF assignments. The secondary corrections were easily represented by linear combinations of global radial functions and required no additional Gaussian functions. Also, no additional shift functions were supported, indicating that the determination of R_e had converged after the first cycle.

A total of 94 DF($B \rightarrow X$) bands was included in fit B which can be compared with the previously identified 41 bands from the conventional analysis. A total of 2374 fitted DF($B \rightarrow X$) lines in this analysis can also be compared with the 1240 fitted lines from the conventional analysis. The assignments for the electronic spectrum of DF are now approximately 75% complete. A significant portion of the remaining 25% of the measurements can be attributed to other sources and are not necessarily due to DF. A computer-aided search revealed the presence of the HF($B \rightarrow X$) system on the DF plates; obviously the small amount of HF impurity in the DF gas was sufficient to excite the strongest HF bands. The few remaining lines are probably due to

incomplete spectral order separation. Although a serious attempt was made to separate different spectral orders by employing a prism/cylinder combination, the degree of order separation breakdown was not investigated rigorously. A valuable method of evaluating the extent of this effect would consist of recording atomic standards, under identical conditions as the molecular spectra, followed by a critical examination of the photographic plates.

A total of 5213 line positions was included in fit B, 2482 for DF and 2729 for HF. The final assignments for the DF($B \rightarrow X$) band system can be found in Appendix A-6. Here, all DF experimental lines included in the final fit are provided, as well as estimates of their positions calculated from the quantum mechanical eigenvalues of the corrected operators. Also listed here are the hydrogen fluoride lines employed in fit B, including those of the $B^1\Sigma^+ \rightarrow X^1\Sigma^+$ emission band system (87). The present work has revealed previously undetected systematic error in the 155 nm region. A small portion of the data in this region, for more than one band, is found to be systematically inconsistent ($\approx 0.2 \text{ cm}^{-1}$) with the rest of the measurements. It appears that although Di Lonardo and Douglas (87) allude to an attempt to correct their plates for systematic inconsistencies, they were not fully successful. There were a few additional incorrect assignments found quite readily by using the present fitting procedure. These were primarily pairs of lines which satisfied upper state combination differences but not those of the lower state. Here, then, is a distinct advantage of the Hamiltonian correction approach; *all* line positions must arise from the same radial operators. The approach of fitting molecular constants to *individual* bands often masks incorrect assignments, particularly at high- J . The resulting representations need not then be characterized by a self-consistent set of

molecular constants. Although the process of merging constants from individual bands to a nonredundant set might reveal such inconsistencies, this approach was not followed for the HF(*B* - *X*) data (87).

7.3 Results and Discussion

7.3.1 Radial Functions and Eigenvalues for HF and DF

The functions $U_X^H(R)$ and $U_B^H(R)$ are shown in Figures 7.2 and 7.3, respectively. There is a striking qualitative similarity between these functions for HF/DF and the corresponding functions derived for HCl/DCl. A similar observation is made for the $\tilde{R}_X^H(R)$ function obtained here for HF/DF (Fig. 7.4) and that given in Fig. 6.4 for HCl/DCl. The experimental function $\tilde{R}_X^H(R)$ for HF/DF, however, increases in magnitude more rapidly than the corresponding HCl/DCl function. This indicates that the perturbing $^1\Pi$ state and the $X^1\Sigma^+$ ground state are approaching each other at a faster rate in the case of HF than for HCl; this is confirmed from the results of *ab initio* calculations (127, 149).

These observations are significant and provide experimental evidence for the large similarity between the structure and arrangement of electronic states in the two hydrogen halides.

The final operators are available in numerical form only. A detailed listing of relevant radial functions is found in Appendix A-7 but for certain applications it may simply be sufficient to refer to the functions given in Tables 7.2 and 7.3, arranged in RKR-style output. The energies corresponding to the vibrational levels are the quantum mechanical eigenvalues of the rotationless functions, and the turning points were obtained by inverse interpolation. The mass-independent part of the function $g_X(R)$ can be

Figure 7.2

The experimentally determined function $U_X^H(R)$ for HF/DF($X^1\Sigma^+$). The two broken curves represent the 95% confidence limits of the fitted function. For the definitions of R_{\min} and R_{\max} and the filled circles see the legend to Figure 3.2. J_{\max} is not shown for HF level $v = 19$.

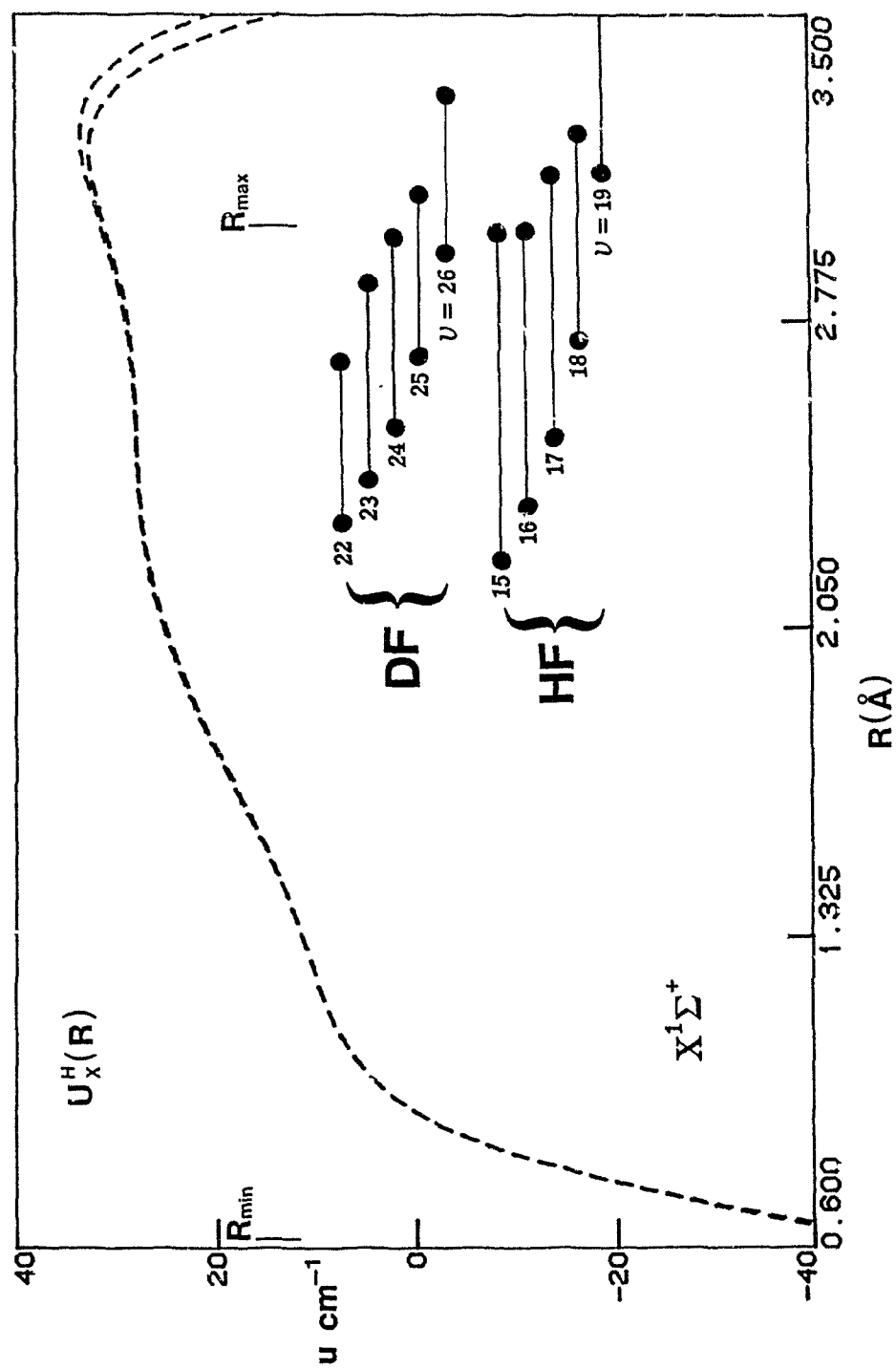


Figure 7.2

Figure 7.3

The experimentally determined function $U_B^H(R)$ for HF/DF($B^1\Sigma^+$). The two broken curves represent the 95% confidence limits of the fitted function. For the definitions of R_{\min} and R_{\max} and the filled circles see the legend to Figure 3.2. J_{\max} is not shown for HF level $v = 10$.

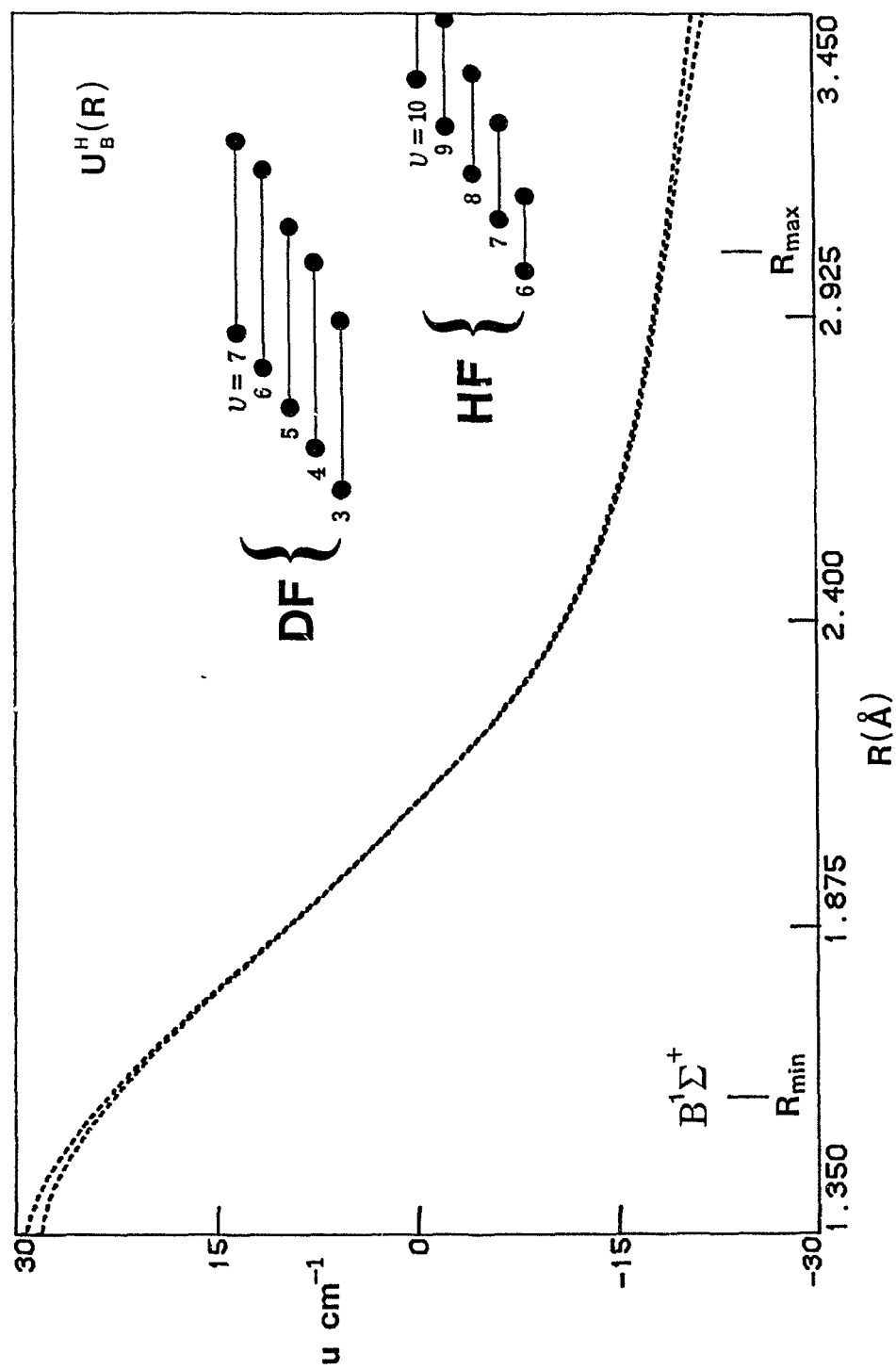


Figure 7.3

Figure 7.4

The function $\tilde{R}_X^H(R)$ for the $X^1\Sigma^+$ state of HF/DF. The two solid curves represent the 95% confidence limits of the fitted function.

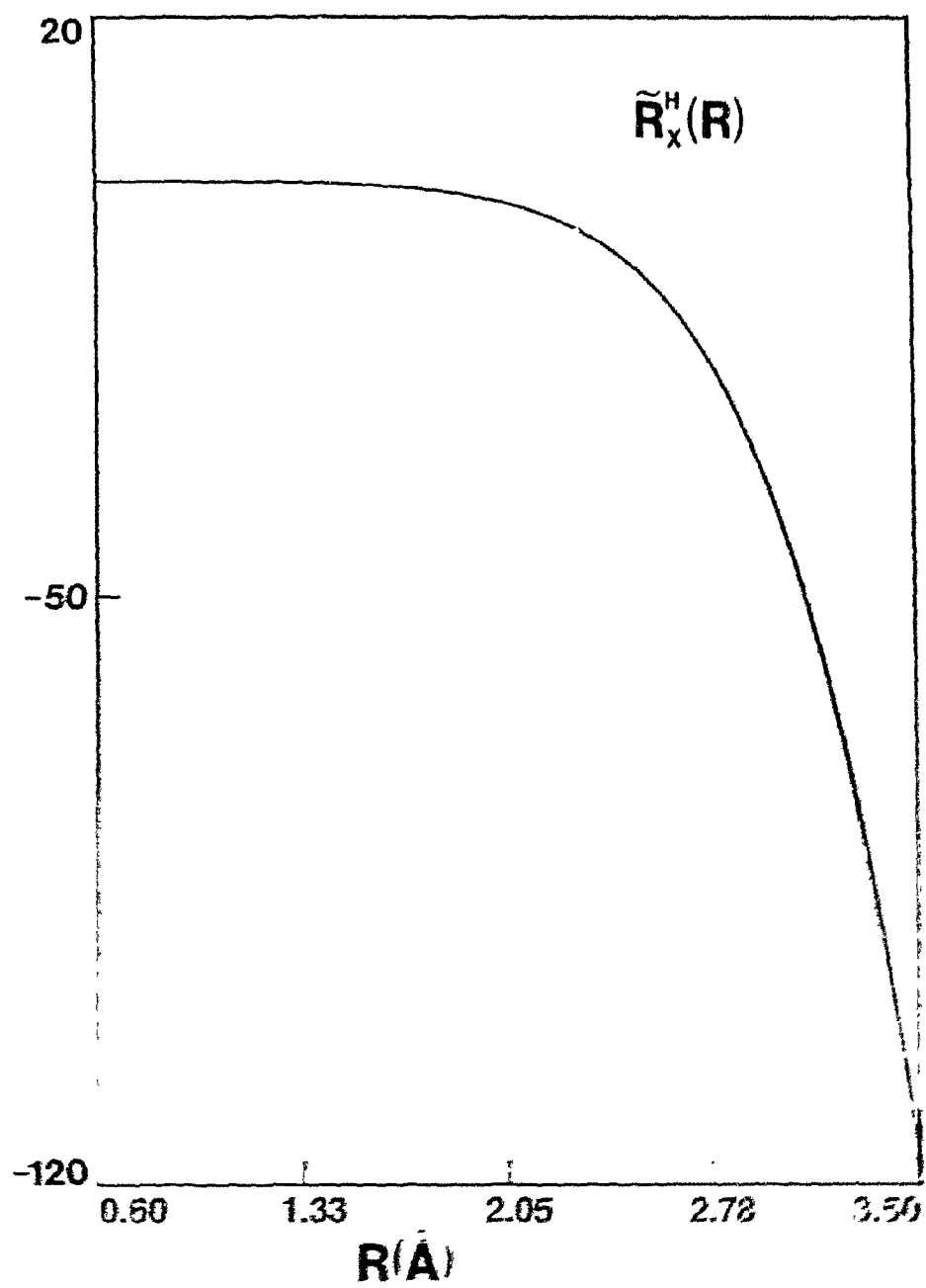


FIGURE 7.4.1

TABLE 7.2

Internuclear Potentials for the $X^1\Sigma^+$ States of HF and DF^a

v	HF($X^1\Sigma^+$)			DF($X^1\Sigma^+$)		
	$E_v(\text{cm}^{-1})$	$R_{\min}(\text{\AA})$	$R_{\max}(\text{\AA})$	$E_v(\text{cm}^{-1})$	$R_{\min}(\text{\AA})$	$R_{\max}(\text{\AA})$
0	2 050.771	0.834 164	1.020 550	1 490.304	0.845 388	1.003 648
1	6 012.194	0.784 496	1.113 087	4 396.966	0.801 118	1.078 758
2	9 801.566	0.754 791	1.186 891	7 212.122	0.774 065	1.137 284
3	13 423.603	0.733 069	1.254 045	9 937.659	0.753 947	1.189 533
4	16 882.448	0.715 908	1.318 066	12 575.326	0.737 814	1.238 503
5	20 181.824	0.701 767	1.380 656	15 126.697	0.724 331	1.285 559
6	23 324.620	0.689 804	1.442 824	17 593.323	0.712 762	1.331 487
7	26 313.146	0.679 499	1.505 310	19 976.491	0.702 655	1.376 810
8	29 148.927	0.670 513	1.568 760	22 277.236	0.693 708	1.421 889
9	31 832.367	0.662 607	1.633 766	24 496.553	0.685 708	1.467 016
10	34 362.909	0.655 612	1.701 027	26 635.187	0.678 499	1.512 448
11	36 738.405	0.649 403	1.771 358	28 693.560	0.671 965	1.558 424
12	38 954.943	0.643 888	1.845 822	30 671.873	0.666 015	1.605 167
13	41 006.593	0.639 001	1.925 881	32 570.069	0.660 578	1.652 923
14	42 884.443	0.634 696	2.013 706	34 387.697	0.655 598	1.701 981
15	44 576.055	0.630 945	2.112 621	36 123.796	0.651 030	1.752 658
16	46 064.207	0.627 740	2.228 215	37 777.013	0.646 838	1.805 331
17	47 325.663	0.625 087	2.370 656	39 345.461	0.642 993	1.860 502
18	48 328.541	0.623 019	2.561 877	40 826.504	0.639 472	1.918 780
19	49 026.508	0.621 598	2.867 114	42 216.725	0.636 259	1.980 990
20				43 511.763	0.633 341	2.048 302
21				44 705.951	0.630 711	2.122 254
22				45 792.421	0.628 367	2.205 242
23				46 762.391	0.626 312	2.300 913
24				47 605.014	0.624 555	2.415 284
25				48 306.664	0.623 111	2.559 779
26				48 848.868	0.622 006	2.760 675

^a E_v are the eigenvalues of the fitted operators for $J = 0$. The R_e values are found in Table 7.13 as the quantities R_e^{QM} .

TABLE 7.3

281

Internuclear Potentials for the $B^1\Sigma^+$ States of HF and DF^a

v	HF($B^1\Sigma^+$)			DF($B^1\Sigma^+$)		
	$E_v(\text{cm}^{-1})$	$R_{\min}(\text{\AA})$	$R_{\max}(\text{\AA})$	$E_v(\text{cm}^{-1})$	$R_{\min}(\text{\AA})$	$R_{\max}(\text{\AA})$
0	572.063	1.924 812	2.274 901	416.314	1.947 980	2.245 681
1 1	695.839	1.810 700	2.425 988	1 238.076	1.849 486	2.370 632
2 2	785.236	1.735 175	2.540 126	2 041.493	1.784 075	2.463 405
3 3	841.363	1.675 277	2.640 226	2 827.016	1.732 106	2.543 554
4 4	865.358	1.624 431	2.732 818	3 595.063	1.687 937	2.616 743
5 5	858.351	1.579 658	2.820 844	4 346.103	1.649 008	2.685 506
6 6	821.455	1.539 306	2.905 935	5 080.534	1.613 904	2.751 255
7 7	755.644	1.502 346	2.989 174	5 798.834	1.581 743	2.814 838
8 8	661.873	1.468 079	3.071 041			
9 9	541.073	1.436 001	3.152 239			
10 10	394.194	1.405 725	3.232 950			

^a E_v are the eigenvalues of the fitted operators for $J = 0$. $R_e^{\text{HF}}(B^1\Sigma^+) = 2.091024(1) \text{ \AA}$ and $R_e^{\text{DF}}(B^1\Sigma^+) = 2.090461(3) \text{ \AA}$.

calculated from the $d_{\kappa i}$ coefficients and other required information listed in Table 7.4. The full set of eigenvalues for both electronic states of both isotopomers is found in Appendix A-8.

7.3.2 Predissociation in $X^1\Sigma^+$

Johns and Barrow (151) as well as Di Lonardo and Douglas (87) observed the sudden breaking-off of rotational structure at high- J for several bands of the $\text{HF}(B \rightarrow X)$ system. These observations were independent of the vibrational quantum number of the upper electronic state and were thus attributed to a rotational predissociation mechanism in the ground $X^1\Sigma^+$ state. Further support for a predissociation mechanism was provided by the observation of measurably broadened contours for the last observed lines in several bands involving $v'' = 16$ and 17. For the case of DF, Johns and Barrow (151) reported a similarly abrupt cutoff in rotational structure at high- J , but no unusual broadening of any rotational lines. In the present analysis of the $B - X$ emission band system of DF, similar observations were made, although the range of observed J was increased slightly.

The observation of broadened line positions immediately prior to a complete disappearance of rotational structure at high- J can in many cases be explained adequately by a pure rotational predissociation mechanism. However, this adiabatic mechanism need not be solely responsible for the predissociation observations for HF/DF. Predissociation mechanisms have been categorized by Herzberg (198) and by Mulliken (199). A useful review has been given recently by Lefebvre-Brion and Field (200). A broadening of line contours with increasing J can also be due to a gyroscopic predissociation mechanism involving a nonadiabatic mixing of the rovibronic wavefunctions of

TABLE 7.4
Coefficients d_{Xi} for Nuclear-Mass-Independent
Part of $g(R)^a$

$d_{X3} = -2.154\,796 \times 10^{-3}$
$d_{X4} = 9.484\,920 \times 10^{-4}$
$d_{X5} = -5.062\,229 \times 10^{-4}$
$R_e = 0.916\,843 \text{ \AA}$
$\mathcal{R}_X = 0.60 \text{ \AA}$

^aThe function is defined by Eqs. (3.47, 3.48) (see text).

two different electronic states. This type of mechanism is most appropriate for HF/DF where the $A^1\Pi$ state interacts significantly with high-lying rovibrational levels of $X^1\Sigma^+$. The classical effect of this interaction is to cause the $X^1\Sigma^+$ levels to occur at lower energy than they would in the absence of $A^1\Pi$; the $R_X^H(R)$ function, for both HF and HCl, adds negatively to the kinetic energy of rotation. However, as there exists an infinite number of short-lived collision induced energy levels for the repulsive $A^1\Pi$ state, for every orbiting resonance in $X^1\Sigma^+$ there must exist a degenerate interaction with the wavefunction of a continuum level lying at the same energy. This is shown graphically in Figure 7.5. The interaction provides an additional avenue by which penetration of the potential barrier can occur. The wavefunction mixing reduces the lifetimes of the $X^1\Sigma^+$ quasibound levels and must therefore contribute positively to the observed line widths.

This can be interpreted in yet another way. The orbiting resonances that can be detected by classical spectrography all lie below the barrier maximum. Since the effect of $q(R)$ is to add negatively to the energy of rotation in a *monotonic* way, it follows that $q(R)$ would decrease the position of the barrier maximum *more* than it decreases the position of a bound level. The energy level is therefore brought relatively closer to the barrier top than it would otherwise be. This induces a decrease in the lifetime of the quasibound state and provides a contribution to the width additional to that predicted on a simple rotational predissociation mechanism alone. Also, since $q(R)$ increases negatively with increasing R , it must displace the third turning point towards smaller R by a *greater* amount than it does the second turning point; this decreases the barrier width and hence the lifetimes of quasibound levels.

Due to the $A^1\Pi \approx X^1\Sigma^+$ interaction the observed width is a composite of

Figure 7.5

Interaction between the $A^1\Pi$ and $X^1\Sigma^+$ states of HF(DF). The rovibrational wavefunction of ground state level v is seen to interact with the continuum wavefunction of the repulsive state near an energy E_{vj} . The wavefunction mixing is found to reduce the non-radiative lifetime of the $X^1\Sigma^+$ state quasibound level.

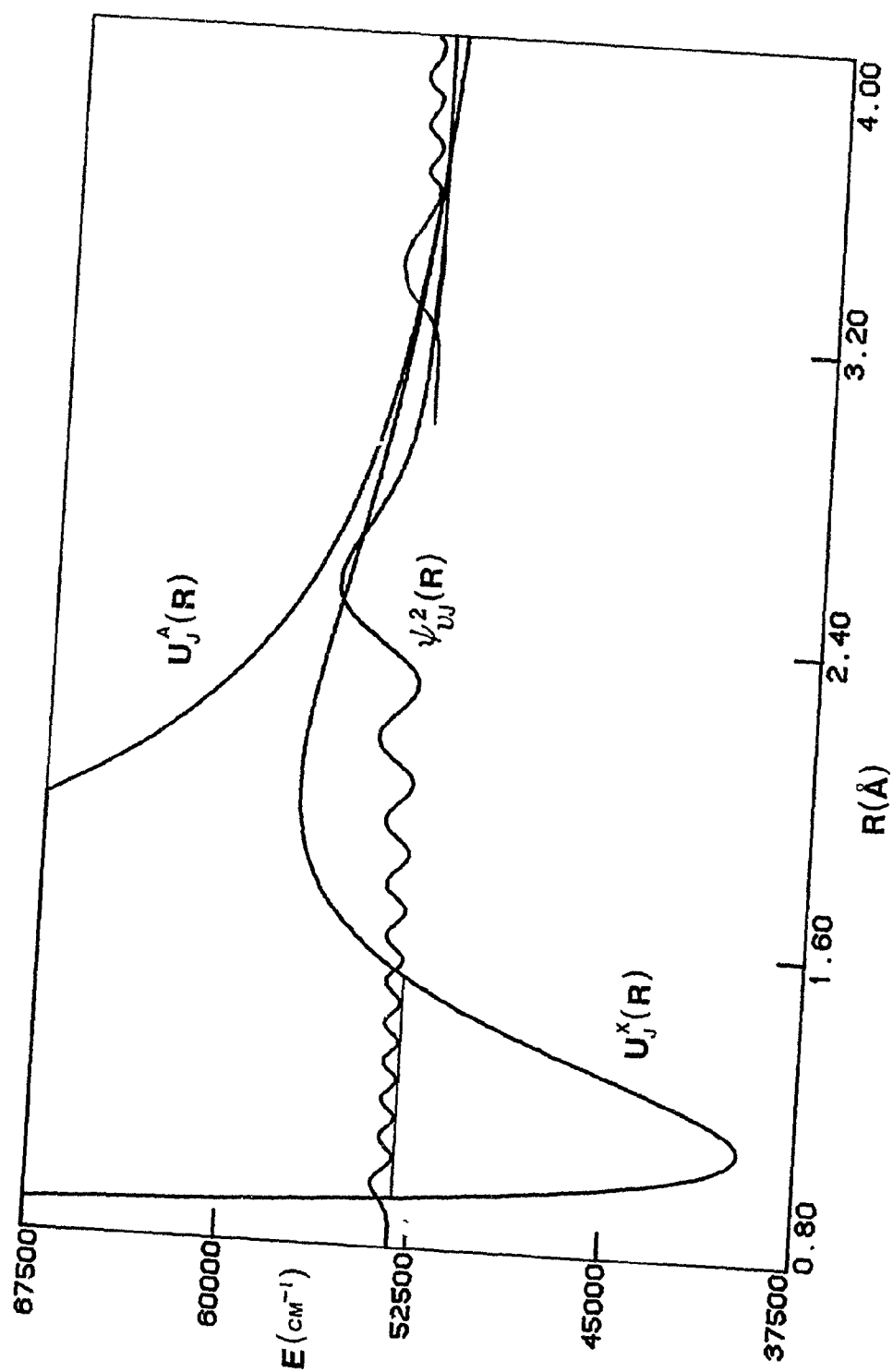


Figure 7.5

the two mechanisms, and a reliable resolution to the individual contributions is difficult to achieve in the absence of a proper quantum mechanical model. It is then not correct to invert observed widths, either quantum mechanically or semiclassically, on the basis of the usual centrifugal barrier expression, to obtain the rotationless potential or the dissociation limit. In the present work, however, it was possible to decompose the total calculated widths, which predict magnificently their observed counterparts, to the gyroscopic and pure centrifugal contributions.

Table 7.5 lists energies and calculated widths for several selected levels of ground state HF and DF. The agreement with widths measured experimentally for levels $v'', J'' = 16, 23$ and $v'', J'' = 17, 19$ is a good indication of the physical significance of the present results. It is noted, also, that experimental estimates are Doppler limited values and that typical widths of normal lines on the plates of Ref. (87) were approximately 0.30 cm^{-1} . The Heisenberg widths calculated in the present work should therefore be slightly smaller than those observed experimentally, as is indeed the case. Also shown in Table 7.5 are the energies and widths calculated in the absence of J -dependent coupling, *i.e.* with $q(R)$ set to zero. The contribution from the pure centrifugal barrier then becomes apparent; it can be seen that $q(R)$ contributes significantly both to the energies and widths of quasibound levels. Experimental observation cannot be rationalized without an explicit consideration of $q(R)$.

7.3.3 The Dissociation Energy of $X^1\Sigma^+$

The determination of the dissociation energy of $X^1\Sigma^+$ states of HF and DF can be accomplished by a variety of methods. The LCD method has been

TABLE 7.5

Rotational Predissociation in $X^1\Sigma^+$: Calculated Energies
and Widths of Selected Quasibound Levels for HF and DF^a

Hydrogen Fluoride					
v	J	E_{vJ}^A	Γ_{fwhm}^A	E_{vJ}^L	Γ_{fwhm}^B
9	44 *	53 150.78	0.82	53 160.99	0.57
10	41 *	52 358.26	0.16	52 367.39	0.10
10	42 *	52 902.45	6.18	52 914.87	5.22
11	38	51 689.46	0.04	51 697.81	0.02
11	39 *	52 197.62	2.78	52 208.78	1.97
12	35 *	51 143.67	0.02	51 151.44	0.01
12	36 *	51 607.16	1.41	51 617.43	0.91
13	32 *	50 716.29	0.01	50 723.65	0.004
13	33 *	51 128.24	1.13	51 137.98	0.69
14	29	50 398.45	0.02	50 405.58	0.01
14	30 *	50 752.98	1.68	50 762.57	1.02
15	26	50 175.91	0.08	50 183.10	0.03
15	27 *	50 467.28	4.61	50 477.20	3.01
16	23	50 026.64	1.16 (1.25)	50 034.59	0.54
17	19	49 746.14	0.65 (0.86)	49 753.00	0.32
18	14	49 473.15	0.20	49 477.58	0.16
Deuterium Fluoride					
v	J	E_{vJ}^A	Γ_{fwhm}^A	E_{vJ}^B	Γ_{fwhm}^B
9	70	54 943.35	0.10	54 948.29	0.08
10	67	54 145.01	0.01	54 149.54	0.008
11	65	53 901.92	0.09	53 906.91	0.07
12	63 *	53 672.04	0.69	53 677.68	0.57
13	60	53 041.03	0.14	53 046.15	0.11
14	58 *	52 867.91	1.49	52 873.86	1.22

TABLE 7.5 (Cont'd)

Rotational Predissociation in $X^1\Sigma^+$: Calculated Energies
and Widths of Selected Quasibound Levels for HF and DF^a

v	J	E_{vJ}^A	Γ_{fwhm}^A	E_{vJ}^B	Γ_{fwhm}^B
15	55	52 346.21	0.50	52 351.67	0.39
16	52	51 885.26	0.20	51 890.36	0.15
17	49	51 484.71	0.11	51 489.53	0.08
18	47 *	51 425.62	2.98	51 431.65	2.46
19	43	50 856.53	0.12	50 861.08	0.08
19	44 *	51 111.16	3.55	51 117.10	2.90
20	40	50 621.06	0.27	50 625.63	0.19
21	37 *	50 429.54	1.01	50 434.31	0.73
22	33	50 101.33	0.20	50 105.31	0.12
22	34 *	50 272.28	4.63	50 277.43	3.75
23	29	49 859.59	0.07	49 863.04	0.04
23	30 *	50 004.75	3.13	50 009.22	2.26
24	25	49 695.74	0.08	49 698.96	0.05
24	26 *	49 810.09	4.24	49 814.47	2.98
25	21 *	49 592.25	0.68	49 595.79	0.50
26	15 *	49 413.39	0.26	49 415.32	0.24
26	16 *	49 469.03	1.36	49 471.76	1.22

^aQuantities X^A and X^B are from calculations including and excluding $q(R)$, respectively. For HF, widths given in parentheses are experimental estimates from Ref. (87). E are energies (cm^{-1}) and Γ_{fwhm} (cm^{-1}) are full widths at half maximum of intensity, and entries marked with an asterisk (*) have not been experimentally observed.

considered previously in this work and the cautionary measures associated with its use were discussed. One method not discussed so far is Bernstein's Locus of Barrier Maximum (LBM) (201) procedure. A natural extension of the LCD method, the LBM assumes an explicit form for the internuclear potential as predicted by long-range theory. For a potential that varies asymptotically as,

$$U(R) = \mathcal{D}_e - C_n/R^n, \quad (7.8)$$

the energy of the barrier maximum is given by

$$E = \mathcal{D}_e + S_n[J(J+1)]^{n/(n-2)}, \quad (7.9)$$

where

$$S_n/\text{cm}^{-1} = \frac{n-2}{4\pi c} \left[\frac{\hbar^{n+2}}{(n\mu)^n C_n^2} \right]^{1/(n-2)}, \quad (7.10)$$

involving the reduced mass μ and a collection of constants, including the long-range potential parameter C_n . However, in order for this method to be applicable it is necessary to employ data that fall into the long-range region of the potential so that Eq. (7.9) is a valid representation. Le Roy (49) has proposed a criterion for determining the onset of the long-range region as,

$$\mathcal{R}_{LR} > 2(\langle r_A^2 \rangle^{1/2} + \langle r_B^2 \rangle^{1/2}), \quad (7.11)$$

where the expectation values of atomic centres A/B are over electronic coordinates and refer to the first state with an outermost unfilled shell. This expression attempts to justify the use of Eq. (7.8) for an internuclear separation \mathcal{R}_{LR} beyond which the electron clouds do not overlap significantly. For the case of HF/DF, using the relativistic $\langle r_F^2 \rangle$ value of Lu *et al.* (202) for the fluorine ground state, $^2P_{3/2}$, and estimating the hydrogenic

expectation value from the analytical $1s$ orbitals (203), it is found that $\mathcal{R}_{LR}(\text{HF}) > 3.12 \text{ \AA}$. This is greater than the outermost turning points of HF and DF and indicates that the use of the LBM procedure is not warranted. The validity of a previous LBM analysis for HF/DF by Byrne *et al.* (204) has been questioned (49) despite the deceptively linear behaviour of the associated plots. When valid, the LBM method gives an estimate for the leading inverse power dispersion coefficient, C_6 for $\text{HF}(X^1\Sigma^+)$, for which *ab initio* estimates are unavailable. An approximate estimate has been obtained (205) as $C_6 = 37\,856 \text{ cm}^{-1} \text{ \AA}^6$; this was calculated by scaling the C_6 value for NeH (206) with the polarizabilities of hydrogen, neon and fluorine. S_6 is given by the expression,

$$S_6/\text{cm}^{-1} = \frac{\hbar^2}{\pi c} \left[\frac{1}{(6\mu)^6 C_6^2} \right]^{1/4}, \quad (7.12)$$

for C_6 in erg cm^6 units. From this, the limiting slopes of the LBM for HF/DF($X^1\Sigma^+$) were estimated. LBM plots were then constructed for HF and DF as shown in Figure 7.6 and extrapolated to $J = 0$. The limiting slopes are also included and it is obvious that they deviate significantly from those which are suggested from a simple extrapolation of the plotted data. This demonstrates the danger of using the LBM blindly, as it is clear that in the long-range region, the behaviour of the curve is altered dramatically. The results indicate that the LBM \mathcal{D}_e values for HF/DF will be slight overestimates if the extrapolation is carried out on the basis of the existing data.

Since internuclear potentials are available in this work, it is possible, in principle, to employ more direct methods for estimating \mathcal{D}_e . It could be possible to fit the outer limb potential points to an inverse power potential expansion,

Figure 7.6

Locus of barrier maximum (LBM) plots for HF/DF($X^1\Sigma^+$). The filled circles represent the last observed rotational levels of given v . The open circles represent extrapolated energies for J one unit higher than the last observed levels. The limiting slopes indicated by dashed lines were calculated on the basis of $C_6 = 37856 \text{ cm}^{-1} \text{ \AA}^6$ (205) and Eq. (7.12). The dissociation limits $\mathscr{D}_e^{\text{HF}} = 49335(30) \text{ cm}^{-1}$ and $\mathscr{D}_e^{\text{DF}} = 49310(40) \text{ cm}^{-1}$ are obtained from the intercepts of the dashed curves.

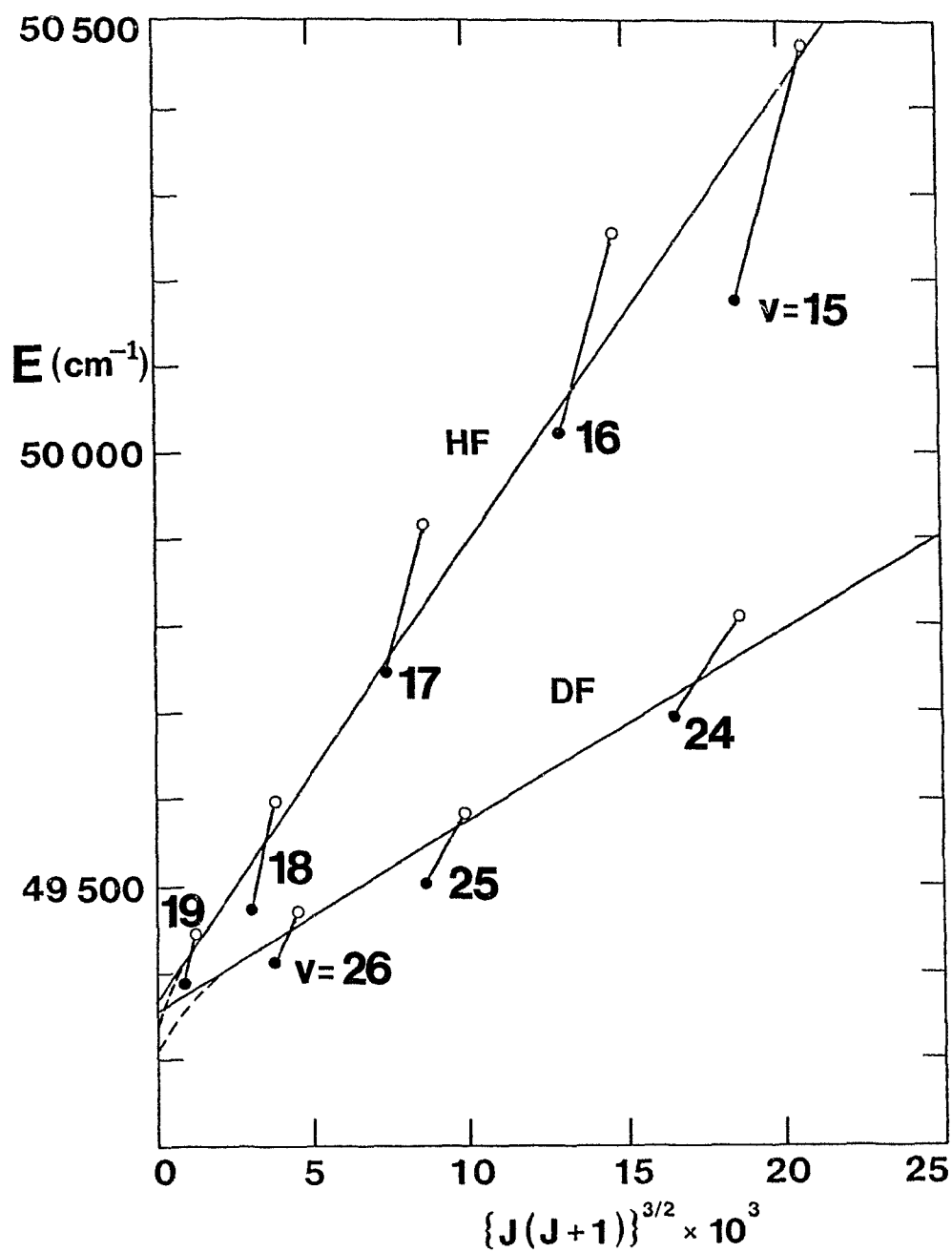


Figure 7.6

$$U(R) = \mathcal{D}_e - C_6/R^6 - C_8/R^8 - C_{10}/R^{10} - \dots, \quad (7.13)$$

a result predicted by a perturbational treatment of the polarization of the electronic clouds as the two atoms approach each other from infinity, but which is inapplicable in the chemical bonding region, at intermediate R . It is found, unfortunately, that this method of estimating \mathcal{D}_e is sensitive to the range of R considered, and the number of terms included in the potential expansion. Employing C_n and \mathcal{D}_e as free-floating parameters, it is even possible to obtain unphysical negative values for C_6 , C_8 , etc. Using the approximate values $C_8 = 172\,470\text{ cm}^{-1}\text{ Å}^8$, and $C_{10} = 103\,810\text{ cm}^{-1}\text{ Å}^{10}$ (205) along with the C_6 estimate given above, it was possible to obtain a more physically meaningful fit to \mathcal{D}_e and an additional constant C_{12} . It was found that $\mathcal{D}_e(\text{HF}) = 49\,370 \pm 30\text{ cm}^{-1}$, where the error limit is intuitive. The value of the fitted constant $C_{12} \approx 72 \times 10^6\text{ cm}^{-1}\text{ Å}^{12}$ is positive and of the right order of magnitude but it is not clear that any strict physical significance should be attached to it. The correlation between \mathcal{D}_e and C_{12} could not be obtained since the geometrical simplex fitting method (207) was employed. The fitted \mathcal{D}_e value appears to be consistent with the LCD estimate given in Chapter 5. The same methodology applied to $\text{DF}(X^1\Sigma^+)$ furnished the fitted constants $\mathcal{D}_e = 49\,355 \pm 40\text{ cm}^{-1}$ and $C_{12} \approx 71 \times 10^6\text{ cm}^{-1}\text{ Å}^{12}$.

A different method exploiting the behaviour of the internuclear potential was also used to estimate \mathcal{D}_e . It was reasoned that as the potential approaches the dissociation limit, the slope of $U(R)$ tends asymptotically to zero. If a plot is constructed with the potential slope as the abscissa and energy as the ordinate, the y-intercept corresponding to zero slope would give precisely \mathcal{D}_e . In mathematical terms, $E_R = f\{U'(R)\}$. It was found that

$f\{U'(R)\}$ could be well represented by,

$$E_R = \mathcal{D}_e + d_1(\partial U/\partial R)_R + d_2(\partial U/\partial R)_R^2 + d_3(\partial U/\partial R)_R^3 + \dots \quad (7.14)$$

Also, an expression involving half-powers of the slope was used, giving similar results. This method appears to give estimates for \mathcal{D}_e which are consistently lower than those obtained with the methods described above. For HF the value $\mathcal{D}_e = 49\,315 \pm 30 \text{ cm}^{-1}$ was obtained and for DF $\mathcal{D}_e = 49\,295 \pm 40 \text{ cm}^{-1}$ was determined. It is interesting to note that the results derived from the radial functions infer that \mathcal{D}_e for HF is approximately 20 cm^{-1} higher than that of DF. Although this, of course, is inconclusive on the basis of the error estimates, it should be noted that the difference appears to be somewhat supported by the use of *identical* models throughout for both HF and DF. Another piece of evidence supporting this small difference is the behaviour of the $\Delta U_X^H(R)$ function, which is essentially one half of the mirror image of the function $U_X^H(R)$, shown in Fig. (7.2). At large- R , if one disregards the obviously unphysical anomaly beyond the outermost v, J turning point (R_{\max}), we see that the difference function $U_X(\text{DF}) - U_X(\text{HF})$, or $\Delta U_X^H(R)$, begins to approach constancy at a value of approximately $-(15\text{--}20) \text{ cm}^{-1}$, indicating that the potential asymptote for HF lies higher than that of DF. These arguments are not conclusive, but it would seem unlikely that the potential difference function would change its behaviour in the long-range region. A situation similar to the present was found for the ground state of LiH (208). As R increases, homogeneous mixing contributions to the rotationless curve approach zero so that the dominant contribution to any difference in the dissociation limits of the two isotopomers becomes the difference in the adiabatic contributions to the separated atoms H/D, as compared to the total adiabatic

and nonadiabatic corrections at the potential minima of HF and DF.

There appears to be, however, an inconsistency between these results and those obtained from the LCD method. For comparison purposes the estimates of \mathscr{D}_e obtained in this work by different methods are listed in Table 7.6. The LCD method infers slightly that the dissociation limit of DF lies higher than that of HF. There is significant disagreement between the \mathscr{D}_e value for DF obtained by the LCD method and the slope/energy method. This could be explained only if the LCD gives estimates which are in fact less precise than first thought.

In Chapter 5 a semiclassical potential for $\text{DF}(X^1\Sigma^+)$ was obtained by interpolating $\Delta G(v + \frac{1}{2})$ and B_v values in the region $v'' = 5-15$. Despite the care exercised in accomplishing these interpolations, the present results show unequivocally that the previous absolute energy estimates above G_{16} are in large error. Specifically, the energies of the RKR potential given in Table 5.7 should be lowered by approximately 20 cm^{-1} . Similarly, the \mathscr{D}_e estimate for the ground state obtained by the LCD method should be lowered by the same amount. This is yet another demonstration of the problems that can be encountered in traditional methods of analysis.

The most reliable results are perhaps those obtained by using Eq. (7.13) with constrained estimates of the C_n . Averaging all results, however, the final values reported in this work are $\mathscr{D}_e(\text{HF}) = 49\,350 \pm 40 \text{ cm}^{-1}$ and $\mathscr{D}_e(\text{DF}) = 49\,338 \pm 45 \text{ cm}^{-1}$. More precise values may be obtained only through the observation of higher vibrational levels of $X^1\Sigma^+$ and further manipulation of the present data *will not* reduce the error estimates. Alternatively, the behaviour of the long-range section of the potential could be obtained by improved theoretical calculations to give more precise estimates of \mathscr{D}_e .

TABLE 7.6

The Dissociation Energies (cm^{-1}) of Ground State HF and DF:
A Comparison of Several Methods of Determination

Method	HF	DF
Eq. (7.13)	49 370 \pm 30	49 355 \pm 40
Energy-Slope	49 315 \pm 30	49 295 \pm 40
LCD	49 380 \pm 60	49 390 \pm 50
LBM (Corrected)	49 335 \pm 30	49 310 \pm 40
Average	49 350 \pm 40	49 338 \pm 45

7.3.4 The Electronic Isotope Shift

The present analysis furnishes a more reliable estimate of the electronic isotope shift, $\Delta T_e = T_e^{\text{HF}} - T_e^{\text{DF}}$, than was reported in Chapter 5. The error estimate of $\pm 5 \text{ cm}^{-1}$ given therein has now been reduced by two orders of magnitude. This is made possible by the plentiful newly assigned DF($B \rightarrow X$) data which provide information that reduces the gap in $X^1\Sigma^+$. Also, the reduction in the uncertainty of this quantity is due to the *smooth* behaviour of the $U_X^{\text{H}}(R)$ function in the region of missing DF experimental information.

The electronic terms of $B^1\Sigma^+$ obtained here are $T_e^{\text{HF}} = 84\,783.93(3) \text{ cm}^{-1}$ and $T_e^{\text{DF}} = 84\,786.41(7) \text{ cm}^{-1}$, giving an electronic term value difference of $-2.48(7) \text{ cm}^{-1}$. There is now a large discrepancy between this experimental result and the approximate theoretical estimate presented earlier, $\Delta T_e = -14.1 \text{ cm}^{-1}$.

7.3.5 Perturbation Calculation of Centrifugal Distortion

The interaction between $A^1\Pi$ and $X^1\Sigma^+$ contributes significantly to the molecular constants of bound vibrational levels of $X^1\Sigma^+$. As Herzberg indicates (209), such coupling requires that the rotational energy be expressed as,

$$F_v(J) = B_v[J(J+1)] - D_v[J(J+1)]^2 + \dots + \Phi_v(J), \quad (7.15)$$

where $\Phi_v(J)$ is a small nonadiabatic contribution to the energy levels. Although Herzberg (209) obtained this expression for $\Lambda \geq 1$ states, it was also stated that $^1\Sigma$ states also require a function $\Phi_v(J)$ to account for electronic state mixing. The nonadiabatic function $\Phi_v(J)$ can be written as,

$$\Phi_v(J) = \phi_{v0} + \phi_{v1}[J(J+1)] + \phi_{v2}[J(J+1)]^2 + \dots, \quad (7.16)$$

where ϕ_{v0} can be regarded as a purely homogeneous contribution to the rotationless eigenvalues. The experimentally derived quantities,

$$B_v^{\text{eff}} = B_v + \phi_{v1}, \quad (7.17)$$

$$D_v^{\text{eff}} = D_v + \phi_{v2}, \quad (7.18)$$

are written in terms of the mechanical B_v and D_v values and the nonmechanical contributions ϕ_{v1} and ϕ_{v2} . From Eqs. (2.53, 2.54) it follows that,

$$\phi_{v1} = \beta_{\text{at}}^2 \langle \psi_v^{(0)} | q(R)/R^2 | \psi_v^{(0)} \rangle, \quad (7.19)$$

$$\phi_{v2} = \beta_{\text{at}}^4 \langle \psi_v^{(0)} | q(R)/R^2 | \psi_v^{(1)} \rangle, \quad (7.20)$$

where $\psi_v^{(0)}$ is the zeroth-order wavefunction and $\psi_v^{(1)}$ the first-order wavefunction correction.

The modified version of Hutson's computer program was employed to calculate rotational and centrifugal distortion constants which are quantum mechanically consistent with the derived Hamiltonian operators. These constants should compare well with experimentally derived estimates. Calculated constants are listed in Tables 7.7-7.8 for both electronic states of HF and DF. Also shown in these tables are constants which have been deperturbed from $^1\Pi - ^1\Sigma$ coupling, as well as some experimentally derived estimates. As was the case for HCl/DCI, the calculated constants fail to predict the high- v, J energy levels within the experimental uncertainties. It is thus currently not possible to employ calculated constants to represent the eigenvalues in a compact fashion. Additional constants beyond M_v are required to remove the discrepancy.

TABLE 7.7

Quantum Mechanical Molecular Constants for HF/DF($X^1\Sigma^+$)^a

HF($X^1\Sigma^+$)						
v	G_v	B_v	D_v	H_v	L_v	M_v
0	2050.7710	20.5597286	2.119864-3	1.638279-7	-1.55883-11	1.5866-15
	2050.7710	20.5597459	2.119800-3	1.638472-7	-1.55853-11	1.5870-15
1	6012.1941	19.787464	2.06366-3	1.5910-7	-1.551-11	1.53-15
	6012.1941	19.787521	2.06357-3	1.5912-7	-1.550-11	1.54-15
2	9801.5656	19.034953	2.00993-3	1.5395-7	-1.563-11	1.49-15
	9801.5656	19.035057	2.00982-3	1.5398-7	-1.563-11	1.49-15
3	13423.603	18.30054	1.9594-3	1.484-7	-1.55-11	1.5-15
	13423.603	18.30070	1.9592-3	1.485-7	-1.55-11	1.5-15
4	16882.448	17.58250	1.9119-3	1.426-7	-1.62-11	8.1-16
	16882.448	17.58273	1.9117-3	1.426-7	-1.62-11	8.1-16
5	20181.824	16.8789	1.8692-3	1.348-7	-1.6-11	2-15
	20181.824	16.8792	1.8689-3	1.349-7	-1.6-11	2-15
6	23324.620	16.1866	1.8308-3	1.283-7	-1.7-11	
	23324.620	16.1870	1.8305-3	1.284-7	-1.7-11	
7	26313.146	15.50367	1.79605-3	1.17866-7	-1.8832-11	1.918-15
	26313.146	15.50419	1.79770-3	1.17969-7	-1.8805-11	1.925-15
8	29148.927	14.82591	1.77324-3	1.07709-7	-1.8968-11	-2.245-16
	29148.927	14.82557	1.77281-3	1.07845-7	-1.8929-11	-2.119-16
9	31832.367	14.14955	1.75630-3	9.41247-8	-2.3822-11	-9.63-16
	31832.367	14.15037	1.75576-3	9.43083-8	-2.3761-11	-9.41-16
10	34362.909	13.46938	1.75184-3	7.54613-8	-2.7967-11	-8.41-16
	34362.909	13.47041	1.75115-3	7.57169-8	-2.7871-11	-8.02-16
11	36738.405	12.77819	1.76272-3	5.33445-8	-3.2861-11	-5.60-15
	36738.405	12.77945	1.76184-3	5.37111-8	-3.2703-11	-5.52-15
12	38954.943	12.06805	1.79254-3	2.03685-8	-4.9355-11	-1.03-14
	38954.943	12.06963	1.79139-3	2.09184-8	-4.9072-11	-1.01-14
13	41006.593	11.32752	1.85214-3	-2.71396-8	-6.5140-11	-2.05-14
	41006.593	11.32950	1.85059-3	-2.62693-8	-6.4613-11	-2.02-14
14	42884.443	10.54127	1.95094-3	-9.93635-8	-1.0864-10	-4.532-14
	42884.443	10.54377	1.94875-3	-9.78894-8	-1.0755-10	-4.447-14
15	44576.055	9.68820	2.11135-3	-2.15406-7	-1.7531-10	-9.859-14
	44576.055	9.69144	2.10810-3	-2.12674-7	-1.7281-10	-9.619-14

TABLE 7.7 (Cont'd)

Quantum Mechanical Molecular Constants for HF/DF($X^1\Sigma^+$)^a

HF($X^1\Sigma^+$)						
v	G_v	B_v	D_v	H_v	L_v	M_v
16	46064.207	8.73866	2.36411-3	-4.20960-7	-3.6377-10	-2.769-13
	46064.207	8.74300	2.35886-3	-4.15214-7	-3.5691-10	-2.683-13
17	47325.663	7.64712	2.78434-3	-8.28972-7	-8.1981-10	-1.004-12
	47325.663	7.65327	2.77468-3	-8.14288-7	-7.9543-10	-9.603-13
18	48328.541	6.33740	3.5528-3	-1.97089-6	-2.9881-9	-5.6478-12
	48328.541	6.34701	3.5306-3	-1.91658-6	-2.8402-9	-5.2110-12
19	49026.508	4.62302	5.5237-3	-7.99298-6	-2.6476-8	-8.6457-11
	49026.508	4.64212	5.4335-3	-7.49756-6	-2.3626-8	-7.1805-11
DF($X^1\Sigma^+$)						
v	G_v	B_v	D_v	H_v	L_v	M_v
0	1490.30435	10.8603442	5.87456-4	2.3856-8	-1.189-12	6.4-17
0	1490.30435	10.8603475	5.87447-4	2.3857-8	-1.189-12	6.4-17
1	4396.96596	10.5640266	5.76080-4	2.3367-8	-1.188-12	6.4-17
1	4396.96596	10.5640370	5.76070-4	2.3368-8	-1.188-12	6.4-17
2	7212.122	10.273310	5.65060-4	2.288-8	-1.19-12	
2	7212.122	10.273329	5.65047-4	2.288-8	-1.19-12	
3	9937.659	9.987962	5.54433-4	2.229-8	-1.20-12	
3	9937.659	9.987990	5.54417-4	2.230-8	-1.20-12	
4	12575.33	9.70753	5.4430-4	2.17-8	-1.2-12	
4	12575.33	9.70757	5.4428-4	2.17-8	-1.2-12	
5	15126.70	9.43175	5.3448-4	2.12-8	-1.2-12	
5	15126.70	9.43181	5.3445-4	2.12-8	-1.2-12	
6	17593.32	9.16036	5.2532-4	2.04-8	-1.2-12	
6	17593.32	9.16043	5.2530-4	2.04-8	-1.2-12	
7	19976.49	8.89260	5.1692-4	1.97-8	-1.2-12	
7	19976.49	8.89268	5.1688-4	1.97-8	-1.2-12	
8	22277.24	8.62808	5.0892-4	1.90-8	-1.3-12	
8	22277.24	8.62818	5.0888-4	1.90-8	-1.3-12	

TABLE 7.7 (Cont'd)

Quantum Mechanical Molecular Constants for HF/DF($X^1\Sigma^+$)^a

DF($X^1\Sigma^+$)						
v	G_v	B_v	D_v	H_v	L_v	M_v
9	24496.553	8.366478	5.01781-4	1.79888-8	-1.3601-12	4.757-17
9	24496.553	8.366596	5.01739-4	1.79952-8	-1.3593-12	4.769-17
10	26635.187	8.106936	4.95713-4	1.69437-8	-1.3283-12	6.875-17
10	26635.187	8.107077	4.95664-4	1.69514-8	-1.3272-12	6.890-17
11	28693.560	7.848704	4.90587-4	1.58876-8	-1.4755-12	3.435-17
11	28693.560	7.848870	4.90530-4	1.58970-8	-1.4741-12	3.458-17
12	30671.873	7.591084	4.86605-4	1.46594-8	-1.6280-12	-1.273-16
12	30671.873	7.591280	4.86538-4	1.46710-8	-1.6261-12	-1.269-16
13	32570.069	7.333189	4.84164-4	1.28246-8	-1.9593-12	4.097-17
13	32570.069	7.333419	4.84085-4	1.28392-8	-1.9567-12	4.148-17
14	34387.697	7.073612	4.83811-4	1.08876-8	-1.9602-12	3.103-17
14	34387.697	7.073881	4.83716-4	1.09062-8	-1.9565-12	3.178-17
15	36123.796	6.810974	4.85380-4	8.79691-9	-2.4364-12	-2.603-16
15	36123.796	6.811289	4.85267-4	8.82094-9	-2.4311-12	-2.590-16
16	37777.013	6.543884	4.89551-4	5.72304-9	-3.1552-12	-2.885-16
16	37777.013	6.544253	4.89414-4	5.75486-9	-3.1473-12	-2.864-16
17	39345.461	6.270235	4.97372-4	1.73736-9	-3.7806-12	-2.621-16
17	39345.461	6.270667	4.97204-4	1.78059-9	-3.7687-12	-2.587-16
18	40826.504	5.987431	5.09441-4	-2.97870-9	-4.7748-12	-9.348-16
18	40826.504	5.987940	5.09233-4	-2.91849-9	-4.7560-12	-9.284-16
19	42216.725	5.692641	5.26927-4	-1.01133-8	-7.4062-12	-1.340-15
19	42216.725	5.693243	5.26663-4	-1.00260-8	-7.3745-12	-1.328-15
20	43511.763	5.381704	5.52572-4	-1.96418-8	-8.8254-12	-1.538-15
20	43511.763	5.382425	5.52227-4	-1.95101-8	-8.7714-12	-1.515-15
21	44705.951	5.049735	5.87204-4	-3.22107-8	-1.5123-11	-6.306-15
21	44705.951	5.050508	5.86739-4	-3.20026-8	-1.5020-11	-6.251-15
22	45792.421	4.690747	6.36854-4	-5.46591-8	-2.3155-11	-5.810-15
22	45792.421	4.691824	6.36199-4	-5.43034-8	-2.2946-11	-5.686-15
23	46762.391	4.295201	7.06882-4	-8.49462-8	-3.9393-11	-2.325-14
23	46762.391	4.296563	7.05901-4	-8.42886-8	-3.8915-11	-2.287-14
24	47605.014	3.85212	8.0910-4	-1.4701-7	-8.568-11	-5.308-14
24	47605.014	3.85391	8.0750-4	-1.4561-7	-8.434-11	-5.171-14

TABLE 7.7 (Cont'd)

Quantum Mechanical Molecular Constants for HF/DF($X^1\Sigma^+$)^a

DF($X^1\Sigma^+$)						
v	G_v	B_v	D_v	H_v	L_v	M_v
25	48306.664	3.34091	9.7460-4	-2.7546-7	-2.132-10	-2.125-13
25	48306.664	3.34341	9.7162-4	-2.7174-7	-2.081-10	-2.050-13
26	48848.868	2.72418	1.2835-3	-6.6639-7	-9.078-10	-1.724-13
26	48848.868	2.72809	1.2762-3	-6.5121-7	-8.710-10	-1.626-12

^aAll quantities are in cm^{-1} units. For each vibrational level the top and bottom entries represent perturbed and deperturbed constants, respectively. 5.87456-4 reads as 5.87456×10^{-4} .

TABLE 7.8

Quantum Mechanical Molecular Constants for HF/DF($B^1\Sigma^+$)^a

HF($B^1\Sigma^+$)						
v	G_v	B_v	D_v	H_v	L_v	M_v
0	572.063	4.02042	2.0494-4	1.9332-8	-3.674-12	8.33-16
1	1695.839	4.00106	2.2574-4	2.4880-8	-5.353-12	1.41-15
2	2785.236	3.98038	2.4752-4	3.1595-8	-7.601-12	2.23-15
3	3841.363	3.95895	2.7033-4	3.9345-8	-1.048-11	3.46-15
4	4865.358	3.93681	2.9415-4	4.8438-8	-1.429-11	5.27-15
5	5858.351	3.91413	3.1910-4	5.9213-8	-1.937-11	7.76-15
6	6821.455	3.89119	3.4558-4	7.1586-8	-2.571-11	1.15-14
7	7755.644	3.86793	3.7355-4	8.6515-8	-3.413-11	1.62-14
8	8661.873	3.84469	4.0326-4	1.0364-7	-4.386-11	2.21-14
9	9541.073	3.82169	4.3436-4	1.2257-7	-5.609-11	2.94-14
10	10394.194	3.79872	4.6745-4	1.4379-7	-6.659-11	3.66-14

DF($B^1\Sigma^+$)						
v	G_v	B_v	D_v	H_v	L_v	M_v
0	416.314	2.11520	5.5878-5	2.7060-9	-2.651-13	3.073-17
1	1238.076	2.10799	6.0002-5	3.2590-9	-3.494-13	4.576-17
2	2041.493	2.10034	6.4251-5	3.9042-9	-4.583-13	6.526-17
3	2827.016	2.09243	6.8666-5	4.6289-9	-5.818-13	8.899-17
4	3595.063	2.08432	7.3192-5	5.4130-9	-7.441-13	1.277-16
5	4346.103	2.07595	7.7909-5	6.3401-9	-9.206-13	1.643-16
6	5080.534	2.06746	8.2711-5	7.3310-9	-1.171-12	2.322-16
7	5798.833	2.05882	8.7760-5	8.4788-9	-1.431-12	2.999-16

^aAll quantities are in units of cm^{-1} . 2.0494-4 reads as 2.0494×10^{-4} .

The calculated constants for $v'' = 0$ of HF and DF were employed to calculate the very highly precise far-infrared measurements. The comparison shown in Table 7.9 is very satisfactory, providing support for the physical significance of the present results.

7.3.6 *Vibrational Index at Dissociation*

Estimates of the vibrational index of dissociation, v_D , have been reported for the ground states of HF and DF (48, 210). These were derived from experimental estimates of centrifugal distortion constants which are admixtures of mechanical with nonmechanical effects. Effects from excited $^1\Pi$ states were not subtracted from these constants before they were employed to obtain v_D .

These contributions were separated from the molecular constants in the previous section. The resulting constants are only *partially* deperturbed from excited states; the homogeneous contributions to the rovibrational eigenfunctions cannot be estimated. The concept of a rotationless potential in this work is of one which contains homogeneous contributions. This is an unavoidable consequence of the electronic contact transformation, the inability of the nuclear Laplacian operator to commute with Born-Oppenheimer homogeneous breakdown matrix elements, and the subsequent manipulation of the radial wave equation to overcome this problem. This means that the estimate of v_D obtained here will be for such an effective rotationless potential. The heterogeneous contributions become especially significant as the dissociation limit is approached and must be subtracted from the effective constants. The extrapolation to v_D is particularly sensitive on the constants of these higher vibrational levels and it is thus plausible that the determination of v_D could

TABLE 7.9

Calculation of $\text{HF}(X^1\Sigma^+)$ Pure Rotational Transitions from
Quantum Mechanical Rotational and Centrifugal Distortion
Constants^a

$J+1 \leftarrow J$	$\bar{\nu}_{\text{obs}}(\text{cm}^{-1})$	$\bar{\nu}_{\text{calc}}(\text{cm}^{-1})$	$\Delta\bar{\nu}(\text{cm}^{-1})$
1 0	41.110 983 2(30)	41.110 979 1	0.000 004 1
2 1	82.171 117 9(60)	82.171 112 8	0.000 005 1
3 2	123.129 670 3(90)	123.129 673 6	-0.000 003 3
4 3	163.936 164 5(120)	163.936 168 9	-0.000 004 4
5 4	204.540 45(20)	204.540 46	-0.000 01
6 5	244.892 83(20)	244.892 86	-0.000 03
7 6	284.944 44(30)	284.944 28	0.000 16

^a $\bar{\nu}_{\text{obs}}$ are taken from Ref. (142) with precision estimates in parentheses. $\bar{\nu}_{\text{calc}}$ are line positions calculated on the basis of the quantum mechanical constants found in Table 7.7. The $\Delta\bar{\nu}$ are the differences $\bar{\nu}_{\text{obs}} - \bar{\nu}_{\text{calc}}$.

be significantly influenced.

The prescription described by Barwell (48) was followed to estimate v_D for the ground states of HF and DF. The equations,

$$D_v^{-1} = (v_D - v)|X_6(2)|^{-1}, \quad (7.21)$$

$$|H_v|^{-1/3} = (v_D - v)|X_6(3)|^{-1/3}, \quad (7.22)$$

$$|L_v|^{-1/5} = (v_D - v)|X_6(4)|^{-1/5}, \quad (7.23)$$

were employed to construct the plots shown in Figures 7.7 and 7.8 for HF and DF, respectively. The average extrapolated values are $v_D^{\text{HF}} = 20.4(4)$ and $v_D^{\text{DF}} = 29.2(5)$. These are not found to be significantly different from the values reported previously (48, 210).

The value quoted by Barwell (48), $v_D^{\text{HF}} = 20.9(5)$, suggests the possible existence of vibrational level $v = 21$, whereas the present estimate casts doubt on this. In fact, even vibrational level $v = 20$ is not predicted unequivocally to exist from the present estimate. In preliminary stages of the Hamiltonian correction analysis an attempt was made to assign the most probable Franck-Condon transitions to $v'' = 20$ on the HF emission plates (87). No definite assignments could be made. The final results from this work predict that, if $v'' = 20$ in fact exists, it must extend so far into the long-range region that the Franck-Condon overlap with the most populated $B^1\Sigma^+$ ($v' = 0-3$) levels is very small. An additional problem is apparent from the observation that under discharge excitation conditions, the rotational level populations shift to higher J . Since the predicted maximum value of J in a $v' - 20$ band is approximately 5, it is highly unlikely that these transitions would be observed in discharge spectra.

Figure 7.7

Estimation of v_D for $\text{HF}(X^1\Sigma^+)$. The plots according to Eqs. (7.21-7.23) give an average value $v_D = 20.4 \pm 0.4$.

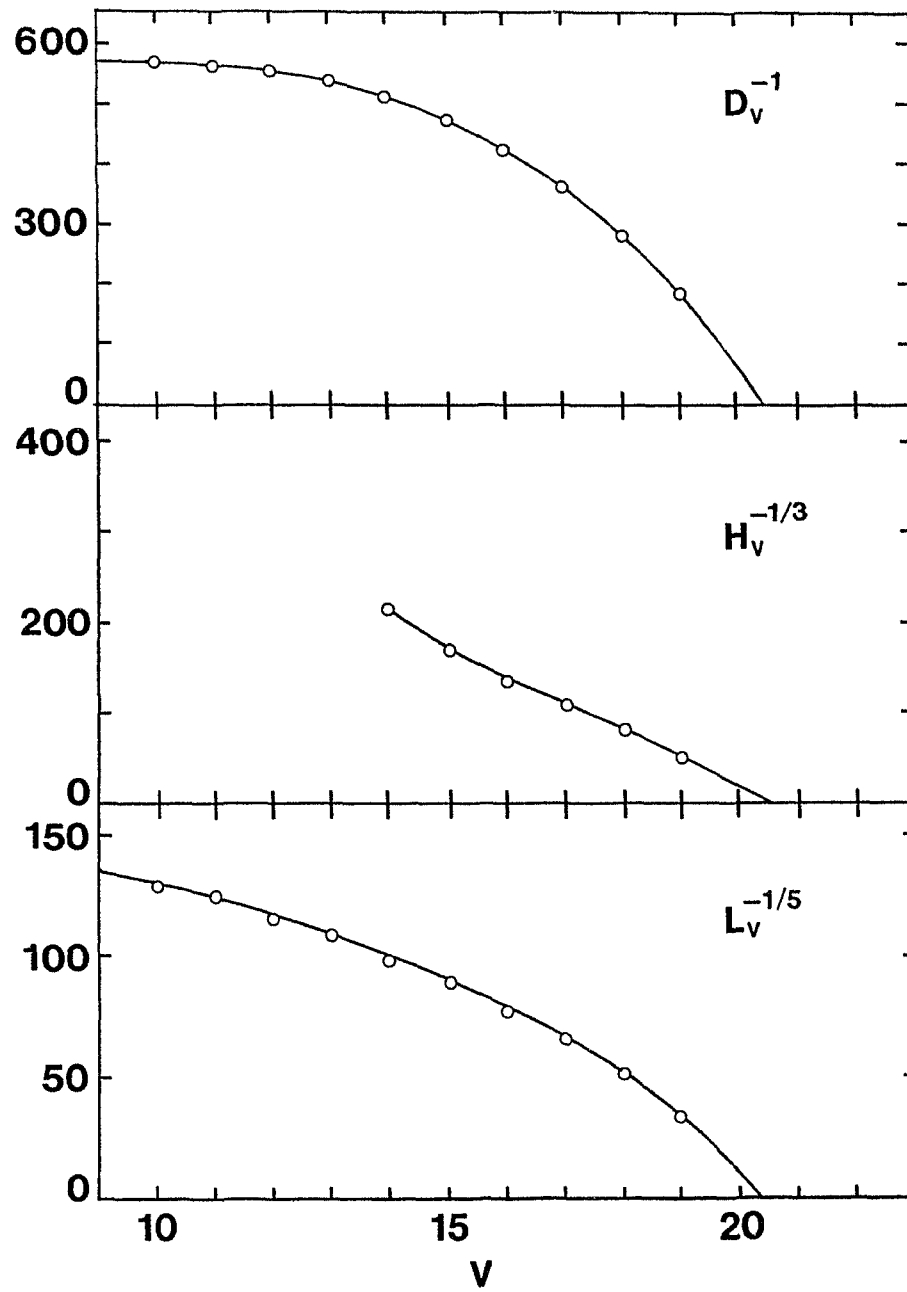


Figure 7.7

Figure 7.8

Estimation of v_D for $DF(X^1\Sigma^+)$. The plots according to Eqs. (7.21-7.23) give an average value $v_D = 29.2 \pm 0.5$.

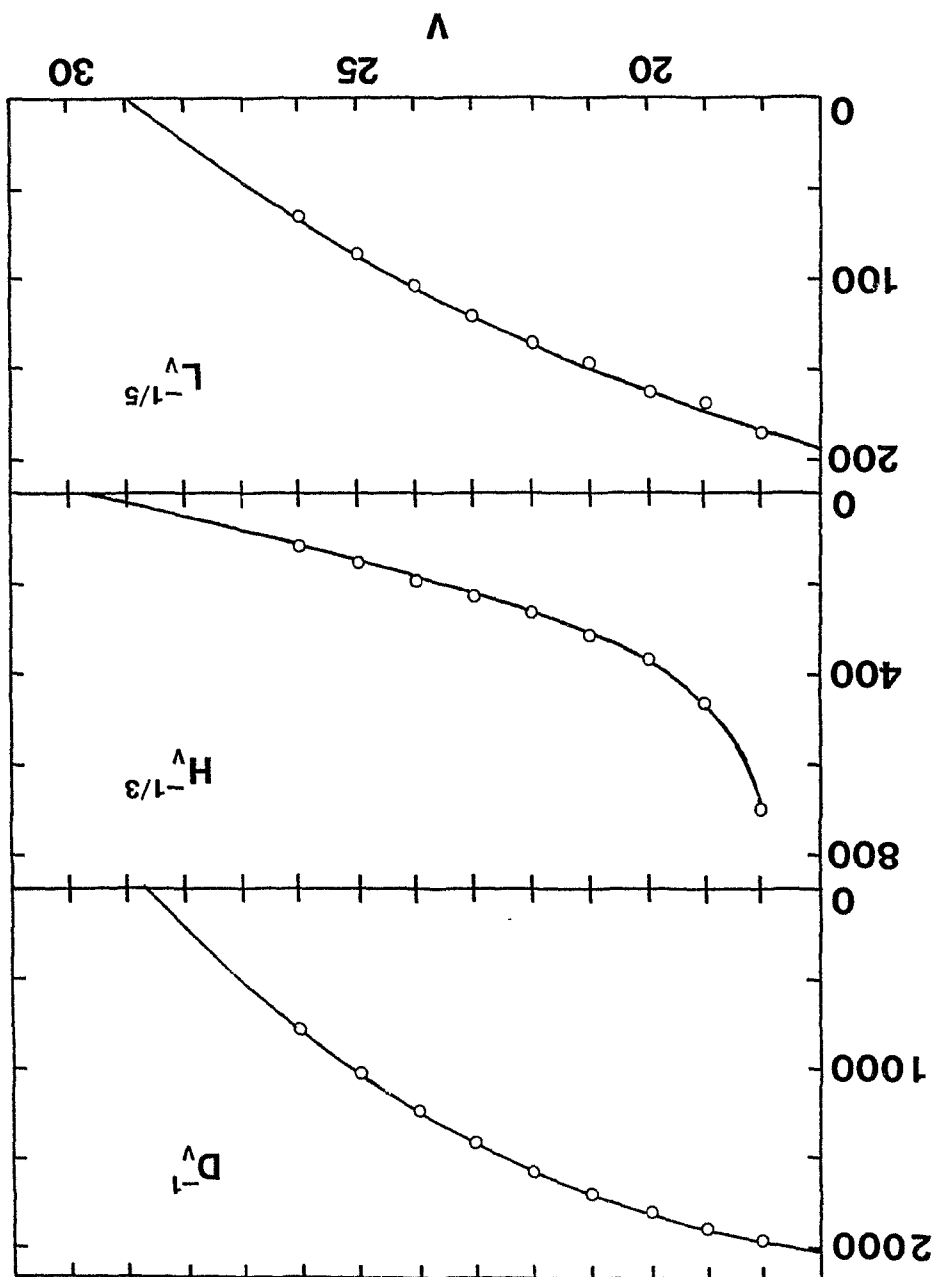


Figure 7.8

The v_D estimate for DF predicts with confidence the existence of level $v'' = 27$. The search for lines of the 6-27 band, which has the largest $v'' = 27$ calculated J -dependent Franck-Condon factors, resulted in several promising lines. These satisfied the known $v' = 6$ combination differences but no additional $v'' = 27$ bands could be found to confirm the lower state combination differences. The assignments for the 6-27 band, listed in Table 7.10, thus remain tentative. The position of $v'' = 27$ with respect to the potential minimum is nevertheless predicted at $G_{27} = 49\,203 \pm 1\text{ cm}^{-1}$, a mere 135 cm^{-1} away from the estimated dissociation limit. Owing to the uncertainty in the assignments, however, this band was not included in the Hamiltonian correction analysis.

7.3.7 Tritium Fluoride

The combined treatment of HF and DF spectral data has resulted in functions $U_{X/B}^H(R)$ and $q_X(R)$. These can be employed to construct synthetic Hamiltonian operators for TF. The rotationless potential function for TF is given by,

$$U^{\text{TF}}(R) = (1 + \mathcal{M}) U^{\text{HF}}(R) - \mathcal{M} U^{\text{DF}}(R), \quad (7.24)$$

where \mathcal{M} has been given previously by Eq. (6.38). The $q(R)$ function for TF is found from,

$$q^{\text{TF}}(R) = (M_H/M_T) q^{\text{HF}}(R). \quad (7.25)$$

The only experimental information available for TF consists of relatively low resolution spectrographic data for the fundamental and first-overtone bands in the infrared (211). These line positions could not be predicted satisfactorily from (simple) mass-transformed molecular constants for HF and

TABLE 7.10

Tentative Rotational Assignments (cm^{-1}) for the 6-27 Band
of the $B - X$ System of Deuterium Fluoride

J	$P(J)$	$R(J)$
2	40 655.736	40 676.334
3	40 652.802	40 681.735
4	40 650.587	40 687.800
5	40 649.227	40 694.635
6		40 703.177
7		40 712.899
8		40 724.526

DF. Part of the reason for this inconsistency is due to semiclassical and Born-Oppenheimer breakdown errors, but even when such effects were considered (190), there was a residual disagreement. This implies that unreliable calibration standards are at least partly responsible. Additional evidence for the lack of reliability in the absolute line positions is provided by the anomaly in the sign of the constant β_e and the apparent inaccuracy in the reported value of R_e . Coxon and Ogilvie (190) excluded TF data in determining isotopically invariant parameters U_{kl} because of a clear inconsistency.

It was decided to repeat the analysis of the TF data in order to obtain estimates for the parameters which have a full statistical significance. Although the method of least-squares was employed in Ref. (211), a merge of separately fitted constants could not be undertaken. In the present work, the two bands were fitted individually and the constants were merged together to provide the best set of nonredundant constants for TF($v'' = 0-2$). The data were fitted with a merge standard deviation of $\hat{\sigma}_M = 2.7$, which is reasonable for just two degrees of freedom. The merged parameters and error estimates are listed in Table 7.11.

When the quantum mechanical eigenvalues of the present synthetic TF operators were employed to calculate the 1-0 and 2-0 rotational transitions, it was found that there was a smooth wavelength dependent deviation from the experimental spectral lines of the fundamental band, and a constant ($\approx 0.4 \text{ cm}^{-1}$) discrepancy from the experimental first-overtone transitions. A resolution of this disagreement appears to be almost certainly in favour of the present results; however, new, more highly resolved spectra for TF are required to make an unequivocal statement. The quantum mechanical molecular

TABLE 7.11

Merged Molecular Constants (cm^{-1}) for $\text{TF}(X^1\Sigma^+)$

Constant	Estimate	Standard Error
B_0	7.60598	4.68×10^{-3}
B_1	7.43385	4.52×10^{-3}
B_2	7.26354	7.20×10^{-3}
D_0	2.7034×10^{-4}	1.81×10^{-5}
D_1	2.7821×10^{-4}	1.60×10^{-5}
D_2	2.783×10^{-4}	4.89×10^{-5}
ν_{1-0}	2443.86	0.07
ν_{2-0}	4823.80	0.12

constants of $\text{TF}(X^1\Sigma^+)$ have been calculated from the synthetic operators and are listed in Table 7.12. It would be of interest to compare these with molecular constants extracted from improved experimental spectra.

7.3.8 Equilibrium Bond Lengths

A comparison of the $X^1\Sigma^+$ equilibrium bond lengths obtained by direct fitting of the effective potentials from this work (R_e^{QM}) and those obtained from the Y_{01} Dunham coefficients (R_e^{DUN}) estimated from the results of Coxon and Ogilvie (190), is given in Table 7.13.

Agreement between the two sets of values need not necessarily be found. Dunham has shown (16) that the semiclassical estimates are slightly deficient because of the incompleteness of the JWKB approximation in his theory and, by extension, the slight inappropriateness of a $(v + 1/2)$ expansion variable in the representation of the vibrational dependence of rotational constants. This leads to a small difference between Y_{01} and B_e which is proportional to B_e^3/ω_e^2 , or dependent on μ^{-2} , predicting in turn that the difference $R_e^{\text{QM}} - R_e^{\text{DUN}}$ should be proportional to μ^{-1} . This is confirmed from the results in Table 7.13; the quantity $\mu\Delta R_e$ is shown to be nearly constant for all three isotopomers.

Since there is only one stable fluorine nuclide, it is not possible to determine the Born-Oppenheimer potential from a combined treatment of HF/DF data. It is similarly impossible to perform a fit to the expression (182),

$$R_e^{\text{DUN}} = R_e^{\text{BO}}[1 + m_e(d_{\text{H}}/M_{\text{H/D}} + d_{\text{F}}/M_{\text{F}})], \quad (7.26)$$

unless the term $d_{\text{F}}/M_{\text{F}}$ is ignored. This neglect would result in an effective R_e^{BO} value that deviates from the true value by

TABLE 7.12

Quantum Mechanical Molecular Constants (cm^{-1}) for $\text{TF}(X^1\Sigma^+)$

v	G_v	B_v	$10^4 D_v$	$10^9 H_v$	$10^{13} L_v$
0	1247.8523	7.615 075 6	2.879 776	8.181 01	-2.846 3
1	3691.7500	7.441 131 1	2.832 942	8.041 14	-2.856 8
2	6071.3004	7.269 952	2.787 456	7.907 14	-2.823 8
3	8387.6086	7.101 476	2.743 031	7.748 16	-2.870 7

TABLE 7.13

Isotopic Dependence of Equilibrium Internuclear Separations^a

Isotopomer	$R_e^{\text{QM}}(\text{\AA})$	$R_e^{\text{DUN}}(\text{\AA})$	$\mu\Delta R_e(\text{\AA})$
HF($X^1\Sigma^+$)	0.916 839 54(4)	0.916 852 3	-0.000 012 3
DF($X^1\Sigma^+$)	0.916 910 9(5)	0.916 918 0	-0.000 012 9
TF($X^1\Sigma^+$)	0.916 934 5(6)	0.916 939 9	-0.000 014 1

^a R_e^{QM} are the minima of the quantal potentials constructed in this work. R_e^{DUN} were estimated from the results of Ref. (190).

$$R_e^{\text{BO}}(\text{eff}) = R_e^{\text{BO}}(\text{true})[1 + m_e d_F/M_F], \quad (7.27)$$

estimated as a difference of the order of 10^{-5} Å. The effective value obtained here is $R_e^{\text{BO}}(\text{eff}) = 0.916\,982\,1(7)$ Å, in good agreement with the estimate of Coxon and Ogilvie (192), $R_e^{\text{BO}}(\text{eff}) = 0.916\,983\,9(23)$ Å.

The equilibrium internuclear separation for TF calculated from Eq.(7.26), $R_e^{\text{DUN}} = 0.916\,940(2)$ Å, differs from the present least-squares estimate, $R_e = 0.917\,65(32)$ Å, by more than three standard errors. This might be indicative of a problem with the data employed in the determination of the latter estimate.

7.3.9 Radiative Transition Probabilities

The effect of nonadiabatic coupling on transition probabilities has not been investigated for the hydrogen halide diatomics considered here. Recently, the vibrational-rotational dependence of Einstein coefficients for spontaneous emission has been examined by Oba *et al.* (212) for the isotopomers HF/DF and HCl/DCI. The calculations were performed with a variety of dipole moment functions derived from *ab initio* as well as experimental studies. Internuclear potentials were constructed with the RKR procedure from molecular constants found in the literature. No consideration was given to a nonadiabatic $q(R)$ function and it was thus decided to investigate here whether neglect of $q(R)$ has a serious effect on the calculated transition probabilities.

A computer program was written to employ rovibronic wavefunctions from a solution of the effective nonadiabatic radial wave equation to estimate the transition matrix elements,

$$R_{v'J'}^{v''J''} = \int_0^\infty \psi_{v''J''}(R) \mu(R) \psi_{v'J'}(R) dR, \quad (7.28)$$

required for a calculation of the Einstein coefficients for spontaneous emission. $\mu(R)$ is the electric dipole moment function normally expressed as a power series,

$$\mu(R) = \sum_i M_i (R - R_e)^i. \quad (7.29)$$

The Einstein coefficients for spontaneous emission, $A_{v'J'}^{v''J''}$, are obtained as,

$$A_{v'J'}^{v''J''} = \frac{64\pi^4}{3h} \nu^3 f(J) |R_{v'J'}^{v''J''}|^2, \quad (7.30)$$

where the rotational factor is,

$$f(J) = 1 \quad (J = 0), \quad (7.31)$$

$$f(J) = |m|/(2J + 1) \quad (J > 0), \quad (7.32)$$

with $m = J'' + 1$ for the R -branch and $m = -J$ for a P -branch line.

In preliminary work it quickly became apparent that the dipole moment function has a greater effect on the transition matrix elements than the form of the internuclear potential. Furthermore, since dipole functions are usually known with certainty only for fairly low- ν , it is necessary to extrapolate $\mu(R)$. This form of the extrapolation is *critical* and must be considered carefully. The best available experimental dipole moment is that of Sileo and Cool (156) obtained by a meticulous treatment of infrared band intensity ratios from a chemical laser emission source. The simple extrapolation on the basis of Eq. (7.29) is hopeless; large negative values for $\mu(R)$ arise at large R . A model devised here to ensure both a flexible representation in the region of R where $\mu(R)$ is known experimentally, and a

sensible extrapolation to larger and smaller R is,

$$\mu(R) = e^{-(R-R_e)^4} \sum_i D_i (R - R_e)^i. \quad (7.33)$$

Sileo and Cool's dipole moment functions for HF and DF given in Table IV of Ref. (156) were employed in a fit to this expression; results are listed in Table 7.14. D_0 of this model is equivalent to M_0 of Eq. (7.29).

Vibrational ($J = 0$) Einstein coefficients were calculated here for HF/DF. The rotational dependence of $A_{v'',J''}^{v',J'}$ is quite interesting (212) and will be investigated thoroughly in the future. It would appear, however, that on account of the uncertainty in the exact form of $\mu(R)$ at large R , the effect of $q(R)$ cannot be properly evaluated at present. The results in Tables 7.15-7.16 for HF and DF respectively, are in excellent agreement with those tabulated by Oba *et al.* (212) for lower vibrational levels of both isotopomers. For HF, however, there are clear discrepancies for $v \geq 13$. This is most likely due to the difference in the extrapolation of $\mu(R)$ beyond the region sampled by the experimental data. It is obvious from this that the transition matrix elements are more sensitive to the radial variation of $\mu(R)$ than to that of $U(R)$. Additional support for this is provided by the excellent agreement found for DF, where an RKR potential from the molecular constants of Johns and Barrow (151) was used in Ref. (156). This potential is different from our final potential since there was an earlier error (151) in the absolute vibrational terms of approximately 40 cm^{-1} ; apparently this has little effect on the matrix elements. A comprehensive interpretation of the differences between the results of this work and those of Oba and co-workers (212) is not possible since these investigators failed to define explicitly the fashion in which $\mu(R)$ was extrapolated in their study.

TABLE 7.14

Dipole Moment Coefficients for the $X^1\Sigma^+$ States of HF and DF^a

D_i	HF		DF	
	Estimate	Error	Estimate	Error
D_0	1.796115	1.4×10^{-4}	1.795866	2.8×10^{-4}
D_1	1.52116	1.1×10^{-3}	1.51979	2.0×10^{-3}
D_2	-0.14816	8.0×10^{-3}	0.05703	1.5×10^{-2}
D_3	-1.1293	2.1×10^{-2}	-1.3981	3.7×10^{-2}
D_4	1.8315	7.7×10^{-2}	1.0811	1.5×10^{-1}
D_5	1.756	2.1×10^{-1}	2.563	3.8×10^{-1}
D_6	-1.565	1.4×10^{-1}	-2.016	2.6×10^{-1}

^aParameters and their standard errors are in Debye units. The D_i are defined in Eq. (7.33). $\hat{\sigma}_{\text{HF}} = 0.00028$; $\hat{\sigma}_{\text{DF}} = 0.00056$.

TABLE 7.15

Rotationless Matrix Elements and Einstein Coefficients for HF($X^1\Sigma^+$)^a

v''	v'	$\langle v'' \mu(R) v'\rangle$	$A_{v'v''}$	v''	v'	$\langle v'' \mu(R) v'\rangle$	$A_{v'v''}$
0	1	9.8376-20	1.8868+02				
0	2	-1.2771-20	2.3816+01	1	2	1.3742-19	3.2223+02
0	3	1.8847-21	1.6386+00	1	3	-2.2863-20	6.6739+01
0	4	-3.6123-22	1.3352-01	1	4	3.9343-21	6.2352+00
0	5	7.9756-23	1.1890-02	1	5	-8.6432-22	6.6653-01
0	6	-2.0337-23	1.2488-03	1	6	2.1352-22	7.4188-02
0	7	6.2044-24	1.7242-04	1	7	-5.9389-23	9.2545-03
0	8	-2.3878-24	3.5580-05	1	8	1.9029-23	1.4065-03
0	9	1.1756-24	1.1449-05	1	9	-7.3214-24	2.8937-04
0	10	-6.9901-25	5.1696-06	1	10	3.4992-24	8.7504-05
0	11	4.6475-25	2.8272-06	1	11	-2.0291-24	3.7456-05
0	12	-3.2785-25	1.6943-06	1	12	1.3370-24	2.0042-05
0	13	2.3866-25	1.0560-06	1	13	-9.4673-25	1.2046-05
0	14	-1.7687-25	6.6800-07	1	14	6.9886-25	7.6785-06
0	15	1.3264-25	4.2430-07	1	15	-5.2997-25	5.0517-06
0	16	-1.0034-25	2.6922-07	1	16	4.0900-25	3.3707-06
0	17	7.6240-26	1.6917-07	1	17	-3.1791-25	2.2349-06
0	18	-5.7401-26	1.0241-07	1	18	2.4427-25	1.4179-06
0	19	4.0483-26	5.3279-08	1	19	-1.7479-25	7.6258-07
2	3	1.6534-19	4.0740+02				
2	4	-3.3435-20	1.2447+02	3	4	1.8632-19	4.5049+02
2	5	6.4716-21	1.4691+01	3	5	-4.4689-20	1.9333+02
2	6	-1.5967-21	1.9772+01	3	6	9.4929-21	2.7430+01
2	7	4.3565-22	2.6794+01	3	7	-2.5946-21	4.5210+00
2	8	-1.3154-22	3.9298-02	3	8	7.7466-22	7.3184-01
2	9	4.4651-23	6.6856-03	3	9	-2.5214-22	1.2438-01
2	10	-1.7417-23	1.4096-03	3	10	9.1069-23	2.3879-02
2	11	8.0738-24	3.9957-04	3	11	-3.6879-23	5.4057-03
2	12	-4.5037-24	1.5761-04	3	12	1.7051-23	1.5174-03
2	13	2.9215-24	8.1338-05	3	13	-9.1372-24	5.4947-04
2	14	-2.0830-24	4.9268-05	3	14	5.6369-24	2.5481-04
2	15	1.5602-24	3.2102-05	3	15	-3.8828-24	1.4294-04
2	16	-1.1963-24	2.1403-05	3	16	2.8719-24	8.9951-05
2	17	9.2464-25	1.4167-05	3	17	-2.2011-24	5.9204-05
2	18	-7.0701-25	8.9649-06	3	18	1.6888-24	3.8037-05
2	19	5.0429-25	4.8133-06	3	19	-1.2115-24	2.0774-05

TABLE 7.15 (Cont'd)

Rotationless Matrix Elements and Einstein Coefficients for HF($X^1\Sigma^+$)^a

v''	v'	$\langle v'' \mu(R) v' \rangle$	$A_{v'v''}$	v''	v'	$\langle v'' \mu(R) v' \rangle$	$A_{v'v''}$
4	5	2.0152-19	4.5743+02				
4	6	-5.6796-20	2.7047+02	5	6	2.1106-19	4.3366+02
4	7	1.2989-20	4.4376+01	5	7	-6.9992-20	3.5412+02
4	8	-3.8921-21	8.7687+00	5	8	1.6958-20	6.5029+01
4	9	1.2661-21	1.6798+00	5	9	-5.5195-21	1.5109+01
4	10	-4.4216-22	3.2750-01	5	10	1.9523-21	3.4088+00
4	11	1.6956-22	7.0582-02	5	11	-7.2954-22	7.5753-01
4	12	-7.1784-23	1.7378-02	5	12	2.9700-22	1.8302-01
4	13	3.3827-23	5.0382-03	5	13	-1.3246-22	4.9691-02
4	14	-1.7953-23	1.7769-03	5	14	6.4634-23	1.5330-02
4	15	1.0739-23	7.6817-04	5	15	-3.4635-23	5.4612-03
4	16	-7.1136-24	3.9438-04	5	16	2.0424-23	2.2682-03
4	17	5.0577-24	2.2634-04	5	17	-1.3121-23	1.0798-03
4	18	-3.7072-24	1.3402-04	5	18	8.9207-24	5.5651-04
4	19	2.5952-24	7.0154-05	5	19	-5.9577-24	2.6714-04
6	7	2.1434-19	3.8456+02				
6	8	-8.4585-20	4.4332+02	7	8	2.1012-19	3.1577+02
6	9	2.1424-20	8.8641+01	7	9	-1.0101-19	5.3796+02
6	10	-7.4952-21	2.3696+01	7	10	2.6482-20	1.1472+02
6	11	2.8866-21	6.3068+00	7	11	-9.8131-21	3.4219+01
6	12	-1.1540-21	1.5947+00	7	12	4.1285-21	1.0799+01
6	13	4.9732-22	4.2880-01	7	13	-1.7739-21	3.1306+00
6	14	-2.3416-22	1.2868-01	7	14	8.0911-22	9.3429-01
6	15	1.1990-22	4.3274-02	7	15	-4.0168-22	3.0823-01
6	16	-6.6476-23	1.6296-02	7	16	2.1666-22	1.1343-01
6	17	3.9717-23	6.8398-03	7	17	-1.2567-22	4.5952-02
6	18	-2.5177-23	3.1077-03	7	18	7.7153-23	1.9919-02
6	19	1.5941-23	1.3530-03	7	19	-4.7488-23	8.2871-03
8	9	1.9645-19	2.3388+02				
8	10	-1.1973-19	6.3729+02	9	10	1.7051-19	1.4775+02
8	11	3.2392-20	1.4385+02	9	11	-1.4113-19	7.3766+02
8	12	-1.2436-20	4.5735+01	9	12	3.9749-20	1.7905+02
8	13	5.7286-21	1.7159+01	9	13	-1.5315-20	5.6795+01
8	14	-2.6720-21	5.8025+00	9	14	7.6877-21	2.5022+01
8	15	1.2957-21	1.9332+00	9	15	-3.9480-21	1.0117+01
8	16	-6.7731-22	6.9632-01	9	16	2.0621-21	3.8440+00
8	17	3.8367-22	2.7724-01	9	17	-1.1384-21	1.5115+00
8	18	-2.3166-22	1.1875-01	9	18	6.7041-22	6.3274-01
8	19	1.4092-22	4.8912-02	9	19	-4.0129-22	2.5672-01

TABLE 7.15 (Cont'd)

Rotationless Matrix Elements and Einstein Coefficients for HF($X^1\Sigma^+$)^a

v''	v'	$\langle v'' \mu(R) v' \rangle$	$A_{v'v''}$	v''	v'	$\langle v'' \mu(R) v' \rangle$	$A_{v'v''}$
10	11	1.2853-19	6.9452+01				
10	12	-1.6509-19	8.2769+02	11	12	6.6006-20	1.4879+01
10	13	4.9733-20	2.2746+02	11	13	-1.9011-19	8.8135+01
10	14	-1.8522-20	6.6580+01	11	14	6.4364-20	3.0163+02
10	15	9.8923-21	3.2694+01	11	15	-2.2660-20	7.7528+01
10	16	-5.6553-21	1.6070+01	11	16	1.2109-20	3.7299+01
10	17	3.2425-21	7.1818+00	11	17	-7.6180-21	2.1599+01
10	18	-1.9076-21	3.1084+00	11	18	4.8295-21	1.1388+01
10	19	1.1274-21	1.2568+00	11	19	-2.9547-21	5.0803+00
12	13	-2.1603-20	1.2640+00				
12	14	-2.1175-19	8.5320+02	13	14	-1.3689-19	3.8916+01
12	15	8.6421-20	4.1601+02	13	15	-2.2005-19	6.9064+02
12	16	-2.9826-20	1.0025+02	13	16	1.1771-19	5.6219+02
12	17	1.4454-20	3.8428+01	13	17	-4.4983-20	1.6012+02
12	18	-9.2297-21	2.2003+01	13	18	1.9422-20	4.6436+01
12	19	6.0160-21	1.1596+01	13	19	-1.0448-20	1.7661+01
14	15	-2.7634-19	1.1592+02				
14	16	-1.9679-19	3.9045+02	15	16	-4.2321-19	1.8512+02
14	17	1.5277-19	6.4116+02	15	17	-1.1665-19	8.8715+01
14	18	-7.4408-20	2.8016+02	15	18	1.6425-19	4.4705+02
14	19	3.4372-20	8.5849+01	15	19	-1.0583-19	3.0964+02
16	17	-5.3954-19	1.8325+02				
16	18	3.4623-20	4.3646+00	17	18	-5.6821-19	1.0213+02
16	19	9.1824-20	6.8738+01	17	19	2.0380-19	6.4091+01
18	19	-4.5986-19	2.2550+01				

^a9.8376-20 reads as 9.8376×10^{-20} .

TABLE 7.16

Rotationless Matrix Elements and Einstein Coefficients for $\text{DF}(X^1\Sigma^+)^a$

v''	v'	$\langle v'' \mu(R) v' \rangle$	$A_{v'v''}$	v''	v'	$\langle v'' \mu(R) v' \rangle$	$A_{v'v''}$
0	1	8.4216-20	5.4621+01	1	2	1.1844-19	9.8154+01
0	2	-8.4344-21	4.1794+00	1	3	-1.5224-20	1.2364+01
0	3	8.2692-22	1.2926-01	1	4	1.7514-21	5.2623-01
0	4	-1.0788-22	4.9717-03	1	5	-2.5945-22	2.6078-02
0	5	1.9344-23	2.9758-04	1	6	4.9448-23	1.7622-03
0	6	-5.9293-24	4.6039-05	1	7	-1.4944-23	2.6483-04
0	7	2.8481-24	1.6071-05	1	8	7.1886-24	9.2642-05
0	8	-1.6223-24	7.4133-06	1	9	-4.2429-24	4.5843-05
0	9	9.6484-25	3.5550-06	1	10	2.6277-24	2.3814-05
0	10	-5.8070-25	1.6813-06	1	11	-1.6434-24	1.2148-05
0	11	3.5047-25	7.7547-07	1	12	1.0351-24	6.0949-06
0	12	-2.1109-25	3.4726-07	1	13	-6.5626-25	3.0203-06
0	13	1.2686-25	1.5151-07	1	14	4.1729-25	1.4731-06
0	14	-7.6484-26	6.5316-08	1	15	-2.6558-25	7.0645-07
0	15	4.6686-26	2.8397-08	1	16	1.6991-25	3.3672-07
0	16	-2.9108-26	1.2696-08	1	17	-1.1046-25	1.6334-07
0	17	1.8655-26	5.9203-09	1	18	7.3971-26	8.2962-08
0	18	-1.2349-26	2.9110-09	1	19	-5.1494-26	4.4984-08
0	19	8.4967-27	1.5294-09	1	20	3.7258-26	2.6052-08
0	20	-6.1226-27	8.7233-10	1	21	-2.7785-26	1.5857-08
0	21	4.6431-27	5.4568-10	1	22	2.1114-26	9.9178-09
0	22	-3.6937-27	3.7204-10	1	23	-1.6186-26	6.2473-09
0	23	3.0429-27	2.6944-10	1	24	1.2429-26	3.9082-09
0	24	-2.5492-27	1.9986-10	1	25	-9.4906-27	2.3915-09
0	25	2.1257-27	1.4541-10	1	26	7.0833-27	1.3821-09
0	26	-1.7119-27	9.7624-11				
2	3	1.4375-19	1.3120+02	2	15	9.8686-25	7.3811-06
2	4	-2.2424-20	2.4327+01	2	16	-6.6516-25	3.9620-06
2	5	2.9272-21	1.3323+00	2	17	4.5265-25	2.1320-06
2	6	-4.8377-22	8.2115-02	2	18	-3.0992-25	1.1441-06
2	7	9.7998-23	6.2637-03	2	19	2.1355-25	6.1344-07
2	8	-2.9072-23	9.0630-04	2	20	-1.4868-25	3.3162-07
2	9	1.3637-23	3.0116-04	2	21	1.0524-25	1.8308-07
2	10	-8.2342-24	1.5581-04	2	22	-7.6124-26	1.0436-07
2	11	5.3314-24	8.8362-05	2	23	5.6361-26	6.1630-08
2	12	-3.4749-24	4.8892-05	2	24	-4.2594-26	3.7499-08
2	13	2.2631-24	2.6190-05	2	25	3.2537-26	2.3041-08
2	14	-1.4843-24	1.3867-05	2	26	-2.4534-26	1.3625-08

TABLE 7.16 (Cont'd)

Rotationless Matrix Elements and Einstein Coefficients for $\text{DF}(X^1\Sigma^+)^a$

v''	v'	$\langle v'' \mu(R) v' \rangle$	$A_{v'v''}$	v''	v'	$\langle v'' \mu(R) v' \rangle$	$A_{v'v''}$
3	4	1.6381-19	1.5443+02				
3	5	-3.0145-20	3.9820+01	4	5	1.7988-19	1.6853+02
3	6	4.3687-21	2.6857+00	4	6	-3.8442-20	5.8560+01
3	7	-7.9481-22	2.0044-01	4	7	6.0904-21	4.7161+00
3	8	1.7118-22	1.7266-02	4	8	-1.2084-21	4.1818-01
3	9	-5.0350-23	2.4535-03	4	9	2.7631-22	4.0566-02
3	10	2.2689-23	7.5158-04	4	10	-8.1214-23	5.7491-03
3	11	-1.3640-23	3.8498-04	4	11	3.5227-23	1.6297-03
3	12	9.1258-24	2.3281-04	4	12	-2.0807-23	8.0461-04
3	13	-6.2422-24	1.4167-04	4	13	1.4089-23	4.9759-04
3	14	4.2582-24	8.3118-05	4	14	-9.9406-24	3.2161-04
3	15	-2.8939-24	4.7161-05	4	15	7.0683-24	2.0460-04
3	16	1.9739-24	2.6365-05	4	16	-5.0172-24	1.2636-04
3	17	-1.3621-24	1.4798-05	4	17	3.5538-24	7.5986-05
3	18	9.5492-25	8.4282-06	4	18	-2.5226-24	4.4999-05
3	19	-6.7988-25	4.8756-06	4	19	1.8057-24	2.6630-05
3	20	4.9017-25	2.8517-06	4	20	-1.3105-24	1.5946-05
3	21	-3.5695-25	1.6794-06	4	21	9.6719-25	9.7314-06
3	22	2.6237-25	9.9511-07	4	22	-7.2595-25	6.0575-06
3	23	-1.9477-25	5.9407-07	4	23	5.5270-25	3.8279-06
3	24	1.4607-25	3.5761-07	4	24	-4.2506-25	2.4356-06
3	25	-1.1017-25	2.1502-07	4	25	3.2744-25	1.5339-06
3	26	8.2023-26	1.2431-07	4	26	-2.4748-25	9.1675-07
5	6	1.9244-19	1.7430+02				
5	7	-4.7364-20	8.0254+01	6	7	2.0160-19	1.7252+02
5	8	8.1075-21	7.5368+00	6	8	-5.6983-20	1.0464+02
5	9	-1.7415-21	7.8246-01	6	9	1.0441-20	1.1248+01
5	10	4.2350-22	8.5735-02	6	10	-2.4117-21	1.3484+00
5	11	-1.2528-22	1.2291-02	6	11	6.2455-22	1.6731-01
5	12	5.2179-23	3.2075-03	6	12	-1.8799-22	2.4794-02
5	13	-2.9996-23	1.4976-03	6	13	7.5451-23	5.9976-03
5	14	2.0394-23	9.3205-04	6	14	-4.1580-23	2.5684-03
5	15	-1.4682-23	6.2579-04	6	15	2.8033-23	1.5682-03
5	16	1.0733-23	4.1985-04	6	16	-2.0520-23	1.0858-03
5	17	-7.8806-24	2.7668-04	6	17	1.5387-23	7.6419-04
5	18	5.7988-24	1.7900-04	6	18	-1.1608-23	5.2994-04
5	19	-4.2778-24	1.1410-04	6	19	8.7861-24	3.6144-04
5	20	3.1692-24	7.2038-05	6	20	-6.6795-24	2.4362-04
5	21	-2.3643-24	4.5369-05	6	21	5.1066-24	1.6299-04
5	22	1.7813-24	2.8696-05	6	22	-3.9289-24	1.0856-04
5	23	-1.3572-24	1.8291-05	6	23	3.0416-24	7.2006-05
5	24	1.0448-24	1.1728-05	6	24	-2.3661-24	4.7462-05
5	25	-8.0681-25	7.4571-06	6	25	1.8382-24	3.0702-05
5	26	6.1200-25	4.5045-06	6	26	-1.3985-24	1.8727-05

TABLE 7.16 (Cont'd)

Rotationless Matrix Elements and Einstein Coefficients for $\text{DF}(X^1\Sigma^+)^a$

v''	v'	$\langle v'' \mu(R) v' \rangle$	$A_{v',v''}$	v''	v'	$\langle v'' \mu(R) v' \rangle$	$A_{v',v''}$
7	8	2.0725-19	1.6405+02				
7	9	-6.7368-20	1.3144+02	8	9	2.0910-19	1.4988+02
7	10	1.3117-20	1.5931+01	8	10	-7.8599-20	1.6035+02
7	11	-3.2381-21	2.1781+00	8	11	1.6169-20	2.1657+01
7	12	8.9354-22	3.0634-01	8	12	-4.2401-21	3.3354+00
7	13	-2.7605-22	4.7732-02	8	13	1.2486-21	5.3315-01
7	14	1.0804-22	1.0957-02	8	14	-3.9878-22	8.8581-02
7	15	-5.6764-23	4.2544-03	8	15	1.5395-22	1.9731-02
7	16	3.7273-23	2.4574-03	8	16	-7.7326-23	6.9827-03
7	17	-2.7374-23	1.7077-03	8	17	4.8877-23	3.7254-03
7	18	2.0954-23	1.2481-03	8	18	-3.5443-23	2.5144-03
7	19	-1.6231-23	9.0887-04	8	19	2.7352-23	1.8600-03
7	20	1.2614-23	6.5055-04	8	20	-2.1607-23	1.4019-03
7	21	-9.8313-24	4.5842-04	8	21	1.7202-23	1.0471-03
7	22	7.6952-24	3.1952-04	8	22	-1.3735-23	7.6936-04
7	23	-6.0518-24	2.2074-04	8	23	1.0983-23	5.5537-04
7	24	4.7755-24	1.5083-04	8	24	-8.7825-24	3.9303-04
7	25	-3.7554-24	1.0057-04	8	25	6.9780-24	2.6931-04
7	26	2.8839-24	6.2779-05	8	26	-5.4000-24	1.7157-04
9	10	2.0670-19	1.3106+02				
9	11	-9.0781-20	1.9108+02	10	11	1.9942-19	1.0877+02
9	12	1.9650-20	2.8515+01	10	12	-1.0402-19	2.2319+02
9	13	-5.4362-21	4.8772+00	10	13	2.3640-20	3.6639+01
9	14	1.7112-21	8.8862-01	10	14	-6.8442-21	6.8448+00
9	15	-5.6939-22	1.5982-01	10	15	2.3060-21	1.4247+00
9	16	2.1930-22	3.5327-02	10	16	-8.0560-22	2.8152-01
9	17	-1.0593-22	1.1523-02	10	17	3.1331-22	6.3213-02
9	18	6.4020-23	5.5973-03	10	18	-1.4711-22	1.9398-02
9	19	-4.5237-23	3.5710-03	10	19	8.4882-23	8.5478-03
9	20	3.4744-23	2.6030-03	10	20	-5.7744-23	5.0265-03
9	21	-2.7697-23	1.9858-03	10	21	4.3532-23	3.5071-03
9	22	2.2409-23	1.5210-03	10	22	-3.4599-23	2.6395-03
9	23	-1.8214-23	1.1485-03	10	23	2.8133-23	2.0239-03
9	24	1.4791-23	8.4668-04	10	24	-2.3022-23	1.5327-03
9	25	-1.1904-23	5.9988-04	10	25	1.8704-23	1.1167-03
9	26	9.3004-24	3.9176-04	10	26	-1.4739-23	7.4676-04

TABLE 7.16 (Cont'd)

Rotationless Matrix Elements and Einstein Coefficients for $DF(X^1\Sigma^+)^a$

v''	v'	$\langle v'' \mu(R) v'\rangle$	$A_{v'v''}$	v''	v'	$\langle v'' \mu(R) v'\rangle$	$A_{v'v''}$
11	12	1.8648-19	8.4441+01	12	13	1.6689-19	5.9739+01
11	13	-1.1839-19	2.5606+02	12	14	-1.3392-19	2.8859+02
11	14	2.8265-20	4.6256+01	12	15	3.3725-20	5.7801+01
11	15	-8.4811-21	9.2535+00	12	16	-1.0367-20	1.2091+01
11	16	3.0607-21	2.2018+00	12	17	4.0018-21	3.2773+00
11	17	-1.1318-21	4.8555-01	12	18	-1.5813-21	8.2109-01
11	18	4.4973-22	1.1329-01	12	19	6.5009-22	2.0394-01
11	19	-2.0803-22	3.3565-02	12	20	-3.0016-22	5.9813-02
11	20	1.1535-22	1.3578-02	12	21	1.6186-22	2.2711-02
11	21	-7.5038-23	7.2499-03	12	22	-1.0108-22	1.1077-02
11	22	5.4697-23	4.6906-03	12	23	7.0669-23	6.5247-03
11	23	-4.2653-23	3.3658-03	12	24	-5.3184-23	4.3069-03
11	24	3.4353-23	2.5033-03	12	25	4.1475-23	2.9586-03
11	25	-2.7820-23	1.8313-03	12	26	-3.2127-23	1.9440-03
11	26	2.1959-23	1.2382-03				
13	14	1.3945-19	3.6622+01	14	15	1.0281-19	1.7346+01
13	15	-1.5055-19	3.1899+02	14	16	-1.6793-19	3.4432+02
13	16	4.0335-20	7.2031+01	14	17	4.8554-20	9.0096+01
13	17	-1.2542-20	1.5345+01	14	18	-1.5098-20	1.9083+01
13	18	5.1490-21	4.6796+00	14	19	6.5101-21	6.3780+00
13	19	-2.1949-21	1.3563+00	14	20	-3.0161-21	2.1670+00
13	20	9.4832-22	3.6946-01	14	21	1.3938-21	6.6924-01
13	21	-4.4394-22	1.1047-01	14	22	-6.7517-22	2.1207-01
13	22	2.3584-22	4.0323-02	14	23	3.5979-22	7.6930-02
13	23	-1.4267-22	1.8247-02	14	24	-2.1373-22	3.3079-02
13	24	9.5910-23	9.8045-03	14	25	1.3902-22	1.6344-02
13	25	-6.9072-23	5.8308-03	14	26	-9.5025-23	8.5641-03
13	26	5.0837-23	3.4965-03				
15	16	5.5534-20	4.3701+00	16	17	-3.7243-21	1.6784-02
15	17	-1.8531-19	3.6011+02	16	18	-2.0125-19	3.6019+02
15	18	5.9023-20	1.1363+02	16	19	7.2574-20	1.4455+02
15	19	-1.8243-20	2.3608+01	16	20	-2.2443-20	2.9792+01
15	20	8.0795-21	8.2555+00	16	21	9.8687-21	1.0160+01
15	21	-4.0785-21	3.2975+00	16	22	-5.3748-21	4.6656+00
15	22	2.0516-21	1.1931+00	16	23	2.9848-21	2.0269+00
15	23	-1.0530-21	4.1874-01	16	24	-1.6653-21	8.2557-01
15	24	5.7659-22	1.5780-01	16	25	9.6252-22	3.3920-01
15	25	-3.4277-22	6.6626-02	16	26	-5.8249-22	1.4442-01
15	26	2.1716-22	3.0476-02				

TABLE 7.16 (Cont'd)

Rotationless Matrix Elements and Einstein Coefficients for $\text{DF}(X^1\Sigma^+)^a$

v''	v'	$\langle v'' \mu(R) v' \rangle$	$A_{v'v''}$	v''	v'	$\langle v'' \mu(R) v' \rangle$	$A_{v'v''}$
17	18	-7.5901-20	5.8694+00	18	19	-1.6092-19	2.1820+01
17	19	-2.1317-19	3.3734+02	18	20	-2.1692-19	2.8572+02
17	20	9.0054-20	1.8393+02	18	21	1.1189-19	2.2922+02
17	21	-2.8643-20	3.9631+01	18	22	-3.8507-20	5.6948+01
17	22	1.2039-20	1.2180+01	18	23	1.5254-20	1.5261+01
17	23	-6.8333-21	5.9748+00	18	24	-8.4249-21	6.9332+00
17	24	4.1864-21	3.0970+00	18	25	5.4811-21	3.9433+00
17	25	-2.5784-21	1.5004+00	18	26	-3.6497-21	2.1568+00
17	26	1.5988-21	6.8801-01				
19	20	-2.5679-19	4.4915+01	20	21	-3.5836-19	6.8588+01
19	21	-2.0626-19	2.0579+02	20	22	-1.7298-19	1.1132+02
19	22	1.3695-19	2.6893+02	20	23	1.6036-19	2.7700+02
19	23	-5.4480-20	8.7429+01	20	24	-7.8642-20	1.3302+02
19	24	2.1414-20	2.2497+01	20	25	3.4393-20	4.0895+01
19	25	-1.0724-20	8.1454+00	20	26	-1.6428-20	1.2868+01
19	26	6.6620-21	4.0604+00				
21	22	-4.5572-19	8.3531+01	22	23	-5.3354-19	8.1472+01
21	23	-1.0838-19	3.2035+01	22	24	-8.1163-21	1.2303-01
21	24	1.7021-19	2.2137+02	22	25	1.4509-19	1.0493+02
21	25	-1.0811-19	1.7113+02	22	26	-1.2422-19	1.3818+02
21	26	5.7684-20	7.4203+01				
23	24	-5.7243-19	6.1481+01	24	25	-5.5489-19	3.3356+01
23	25	1.1756-19	1.5961+01	24	26	2.3107-19	3.2224+01
23	26	6.1870-20	1.0904+01				
25	26	-4.7315-19	1.1191+01				

^a8.4216-20 reads as 8.4216×10^{-20} .

Table 7.17 lists the averages $\langle \psi_v | \mu(R) | \psi_v \rangle$ found in the present work and compares them to the results of Sileo and Cool (156), as well as to those of Huffaker (108) for HF.

A low sensitivity to the potential form is found for the DF(B - X) Franck-Condon factors also. An extensive calculation including the rotational dependence has been performed here; the results are listed in Table 7.18. The effect of $q(R)$ on the radial wavefunctions has been considered explicitly in the present calculation. The factors are not significantly different when $q(R)$ is neglected in the calculation.

TABLE 7.17

Electric Dipole Moment (D) for the Ground States of HF and DF

v	Present work		Sileo and Cool ^a		Huffaker ^b
	HF	DF	HF	DF	HF
0	1.823	1.817	1.819	1.814	1.819
1	1.869	1.852	1.865	1.848	1.865
2	1.913	1.885	1.909	1.882	1.907
3	1.956	1.918	1.953	1.915	1.953
4	1.997	1.950	1.994	1.947	1.994
5	2.035	1.981	2.032	1.977	2.032
6	2.069	2.009	2.066	2.006	2.066
7	2.096	2.035	2.094	2.032	2.094
8	2.115	2.058	2.113	2.056	2.113
9	2.122	2.078	2.121	2.075	2.122
10	2.112	2.093		2.090	2.113
11	2.079	2.102		2.100	2.093
12	2.013	2.103		2.102	2.047
13	1.905	2.096			1.973
14	1.746	2.078			1.866
15	1.531	2.046			1.720
16	1.268	1.998			1.528
17	0.980	1.930			1.281
18	0.698	1.839			0.971
19	0.412	1.724			0.587
20		1.582			
21		1.415			
22		1.229			
23		1.034			
24		0.841			
25		0.656			
26		0.467			

^aRef. (156); ^bRef. (108).

TABLE 7.18

A Calculation of the Rotational Dependence of Franck-Condon Factors
for the $B^1\Sigma^+ - X^1\Sigma^+$ Band System of DF^a

v''	J	$v'=0$	$v'=1$	$v'=2$	$v'=3$	$v'=4$	$v'=5$	$v'=6$	$v'=7$
9	0	9.69-9	1.77-7	1.63-6	1.00-5	4.65-5	1.73-4	5.33-4	1.41-3
	6	1.04-8	1.89-7	1.72-6	1.05-5	4.83-5	1.78-4	5.46-4	1.43-3
	12	1.28-8	2.26-7	2.01-6	1.20-5	5.39-5	1.95-4	5.85-4	1.51-3
	18	1.83-8	3.09-7	2.64-6	1.52-5	6.57-5	2.29-4	6.68-4	1.67-3
	24	3.11-8	4.95-7	3.99-6	2.17-5	8.96-5	2.98-4	8.32-4	2.00-3
	30	6.51-8	9.58-7	7.18-6	3.64-5	1.41-4	4.40-4	1.16-3	2.63-3
	36	1.74-7	2.32-6	1.58-5	7.36-5	2.61-4	7.55-4	1.84-3	3.91-3
	42	6.21-7	7.30-6	4.42-5	1.84-4	5.88-4	1.54-3	3.42-3	6.63-3
	50	5.69-6	5.34-5	2.63-4	8.97-4	2.38-3	5.22-3	9.82-3	1.62-2
	56	4.75-5	3.52-4	1.39-3	3.86-3	8.45-3	1.54-2	2.43-2	3.37-2
10	0	9.40-8	1.52-6	1.23-5	6.65-5	2.70-4	8.76-4	2.36-3	5.38-3
	6	1.02-7	1.62-6	1.30-5	6.98-5	2.81-4	9.05-4	2.42-3	5.49-3
	12	1.26-7	1.96-6	1.53-5	8.01-5	3.15-4	9.94-4	2.60-3	5.80-3
	18	1.82-7	2.70-6	2.02-5	1.02-4	3.86-4	1.18-3	2.98-3	6.45-3
	24	3.14-7	4.38-6	3.09-5	1.47-4	5.28-4	1.53-3	3.70-3	7.67-3
	30	6.69-7	8.56-6	5.58-5	2.46-4	8.24-4	2.23-3	5.07-3	9.90-3
	36	1.81-6	2.08-5	1.22-4	4.90-4	1.50-3	3.72-3	7.77-3	1.40-2
	42	6.49-6	6.48-5	3.34-4	1.18-3	3.21-3	7.12-3	1.34-2	2.18-2
	50	5.90-5	4.54-4	1.84-3	5.18-3	1.13-2	2.04-2	3.13-2	4.17-2
	56	4.84-4	2.78-3	8.60-3	1.88-2	3.24-2	4.60-2	5.57-2	5.81-2
11	0	7.98-7	1.12-5	7.89-5	3.70-4	1.30-3	3.63-3	8.33-3	1.61-2
	6	8.64-7	1.20-5	8.37-5	3.89-4	1.35-3	3.75-3	8.54-3	1.64-2
	12	1.08-6	1.46-5	9.87-5	4.48-4	1.52-3	4.11-3	9.19-3	1.73-2
	18	1.58-6	2.03-5	1.31-4	5.70-4	1.86-3	4.85-3	1.05-2	1.91-2
	24	2.75-6	3.30-5	2.00-4	8.19-4	2.52-3	6.22-3	1.27-2	2.22-2
	30	5.91-6	6.46-5	3.59-4	1.35-3	3.85-3	8.81-3	1.68-2	2.73-2
	36	1.61-5	1.56-4	7.72-4	2.61-3	6.69-3	1.39-2	2.41-2	3.56-2
	42	5.72-5	4.73-4	2.02-3	5.90-3	1.32-2	2.40-2	3.65-2	4.73-2
	50	5.06-4	3.06-3	9.79-3	2.17-2	3.72-2	5.17-2	6.00-2	5.84-2
	56	3.98-3	1.64-2	3.71-2	5.89-2	7.23-2	7.10-2	5.57-2	3.35-2
12	0	5.93-6	7.14-5	4.30-4	1.72-3	5.12-3	1.20-2	2.29-2	3.62-2
	6	6.43-6	7.66-5	4.56-4	1.81-3	5.33-3	1.24-2	2.34-2	3.67-2
	12	8.07-6	9.31-5	5.39-4	2.08-3	5.95-3	1.35-2	2.49-2	3.83-2
	18	1.19-5	1.30-4	7.15-4	2.63-3	7.21-3	1.57-2	2.78-2	4.11-2
	24	2.08-5	2.11-4	1.08-3	3.71-3	9.55-3	1.95-2	3.26-2	4.54-2
	30	4.47-5	4.09-4	1.90-3	5.94-3	1.40-2	2.61-2	4.01-2	5.13-2
	36	1.21-4	9.63-4	3.92-3	1.08-2	2.25-2	3.73-2	5.07-2	5.72-2
	42	4.24-4	2.79-3	9.51-3	2.21-2	3.87-2	5.42-2	6.17-2	5.71-2
	50	3.55-3	1.58-2	3.73-2	6.05-2	7.38-2	6.98-2	5.04-2	2.56-2

TABLE 7.18 (Cont'd)

A Calculation of the Rotational Dependence of Franck-Condon Factors
for the $B^1\Sigma^+ - X^1\Sigma^+$ Band System of DF

v''	J	$v'=0$	$v'=1$	$v'=2$	$v'=3$	$v'=4$	$v'=5$	$v'=6$	$v'=7$
13	0	3.85-5	3.90-4	1.97-3	6.57-3	1.61-2	3.06-2	4.64-2	5.64-2
	6	4.18-5	4.19-4	2.09-3	6.88-3	1.67-2	3.14-2	4.71-2	5.67-2
	12	5.26-5	5.09-4	2.46-3	7.84-3	1.84-2	3.37-2	4.92-2	5.74-2
	18	7.74-5	7.06-4	3.22-3	9.76-3	2.18-2	3.79-2	5.26-2	5.84-2
	24	1.36-4	1.14-3	4.78-3	1.34-2	2.77-2	4.47-2	5.73-2	5.86-2
	30	2.90-4	2.15-3	8.09-3	2.03-2	3.76-2	5.43-2	6.21-2	5.57-2
	36	7.71-4	4.86-3	1.56-2	3.34-2	5.32-2	6.54-2	6.24-2	4.49-2
	42	2.61-3	1.30-2	3.34-2	5.74-2	7.25-2	6.89-2	4.81-2	2.17-2
	50	1.99-2	5.86-2	9.07-2	9.20-2	6.29-2	2.55-2	2.71-3	2.39-3
14	0	2.18-4	1.82-3	7.48-3	2.01-2	3.89-2	5.68-2	6.30-2	5.13-2
	6	2.37-4	1.94-3	7.90-3	2.09-2	4.00-2	5.77-2	6.30-2	5.06-2
	12	2.97-4	2.35-3	9.19-3	2.35-2	4.32-2	6.00-2	6.31-2	4.82-2
	18	4.36-4	3.22-3	1.18-2	2.83-2	4.90-2	6.37-2	6.22-2	4.33-2
	24	7.59-4	5.07-3	1.69-2	3.68-2	5.77-2	6.77-2	5.86-2	3.46-2
	30	1.59-3	9.23-3	2.68-2	5.07-2	6.89-2	6.87-2	4.85-2	2.07-2
	36	4.10-3	1.94-2	4.60-2	7.12-2	7.74-2	5.90-2	2.80-2	4.66-3
	42	1.31-2	4.56-2	8.01-2	8.97-2	6.62-2	2.85-2	3.24-3	2.61-3
	50	8.46-2	1.34-1	1.04-1	3.99-2	2.33-3	7.18-3	2.86-2	3.76-2
15	0	1.07-3	7.08-3	2.29-2	4.71-2	6.73-2	6.78-2	4.52-2	1.54-2
	6	1.16-3	7.55-3	2.40-2	4.86-2	6.83-2	6.75-2	4.38-2	1.41-2
	12	1.45-3	9.02-3	2.74-2	5.30-2	7.09-2	6.61-2	3.97-2	1.08-2
	18	2.11-3	1.21-2	3.40-2	6.06-2	7.44-2	6.24-2	3.20-2	5.71-3
	24	3.60-3	1.83-2	4.56-2	7.17-2	7.64-2	5.35-2	2.00-2	8.62-4
	30	7.34-3	3.12-2	6.49-2	8.42-2	7.12-2	3.56-2	5.84-3	1.59-3
	36	1.79-2	5.83-2	9.21-2	8.74-2	4.83-2	1.01-2	7.21-4	1.64-2
	42	5.20-2	1.10-1	1.09-1	5.55-2	8.33-3	2.75-3	2.40-2	3.79-2
16	0	4.48-3	2.26-2	5.41-2	7.85-2	7.23-2	3.78-2	5.86-3	2.42-3
	6	4.85-3	2.40-2	5.62-2	7.98-2	7.14-2	3.58-2	4.80-3	3.14-3
	12	6.02-3	2.81-2	6.21-2	8.27-2	6.84-2	3.00-2	2.33-3	5.64-3
	18	8.61-3	3.64-2	7.25-2	8.60-2	6.11-2	2.02-2	1.10-4	1.14-2
	24	1.43-2	5.17-2	8.75-2	8.57-2	4.62-2	7.64-3	2.27-3	2.21-2
	30	2.77-2	7.88-2	1.03-1	7.26-2	2.16-2	8.38-7	1.55-2	3.57-2
	36	6.21-2	1.20-1	1.01-1	3.54-2	4.03-4	1.50-2	3.85-2	3.62-2
	42	1.55-1	1.45-1	4.39-2	7.61-6	2.56-2	4.74-2	3.22-2	6.65-3
17	0	1.59-2	5.71-2	9.18-2	7.95-2	3.16-2	8.22-4	1.19-2	3.49-2
	6	1.72-2	5.99-2	9.36-2	7.81-2	2.90-2	3.67-4	1.36-2	3.60-2
	12	2.10-2	6.80-2	9.78-2	7.32-2	2.18-2	5.98-5	1.87-2	3.83-2
	18	2.93-2	8.29-2	1.02-1	6.20-2	1.09-2	2.95-3	2.80-2	3.97-2
	24	4.65-2	1.06-1	1.01-1	4.05-2	9.66-4	1.45-2	3.96-2	3.50-2
	30	8.34-2	1.33-1	8.03-2	1.09-2	6.24-3	3.71-2	4.23-2	1.76-2
	36	1.63-1	1.36-1	2.67-2	4.02-3	4.11-2	4.72-2	1.75-2	2.57-5
	42	3.12-1	4.40-2	1.03-2	6.05-2	4.47-2	5.89-3	4.54-3	2.45-2

TABLE 7.18 (Cont'd)

A Calculation of the Rotational Dependence of Franck-Condon Factors
for the $B^1\Sigma^+ - X^1\Sigma^+$ Band System of DF

v''	J	$v'=0$	$v'=1$	$v'=2$	$v'=3$	$v'=4$	$v'=5$	$v'=6$	$v'=7$
18	0	4.71-2	1.07-1	9.55-2	2.95-2	1.92-4	2.57-2	4.38-2	2.38-2
	6	5.03-2	1.10-1	9.38-2	2.62-2	6.59-4	2.82-2	4.38-2	2.18-2
	12	6.02-2	1.19-1	8.76-2	1.75-2	3.43-3	3.49-2	4.26-2	1.61-2
	24	1.19-1	1.37-1	4.30-2	3.55-4	3.35-2	4.90-2	2.05-2	7.50-5
	30	1.90-1	1.15-1	6.08-3	2.27-2	5.61-2	3.11-2	1.31-3	9.78-3
	36	2.98-1	3.35-2	2.00-2	6.78-2	3.34-2	3.02-4	1.56-2	3.27-2
19	0	1.12-1	1.32-1	3.69-2	1.93-3	4.10-2	4.59-2	1.06-2	2.38-3
	6	1.18-1	1.31-1	3.24-2	3.43-3	4.40-2	4.42-2	8.39-3	3.62-3
	12	1.37-1	1.28-1	2.05-2	9.74-3	5.11-2	3.81-2	3.37-3	8.23-3
	24	2.29-1	7.31-2	2.49-3	5.58-2	4.76-2	4.50-3	9.29-3	3.23-2
	30	3.01-1	1.10-2	4.62-2	6.77-2	1.15-2	6.63-3	3.40-2	2.76-2
	36	3.19-1	5.98-2	8.75-2	1.02-2	1.50-2	4.16-2	2.07-2	1.70-4
20	0	2.06-1	7.52-2	2.33-3	5.73-2	4.39-2	1.52-3	1.64-2	3.55-2
	6	2.14-1	6.85-2	4.50-3	6.08-2	4.03-2	5.38-4	1.94-2	3.55-2
	12	2.36-1	4.91-2	1.41-2	6.79-2	2.92-2	4.78-4	2.75-2	3.31-2
	24	3.00-1	9.18-4	8.39-2	4.09-2	7.09-4	3.38-2	3.42-2	4.62-3
	30	2.81-1	9.64-2	7.68-2	2.33-4	3.61-2	3.89-2	4.56-3	6.68-3
21	0	2.74-1	3.16-4	7.72-2	4.43-2	7.08-4	3.66-2	3.21-2	1.61-3
	6	2.77-1	6.80-5	8.29-2	3.86-2	2.19-3	3.97-2	2.91-2	5.76-4
	12	2.81-1	7.09-3	9.40-2	2.24-2	1.03-2	4.53-2	1.93-2	4.84-4
	24	2.24-1	1.79-1	3.64-2	1.47-2	5.51-2	1.34-2	4.42-3	2.83-2
	30	1.03-1	3.63-1	3.02-2	5.35-2	1.69-2	8.94-3	3.12-2	1.60-2
22	0	2.32-1	1.10-1	6.09-2	7.06-3	5.58-2	1.68-2	4.60-3	3.10-2
	6	2.24-1	1.30-1	5.13-2	1.20-2	5.67-2	1.22-2	7.51-3	3.22-2
	12	1.98-1	1.88-1	2.41-2	3.04-2	5.27-2	2.63-3	1.78-2	3.18-2
	18	1.43-1	2.85-1	1.89-4	6.13-2	2.83-2	3.62-3	3.36-2	1.92-2
	24	6.00-2	3.39-1	1.10-1	4.06-2	1.30-5	3.62-2	2.36-2	1.90-4
23	0	9.73-2	3.02-1	2.54-2	7.07-2	3.05-3	2.88-2	3.16-2	8.02-4
	6	8.59-2	3.08-1	4.24-2	6.57-2	7.07-4	3.41-2	2.75-2	3.80-5
	12	5.64-2	3.09-1	1.13-1	4.07-2	2.77-3	4.45-2	1.41-2	2.98-3
	18	1.93-2	2.45-1	2.81-1	2.21-4	2.32-2	3.88-2	4.08-6	1.82-2
	24	1.04-4	7.47-2	3.99-1	1.62-1	6.17-3	7.29-3	3.27-2	1.49-2
24	0	9.08-3	1.74-1	3.33-1	1.67-2	4.11-2	1.33-2	1.38-2	2.81-2
	6	5.91-3	1.50-1	3.54-1	3.66-2	3.75-2	8.20-3	1.98-2	2.57-2
	12	9.33-4	8.60-2	3.73-1	1.34-1	1.60-2	4.85-4	3.65-2	1.38-2
	18	6.15-4	1.20-2	2.53-1	3.67-1	1.56-2	1.28-3	4.95-2	4.06-4

TABLE 7.18 (Cont'd)

A Calculation of the Rotational Dependence of Franck-Condon Factors
for the $B^1\Sigma^+ - X^1\Sigma^+$ Band System of DF

v''	J	$v'=0$	$v'=1$	$v'=2$	$v'=3$	$v'=4$	$v'=5$	$v'=6$	$v'=7$
25	0	6.13-4	3.57-3	1.68-1	4.05-1	6.44-2	6.97-3	2.36-2	1.59-2
	6	8.47-4	7.26-4	1.28-1	4.16-1	1.08-1	3.25-3	1.95-2	2.50-2
	12	1.06-3	2.32-3	3.67-2	3.59-1	2.67-1	4.63-3	1.28-2	5.65-2
	18	2.12-4	9.35-3	7.69-3	7.86-2	3.75-1	1.36-1	2.61-2	1.11-1
26	0	7.91-5	5.87-3	9.72-3	4.16-2	3.65-1	2.15-1	1.63-2	6.15-2
	6	1.69-5	4.95-3	1.71-2	1.28-2	3.03-1	2.64-1	3.04-2	6.32-2
	12	5.87-5	1.19-3	2.66-2	1.42-2	8.72-2	2.87-1	8.94-2	6.77-2

^a9.69-9 reads as 9.69×10^{-9} .

CHAPTER 8

REVIEW OF HAMILTONIAN CORRECTION APPROACH

8.1 Comparison with a Conventional Rotational Analysis

8.1.1 Physical Significance

The approach of reducing a set of spectroscopic line positions to molecular constants often yields parameters that lack a strict physical significance. Before proceeding any further, it is important to define what is meant by "physical significance".

Our understanding of a molecular system can be described easily in qualitative terms, often involving such classically influenced terminology as "electron cloud", "internuclear bond", "angles", etc. A quantitative description is obtained by adopting a theoretical or mathematical model, which approaches the physical reality of the system to a varying extent. What is meant by physical significance here, then, is the ability of derived parameters obtained empirically to correspond to those predicted by a formal theoretical treatment of the assumed model. The ability of such derived parameters to describe the physical reality of a system can only be as good as, and is often worse than, that of the theoretical model.

Returning to the subject under discussion, finite measurement errors and J ranges limit the number of higher-order centrifugal constants that can be determined significantly, in the statistical sense. Furthermore, high correlations among parameters and truncation of the power series force the constants that are determined to absorb unphysical contributions. As a

result, inversion of such diatomic constants to the potentials governing nuclear motion will result in functions having reduced physical meaning.

The Hamiltonian Correction Approach (HCA) employed here goes a step further furnishing functions that have improved physical significance. The corrected operators are fully quantum mechanically consistent with the observables from which they were derived. Moreover, an extension of the HCA has been devised to evaluate quantum mechanical estimates of the molecular constants. From this effort, it has been shown conclusively for the systems studied, that considerably higher orders in $J(J + 1)$ than normally employed are in fact required to describe the data within the measurement errors for the experimentally derived constants to preserve their proper quantum mechanical meanings.

Here, it is interesting to note that with each progressive application of a contact transformation, *explicit* information is lost. For example, the theorist begins with the exact infinite block Hamiltonian of a diatomic system and applies the electronic contact transformation to obtain a perturbational expansion that operates within a single electronic state. The experimentalist applying such an effective operator to the interpretation of spectroscopic line positions obtains the total effect of all perturbing states but cannot separate the perturbation into its individual components. An example of this is found in the present work where the fitted functions $\tilde{S}_i^{(n)}(R)$ and $\tilde{R}_i^{(n)}(R)$ describe adiabatic effects and nonadiabatic coupling well but cannot provide information on the *individual* perturbations exerted by other states. A rare case where the perturbation has been decomposed into individual electronic state contributions, concerns an elegant *ab initio* study of the spin-orbit interaction in the ground state of the hydroxyl radical (213). This type of

decomposition is only possible for direct theoretical studies.

Similarly, when a vibrational contact transformation is applied to the Van Vleck transformed operator, the perturbational coefficients B_v , D_v , etc., obtained experimentally on the basis of the associated model, cannot yield information explicitly on nonadiabatic perturbations, even though these are contained implicitly in such estimates. It is clear from these considerations that although the approach of molecular constants can provide a satisfactory description of the observables, it fails to achieve a separation of mechanical and nonmechanical contributions to the energy levels. Due to this unpreventable loss of information, the HCA, which also achieves an equally satisfactory description of the observables, is to be preferred.

An additional benefit of the HCA is that the corrected operators are found to predict information not included in the least-squares fits, such as widths of spectral lines and line positions of isotopomers not considered explicitly in the fitting procedure. Although an analogous procedure exists, describing the isotopic variation of molecular constants and accounting fully for Born-Oppenheimer breakdown, it is found that constants obtained in this fashion fail to correspond to the formal perturbational coefficients.

8.1.2 General Fitting, Extrapolation, and Interpolation Ability

The work performed in this thesis provides a rare opportunity to compare reliably the properties of the molecular constant and Hamiltonian correction approaches. It has been demonstrated that the use of local correction functions in the HCA is of undeniable advantage. As Coxon has shown (120), the distribution of these functions is not critical as long as adjacent Gaussians are placed as to ensure sufficient overlap and smooth corrections

throughout. The results of the model testing showed that the fitted residuals actually represent the random errors quite closely, indicating that the model has a lot of flexibility and can be very accurate, not merely precise.

From the conventional rotational analyses described in Chapters 4 and 5 it became apparent that polynomial representations in $J(J + 1)$ for the rotational energy do not have satisfactory extrapolation properties; in fact, the extrapolation over a single J is often highly uncertain. On the other hand, the fit of spectroscopic lines to a *global* model improves tremendously the extrapolation to highly excited J levels. This feature of the HCA proved to be particularly helpful in rationalizing predissociation observations in the HF and DF ground states.

Another demonstration of the extrapolation properties of the HCA operators was given by the successful prediction of the $T^{35}\text{Cl}$ and $T^{37}\text{Cl}$ microwave transitions. It must be noted that the levels involved in these transitions lie *below* the lowest levels of HCl and DCl employed in the least-squares fit so that their prediction is essentially an extrapolation.

The matter of interpolation was settled quite decidedly from the results of the model calculations in Chapter 3, and also by the ability of an intermediate operator for $\text{DF}(X^1\Sigma^+)$ in Chapter 7 to provide effortlessly sound rotational assignments for intermediate ($v'' = 9-15$) vibrational levels not detected previously from a conventional analysis. The prediction of the intermediate $\text{DF}(X^1\Sigma^+)$ levels by a conventional treatment was fraught with large error.

It is concluded that the general fitting ability, extrapolation and interpolation properties of the HCA are considerably better than those of a conventional rotational analysis.

8.1.3 Stability

The stability of a fit of spectroscopic lines in accord with a power series expansion for the rotational energy in terms of $J(J + 1)$ is dependent largely on the quality of the matrix inversion method employed in the least-squares procedure. It is often found that inclusion of one more parameter than is warranted by the precision of the data results in the deterioration of the lower-order constants. Also, in the extended Dunham treatment of data from several isotopomers (*cf.* Eq. (2.47)), Watson (42) has shown that large (unphysical) values of the Δ_{kl} can be associated with accidentally small values of some U_{kl} . There are cases, then, where stability can be a problem for the conventional approach.

The stability of the HCA depends squarely on the choice and distribution of basis functions and the local weights along the radial coordinate. If, for example, a Gaussian function is placed in a region of low weighting the fit runs the risk of becoming unstable, the calculation often diverging. Additional instability can result in the extreme inner and outer regions of the fitted correction functions which can cause subsequent problems with the numerical solution of the radial wave equation. The HCA has its special types of problems but these were understood in the model testing. To quote Albritton *et al.* (57): "a devil known is better than a devil unknown even though it cannot be exorcised."

8.1.4 Compactness

A considerable amount of effort was expended in devising a method by

which initial operators could be represented by flexible analytic functions. This would not only eliminate ambiguities in the definitions of the trial operators, but also lead to more compact representations of the final functions. Such an approach was possible for HCl/DCI but could not be followed for HF/DF.

For HCl/DCI, eight Hamiltonian operators were represented by approximately 100 parameters, that is, approximately 12 parameters per operator. One ought to consider that highly precise data ($\sim 10^{-6} \text{ cm}^{-1}$) were incorporated, and that *all* the reliable data included for all four isotopomers and two electronic states could be described simultaneously. This is a testament not only to the relative compactness that can be achieved in this fashion but also the general success of the fitting procedure.

Clearly, however, a considerable amount of labour is required to reconstruct the corrected operators from the fitted parameters. This is part of the reason RKR-like numerical potentials have been tabulated. Although the interpolated potentials cannot achieve an accuracy of 10^{-6} cm^{-1} , they are far more accurate than first-order RKR potentials. For many purposes, it is not necessary to have an accuracy of 10^{-6} cm^{-1} . Thus, in the end, the HCA can be likened somewhat to the RKR procedure in compactness. This is still as good or better than the approach of constants in representing a set of line positions.

The final HCA representations must be viewed as a compromise between compactness and accuracy. Earlier efforts (119) employed global basis functions which gave more compact representations but had relatively poor flexibility properties. The local basis functions yield the desired flexibility but fail to provide as compact a representation of the radial

functions.

With regard to the representation of eigenvalues, significant advantage would be gained if energy levels could be described more compactly. The problems with fitting terms to $J(J + 1)$ power series have been explained previously. These problems are amplified with decreasing reduced mass. Therefore, efforts were directed in obtaining molecular constants which could not only represent within the measurement errors the experimental data, but also obey the same boundary conditions as the derived operators. Although this approach would lead to a 5-10 fold reduction in the parameters required to specify the energies, it was found that considerably high orders of the perturbation have to be invoked to achieve the desired consistency. The computational algorithm for this purpose has been developed only for a fifth-order energy calculation.

8.2 *Suggestions for Improved Procedures*

8.2.1 *Improved Compactness*

In keeping with the first-order perturbation determination of radial operators in numerical form, with the functions tabulated on a radial grid, it is possible to achieve, in some cases, much improved compactness. Upon reflection, the main weakness of the HCA is its relative complexity; there are simply too many variables left to intuition and much effort is required to reconstruct correction functions. On the other hand, no other method proposed so far has been able to achieve a successful simultaneous fit of data from the potential minimum to the dissociation limit for many isotopomers and more than one electronic state.

An extension of the procedure that improves the compactness in the radial function representations is suggested here. Suppose that the trial potentials can be represented by the general Dunham-type power series (214),

$$U^{(0)}(\xi_{mn}) = d_0^{mn} \xi_{mn}^2 (1 + \sum_{i=1} d_i^{mn} \xi_{mn}^i), \quad (8.1)$$

where

$$\xi_{mn} = (m + n)(R - R_e)/(mR + nR_e). \quad (8.2)$$

A correction function $\Delta U(R)$ could be modelled as,

$$\Delta U(\xi_{mn}) = \sum_{i=1} c_i^{mn} \xi_{mn}^i, \quad (8.3)$$

where a *linear* term has also been included here to take into account the probability that the adiabatic component of the correction possesses a finite slope at R_e . This correction function could then be estimated with the Hamiltonian correction approach. The final, corrected, potential would be expressed as,

$$\begin{aligned} U(\xi_{mn}) = & c_1^{mn} \xi_{mn} + (d_0^{mn} + c_2^{mn}) \xi_{mn}^2 + (d_0^{mn} d_1^{mn} + c_3^{mn}) \xi_{mn}^3 \\ & + (d_0^{mn} d_2^{mn} + c_4^{mn}) \xi_{mn}^4 + (d_0^{mn} d_3^{mn} + c_5^{mn}) \xi_{mn}^5 + \dots, \end{aligned} \quad (8.4)$$

in other words, one additional term only is generated; small corrections (c_i^{mn}) are imposed onto the known coefficients of the trial function. An iteration, should it prove necessary, would not increase the total number of parameters but simply refine already existing ones.

The effectiveness of this procedure is controlled critically by the radius of convergence of the reduced internuclear coordinate ξ_{mn} . It is not expected, for *any* choice of m and n , that the long-range region could be represented well by such an expansion. This type of model should be used with

care and only for low and intermediate vibrational levels.

8.2.2 Extension to Higher-Order Perturbation Theory

It is possible, with a proportional increase in labour, to extend the HCA to higher-order in the perturbation. First, let us examine the breakdown of first-order perturbation theory more closely.

Employing the trial potential given in Table 6.2 for the $X^1\Sigma^+$ state of HCl, as the zeroth-order function, and the model correction function $\Delta U(R)$, plotted in Fig. 3.2, as the perturbation, it is possible to calculate exactly the first-order correction,

$$E_v^{(1)} = \langle \psi_v^{(0)} | \Delta U(R) | \psi_v^{(0)} \rangle, \quad (8.5)$$

add it onto the trial eigenvalues $E_v^{(0)}$ and examine to what degree first-order perturbation theory can approach the eigenvalues $E_v^{(\text{cor})}$ of the known corrected potential. Subsequently, the perturbation is doubled, a new corrected potential and new $E_v^{(\text{cor})}$ are obtained, and the ability of first-order perturbation theory in recovering these is reexamined. The perturbation is then tripled and similar calculations are carried out.

Table 8.1 shows that as the perturbation is doubled, the discrepancies from the true exact eigenvalues are slightly more than quadrupled and when the perturbation is tripled the discrepancies are a bit over nine times the initial values. This is in accord with the expectation that the omitted second-order corrections go as the square of the expectation value (*cf.* Eq. (8.6)), and hence as the square of the perturbation. The ratios given in Table 8.1 provide general support for this argument, the small disagreement from the exact squares most likely due to third-order corrections.

TABLE 8.1

Test of First-Order Perturbation Theory^a

$\mathcal{H} = \Delta U(R)$		$\mathcal{H} = 2\Delta U(R)$		$\mathcal{H} = 3\Delta U(R)$	
v	ΔE_1	ΔE_2	$\Delta E_2/\Delta E_1$	ΔE_3	$\Delta E_3/\Delta E_1$
0	0.000 000	0.000 001	-	0.000 003	-
1	0.000 001	0.000 005	-	0.000 012	-
2	0.000 006	0.000 024	4.00	0.000 054	9.00
3	0.000 014	0.000 057	4.07	0.000 128	9.14
4	0.000 019	0.000 077	4.05	0.000 175	9.21
5	0.000 024	0.000 097	4.04	0.000 219	9.13
6	0.000 044	0.000 173	3.93	0.000 391	8.89
7	0.000 094	0.000 375	3.99	0.000 846	9.00
8	0.000 189	0.000 757	4.01	0.001 705	9.02
9	0.000 331	0.001 327	4.01	0.002 991	9.04
10	0.000 511	0.002 050	4.01	0.004 621	9.04
11	0.000 710	0.002 846	4.01	0.006 417	9.04
12	0.000 900	0.003 606	4.01	0.008 132	9.04
13	0.001 052	0.004 219	4.01	0.009 517	9.05
14	0.001 146	0.004 597	4.01	0.010 370	9.05
15	0.001 171	0.004 698	4.01	0.010 601	9.05
16	0.001 133	0.004 545	4.01	0.010 258	9.05
17	0.001 045	0.004 194	4.01	0.009 464	9.06
18	0.000 915	0.003 674	4.02	0.008 292	9.06
19	0.000 908	0.003 642	4.01	0.008 214	9.04

^aQuantities $\Delta E(\text{cm}^{-1})$ are the differences between the exact and first-order perturbation results.

In terms of the absolute magnitudes of the breakdown of first-order perturbation theory, it appears that for the most part first-order theory is sufficient. It is possible, however, to include second and higher orders of the perturbation in the Hamiltonian correction method. The correction to an eigenvalue could be modelled as,

$$\Delta E_{vJ} = \langle \psi_{vJ}^{(0)} | \Delta U(R) | \psi_{vJ}^{(0)} \rangle + \sum_{vJ \neq wK} \frac{|\langle \psi_{vJ}^{(0)} | \Delta U(R) | \psi_{wK}^{(0)} \rangle|^2}{E_{wK}^{(0)} - E_{vJ}^{(0)}}, \quad (8.6)$$

which can be simplified further by avoiding the sum-over-states and writing explicitly,

$$\Delta E_{vJ} = \langle \psi_{vJ}^{(0)} | \Delta U(R) | \psi_{vJ}^{(0)} \rangle + \langle \psi_{vJ}^{(0)} | \Delta U(R) | \psi_{vJ}^{(1)} \rangle. \quad (8.7)$$

If the perturbation is expanded as in Eq. (3.15), then we obtain,

$$\begin{aligned} \Delta E_{vJ} = & c_1 \{ \langle 0 | f_1 | 0 \rangle + \langle 0 | f_1 | 1 \rangle \} + c_2 \{ \langle 0 | f_2 | 0 \rangle + \langle 0 | f_2 | 1 \rangle \} \\ & c_3 \{ \langle 0 | f_3 | 0 \rangle + \langle 0 | f_3 | 1 \rangle \} + c_4 \{ \langle 0 | f_4 | 0 \rangle + \langle 0 | f_4 | 1 \rangle \} + \dots, \end{aligned} \quad (8.8)$$

which requires simply the additional generation of expectation values $\langle 0 | f_i | 1 \rangle$ doubling the amount of labour needed to obtain expectation values, but not the time required to perform least-squares fits. The $|1\rangle$ vectors can be obtained by Hutson's (53) method.

3.2.3 Direct Nonlinear Least-Squares Fits to Analytical Operators

In recent work, Gruebele *et al.* (188) explored the possibility of fitting spectral line positions *directly* to the relevant elements of the radial Hamiltonian operators. This calculation is exact within the Schrödinger equation picture but requires nonlinear least-squares optimization and a more

frequent numerical solution of the wave equation. As discussed previously, the HCA can also be interpreted in terms of a pseudolinearized problem with partial derivatives obtained by the Hellmann-Feynman theorem. These derivatives can also be obtained in a brute-force way in accord with,

$$\frac{\partial E_{vJ}}{\partial p_k} = \frac{E_{vJ}(p_k) - E_{vJ}(p_k + \delta p_k)}{\delta p_k}, \quad (8.9)$$

where δp_k is chosen to avoid numerical problems or instabilities. The procedure is iterated, since the brute-force method does not obtain as accurate partial derivatives as the Hellmann-Feynman method. The p_k are parameters defining an analytical potential function, or other elements of the operator.

This method is far more demanding computationally than the HCA. This is because a calculation of new partial derivatives is required with every fit whereas the HCA operates on the same set of expectation values. It is estimated that for models with similar numbers of parameters and identical data sets, the direct method would required approximately 10-20 times the amount of execution time. Work carried out in this laboratory with the direct method has so far been restricted to the lower vibrational levels of $\text{HI}(X^1\Sigma^+)$ and $\text{CO}(X^1\Sigma^+)$. The analytical model Eq. (6.13) has been employed as well as the Perturbed Morse Oscillator expansion, Eq. (3.6).

Despite the increased computational labour, this method is preferable over the HCA since it eliminates a lot of the complexity and ambiguity associated with the indirect numerical procedure. Some effort has gone into, and is still required, in devising flexible analytical functions for use with the direct method. In particular, the PMO and the radial- β Morse functions can only be relied on for up to approximately 50% of \mathcal{D}_e . A model which will

be tested in the future is,

$$U(R) = f_1 U_I(R) + f_2 U_M(R) + f_3 U_O(R), \quad (8.10)$$

where $U_I(R)$, $U_M(R)$, and $U_O(R)$ are analytical forms appropriate for the inner, middle, and outer regions of the potential, respectively. The functions f_i are mathematical filters which allow for a smooth transition from one potential form to another as the internuclear distance is varied.

8.3 *Concluding Remarks*

The work presented in this thesis has extended our understanding of the diatomic molecules HF and HCl and their isotopomers. The interpretation of spectroscopic observables in terms of a fully quantum mechanical model has been demonstrated to be very effective not only in representing information included in the fits, within experimental precision, but also at predicting with remarkable accuracy such information not obtained readily by traditional methods.

Despite this, as the precision of spectroscopic data continues to improve, development of improved procedures will undoubtedly be required. It will indeed be interesting to see to what extent very precise observations over the entire potential well will lend themselves to an interpretation by approximate theoretical models. In Steinfeld's words: "... in every case the molecule has solved its own Schrödinger equation exactly, and is probably laughing at our attempts at attaining to some approximate solution" (215).

It is my belief that through this work we have quieted down some of the laughter.

APPENDICES

The eight appendices contained in this thesis have been numbered separately and are included as eight microfiche sheets on the inside of the back cover of the bound thesis. A list of their titles and page numbers is given below.

	PAGE
APPENDIX A-1 Fortran-77 Source Listing of SPECTRUM	1
APPENDIX A-2 Numerical Information on Radial Functions for HCl and DCl	15
APPENDIX A-3 Quantum Mechanical Eigenvalues for the $X^1\Sigma^+$ and $B^1\Sigma^+$ States of $H^{35}Cl$, $H^{37}Cl$, $D^{35}Cl$, and $D^{37}Cl$	23
APPENDIX A-4 Calculation of Spectroscopic Line Positions for $H^{35}Cl$, $H^{37}Cl$, $D^{35}Cl$, and $D^{37}Cl$	53
APPENDIX A-5 Quantum Mechanical Eigenvalues for the $X^1\Sigma^+$ and $B^1\Sigma^+$ States of $T^{35}Cl$ and $T^{37}Cl$	273
APPENDIX A-6 Calculation of Spectroscopic Line Positions for HF and DF	300
APPENDIX A-7 Numerical Information on Radial Functions for HF and DF	452
APPENDIX A-8 Quantum Mechanical Eigenvalues for the $X^1\Sigma^+$ and $B^1\Sigma^+$ States of HF and DF	459

BIBLIOGRAPHY

1. E. Schrödinger, "The Collected Works," Chelsea, New York, 1978.
2. M. Born and J. R. Oppenheimer, *Ann. Phys.* **84**, 457 (1927).
3. H. Jeffreys, *Proc. London Math. Soc. A* **23**, 428 (1925).
4. G. Wentzel, *Z. Phys.* **38**, 518 (1926).
5. H. A. Kramers, *Z. Phys.* **39**, 828 (1926).
6. L. Brillouin, *J. Phys. Radium* **7**, 353 (1925).
7. N. Fröman, "Semiclassical Methods in Molecular Scattering and Spectroscopy," Chap. 1, Reidel, Dordrecht, 1980.
8. J. L. Dunham, *Phys. Rev.* **41**, 713 (1932).
9. S. M. Kirschner and R. J. Le Roy, *J. Chem. Phys.* **68**, 3139 (1978).
10. R. N. Kesarwani and Y. P. Varshni, *Canad. J. Phys.* **58**, 363 (1980).
11. J. Killingbeck, *J. Phys. A* **13**, L231 (1980).
12. L. A. Young, *Phys. Rev.* **38**, 1612 (1931).
13. W. E. Milne, *Phys. Rev.* **35**, 863 (1930).
14. H. J. Korsch and H. Laurent, *J. Phys. B* **14**, 4213 (1981).
15. H. J. Korsch, H. Laurent and R. Möhlenkamp, *J. Phys. B* **15**, 1 (1982).
16. J. L. Dunham, *Phys. Rev.* **41**, 721 (1932).
17. J. O. Hirschfelder and W. J. Meath, *Adv. Chem. Phys.* **12**, 3 (1967).
18. G. Simons, R. G. Parr and J. M. Finlan, *J. Chem. Phys.* **59**, 3229 (1973).
19. A. J. Thakkar, *J. Chem. Phys.* **62**, 1693 (1975).
20. J. F. Ogilvie, *Proc. R. Soc. London Ser. A* **378**, 287 (1981).
21. R. Rydberg, *Z. Phys.* **73**, 376 (1931).
22. O. Klein, *Z. Phys.* **76**, 226 (1932).
23. A. L. G. Rees, *Proc. Phys. Soc. London* **59**, 998 (1947).

24. J. T. Vanderslice, E. A. Mason and W. G. Maisch, *J. Mol. Spectrosc.* **3**, 17 (1959).
25. W. Kołos, *Adv. Quantum Chem.* **5**, 99 (1970).
26. R. G. Woolley and B. T. Sutcliffe, *Chem. Phys. Lett.* **45**, 393 (1977).
27. H. Essén, *Int. J. Quantum Chem.* **12**, 721 (1977).
28. R. F. W. Bader, *Acc. Chem. Res.* **18**, 9 (1985).
29. H. J. Monkhorst, *Phys. Rev. A* **36**, 1544 (1987).
30. D. M. Bishop and S. Shih, *J. Chem. Phys.* **64**, 162 (1976); erratum *J. Chem. Phys.* **67**, 4313 (1977).
31. E. Corinaldesi and F. Strocchi, "Relativistic Wave Mechanics," Part II, Chap. III, North-Holland, Amsterdam, 1963.
32. D. P. Craig and T. Thirunamachandran, "Molecular Quantum Electrodynamics," Academic Press, New York, 1984.
33. J. M. Hutson and B. J. Howard, *Mol. Phys.* **41**, 1113 (1980).
34. L. C. Wang and R. J. Boyd, *J. Chem. Phys.* **90**, 1083 (1989).
35. D. M. Bishop and L. M. Cheung, *Adv. Quantum Chem.* **12**, 1 (1980).
36. G. Herzberg, *Vistas in Astronomy* **29**, 201 (1986).
37. J. H. Van Vleck, *J. Chem. Phys.* **4**, 327 (1936).
38. H. Lefebvre-Brion and R. W. Field, "Perturbations in the Spectra of Diatomic Molecules," Chap. 3, Academic Press, New York, 1986.
39. R. M. Herman and A. Asgharian, *J. Mol. Spectrosc.* **19**, 305 (1966).
40. P. R. Bunker and R. E. Moss, *Mol. Phys.* **33**, 417 (1977).
41. P. R. Bunker, C. J. McLarnon and R. E. Moss, *Mol. Phys.* **33**, 425 (1977).
42. J. K. G. Watson, *J. Mol. Spectrosc.* **80**, 411 (1980).
43. J. Hoeft and K. P. R. Nair, *Chem. Phys. Lett.* **155**, 273 (1989).

44. M. Bogey, C. Demuyne and J. L. Destombes, *Chem. Phys. Lett.* **155**, 265 (1989).
45. A. G. Maki, *J. Mol. Spectrosc.* **137**, 147 (1989).
46. J. A. Coxon and J. F. Ogilvie, *J. Chem. Soc. Faraday Trans. 2* **78**, 1345 (1982).
47. S. M. Kirschner and J. K. G. Watson, *J. Mol. Spectrosc.* **51**, 321 (1974).
48. M. G. Barwell, M. Sc. thesis, University of Waterloo, 1976.
49. R. J. Le Roy, "Molecular Spectroscopy," Vol. 1, Chap. 3, Specialist Periodical Report of the Chemical Society of London, 1973.
50. S. Z. Moody and C. L. Beckel, *Int. J. Quantum Chem. Symp. No. 3*, 469 (1970).
51. J. Tellinghuisen, *Chem. Phys. Lett.* **18**, 544 (1973).
52. D. L. Albritton, W. J. Harrop, A. L. Schmeltekopf and R. N. Zare, *J. Mol. Spectrosc.* **46**, 25 (1973).
53. J. M. Hutson, *J. Phys. B* **14**, 851 (1981).
54. J. Tellinghuisen, *J. Mol. Spectrosc.* **122**, 455 (1987).
55. P. Pajunen, *J. Mol. Spectrosc.* **124**, 185 (1987).
56. G. Herzberg, "Molecular Spectra and Molecular Structure. I. Spectra of Diatomic Molecules," pp. 175-185, Academic Press, New York, 1986.
57. D. L. Albritton, A. L. Schmeltekopf and R. N. Zare, "Molecular Spectroscopy: Modern Research," Vol II, Chap. 1, Academic Press, New York, 1976.
58. H. I. Britt and R. H. Luecke, *Technometrics* **15**, 233 (1973).
59. J. A. Coxon, *J. Mol. Spectrosc.* **72**, 252 (1978).
60. F. W. Birss, *J. Mol. Spectrosc.* **99**, 133 (1983).

61. H. Hellmann, "Einführung in die Quantenchemie," Franz Deuticke, Vienna, 1937.
62. R. P. Feynman, *Phys. Rev.* **56**, 340 (1939).
63. J. W. Cooley, *Math. Comp.* **15**, 363 (1961).
64. J. K. Cashion, *J. Chem. Phys.* **39**, 1872 (1963); R. N. Zare and J. K. Cashion, University of California, Lawrence Radiation Laboratory Report, UCRL-10881, 1963.
65. B. Numerov, *Publs. Observatoire Central Astrophys. Russ.* **2**, 188 (1933).
66. L. D. Landau and E. M. Lifshitz, "Quantum Mechanics, Non-Relativistic Theory," Pergammon Press, New York, 1977.
67. D. F. Zetic and F. A. Matsen, *J. Mol. Spectrosc.* **24**, 122 (1967).
68. C. S. Lin and G. W. F. Drake, *Chem. Phys. Lett.* **16**, 35 (1972).
69. I. Baraldi, F. Momicchioli and M. C. Bruni, *J. Farad. Trans II* **72**, 887 (1976).
70. B. R. Johnson, *J. Chem. Phys.* **67**, 4086 (1977).
71. H. Kobeissi, M. Dagher and M. A. Alameddine, *Int. J. Quantum Chem.* **20**, 633 (1981).
72. J. Tellinghuisen, *Int. J. Quantum Chem.* **XXXIV**, 401 (1988).
73. R. J. Le Roy and W. K. Liu, *J. Chem. Phys.* **69**, 3622 (1978).
74. J. C. P. Miller, "The Airy Integral," Brit. Assoc. Mathematical Tables, Part-Vol. B, Cambridge, 1946.
75. E. Tiemann, *Mol. Phys.* **65**, 359 (1988).
76. N. Elander, K. Hehenberger and P. R. Bunker, *Phys. Scr.* **20**, 631 (1974).
77. R. J. Le Roy and R. B. Bernstein, *J. Chem. Phys.* **49**, 4312 (1968).
78. R. J. Le Roy, Chemical Physics Research Report CP-230R, University of Waterloo, 1984.

79. J. N. L. Connor and A. D. Smith, *Mol. Phys.* **43**, 397 (1981).
80. T. Tietz, *Canad. J. Phys.* **49**, 1315 (1971).
81. R. N. Zare, *J. Chem. Phys.* **40**, 1934 (1964).
82. S. Weissman, J. T. Vanderslice and R. J. Battino, *J. Chem. Phys.* **43**, 2226 (1965).
83. A. W. Mantz, J. K. G. Watson, K. Narahari Rao, D. L. Albritton, A. L. Schmeltekopf and R. N. Zare, *J. Mol. Spectrosc.* **39**, 180 (1971).
84. J. Tellinghuisen, *J. Mol. Spectrosc.* **44**, 194 (1972).
85. H. Telle and U. Telle, *J. Mol. Spectrosc.* **85**, 248 (1981).
86. G. Guelachvili, *Optics Comm.* **19**, 150 (1976).
87. G. Di Lonardo and A. E. Douglas, *Canad. J. Phys.* **51**, 434 (1973).
88. R. S. Berry, S. A. Rice and J. Ross, "Physical Chemistry," Wiley, New York, 1980.
89. J. T. Vanderslice, R. Davies and S. Weissman, *J. Chem. Phys.* **43**, 1075 (1965).
90. R. H. Davies and J. T. Vanderslice, *J. Chem. Phys.* **45**, 95 (1966).
91. J. W. McKeever, *J. Mol. Spectrosc.* **51**, 306 (1974).
92. R. J. Le Roy, "Semiclassical Methods in Molecular Scattering and Spectroscopy," Chap. 3, Reidel, Dordrecht, 1980.
93. E. W. Kaiser, *J. Chem. Phys.* **53**, 1686 (1970).
94. C. Schwartz and R. J. Le Roy, *J. Chem. Phys.* **81**, 3996 (1984).
95. J. N. Huffaker, *J. Mol. Spectrosc.* **65**, 1 (1977).
96. J. N. Huffaker, *J. Chem. Phys.* **64**, 1726 (1976).
97. R. J. Le Roy, *J. Chem. Phys.* **73**, 6003 (1980).
98. J. B. Bouanich, *J. Quant. Spectrosc. Radiat. Trans.* **19**, 381 (1978).

99. A. Pardo, J. J. Camacho, J. M. L. Poyato and J. I. Fernandez-Alonso, *J. Mol. Struct.* **142**, 319 (1986).
100. J. K. G. Watson, *J. Mol. Spectrosc.* **74**, 319 (1979).
101. G. Gouedard and J. Vigue, *Chem. Phys. Lett.* **96**, 293 (1983).
102. N. Bessis, G. Hadinger and Y. S. Tergiman, *J. Mol. Spectrosc.* **107**, 343 (1984).
103. J. F. Ogilvie, *J. Mol. Spectrosc.* **128**, 216 (1988).
104. J. F. Ogilvie and R. H. Tipping, *Int. J. Rev. Phys. Chem.* **3**, 3 (1983).
105. V. Y. Galin, V. F. Golovko, Y. S. Manushkin and V. G. Tyuterev, *Opt. Spectrosc.* **57**, 582 (1984).
106. A. V. Burenin, *Opt. Spectrosc.* **55**, 638 (1983).
107. J. N. Huffaker, *J. Chem. Phys.* **64**, 4564 (1976).
108. J. N. Huffaker, M. Karimi and L. B. Tran, *J. Mol. Spectrosc.* **124**, 393 (1987).
109. J. N. Huffaker and D. I. Cohen, *J. Chem. Phys.* **85**, 346 (1986).
110. W. H. Miller, *J. Chem. Phys.* **54**, 4174 (1971).
111. R. J. Le Roy and R. B. Bernstein, *J. Chem. Phys.* **49**, 4312 (1968).
112. W. Kołos and L. Wolniewicz, *J. Chem. Phys.* **49**, 404 (1968).
113. M. Kuriyan and H. O. Pritchard, *Canad. J. Phys.* **54**, 1865 (1976).
114. M. Kuriyan and H. O. Pritchard, *Canad. J. Phys.* **55**, 3420 (1977).
115. W. M. Kosman and J. Hinze, *J. Mol. Spectrosc.* **56**, 93 (1975).
116. C. R. Vidal and H. Scheingraber, *J. Mol. Spectrosc.* **65**, 46 (1977).
117. J. I. Musher, *Amer. J. Phys.* **34**, 267 (1966).
118. S. T. Epstein, *Amer. J. Phys.* **22**, 99 (1954).
119. J. A. Coxon, *J. Mol. Spectrosc.* **117**, 361 (1986).
120. J. A. Coxon, *J. Mol. Spectrosc.* **133**, 96 (1989).

121. I. S. Berezin and N. P. Zhidkov, "Computing Methods," Vol. 1, Pergamon Press, New York, 1965.
122. W. H. Beyer, Ed., CRC Standard Mathematical Tables, CRC Press, Boca Raton, 1981.
123. I. P. Hamilton, J. C. Light and K. B. Whaley, *J. Chem. Phys.* **85**, 5151 (1986).
124. C. H. Townes and A. L. Schawlow, "Microwave Spectroscopy," McGraw-Hill, New York, 1955.
125. W. H. Press, B. P. Flannery, S. A. Teukolsky and W. T. Vetterling, "Numerical Recipes: The Art of Scientific Computing," Cambridge University Press, New York, 1986.
126. P. B. Bailey, *J. Math. Phys.* **5**, 1293 (1964).
127. M. Bettendorff, S. D. Peyerimhoff and R. J. Buenker, *Chem Phys.* **66**, 261 (1982).
128. A. E. Douglas and F. R. Greening, *Canad. J. Phys.* **57**, 1650 (1979).
129. I. G. Nolt, J. V. Radostitz, G. Di Lonardo, K. M. Evenson, D. A. Jennings, K. P. Leopold, M. D. Vanek, L. R. Zink, A. Hinz and K. V. Chance, *J. Mol. Spectrosc.* **125**, 274 (1987).
130. J. A. Coxon and U. K. Roychowdhury, *Canad. J. Phys.* **63**, 1485 (1985).
131. R. A. Sawyer, "Experimental Spectroscopy," Dover, New York, 1963.
132. A. E. Douglas and J. G. Potter, *Appl. Opt.* **1**, 727 (1962).
133. A. P. Thorne, "Spectrophysics," Chapman and Hall, New York, 1974.
134. H. M. Crosswhite, *J. Res. Natl. Bur. Stand. Sec. A* **79**, 17 (1974).
135. P. R. Bunker, *J. Mol. Spectrosc.* **28**, 422 (1968).
136. S. G. Tilford, M. L. Ginter and J. T. Vanderslice, *J. Mol. Spectrosc.* **33**, 505 (1970).

137. S. G. Tilford and M. L. Ginter, *J. Mol. Spectrosc.* **40**, 568 (1971).
138. D. S. Ginter and M. L. Ginter, *J. Mol. Spectrosc.* **90**, 177 (1981).
139. R. Callaghan, S. Arepali and R. J. Gordon, *J. Chem. Phys.* **86**, 5273 (1987).
140. C. N. Banwell, "Fundamentals of Molecular Spectroscopy," McGraw-Hill, New York, 1983.
141. P. G. Francis, "Mathematics for Chemists," Chapman and Hall, New York, 1984.
142. D. A. Jennings, K. M. Evenson, L. R. Zink, C. Demuynck, J. L. Destombes, B. Lemoine and J. W. C. Johns, *J. Mol. Spectrosc.* **122**, 477 (1987).
143. U. K. Sengupta, P. K. Das and K. Narahari Rao, *J. Mol. Spectrosc.* **74**, 322 (1979).
144. T. F. Deutsch, *Appl. Phys. Lett.* **10**, 234 (1967).
145. T. F. Deutsch, *Appl. Phys. Lett.* **11**, 18 (1967).
146. D. E. Mann, B. A. Thrush, D. R. Lide, Jr., J. J. Ball and N. Acquista, *J. Chem Phys.* **34**, 420 (1961).
147. D. A. Jennings and J. S. Wells, *J. Mol. Spectrosc.* **130**, 267 (1988).
148. C. A. Coulson, "Valence," Oxford University Press, London, 1961.
149. M. Bettendorff, R. J. Buenker, S. D. Peyerimhoff and J. Römelt, *Z. Phys. A* **304**, 125 (1982).
150. E. Safary, J. Romand and B. Vodar, *J. Chem. Phys.* **19**, 379 (1951).
151. J. W. C. Johns and R. F. Barrow, *Proc. R. Soc. London A* **251**, 504 (1959).
152. L. Tashiro, W. Ubachs and R. N. Zare, *J. Mol. Spectrosc.* **128**, 89 (1989).
153. N. Åslund, *Ark. F. Fysik* **30**, 377 (1965).

154. R. N. Spanbauer, K. Narahari Rao and L. H. Jones, *J. Mol. Spectrosc.* **16**, 100 (1965).
155. A. J. Perkins, *Spectrochim. Acta A* **24**, 285 (1968).
156. R. N. Sileo and T. A. Cool, *J. Chem. Phys.* **65**, 117 (1976).
157. G. Büttgenbender and G. Herzberg, *Ann. Phys.* **21**, 577 (1935).
158. R. Schmid and L. Gerö, *Z. Phys.* **104**, 724 (1937).
159. T. G. Waech and R. B. Bernstein, *J. Chem. Phys.* **46**, 4905 (1967).
160. R. S. Mulliken, cited as private communication in Ref. (171).
161. F. C. De Lucia, P. Helminger and W. Gordy, *Phys. Rev. A* **3**, 1849 (1971).
162. G. Guelachvili, P. Niay and P. Bernage, *J. Mol. Spectrosc.* **85**, 271 (1981).
163. C. M. Clayton, Ph.D. thesis, Pennsylvania State University, 1977.
164. D. H. Rank, B. S. Rao and T. A. Wiggins, *J. Mol. Spectrosc.* **17**, 122 (1965).
165. M. Zughal, cited as private communication in Ref. (46).
166. T. F. Deutsch, *IEEE J. Quantum Electron.* **3**, 419 (1967).
167. D. U. Webb and K. Narahari Rao, *Appl. Opt.* **5**, 1461 (1966).
168. D. U. Webb and K. Narahari Rao, *J. Mol. Spectrosc.* **28**, 121 (1968).
169. A. Levy, I. Rossi and C. Haeusler, *J. Phys. (Paris)* **27**, 526 (1966).
170. P. Niay, C. Coquant, P. Bernage and H. Bocquet, *J. Mol. Spectrosc.* **65**, 388 (1977).
171. D. A. Rank, D. P. Eastman, B. S. Rao and T. A. Wiggins, *Opt. Soc. Amer.* **52**, 1 (1962).
172. J. K. Jacques and R. F. Barrow, *Proc. Phys. Soc. London* **73**, 538 (1958).
173. J. A. Coxon, P. G. Hajigeorgiou and K. P. Huber, *J. Mol. Spectrosc.* **131**, 288 (1988).

174. B. H. Wells, E. B. Smith and R. N. Zare, *Chem. Phys. Lett.* **99**, 244 (1983).
175. J. Tellinghuisen, S. D. Henderson, D. Austin, K. P. Lawley and R. J. Donovan, *Phys. Rev. A* **39**, 925 (1989).
176. J. A. Coxon, *J. Quant. Spectrosc. Radiat. Transfer* **11**, 443 (1971).
177. J. K. G. Watson, *J. Mol. Spectrosc.* **66**, 500 (1977).
178. J. Tellinghuisen, *J. Mol. Spectrosc.* **137**, 248 (1989).
179. J. D. Poll and G. Karl, *Canad. J. Phys.* **44**, 1467 (1966).
180. J. K. G. Watson, *J. Mol. Spectrosc.* **45**, 99 (1973).
181. A. H. Wapstra and K. Bos, *At. Data Nuc. Data Tables* **19**, 185 (1977).
182. I. G. M. Mills, Ed., "Quantities, Units and Symbols in Physical Chemistry, IUPAC Commission on Physicochemical Symbols, Terminology and Units," Blackwell Oxford, 1988.
183. S. M. Bass, R. L. De Leon and J. S. Muentert, *J. Chem. Phys.* **86**, 4305 (1987).
184. C. A. Burrus, W. Gordy, B. Benjamin and R. Livingstone, *Phys. Rev.* **97**, 1661 (1955).
185. L. H. Jones and E. S. Robinson, *J. Chem. Phys.* **24**, 1246 (1956).
186. F. L. Keller and A. H. Nielsen, *J. Chem. Phys.* **22**, 294 (1954).
187. L. I. Kleinman and M. Wolfsberg, *J. Chem. Phys.* **60**, 4749 (1974).
188. M. Gruebele, E. Keim, A. Stein and R. J. Saykally, *J. Mol. Spectrosc.* **131**, 343 (1988).
189. L. I. Kleinman and M. Wolfsberg, *J. Chem. Phys.* **60**, 4740 (1974).
190. J. A. Coxon and J. F. Ogilvie, *Canad. J. Spectrosc.* **34**, 137 (1989).
191. J. M. Alvaríño, L. F. González, M. L. Hernández and E. Martínez, *Spectrosc. Lett.* **16**, 541 (1983).

192. D. P. Akitt and J. T. Yardley, *J. Quantum Electron.* **6**, 113 (1970).
193. E. Cuellar and G. C. Pimentel, *J. Chem. Phys.* **71**, 1385 (1979).
194. A. A. Mason and A. H. Nielsen, *J. Opt. Soc. Amer.* **57**, 1464 (1967).
195. V. E. Revich and S. A. Stankevich, *Dokl. Phys. Chem.* **170**, 699 (1966).
196. W. G. Rothschild, *J. Opt. Soc. Amer.* **54**, 20 (1964).
197. S. C. Foster, Ph.D. thesis, Dalhousie University, 1982.
198. G. Herzberg, "Molecular Spectra and Molecular Structure. I. Spectra of Diatomic Molecules," pp. 413-434, Academic Press, New York, 1986.
199. R. S. Mulliken, *J. Chem. Phys.* **33**, 247 (1960).
200. H. Lefebvre-Brion and R. W. Field, "Perturbations in the Spectra of Diatomic Molecules," Chap. 6, Academic Press, New York, 1986.
201. R. B. Bernstein, *Phys. Rev. Lett.* **16**, 385 (1966).
202. C. C. Lu, T. A. Carlson, F. B. Malik, T. C. Tucker and C. W. Nestor, Jr., *Atomic Data* **3**, 1 (1971).
203. L. Pauling and E. B. Wilson, "Introduction to Quantum Mechanics," McGraw-Hill, New York, 1935.
204. M. A. Byrne, W. G. Richards and J. A. Horsley, *Mol. Phys.* **12**, 273 (1967).
205. W. T. Zemke, private communication, 1988.
206. T. R. Proctor and W. C. Stwalley, *J. Chem. Phys.* **66**, 2063 (1977).
207. M. S. Caceci and W. P. Cacheris, *BYTE*, p. 340, May 1984.
208. Y. C. Chan, D. R. Harding, W. C. Stwalley and C. R. Vidal, *J. Chem. Phys.* **85**, 2436 (1986).
209. G. Herzberg, "Molecular Spectra and Molecular Structure. I. Spectra of Diatomic Molecules," pp. 227-228, Academic Press, New York, 1986.
210. J. A. Coxon and P. G. Hajigeorgiou, *J. Mol. Spectrosc.* **133**, 45 (1989).
211. L. H. Jones and M. Goldblatt, *J. Mol. Spectrosc.* **1**, 43 (1957).

- 212. D. Oba, B. S. Agrawalla and D. W. Setser, *J. Quant. Spectrosc. Radiat. Transfer* **34**, 283 (1985).
- 213. S. R. Langhoff, M. L. Sink, R. H. Pritchard and C. W. Kern, *J. Mol. Spectrosc.* **96**, 200 (1982).
- 214. J. F. Ogilvie, *Proc. R. Soc. London A* **378**, 287 (1981).
- 215. J. I. Steinfeld, "Molecules and Radiation," p. 140, Harper & Row, New York, 1974.

UNABLE TO FILM MATERIAL ACCOMPANYING THIS THESIS (I.E.
DISKETTE(S), SLIDES, MICROFICHE, ETC...).

PLEASE CONTACT THE UNIVERSITY LIBRARY.

INCAPABLE DE MICROFILMER LE MATERIEL QUI ACCOMPAGNE CETTE THESE
(EX. DISQUETTES, DIAPOSITIVES, MICROFICHE (S), ETC...).

VEUILLEZ CONTACTER LA BIBLIOTHEQUE DE L'UNIVERSITE.

NATIONAL LIBRARY OF CANADA
CANADIAN THESES SERVICE

BIBLIOTHEQUE NATIONALE DU CANADA
LE SERVICE DES THESES CANADIENNES